Design of a UAV based NavAid Calibration and Testing system

Final Report

H. van Donge, S. Heyer, A.A.J. Hooijen, A. Khoshnewiszadeh, R.R.J. Krook, J. Meyer, J.R. van der Ploeg, T.S.C. Pollack, T.C. Schouten and S.C.E. Smets

Delft University of Technology

TU Delft Delft University of Technology

Challenge the future

This page would be intentionally left blank
if we would not wish to inform about that.

DESIGN OF A UAV BASED NAVAID CALIBRATION AND TESTING SYSTEM

FINAL REPORT

by

H. van Donge, S. Heyer, A.A.J. Hooijen, A. Khoshnewiszadeh, R.R.J. Krook, J. Meyer, J.R. van der Ploeg, T.S.C. Pollack, T.C. Schouten and S.C.E. Smets

Date: June 28, 2016

AE3200 Design Synthesis

Project coordinators

Ir. P.C. Roling (principal tutor), Dr.ir. A.C. in 't Veld (coach) and Dr. A. Elham (coach)

Cover image is property of NAV CANADA, and was accessed through
`http://www.navcanada.ca/EN/media/PublishingImages/Photo%20Library/_K2C0472.jpg`

Name	**Student number**
Henk van Donge	4230345
Stefan Heyer	4151712
Toine Hooijen	4079418
Arwin Khoshnewiszadeh	4137736
Ralph Krook	4234146
Johann Meyer	4303113
Joost van der Ploeg	4293266
Tijmen Pollack	4268644
Tom Schouten	4272196
Stephan Smets	4293517

TU Delft Delft University of Technology

PREFACE

This is the final report concerning the detailed design of a UAV based system that is capable of testing and calibrating the accuracy of aviation navigation equipment. This assignment is part of the course AE3200 Design Synthesis, taught at the Delft University of Technology. This course provides the students the opportunity to obtain design experience in a multidisciplinary design project and is also the final course in the bachelor programme of the study Aerospace Engineering. The final report is the last report in a series of four, preceded by a project plan, a baseline report and a midterm report.

The authors would like to express their gratitude to Ir. P.C. Roling (principal tutor) for his guidance and support during the entire process. Also Dr.ir. A.C. in 't Veld (coach) and Dr. A. Elham (coach) deserve lots of gratitude for their assistance and expertise all the way. Lastly, special appreciation goes to I. Wilmes (external consultant) for guiding and assisting the students in their project and giving them the opportunity to tour the Cessna Citation II and explaining the practises that are currently used in the calibration of aircraft navigation equipment.

H. van Donge, S. Heyer, A.A.J. Hooijen, A. Khoshnewiszadeh, R.R.J. Krook, J. Meyer, J.R. van der Ploeg, T.S.C. Pollack, T.C. Schouten and S.C.E. Smets

Delft, June 28, 2016

SUMMARY

This report presents the design of a UAV based NavAid calibration and testing system. The purpose of this report is to develop the final concept to a preliminary design, where all major design parameters are fixed. This design step is the last design step of the project.

The first part of the project consists of pre-design considerations. In this chapter, all non-engineering preparations for the design process are undertaken and is a brief summary of what is described in the Project Plan [1]. The market analysis elaborates on the market share of the UAV based calibration system. Stakeholders are summed up and their requirements form a key for the design. Based on the functional analysis, more system requirements are created. A driving design factor is the sustainability of the product, affecting materials, operations and production strategies.

Secondly, the conceptual design is discussed. The chapter summarises the Midterm Report [2] where selections were made out of the design option trees, trade-offs were done and four final concepts were chosen. The four concepts are designed in a very preliminary phase and a last trade-off gives the final conceptual design. The conventional fixed wing aircraft is going to be piston powered and uses a pushing propeller.

The next step is to continue with the design of the piston powered fixed-wing aircraft. The aircraft is designed by using an iterative process. This process is performed because the design parameters are dependent others and need to be optimised simultaneously. The process is first explained and the decision flow is presented. Starting with the weight estimation, the matching plots from the Midterm Report are recomputed. From this the 2D lift device and propulsion system is designed. After that, the 3D wing is optimised, and the weight estimation is redone. On this results, the stability is analysed and the landing gear is sized, and so the weight estimation is adjusted to the new criteria and the loop starts again. The iteration process is performed four times, leading to convergent results of an optimal design.

To simplify the process, tools are made so input values can easily be converted to the corresponding outputs. All payload and avionics are defined including the communication systems. A dish in the nose of the UAV will enable satellite communications and the payload bay will be a removable module. Based on the class I weight estimation from the Mid-term Report, the class II weight estimation is performed. With a tool, using the aircraft's dimensions and characteristics, the weights of all major components are estimated. A third tool is determining the aerodynamics of the high-wing aircraft, designing the lift device and all 2D and 3D aerodynamic characteristics. The drag is influencing the propulsion design. In the engine design an off-the-shelf engine is used and the fuel tank is sized to be integrated in the wing. The last contribution in the iteration is the stability and control analysis, where the centre of gravity (c.g.) of the aircraft is determined, and using that, the wing can be located and the landing gear can be sized.

After the design process, the final design results are presented and the general layout of the UAV is designed. With these results, the flight performance of the system is analysed in terms of climb & descent and airfield performance. Also, a loading diagram and the flight envelope are determined. The airframe needs to be designed to carry all loads that are introduced to the frame during operations. Now all lay-out constraints are set, the exact loads are calculated and the structure is designed to it. Regarding the calibration operations, the ground station is sized, the transportability via the LD6 container is designed and the system setup procedures are determined.

After the entire preliminary design is defined, a synthesis on the system is performed. Because noise was a requirement at the start of the project, it needs to be analysed and the noise footprint has to be defined. For sustainability purposes the emissions and recyclability are analysed. Furthermore, the RAMS characteristics and crash rate are analysed. Finally, a cost estimation is done and a quality check is done on the system.

To conclude this phase of the design process, an overview of the future planning is given. This contains the project design and development logic and planning as well as a cost-breakdown structure and production plan.

It can be concluded that the goal of the report, which was to develop the final concept to a preliminary design, was achieved. The next step will be the detailed design, experimental validation and the assembly of the first prototype. However, this will be beyond the scope of the project.

CONTENTS

NOMENCLATURE

Abbreviations

ADF	Automatic Direction Finder
AOA	Angle Of Attack
ATC	Air Traffic Control
BEM	Blade Element Momentum
CFD	Computational Fluid Dynamics
CFR	Code of Federal Regulations
COTS	Commercial off-the-shelf
CSP	Constant Speed Propeller
CSU	Constant Speed Unit
DGPS	Differential Global Positioning System
DME	Distance Measuring Equipment
EOL	End-Of-Life
EOL-RR	EOL Recycling Rate
FAA	Federal Aviation Administration
FAR	Federal Aviation Regulations
FBS	Functional Breakdown Structure
FMC	Flight Management Computer
FPP	Fixed Pitch Propeller
FRP	Fibre-Reinforced Plastic
GPS	Global Positioning System
GS	Glideslope
HAZMAT	Hazardous Materials
IFR	Instrument Flight Rules
ILS	Instrument Landing System
IMU	Inertial Measurement Unit
INM	Integrated Noise Model
INS	Inertial Navigation System
LEMAC	Leading Edge Mean Aerodynamic Chord
LOS	Line Of Sight
LOS	Local Optima Smoothing
MAC	Mean Aerodynamic Chord
MB	Marker Beacon
MFW	Maximum Fuel Weight
MPW	Maximum Payload Weight
MTOW	Maximum Take-Off Weight
OEW	Operating Empty Weight
OSR	Old Scrap Ratio
PAPI	Precision Approach Path Indicator
Q3D	Quasi Three Dimensional
RAMS	Reliability, Availability, Maintainability and Safety
RC	Recycled Content
REE	Rare Earth Element
ROC	Rate of Climb
RPM	Rotations Per Minute
RPS	Rotations Per Second
RTK	Real-Time Kinematic
S.M.	Safety Margin
SATCOM	Satellite Communication
SBAS	Satellite Based Augmentation System
SFC	Specific Fuel Consumption
SNR	Signal-to-Noise Ratio

SQP	Sequential Quadratic Programming
TACAN	Tactical Air Navigator
TAS	True Airspeed
TBO	Time Between Overhaul
UAV	Unmanned Aerial Vehicle
UIP	Unloaded Inflation Pressure
VASI	Visual Approach Slope Indicator
VDB	VHF Data Broadcast
VFR	Visual Flight Rules
VHF	Very High Frequency
VOR	VHF Omnidirectional Range
VPP	Variable Pitch Propeller
WAAS	Wide Area Augmentation System

Greek Symbols

α	Angle of attack	[rad]
ϵ	Downwash angle	[rad]
Γ	Dihedral	[deg]
λ	Wing taper ratio	[–]
Λ_{LE}	Leading edge sweep angle	[deg]
ϕ	Lateral tip-over angle	[rad]
ψ	Lateral ground clearance angle	[rad]
θ	Longitudinal tip-over angle	[°]

Roman Symbols

$\bar{c}$	Mean aerodynamic chord	[m]
η_s	Shock absorber efficiency	[–]
η_t	Tire efficiency	[–]
a_x	Horizontal acceleration	[m/s^2]
C_D	Drag coefficient	[–]
C_l	Lift coefficient airfoil	[-]
$C_{L_{\alpha_h}}$	Lift coefficient slope horizontal tail	[–]
C_{L_α}	Lift coefficient slope	[–]
C_L	Lift coefficient	[-]
$C_{m_{a.c.}}$	Moment coefficient aerodynamic centre	[–]
d_s	Strut diameter	[m]
h_{cg}	Centre of gravity height	[m^2]
L_f	Fuselage length	[m]
l_h	Wing-tail distance	[m]
n	Load factor	[–]
n_s	Number of struts	[–]
S_h	Horizontal tail surface area	[m^2]
s_s	Strut length	[m]
s_t	Tire deflection	[ft]
w_t	Vertical speed	[m/s]
x_{ac}	Aerodynamic Centre	[-]
x_{cg}	Centre of Gravity	[-]
A	Area	[m^2]
a	Acceleration	[m/s^2]
AR	Aspect ratio	[–]
B	Bandwidth	[Hz]
b	Wing span	[m]
c	Chord length	[m]
D	Diameter	[m]
d	Distance	[m]
E	Endurance	[hrs]
e	Oswald factor	[–]
F	Static load	[N]

f	Frequency	[Hz]
g	Gravitational acceleration	[m/s^2]
h	Height	[m]
kW	Power	[Nm/s]
L	Length	[m]
P	Dynamic load	[N]
P	Power	[W]
R	Bit rate	[bit/s]
R	Range	[nm]
S	(Wing) surface area	[m^2]
s	Distance	[m]
t	Thickness	[m]
t	Time	[sec]
V	Airspeed	[m/s]
V	Volume	[m^3]
W	Weight	[N]
w	Width	[m]

1 INTRODUCTION

In these modern days, navigation of aircraft has become an important topic. Aircraft make use of highly accurate equipment to navigate. One of the systems used at airports to provide accurate navigation data is the instrument landing system (ILS). This system will allow aircraft to fly to the runway in all conditions, where the runway might not be visible at all. Depending on the accuracy of the ILS system it can be used up to zero feet decision height and 150 feet visual range (CAT IIIb), only limited by being able to visually drive off the runway. In order to provide such a high accuracy, the navigation equipment needs to be calibrated on a regular basis. Currently, inspection of the equipment is performed mostly by twin-engine business jets or small four seat propeller aircraft. These aircraft are expensive to acquire, operate and maintain. The low altitudes needed for flight inspection means suboptimal fuel use and high noise levels. Moreover, because of the limited amount of flight inspection aircraft in some regions, inspections can only be performed after careful planning and leaves little room for flexibility. At the moment, the industry of UAVs is growing and therefore, a new solution in the form of a UAV will be investigated and designed.

The aim of this report is to provide the reader with a description of the whole design process and to present a final design of the UAV that is able to replace the aircraft that are currently used for the calibration of aerial navigation equipment. The aircraft that is used for calibration in the Netherlands is the Cessna 550 Citation II that the Dutch Aerospace Centre (NLR) owns together with the faculty of Aerospace Engineering. The Citation is fitted with a multitude of extra sensors and systems such as a high-accuracy Global Positioning System with phase tracking, a multi-channel digital data acquisition and recording system and a telemetry system. The goal of the design is to be more efficient, be more sustainable, reduce the interference with aerodrome operations and produce less noise while still meeting the same performance requirements.

The structure of the report is as follows: in Chapter 2, the work done before the actual design is presented. This includes a market analysis and a functional analysis. In Chapter 3 the concept selection process is explained, together with a description of the chosen concept and after this, the design process and iterations are explained in Chapter 4. Chapter 5 covers the determination of the payload and avionics needed for the UAV and the mission that is to be performed. Also the telemetry is designed here. Then Chapter 6 provides an overview of the estimations of all subsystems of the UAV using a class II weight estimation. This is followed by Chapter 7, which covers the analysis and design of the aerodynamics of the UAV. Chapter 8 describes the propulsion system of the UAV, which entails the selection of the engine, propellers and batteries. Subsequently, the stability & control of the UAV are analysed in Chapter 9. After the design of the different subsystems and the iterations between them, the results of the design process are presented in Chapter 10 followed by an analysis on the flight performance in Chapter 11. After the design is finalised, the system can be analysed in more detail. This starts with the structural analysis & design in Chapter 12. Here the critical parts of the UAV are structurally designed. Then the layout of important aircraft systems is described in Chapter 13, followed by a description of the operations & logistics of the whole system in Chapter 14. Chapter 15 provides some additional vital characteristics of the system and Chapter 16 shows a final compliance matrix in which can be seen if all requirements are met. This is followed by a future planning in Chapter 17 and finally in Chapter 18, the conclusion of this report is provided.

2 PRE-DESIGN CONSIDERATIONS

Projects originate from multiple sources. One option is that there is a breakthrough in the technology, with which certain systems can be redesigned and improved, or new systems can be designed that previously were not feasible. This is partly the case, since UAV technology is relatively new for these kind of operations. Another source from which projects originate is a need for a certain system or product. This holds for the current project, since there is a demand for a more efficient system that can calibrate aeronautical navigation equipment. It is of vital importance to understand what a system will have to do in order to start the actual design of the system, so firstly a market analysis is performed in Section 2.1 from which a clear understanding of the actual needs is obtained. Then in Section 2.2 the functions that the product should be able to perform are identified and explained. These function are based on the function determine in the Baseline Report [3]. These function are structured in a Functional Breakdown Structure (FBS) and a Functional Flow Diagram (FFD).

In these modern days, sustainable development has become a key factor in each project. Therefore, an overview of the measures that will be taken is given in Section 2.3. Lastly, to be able to actually design and produce the system, special focus is needed in the identification and mitigation of all risks that can happen during the entire process. This is done in Section 2.4.

2.1. MARKET ANALYSIS

In order to design a system that will improve the current practice in navigation aid calibration services, a proper market analysis should be performed, from which a clear understanding of the actual needs of the system can be obtained. First, an overview of the current and possible future practises in the flight inspection market will be discussed. Then, a cost estimation of the new system will be compared to the cost of current systems. After the costs have been compared, a SWOT analysis can be created to evaluate the strengths, weaknesses, opportunities and threats of the new system.

2.1.1. CURRENT & FUTURE MARKETS

The current market can be subdivided into two main groups. Within the first group, the calibration is performed with the flight inspector on the ground, while the second group performs the inspection with the inspector in the aircraft. The global trend is shifting more and more to inspection with the inspector on the ground, since smaller aircraft can be used and the calibration data is sent to the inspector using a data-link system. This system also decreases operational costs by reducing the payload and enabling direct communication between the inspector and the ground crew [4]. Most current systems require two pilots and an inspector in the back, which is why primarily small business jets are used, like a Cessna Citation, Learjet or Beechcraft King Air. The systems that have been moved because of the data-link can utilise aircraft as small as a Diamond DA-42. These smaller multi-piston engine aircraft however, cannot compete with the larger aircraft with respect to operating speed.

Two major markets have been distinguished: civil and military. The markets have distinct needs and requirements and must thus be treated separately.

Civil Application

Civilian application refers primarily to civilian airports under normal operating conditions with high air traffic throughput. The main interest for civilian operation is to mitigate interference with airport operations and reduce airspace saturation. Civilian operations often use more expensive systems, like ground-based calibration, to reduce this downtime. According to Airbus, this requirement is only going to grow in the coming years as air traffic is concentrating around mega-cities and the airports are thus becoming more and more saturated, as illustrated in Figure 2.1. It can thus be concluded that the driving requirement for the civilian market is reducing interference.

The market for NavAid calibration is currently saturated; however, some regions are still serviced by one provider. Through some consultations with main international flight inspection service providers, current costs are estimated to be between €2000-€3000 per flight hour. In addition, a country with similar airport infrastructure to the Netherlands requires roughly 200 flight hours annually.

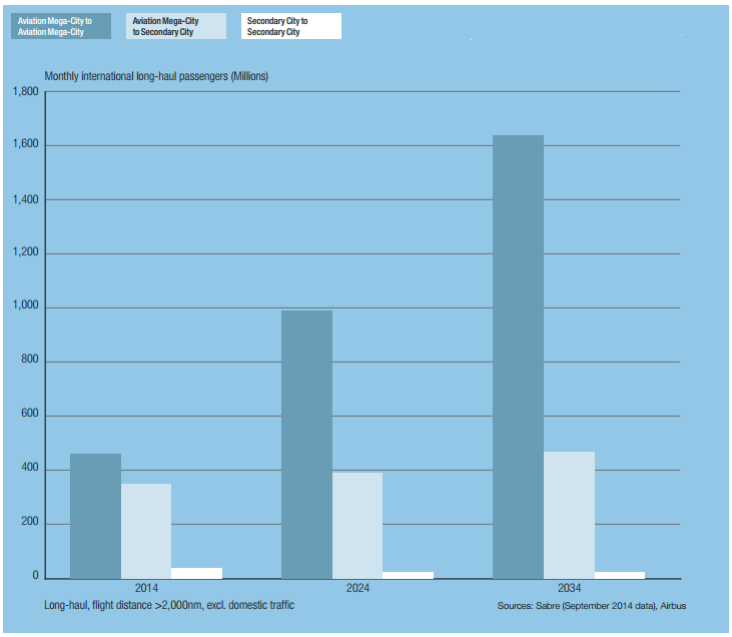

Figure 2.1: Growth of passengers with size of airport [5].

Military Application

The major requirements for military application is ensuring the integrity of their NavAid systems, which are of utmost importance in hostile environments. The main need originates from sabotage and capturing of foreign airports. The systems require frequent calibration to ensure integrity; however, in these hostile environments and at the low altitudes required for these flight inspections, the calibration aircraft is very vulnerable to enemy fire. Removing the pilot from the equation is thus advantageous.

UAVs

Figure 2.2 shows the UAV revenue distribution over the world in the coming years. North America seems to be the largest consumer of drones, followed by Asia and Europe.

Figure 2.2: Commercial Drone Revenue Forecast for different regions [6].

The market experiences some drivers and some killers that determine the growth. Autonomous flying makes it able for aircraft to fly in otherwise dangerous or exhausting conditions for pilots. However, the higher the degree of autonomy, the more investments in technology, regulations and verification research are needed, due to the novelty of the technology. To get full potential out of unmanned vehicles, the vehicle should adapt to ground, sea and manned vehicles without problems and airspace integration is required in order to get UAVs fully operational.

2.1.2. COST & VOLUME ESTIMATION

For the preliminary cost estimation, one can differentiate between development, manufacturing, operational and disposal costs. However, as described by [7], a conceptual design effort is necessary prior to the cost estimation. At this stage the main target is to establish a target for cost and volume for the system. An in-depth cost breakdown will be conducted in Chapter 14.

The stakeholder target is that at least 100 units at a unit price of €250,000 have to be sold. This price is for the empty aircraft, without fuel and payload costs. Comparing with reference aircraft, the cost is out of range, particularly when considering certification and research & development costs for the aircraft for civil use. This is as a direct result of the technology and legislation for UAVs being in its infancy. Furthermore, this problem is exacerbated by the fact that a production of 100 units is not feasible as, currently, there are very few aircraft required to service very large regions. However, a lower unit cost would increase the feasibility of selling a unit to all airports and thereby decreasing the need to transport the system. This would off course also decrease the operational costs of the system.

The €250,000 per unit will comprise of fixed costs and variable costs. The more units produced the more the fixed costs can be spread. The variable costs increase with the number of products created, such as the raw materials. The fixed costs will be related to research & certification of the product. This will be a major fixed cost for the system.

2.1.3. ADDED VALUE

The added value determines where the new system is better compared to currently used systems. It is closely related to the strengths of the system as discussed in the SWOT analysis in the next subsection. For the added value, again a distinction between the civil and military market has been made.

Civil Application
Utilising a UAV can reduce the amount of human resources required to complete the task and the costs to operate the aircraft. A smaller aircraft also reduces the noise impact on housing in the nearby vicinity. The aircraft will also be much cheaper to purchase. Furthermore, the use of UAVs provides more constant flights and the customer has immediate communication with the aircraft and thus reducing the likelihood of having to re-fly a manoeuvre, which further decreases the operating costs and time. The system can also be better integrated into airport operations to mitigate its interference.

Military Application
In hostile regions, NavAid is a very dangerous procedure as the calibration must be performed at very low altitudes making the aircraft vulnerable to ground-based attacks. NavAid has to be performed frequently in these regions, where the risk of sabotage is high and when new airfields are captured. The need to remove people out of the equations is thus necessary for military application.

2.1.4. SWOT ANALYSIS

A SWOT analysis is done in order to evaluate the market position of the design and its elements. The abbreviation of SWOT contains the words strengths, weaknesses, opportunities and threats, referencing to internal and external factors:

- Strength: Advantages over other systems
- Weakness: Disadvantages compared to other systems
- Opportunity: Opportunities for the project
- Threat: Threats for the project

In Figure 2.3, the analysis is summarised. The new, fast-growing market is a large player in affecting the project. Besides the fact that the use of UAVs is quite new, it has it's advantages and disadvantages with respect to current calibration and testing systems.

2.2. FUNCTIONAL ANALYSIS

This section will describe the functions that the system needs to perform in order to fulfil the mission. These functions are structured in a Functional Breakdown Structure (FBS) as can be seen in Figure 2.4

Perform Flight: The first branch of the FBS is concerned with basic functions that the system needs to fulfil in order to be able to fly. These functions include to provide lift, provide thrust, provide stability and provide control. The control function applies only to the flying of different manoeuvres and not to the autonomy of the system.

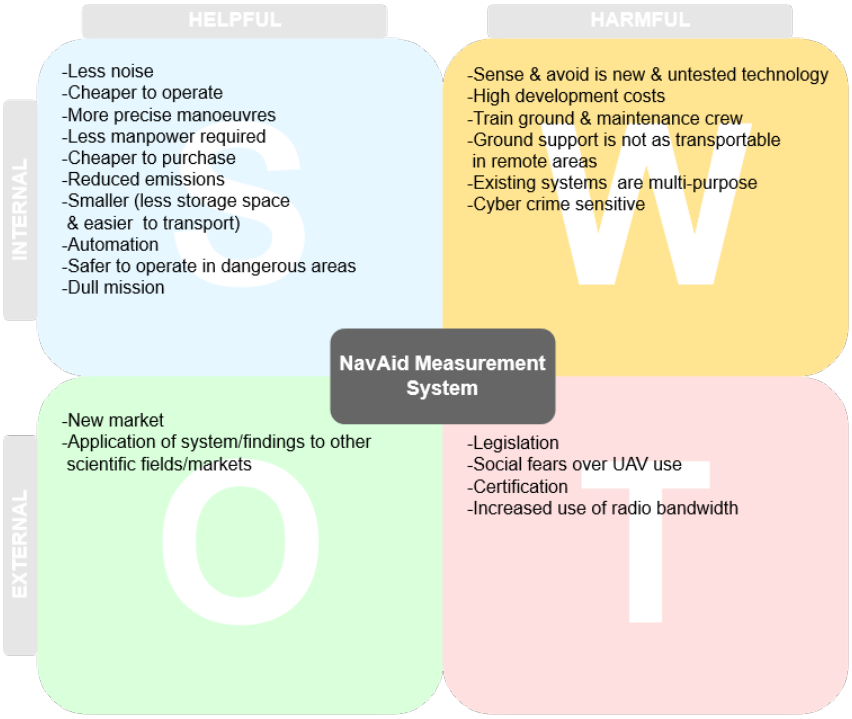

Figure 2.3: SWOT analysis on Navigational Aid measurement systems.

Provide Navigation: The navigation branch is concerned with the autonomy of the UAV and allowing the UAV to track itself during its predetermined flight path. The navigation system will also allow the aircraft to set up it's own flight path and manage the path during flight.

Provide Communication: Another function of the complete system is that different subsystems are able to communicate with each other and that the system can communicate with an end user or an external controlling entity that provides the system with direct control. Other functions that comprise the communications are data storage and status reporting.

Provide Power: The system should provide power to the electrical systems. First of all, this power should be generated. After the power is generated, it should be regulated and distributed to all different systems so that all systems obtain the correct electric power.

Perform Inspection: To perform an inspection of radio navigation aids is a major function of the system. In order to perform this function, the system should be able to measure signals, store the measurements and analyse the measurements.

Provide Structure: The system should also provide a structure to carry the payload, house internal components of the UAV and to provide structural integrity.

Provide Safety: Safety is of major importance for the system. Not only should the internal safety of the system be guaranteed, but also the safety of the direct environment of the system. To ensure this, the system should have a safe mode function, which will transform the system into a certain configuration so that in the first place, the risk of harm to the environment and second harm to the system itself is minimised.

Another way of structuring the system functions is using a Functional Flow Diagram (FFD) as shown in Figure 2.5. The FFD shows the logical time-wise order of functions the system should perform during a mission. This way of structuring the functions gives the opportunity to implement functions which are of short duration and show the relationships between the different subsystems. As can be seen in the FFD, there are five main functions which themselves are comprised of more detailed and smaller functions.

Pre-operational inspection: To ensure a safe, effective and efficient mission, a pre-operational inspection should be done. This inspection consists of checking the state of the UAV itself, e.g. fuel, structural integrity, actuators, etc. But also the payload will have to be inspected before the mission starts and the communication is checked. Lastly, if all inspections are positive, the UAV can be transported to the runway to actually start the mission.

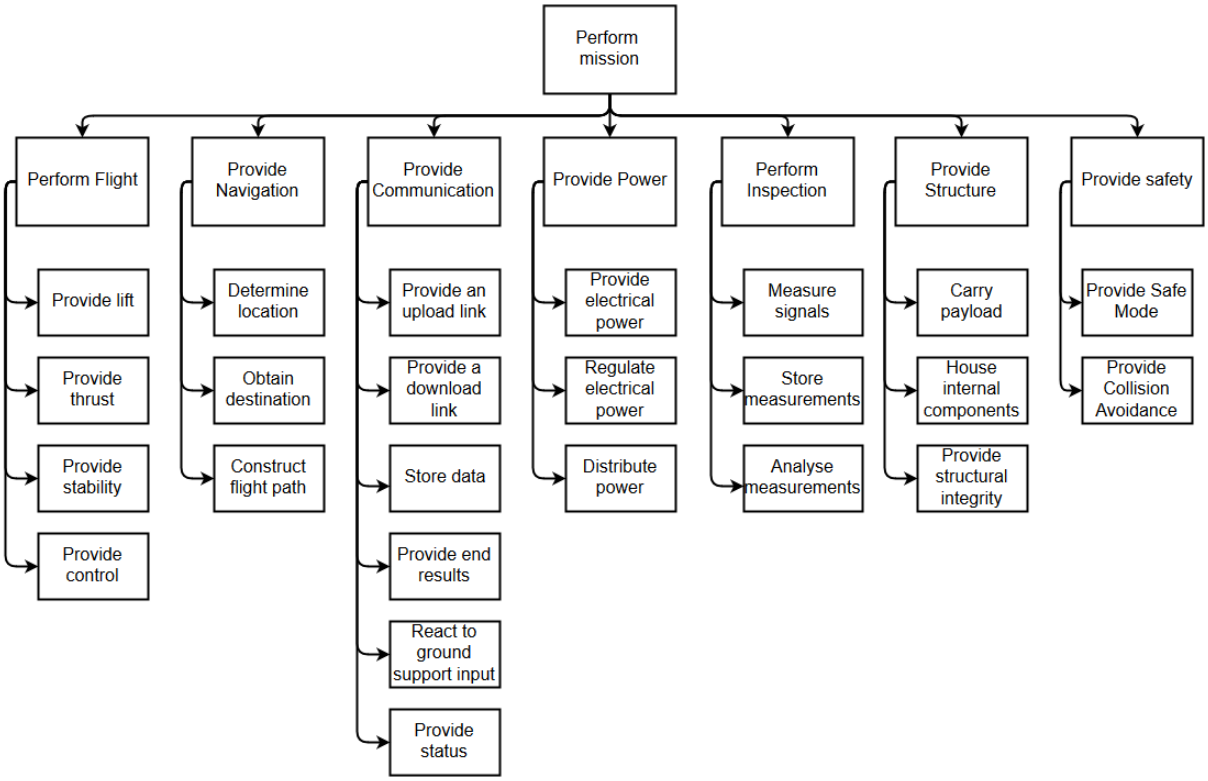

Figure 2.4: Functional Breakdown Structure for the NavAid System.

Take-off: This function is mainly concerned with the aerial part of the mission and makes sure that the aircraft is able to get up into the air to its designated altitude. To do this, the level of autonomy is set after which the UAV or GS needs to receive ATC instructions and needs to transport to the runway. From here on, the conventional take-off function are required, such as gaining velocity, climbing to altitude, at which the actual flight starts.

Fly: The moment the UAV has finished its take-off, UAV enters its flying phase. This entails navigating the UAV from the current location towards the measurement location, where the dedicated paths have to be flown. Simultaneously, the UAV performs the measurements and communicates with the GS to send the data. This is a continuous process during which navigation, communication and measuring are the key functions.

Land: As soon as all measurements are done or the UAV needs to refuel, the UAV has to perform landing. This entails the ability of the aircraft to receive ATC instructions, fly into a designated landing area and safely land without damage. After this, the UAV needs to transport back to the hangar where maintenance takes place.

Maintenance: After landing, some maintenance tasks should be performed. First of all, the post flight inspection is there to ensure no part of the system got damaged during the mission. Secondly, the UAV's fuel level should be checked and if necessary, extra fuel should be added.

2.3. SUSTAINABLE DEVELOPMENT STRATEGY

Ever since the industrial revolution, humans have striven for improving technologies by developing better, faster, lighter and cheaper systems. Although this does sound good, this comes at a price, namely the use of finite resources has grown extensively. The amount of trees is decreasing faster than can be re-grown, fossil fuels are getting scarcer, rare-earth metals are used, etc. Therefore, during the entire design process, special attention will be paid to sustainable development, as well as to the contribution of the system to sustainability. Sustainable development ensures that a system fulfils the needs of the present without affecting the capability of fulfilling any needs in the future. This means that 100 % sustainable systems can operate for eternity. In order to apply this principle in a design process, the design team needs to be aware of the limited availability of the resources and the impact of the materials and substances that will be used, and should always strive to minimise these in the whole process. This chapter illustrates the measures that can be taken for a system in order to maximise its sustainability. The whole process can be divided in the following three processes:

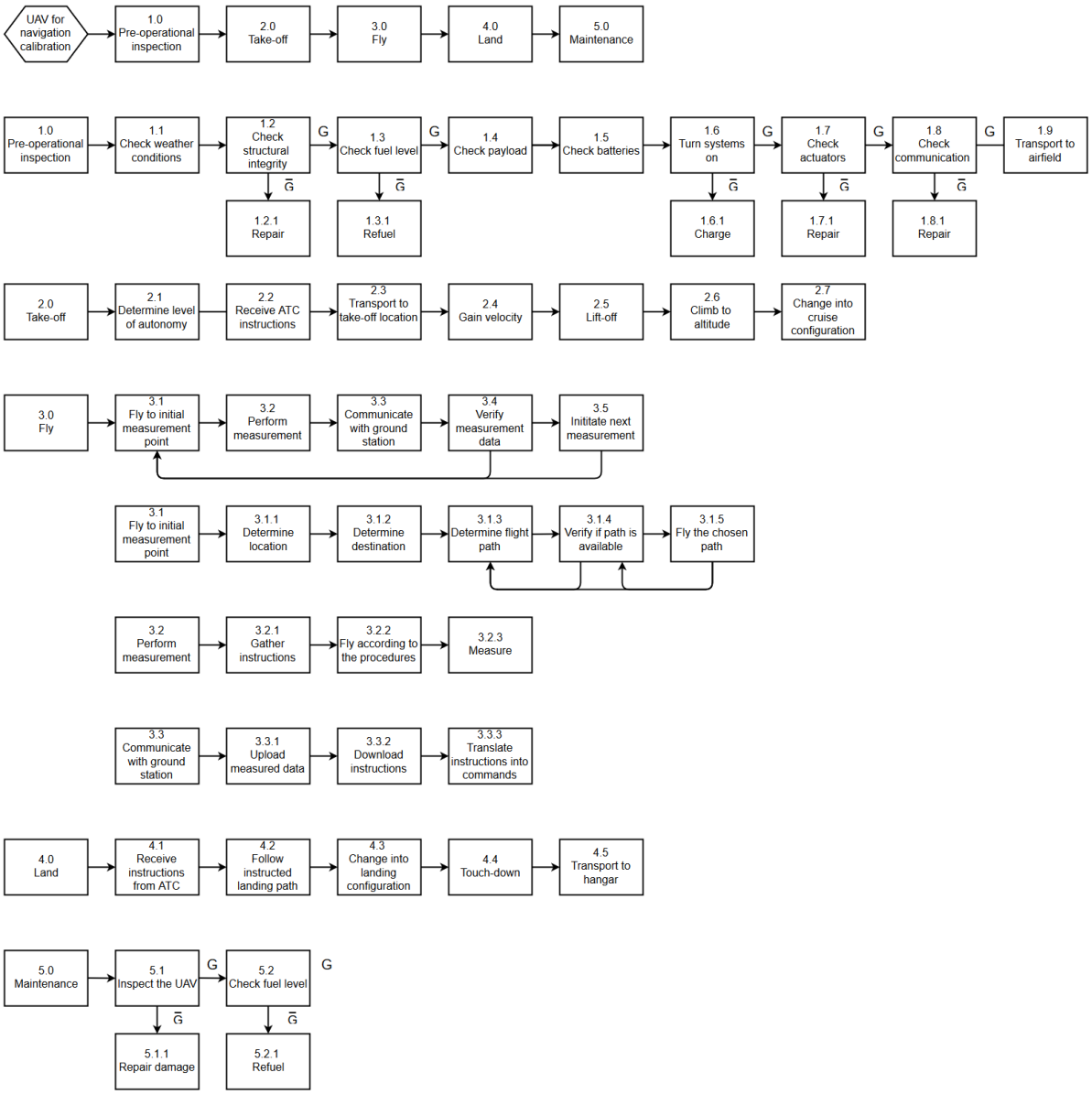

Figure 2.5: Functional Flow Diagram for the NavAid system.

the design process (Subsection 2.3.1), the production process (Subsection 2.3.2) and the operational process (Subsection 2.3.3). An overview of the measures that can be taken to improve the sustainability is illustrated in Figure 2.6.

2.3.1. DESIGN CONSIDERATIONS

Striving for a sustainable development already starts during the design process. Here, the choice for materials will be made, the type of connections between different systems will be determined, which systems will be used will be decided, etc. It defines the recyclability of the product to be designed. The recyclability of the system can be improved in a number of ways.

First of all, making use of materials that are easy to recycle will reduce the environmental impact of the total system by limiting the need for new materials. Easy to recycle materials are mostly metals (especially aluminium, which does not degrade during refining and remelting [1]), because they can be melted, refined and then casted into new products. Composites and plastics need more processing steps and are therefore harder to recycle. Therefore these materials are less environmentally friendly and should therefore be used only if metals do not provide a feasible solution. Another way to improve recyclability is to create easy dismantling techniques (e.g. click systems, screws), which provides easier and more affordable separation of materials for recycling. Fi-

[1] `http://www.world-aluminium.org/media/file_public/2013/01/15/fl0000181.pdf` [cited 08 June 2016]

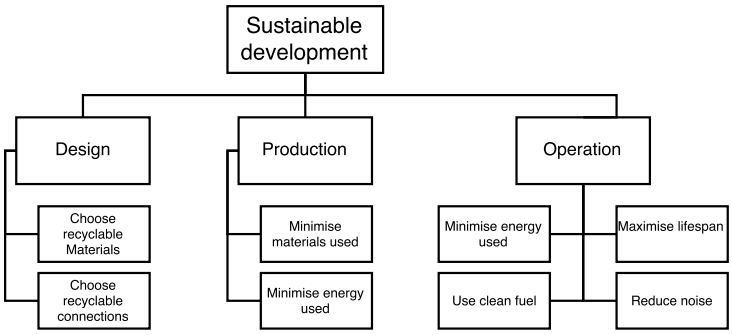

Figure 2.6: Sustainability measures.

nally, making use of less critical materials, less dissimilar materials and overall less number of materials will all improve the recyclability of the system has a whole.

Next to being recyclable, materials and their connections should also be safe, non-toxic and durable. Being safe and durable ensures that the system can operate for a longer period of time, which reduces the need for replacing parts or the whole system. The use of toxic materials or substances has a negative effect on the environment, so these should also be avoided.

2.3.2. PRODUCTION STRATEGY

When optimising a product for sustainable development, one also has to account for a sustainable production process. One way to reduce the energy during manufacturing is for example using electrical injection molding presses instead of traditional hydraulic ones. Using this technology can result in 50% less energy usage for presses and reduce start-up times [2].

Another aspect in optimising the production process is the use of highly efficient machines. If a factory uses air compressor units to run machines, the pressure loss should be kept as small as possible. By fixing leaks in this compressor system the loss of pressure is reduced significantly. An example of the effect of such a defect is Arctic Cat in Minnesota, that inspected the compressors and fixed a leak, which saved the company around $\$21,400$ per year [3].

To improve the sustainability of the production of a system, the "DOWNTIME" should be minimised [4]. The acronym DOWNTIME comprises of the following definitions:

- **D**efects: By doing checks after part production, defects will be spotted quicker and this reduces the chance that the whole product becomes waste.
- **O**verproduction: If too many products are made, a lot of products have to be stored or disposed. Therefore the amount of products produced should be tailored to the demand.
- **W**aiting: If a part needs to wait to be processed, time is wasted. To prevent this waste, the manufacturing line needs to be build in such a way that each product can be processed at the right time. One should aim for a process where as soon as the machine finishes his task, the next (to be processed) part arrives at that machine.
- **N**on-utilised resources: A lack of teamwork, training and communication can lead to waste. By keeping the same crew for the same task, a faster production can be achieved.
- **T**ransportation: When the whole product is produced in one factory, no transportation of parts is needed. This reduces packaging waste and emissions due to the transportation of parts.
- **I**nventory: Product should be bought at the exact time they are needed to minimise storage costs and space.
- **M**otion: By keeping the work station clean, no time is lost to search for specific tools or machines which will reduce the production time.

[2] http://www.harbec.com/wp-content/uploads/2016/04/HARBEC_ECOECONOMICS_2015.pdf [cited 07 June 2016]
[3] http://www.mntap.umn.edu/paint/resources/150-ArcticCat.htm [cited 08 June 2016]
[4] http://www.theproductivitypro.com/FeaturedArticles/article00138.htm [cited 21 April 2016]

- **E**xtra processing: Doing unnecessary tasks leads to waste. For example polishing the surface of a massive cylinder which will be turned into a specific shape in a later stage is totally useless.

2.3.3. OPERATIONAL ASPECTS

Also during the operation of the system, sustainable development should be aimed for. This entails, among others, operating as efficient as possible so that a minimum amount of energy will be used, while maintaining the required performance. This can be done in several ways, e.g. using more efficient engines and reducing the drag experienced by the UAV (which reduces the thrust needed thus reducing energy consumption). Next to that, wasted operating time should be avoided by optimising the operation as much as possible. Every second the system is operating and using energy while it is not actually performing a mandatory action, is wasted. Another measure is using more environmentally friendly fuel. Using fuel might be inevitable, and if this is the case, using a more environmentally friendly fuel might limit the damage induced to the environment, which makes it a more sustainable option.

Besides reducing energy and using cleaner fuel, also noise should be kept to a minimum. In the case of a UAV for navigational equipment calibration, often the UAV will fly in populated areas around airports, while the airports already have issues with noise regulation. In order to be able to continue performing the mission, the civilians living around the mission area should be kept satisfied.

Lastly, the lifespan of the system should be maximised while maintaining all other mentioned measures, which reduces the need for replacing systems frequently. All maintenance is in fact waste, since it does not add any value to the product. This requires no further explanation. For all maintenance, the same principles as for the production process apply, e.g. minimise the materials and energy needed to perform the maintenance.

2.4. RISK MANAGEMENT & MITIGATION

In the design of the final concept, the technical risk management is of key importance in achieving the goal for the final design. It is important to be aware of the possible risks and to know how to mitigate these risks. The technical risk management process is as defined in Figure 2.7 by the ISO31000:2009 standards [8]. During this process, risks need to be identified, analysed and evaluated.

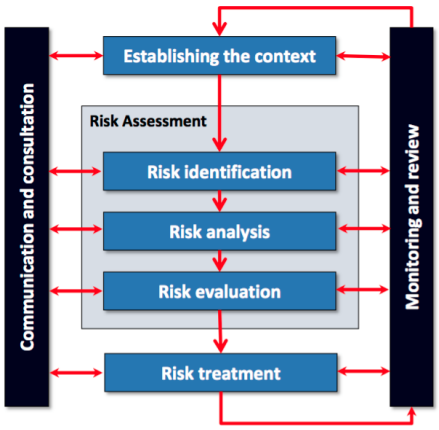

Figure 2.7: Risk assessment as used in ISO31000 [8].

As described in the baseline report [3], some risks are more critical than others to monitor and review. This is why the risks have to be arranged in order of importance. After defining all risks, they are ordered in a Risk Assessment Matrix.

In the risk register, shown in Table 2.3, some risks from the baseline report [3] are still feasible. Other risks related to the final concepts are added. On the left side of the table, the risk event is defined, on the right side, the consequence, likelihood and impact are mentioned. Furthermore, the mitigation is given, to monitor and review a risk.

In Table 2.1 the risk assessment matrix is shown. In the RAM, the critical risks are identified. Creating a hierarchy in risks, they are easier to monitor and manage. From the table, it can be seen that risk number 1, 10 and 14 are having the highest priority.

Table 2.1: Risk assessment matrix.

	Likelihood		
Impact	Low	Medium	High
Low	6,11	3	
Medium	2,5,9,13,15	4,7,8,12	
High	10	1,14	

The uncertainty of the legislation around UAVs (risk 1) is still present, which is due to the infancy of UAVs, especially the kind of UAV that is being designed here. There is a medium likelihood that the legislation changes, but the impact on the design is high. A change in the regulations of UAVs has a direct impact on the design and might result in a complete redesign, which is costly and time-consuming and might even have an effect on the performance. The only solution to this problem is to make agreements with the authorities and to try to legislate it for similar types of aircraft to reduce the likelihood of a need for changes in the design.

Risk 10 is that the aerial calibration market is decreasing, which has a very low likelihood, however, the impact will be disastrous for the project. If the UAV is no longer needed on the market, the project needs to be cancelled. Monitoring the market on NavAid calibration must prevent from continuing the project while it had to be killed. Another option is to design the UAV in such a way that is can fulfil other missions as well, therefore it is not dependent on a single market and thus reducing the impact of this happening.

The risk that a deadline approaches before a viable design is achieved (risk 14) has a medium likelihood, but a high impact. The consequence of this risk is that a sub-optimal design or no design is created. This makes this risk critical for the success of the entire project. In order to mitigate the risk, either the likelihood or the impact should be decreased. This is done by making use of an N^2-chart to manage the iterations. By doing this, the likelihood of the risk is decreased and therefore not critical anymore.

Implementing all these mitigation measures for the previously determined risks results in an updated risk assessment matrix, presented in Table 2.2. As can be observed, there are no critical risks present anymore after the risk mitigation, which implies that the chance of success for this project is high enough to be sold to customers.

Table 2.2: Risk assessment matrix after risk mitigation has taken place.

	Likelihood		
Impact	Low	Medium	High
Low	6,11	3	
Medium	2,5,9,10,13,15	4,7,8,12	
High	1,14		

Table 2.3: Risk register.

#	Category	Cause	Risk Event	Consequence	Promise	Likelihood	Impact	Mitigation
1	Political	UAV legislation is still in its infancy.	New legislation implemented.	Design & feasibility impacted.	Product/Cost/ Schedule.	M	H	Make an agreement with aeronautical authorities.
2	Social	UAVs are new & may scare people through the possibilities of the technology.	Society opposes the new technology.	Project cannot procede.	Product	L	M	Ad campaign in conjunction with the government to show its benefits to society.
3	Political	Middle-east crisis.	War in oil-source areas.	Import costs of fuel.	Cost	M	L	Accept risk.
4	Sustainability	Costs for reusing materials are high.	Product uses materials that are difficult or expensive to reuse.	Sustainability costs increase/overall sustainability reduced.	Cost/Sustainability	M	M	Design product using these costs as a basis for design choices.
5	Economic	Fixed costs are dependent on the number of units produced.(Scales of Economy)	Design is not suited for mass production.	High unit costs for users and delivery is bottle-necked.	Cost/Schedule	L	M	Design with production considerations in mind.
6	Strategic	Product delivery is about timing of entering the market & development in the UAV market is high currently.	Competitors beat us to the market.	Loss of strategic advantage.	Cost	L	L	Make product more desirable than competing products.
7	Project Management	Difficult to state if all generated requirements are achievable or requirements are missing.	Missing or unachievable requirements discovered.	Redesign or reconsideration of requirements may be needed.	Cost/Schedule	M	M	Gather input for requirements from entire group & other stakeholders.
8	Technology	Weight estimation not correct	Wrong/ incomplete estimation is performed.	Redesign of system required.	Performance/ Schedule	M	M	Frequent contigency analysis.
9	Environment	Piston engine too noisy.	Noise related to required power is too loud to meet the requirement.	Consider new propulsion system.	Cost/Schedule	L	M	Perform noise footprint analysis.
10	Strategic	Aerial calibration market decreases.	Improved ground-based calibration systems.	Not meeting mission statement.	Product/Cost	L	H	Make product more attractive.
11	Technology	Payload weight decreases.	UAV designed for heavier payload.	Oversized design	Product/ Performance/Cost	L	L	Monitor payload technology.
12	Project Management	Local extrema act similar to global extrema.	Engineers converge to local extrema.	Sub-optimal design selected.	Performance	M	M	Perform sensitivity analysis.
13	Technology	System too large/ heavy for LD6.	System not able to be transported by pax aircraft.	Rescaling has to be considered.	Product/ Performance	L	M	Perform contingency analysis.
14	Project Management	Projects are time bound.	Deadline approaches before a viable design is achieved.	Sub-optimal design or no design.	Schedule/ Performance	M	H	Use the N^2 chart to manage iterations.
15	Project Management	During design, many uncertainties exist.	Uncertainty leads to a delay in start of the design of a subsystem.	Less time available for other work packages.	Schedule/ Performance	L	M	Perform thorough literature study.

3 Conceptual Design

In the Midterm Report [2], a final concept has been chosen for the calibration of navigational aids. The design process is described in this chapter. It starts with providing the concept selection process that has been followed. After this, the concept will be described including the Class I weight estimation of the chosen concept as this is the starting point of the detailed design phase.

3.1. Concept Selection Process

As a first step of the concept selection process, the design methodology was been defined. It enabled all engineers to follow the same steps and create the same output and a proper trade-off could be made in order to choose the most optimal concept. It is a stepwise process which defines precisely what has to be done in order to be able to perform the final trade-off at the end of the concept selection process. The first part of the process was the same for all concepts and had to be defined before the individual concept design. The second and largest part was the actual concept design. The final part of the process entailed the final trade-off and a more detailed description of the chosen concept.

In the baseline report [3], 17 Design Option Trees (DOTs) were created showing the different design options available for the functions as defined in the Funtional Breakdown Structure (FBS). After some more research, they could be further defined and finalised. The first step in this process was to eliminate non-feasible options and temporary placeholders that were placed for the sake of completeness. After doing this, the DOTs consisted of possible solutions to perform the different functions. After this, the weak points in the DOTs were eliminated. Weak points are design options that are clearly inferior to other options for given functions.

After the finalisation of the DOTs, all available concepts could be developed. Because of the large number of functions, this would create a lot of concepts if all possible combinations were to be selected. In order to decrease this, driving functions were identified which determine the total system more than others. These driving functions were: provide lift, provide thrust and provide launch and recovery. The DOTs of the driving requirements were then used to create the possible concepts. These concepts could be distributed in five different categories: conventional fixed-wing aircraft, conventional rotary wing aircraft (helicopters), gyrodyne aircraft, hybrid and airships.

A first trade-off process was used to eliminate non-feasible or inferior concepts from the initial list of 24 concepts. Four concepts were eventually chosen for the conceptual design phase. The trade-off process started with the definition of the criteria that were used to score the different concepts. For all criteria, weight factors were calculated and normalised. After this , the trade method was determined. Subsequently the definition of the criteria and trade method, the trade-off was performed, the concepts were scored against a comparative benchmark (the conventional piston engine fixed-wing aircraft) on all criteria. The four concepts that were chosen for the conceptual design phase in the trade-off are the piston powered fixed-wing aircraft, the electric powered fixed-wing aircraft, the electrically propelled airship and the turboshaft propelled tiltrotor aircraft.

A basic investigation had to be performed on what must be included as payload for this mission. Since all concepts are required to perform the same mission, the payload will also be the same. First, a general description of the necessary payload was given which defines what systems are needed in order to perform the flight inspection. A detailed list was created presenting all necessary systems. The list was completed with product names, manufacturers and size and mass of the system. The second part of the general concept design was to define the mission profile. All concepts must be able to perform the same mission and therefore follow the same mission profile. The mission profile was used to determine the fuel fraction for an initial weight estimation.

After the design of the four concepts, a second trade-off was performed to select the best concept. The second and final trade-off process again started with defining the trade-off criteria and method. The newly defined trade-off criteria were cost, size and transportability, mass, mission time, RAMS characteristics, producibility, mission diversity, operational flexibility, development risk, noise, emissions and sustainability. The weights for all criteria were again determined and normalised. From the weights, it could be seen that the most important criteria for the trade-off were the mission time, development risk and noise. After the determination of the

trade-off criteria, trade-off method and criteria weights, the trade-off could be performed. The concept with the highest score in this final trade-off was the piston powered fixed-wing aircraft.

3.2. CONCEPT DESCRIPTION

In the concept selection process, the best concept out of all available concept was chosen. This concept is the piston powered fixed-wing aircraft. In this section, the concept is described following the concept design phase as presented in the Midterm report [2].

The piston-fixed wing concept is a conventional and proven concept. The preliminary configuration is a tailplane configuration with a twin-boomed tail system utilising a pusher propeller to increase the effectiveness of the horizontal stabiliser. It uses a high-wing design for ease of access to the payload bay. Furthermore, the design does not use high-lift devices as they consume a significant amount of space in the wing and limit the transportability by making it harder to remove the wings. A concept drawing of the system is included in Figure 3.1. The MTOW is estimated to be $450kg$ of which $140kg$ is fuel. The difference between the ferry and harmonic range is $254nm$, which is representative of its payload flexibility. The design will utilise a wing with a lift coefficient of at least 1.6 and an aspect ratio of 11. The span and chord is estimated to be 8.2 and $0.74m$, respectively. These dimensions mean that the aircraft wings must be detached to fit within the LD6. This means that the take-off and landing distances are 300 and $550m$, respectively, with a stall speed of $61kts$. Finally, the maximum g-loading will be 3.8 at a speed of $140kts$.

3.3. FURTHER DEVELOPMENT

The values mentioned in the previous section are not fixed. During the further development, those values will be analysed more in detail. By doing iterations, the most optimal design configuration will be defined.

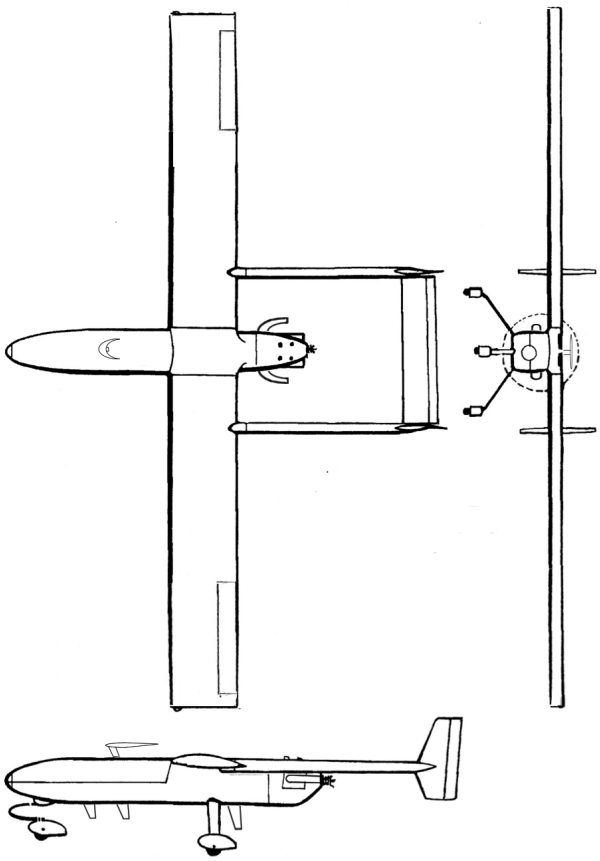

Figure 3.1: Concept drawing of the piston-engine driven concept, adapted from [9].

4 Design Process & Iterations

Aircraft design is a highly multidisciplinary exercise that requires careful monitoring of a wide range of parameters and requirements. A coherent design that consistently meets all requirements can only be achieved if the iteration process is properly managed. In this chapter, this iterative design process which is used in the Final Report will be described thoroughly, and key design decisions will be explained. In following chapters, the primary design and analysis models are described in detail. It is shown what parameters are required for running a calculation or simulation, how the model uses these parameters, and how certain assumptions affect the outcome. Accordingly, these models are both verified and validated. All models will now be used to run through the complete design cycle and get to a converged design. The design is considered to be converged once all iteration parameters do not differ by more than 10% from the previous cycle.

The starting point of the iteration process is formed by the matching diagrams. As shown later, this diagram is used to set a design point that falls within the available design space. This design space is constrained by performance requirements associated with take-off, landing, cruise speed, manoeuvring, climb, stall, and service ceiling. Therefore, compliance with the requirements is fully dependent on selecting the appropriate design point. The success of all other preliminary design steps, including wing design, sizing for stability and control, sizing of high-lift devices and vehicle packaging, is therefore determined by this first step. This is clearly visible in the flow diagram shown in Figure 4.1, were the 'match performance' block is given central importance. The subsequent iteration process will be explained with this flow diagram. For further reference, the parameters associated with each link in this diagram are listed in Table 4.1.

Selecting a design point using the matching diagram will affect the full design cycle. However, its influence is propagated through its direct interfaces with propulsion design, airfoil selection and tree-dimensional wing design. The propulsion design process is mainly related to selecting an engine and propeller that can meet

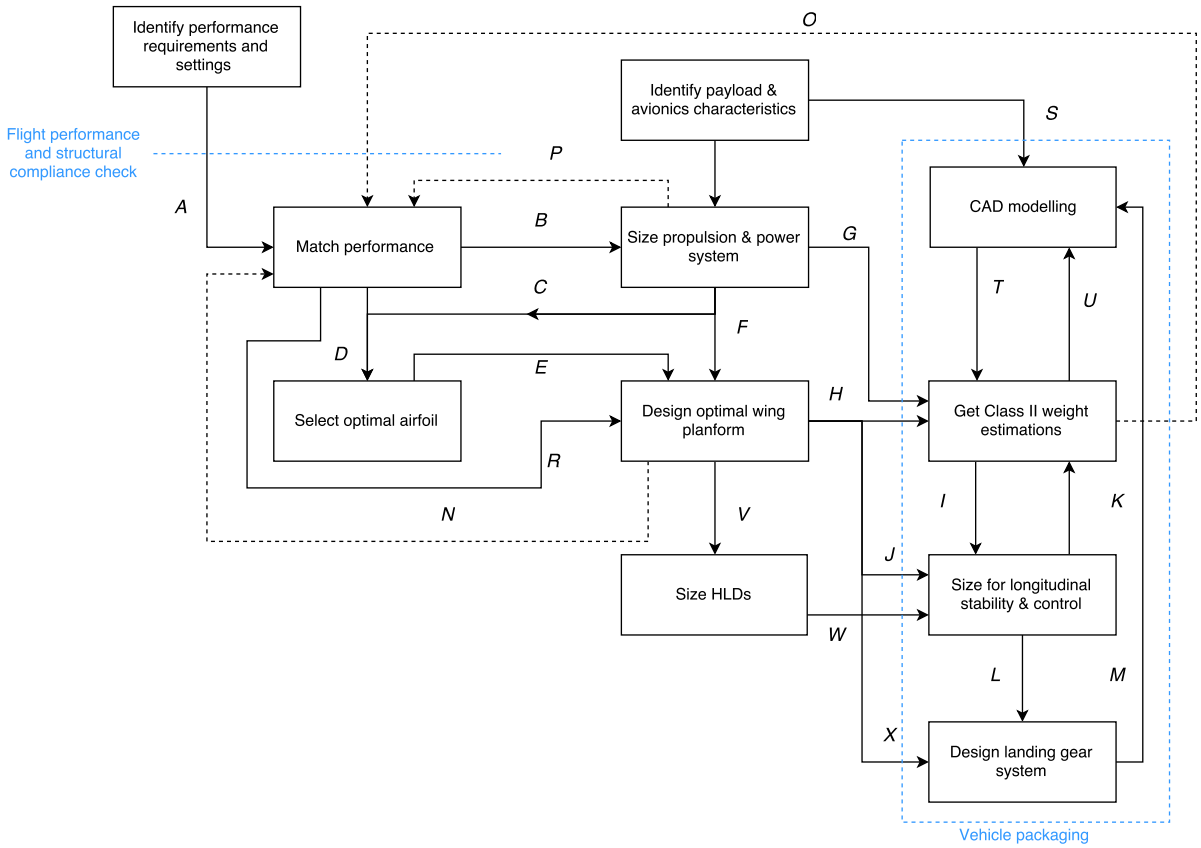

Figure 4.1: Iteration loop procedure.

Table 4.1: Flow path datasets.

ID	Parameters	ID	Parameters
A	V_{s_0}; V_{s_1}; n_{max}; $V_{n_{max}}$; s_{TO}; s_L; W_L/W_{TO}; $V_{c_{max}}$; h_c; $\%P_{max}$; %MTOW	M	$cg_{nosegear}$; $cg_{maingear}$; $h_{nosegear}$; $h_{maingear}$
B	CD_0; A; e; S; MTOW; P_{req}; P_{electr}	N	$CL_{max_{clean}}$; $CL_{max_{flapped}}$; A; e;
C	W_F	O	MTOW; OEW; W_F
D	MTOW; S; $V_{c_{max}}$; h_c; CL_{max};	P	$eta_{p_{cruise}}$; $eta_{p_{climb}}$
E	$C_{L_{cruise}}$; selected airfoil	S	W_{PL}; W_{av}; W_{dish}; position constraints
F	V_{tank}	T	$S_{f_{wet}}$; l_{fus}; D_{fus}; S_{net}
G	D_{prop}; W_F; $N_{engines}$; engine dim.; V_{batt}; W_{batt}; W_{engine}; V_{tank}	U	LEMAC; S_h; l_{tail}
H	c_r; lambda; S; sweep; t/c_{max}; lambda; c_r	V	S; A; w_{fus}; c_r; taper; sweep
I	MTOW; OEW; W_{dish}; PL/AV position constraints; W_{hydr}; W_{FCS}; W_{paint}; W_{av}; W_{fus}; W_{tank}; W_{LG}; W_{electr}; W_{wing}; W_{engine}; W_{fuel}; W_{PL}; l_{fus}	W	Δ Cl_{max}; $CL_{landing_{flapped}}$; Swf/S; c'/c
J	A; MAC; sweep; b; c_r; γ; Γ; S; dC_L/da; dC_M/da; Cm_{ac} airfoil; x_{ac} airfoil; $alpha_{cr}$	X	W/S
K	l_{tail}; LEMAC; S_h; λ_h; Λ_h;	Y	S_{wet}
L	MTOW; CG AFT; CG FWD; l_{fus}; cg prop	R	W/S; MTOW; S; CL_{max};

the power and efficiency requirements associated with the current design point. Accordingly, an estimate is made of the required fuel weight and volume. This fuel weight forms an input for the airfoil selection, which uses parameters for cruising conditions to calculate an optimum C_L and identify an appropriate airfoil. This airfoil, meeting all requirements flowing down from the matching plot in terms of maximum C_L and cruise altitude and speed, then forms the key input for three-dimensional wing design. Using this airfoil, the three-dimensional wing analysis is constrained by the required tank volume, the wing loading and the required wing size.

In addition to the performance requirements identified with the matching plot, the design shall also comply with the constraints imposed by the payload and avionics system. The associated requirements flow down in two ways. First, an electrical power system must be designed that can handle the on-board power requirements. Second, it determines to a large extent the fuselage packaging. What this means in practice for a flight inspection payload will be shown later. In the general case, vehicle packaging is the set of design steps in which the propulsion and power system, the wing, and the payload and avionics systems must all be combined into one coherent design. Accordingly, vehicle packaging consists of four main elements. First, intensive use is made of conceptual CAD drawings to visualise payload constraints and the practical consequences of packaging. Second, there is Class II weight estimations. The group weights are used in combination with the CAD visualisation to make an informed analysis of longitudinal stability and controllability. This iterative sub-cycle is further extended with the sizing of the landing gear. Landing gear design aims at generating a lightweight and small system configuration that meets both ground stability and tail clearance requirements. Accordingly, it can have a large impact on the final configuration of the aircraft.

The four elements of vehicle packaging together shall result in a coherent aircraft configuration. This configuration forms, in addition to the wing design and propulsion characteristics, one of the main elements that enter the iteration loop. Its effect is twofold. First, more information is available on the aircraft group weights, resulting in a new MTOW and OEW. If the difference with the weights used for performance matching is more than the predetermined convergence margin of 10%, the design is not yet converged and another iteration must be performed. Second, the aircraft configuration found in this step may be non-optimal. Conflicting design considerations may result in an inconvenient design, which may be improved by adjusting certain parameters. Re-iterating may then solve the issue. Another possible reason for re-iterating can be non-compliance with flight performance and structural requirements. The weights generated with the Class II estimations are used as primary inputs for subsystem weight allocation. However, these weights are highly sensitive to the maximum load factors encountered at the edges of the aircraft's flight envelope. It must then be assessed whether the aircraft structure is able to carry the ultimate load factors within the allocated weight budgets. These performance checks completely determine the viability of the design and and therefore included explicitly in the iteration loop shown in Figure 4.1.

Decision Flow

The generic iteration process illustrated in Figure 4.1 is used to convert the flight inspection top-level require-

ments into a coherent aircraft design. The success and efficiency of the iterative aircraft design cycle can only be assured if design parameters are managed carefully between different departments. Key design decisions must flow down from conflicting or non-optimum design conditions. In this section, the primary decision flow associated with the design of the flight inspection UAV is described. With this, the reader will get an insight into how the engineering team arrived at the final preliminary design.

The starting point of the iterations is formed by the matching diagram associated with the piston powered vehicle concept. The full concept trade-off was described in the Midterm Report [2]. The selected configuration was briefly illustrated in the previous chapter. In combination with Class I weight estimations, the performance matching parameters form the best starting point for initiating the iteration cycle. The initial design point is illustrated in Figure 4.2, with the associated input and output parameters listed in Table 4.2.

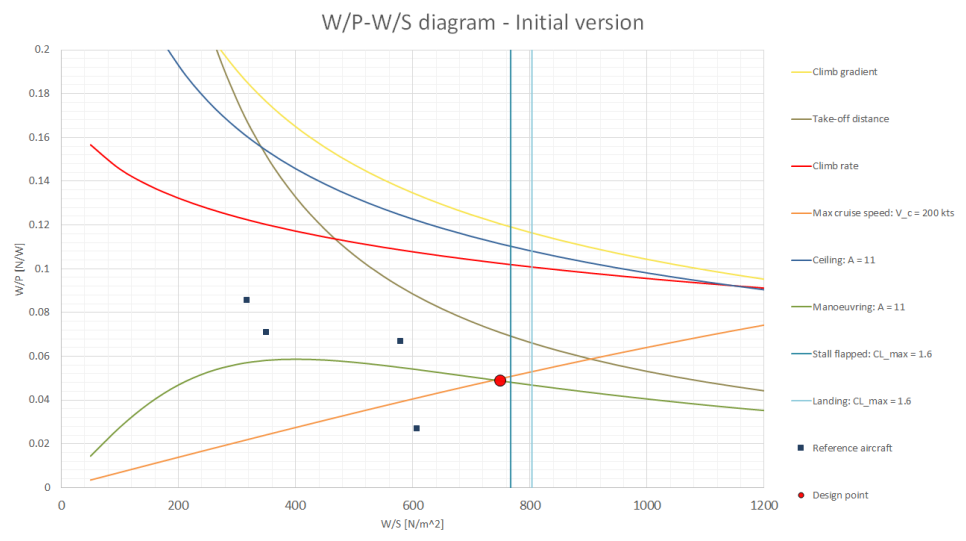

Figure 4.2: Initial matching diagram. The selected design point is chosen as the starting point for the preliminary iteration process.

As was proposed with the conceptual trade-off, the selected vehicle configuration features a piston-powered engine. This decision will be further substantiated in Chapter 8. The feasibility of the design must be verified conducting a market survey on available engines. Throughout the entire multi-iteration cycle, it is seen that a piston powered engine needs to deliver a minimum power of 90 kW. Accordingly, the uninstalled engine weight contributes between 16% to 18% of the maximum take-off weight, and requires a considerable amount of space. Therefore, the engine is seen to be a stringent design driver in terms of fuselage design and aircraft stability. In addition, there is a stringent requirement related to aerodynamic design that flows down from the installed propulsion power. In order to achieve the maximum cruise speed of 200 knots, the parasite drag shall be kept to a certain minimum. With an engine that can deliver 90 kW, the magnitude of C_{D_0} may not exceed a value of 0.0163. This puts considerable pressure on the aerodynamic design of all lifting and non-lifting surfaces.

The design of the wing is characterised by a few degrees of freedom. The design space is constrained by a set of design elements that must be complied with in order to meet the performance characteristics derived from the matching plots. As seen from Table 4.1, these constraining elements are wing loading, wing area, $C_{L_{max}}$, fuel weight and volume, maximum cruise speed and cruise altitude. For the three-dimensional wing, another constraint is formed by the maximum wing span. In order to meet the LD-6 storage requirements, the semi-span of the detached wing may not exceed 4 meters. Accordingly, this translates to a maximum design wing span of 8 meters. Within the remaining design space, the wing can be optimised aerodynamically. This optimisation is characterised by an interplay between airfoil selection and planform design, and is aimed at maximising the lift-to-drag ratio. The reason for optimising for the lift-to-drag ratio is the stringent maximum speed requirements of 200 knots, which is difficult to reach without a highly aerodynamic efficient design. During the multi-iteration cycle, two airfoils were considered, and four different planforms were generated. All planforms featured a wing span of 8 meters, resulting in the lowest induced drag, and a backwards leading edge sweep of only a few degrees. The taper ratio varied between 0.52 and 0.75, showing considerable variation among iteration cycles. All calculations were done based on a Reynolds number of 6 million, which corresponds to the maximum cruise speed of 200 knots.

Initially, an Eppler E593 airfoil was selected for the main wing. This airfoil has excellent performance char-

Table 4.2: Input and output parameters associated with the selected initial design point.

Inputs				Outputs	
V_{s_0} [kts]	61	s_{to} [m]	598	W/S [N/m^2]	750
V_{s_1} [kts]	61	s_l [m]	550	W/P [N/W]	0.0488
$C_{L_{max,clean}}$ [-]	1.6	W_L/W_{TO} [-]	1.00	S [m^2]	5.89
C_{D_0} [-]	0.015	$V_{c_{max}}$ [kts]	200	P [kW]	90.5
e	0.70	h_c [ft]	10,000	OEW [kg]	255
A	11.00	n_{max} [-]	3.8	FW [kg]	140
$\eta_{p_{climb}}$ [-]	0.80	$V_{n_{max}}$ [kts]	140	MTOW [kg]	450
$\eta_{p_{cruise}}$ [-]	0.60	HLDs	no		

acteristics and was seen to be the best airfoil available for the current application. The trade-off behind this conclusion is explained in Section 10.1. Although excellent in terms of performance, this E593 airfoil features a very low thickness-to-chord ratio of only 11.3% at the thickest point, and even very much lower thicknesses at the trailing edge area. Its low thickness was the main reason for switching to the thicker E1098 airfoil, which features a maximum thickness-to-chord ratio of 18.9%. Although it is not the best airfoil available in terms of performance, it still meets the associated minimum requirements listed in Chapter 7. There were two key issues with the small thickness of the E593 airfoil. First, it was expected that using it would lead to very high challenges in terms of structural wing design. Second, it was decided after two iterations to go with simple high lift devices. With plain flaps, the wing loading associated with the stall and landing distance requirements goes up considerably, as well as the allowable power loading. In short, deciding for installing trailing edge high-lift devices allows the wing and engine to be smaller. With the E593, these trailing edge high-lift devices would become extremely thin and therefore again a large challenge to design structurally.

As described in the previous section, packaging of the fuselage consists of four elements including preliminary CAD modelling, Class II weight estimation, longitudinal stability and control sizing, and landing gear design. The main input is formed by the wing layout, the propulsion and power system configuration, and payload and avionics characteristics. As will be described in Chapter 5, there is a wide range of computers, antennas, receivers, and processors that must be installed for both flight inspection as well as aircraft navigation purposes. In addition to a multitude of navigation antennas and communication sensors, there are three large elements that have a large impact on fuselage packaging. These include the payload bay, which has a total volume of 100 litres, the avionics and FMC bay, equalling 37 litres, and a dish antenna with a 36 cm diameter that must be able to look around in all directions. As explained in Subsection 5.4.3, this dish antenna must have a minimum elevation of 23 degrees, and its view may not be obstructed by any other aircraft systems. Also, the payload and avionics systems must be positioned from the engine as far as possible, in order to prevent increased sensor noise due to vibrations. In combination with the large engine size and aircraft stability requirements, these design considerations lead to significant challenges for fuselage packaging. Each requirement must be considered carefully before a final configuration may be arrived at.

Class II weight estimations play a very important role for proper aircraft packaging and design for stability and control. The group weights must be reliable and consistent with what can be achieved in reality, and must therefore be estimated with a reliable method. The fine details are described in Chapter 6. The iterative nature of aircraft packaging leads to constantly updated weight estimations. Tail sizing plays an important role here. The aircraft shall be made stable and controllable by using three elements. First, there is internal packaging of the fuselage, which allows various aircraft systems to be moved around. Second, there is the longitudinal position of the wing. Moving the wing along the longitudinal axis has a very large effect in terms of shifting the centre of gravity of the complete aircraft. However, it cannot be positioned everywhere. Third, there is the sizing of the horizontal tail. This as a direct impact on the stability and controllability characteristics of the aircraft. In addition to these three elements, there is a wide range of parameters that form an input to both component weight as well as stability and control characteristics, but their impact in terms of design sensitivity is limited. An example of this is the moment about the aerodynamic centre of the airfoil. Finally, the aircraft must be configured in such a way that a lightweight and small landing gear system can be installed.

An example of how CAD modelling has played a role in the fuselage packaging part of sizing for stability and control is shown in Figure 4.3. In order to counteract the large tail-heavy moment generated by the empennage and propulsion system, the payload bay is positioned right behind the dish antenna envelope and nose landing gear bay. The reason for the elevated dish position is due to the visibility requirements mentioned in Chapter 5. The avionics system is located in between the payload bay and the engine, with the battery mounted below

it. In order to keep the wetted area and therefore C_{D_0} as low as possible, the fuselage length is kept to an absolute minimum while still allowing a stiff structure to be installed. The proposed push configuration leads to considerable challenges in terms of wing positioning. While the tail-heavy configuration dictates the wing to be installed as far on the back of the fuselage as possible, the ability to do so is restricted by the dimensions of the engine. The associated complexities can be relieved by positioning the wing somewhat outside of the fuselage, and embedding the wing root into an aerodynamic fairing.

Design and location of the horizontal tailplane was done by performing a preliminary stability and control analysis based on both analytical and empirical relationships. The exact details behind this analysis are explained in Chapter 9. Based on reference UAVs, it was decided to assign an aspect ratio of 4.0 to the horizontal tailplane. As it was seen that the landing gear should be wing-mounted and housed in pod systems because of ground stability issues, this aspect ratio would, in combination with the computed horizontal tailplane area, directly determine the lateral spacing of the main gear struts. Throughout the entire multi-iteration cycle, the length of the empennage system would not exceed the dimensions constraints imposed by the LD-6 requirements. After the initial sizing of the landing gear, it was decided to go with a high-wing system. Having used a low-wing configuration initially, the issues associated with the wing integration and propulsion packaging required the wing to be installed significantly below the fuselage. In combination with the pod size, this would lead to a very high length of the nose gear which, as can be seen from Figure 4.3, cannot be easily accommodated for. Switching to a high-wing configuration would lessen the nose gear length at the expense of the size of the main gear. However, the size of the storage pods can be more easily increased than the nose gear storage bay.

The multi-iteration cycle was terminated after five iteration loops. Within these five iterations, new solutions were introduced, and the final design converged to a margin of 7.5% with respect to the second-to-last iteration. Accordingly, a coherent design was obtained that includes all proposed solutions for conflicting requirements and design considerations. The converged configuration is analysed on both flight performance and structural feasibility. As will be described in Chapter 11, the vehicle seems to be highly sensitive to gust loads. The reason for this is the low wing loading, making it particularly vulnerable to sudden loads. This implies that the aircraft structure must be able to cope with higher load factors, which fall outside of the manoeuvring envelope. Another issue arises with the weight budgets derived from the Class II weight estimations. Large structural elements such as the wing or the fuselage are assigned a maximum weight of 51.5 and 26.7 kg, without even including contingency. However, structural analysis of some structural systems seems to indicate that these loads may be coped with within the available weight budgets. This is described in Chapter 12. The full description of the converged vehicle is given in Chapter 10.

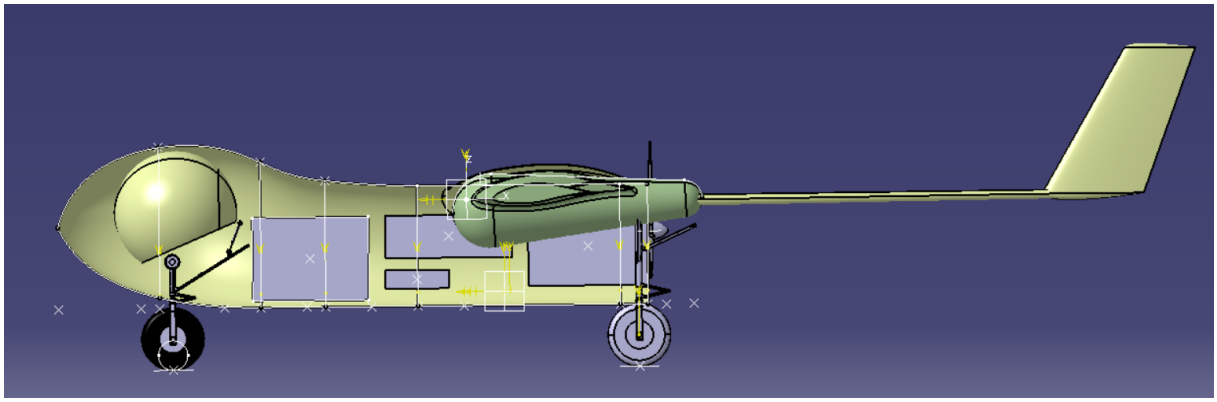

Figure 4.3: Illustration of how CAD modelling is used for initial vehicle packaging. The grey blocks represent the outer boundaries of the primary aircraft systems.

5 PAYLOAD & AVIONICS

The payload and avionics subsystem encompasses both the internal and external systems used for the inspection of NavAid systems (i.e. the mission) as well as the systems necessary to perform both autonomous and remote controlled flight. The first steps of the design for any subsystem are to identify the functions the subsystem should perform (Section 5.1) and the requirements related to these functions (Section 5.2). After these are determined, the payload will be described in a general description and by determining the components and installation in Section 5.3. Roughly the same procedure will be performed for the communications architecture (Section 5.4) and the avionics (Section 5.5) that are needed in the system. After this, the payload & avionics integration into the fuselage will be discussed in Section 5.6. Then, the verification and validation of the overall subsystem will be performed in Section 5.9, in which an interference analysis will be conducted to show that all signals can be received and transmitted correctly by the system. Finally, in Section 5.10, a compliance matrix will indicate whether the subsystem adheres to all requirements and functions will be shown.

5.1. FUNCTIONAL ANALYSIS

In order to know what the subsystem should be able to do for the system to perform its mission, it is important to identify the functions from the FBS as derived in the Baseline Report [3] that are applicable to the payload and avionics subsystem. An overview of the functions related to avionics and payload is illustrated in Figure 5.1. As can be seen, these functions can be divided into aircraft functions and mission specific functions. This distinction is made because the payload will be removable and a different payload will yield other functions.

The aircraft functions related to avionics and payload are navigation and communication. Navigation consists of determining the current location, determining the destination and constructing a flight path to get to the destination. Communication involves not only the up- and down-link, but also the storage of data, implementing commands and providing information of the system status and measurement data. These communication functions are not only related to the avionics of the aircraft, but also the payload needs to be able to perform these. Next to that, the actual inspection of the NavAid systems is the key function that the system has to perform. This includes measuring signals, storing the measured data and analysing the data.

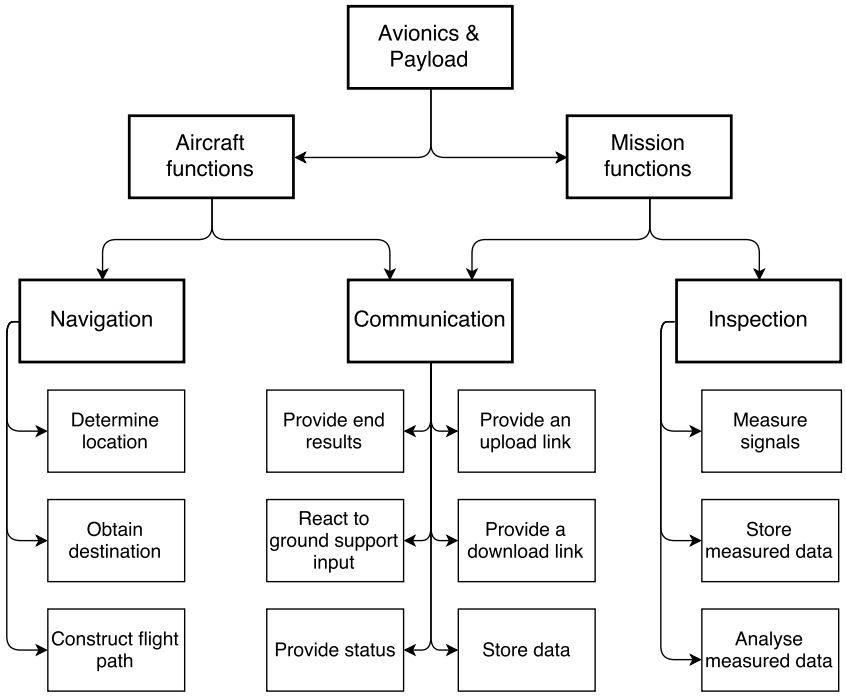

Figure 5.1: Overview of the functions that the avionics and payload subsystems have to perform.

5.2. REQUIREMENTS

From the functions as identified in the previous section, the requirements as presented in Table 5.1 can be determined. These are selected from the overall requirements as determined in the Baseline Report [3].

Table 5.1: Requirement table for the payload and avionics subsystem.

ID	Requirement
NVD-Syst-02	The system shall be able to navigate through Class A, B, C, D, E, F, G airspace.
NVD-Syst-02-01	The system shall be IFR certified.
NVD-Syst-02-02	The system shall be able to determine its flight path between two generic locations that are fixed in space.
NVD-Syst-02-02-01	The system shall have the adequate systems installed to compute its path through the air, independent of class, using the information it extracts from its sensors.
NVD-Syst-02-02-02	The system shall have access to a navigation database, from which navigation information can be extracted.
NVD-Syst-02-02-03	The system shall have real-time knowledge of the three-dimensional position of the airborne element.
NVD-Syst-02-02-04	At all times, the system shall have full knowledge about a destination for the airborne element.
NVD-Syst-08	The system shall enable for operations on the ground.
NVD-Syst-08-02	The system shall allow for ground support of the airborne element, in the form of system monitoring and maintenance.
NVD-Syst-08-02-01	The operator shall be able to monitor key system parameters from the ground system during all phases of the mission.
NVD-Syst-08-02-02	All system elements must be maintainable.
NVD-Syst-08-04	The system shall have a set-up time of no longer than 1 hour.
NVD-Syst-08-05	The payload shall be readily accessible.
NVD-Syst-09	The system shall comply with all technical constraints.
NVD-Syst-09-02	The airborne element shall be able to operate in diverse environments.
NVD-Syst-09-02-02	The airborne element shall be operable under all temperatures ranging from -30 degrees to +50 degrees Celsius.
NVD-Syst-09-02-03	At all times during the mission, the system shall have access to weather reports.

With these requirements, the design of the payload, antennas and avionics can be started. This is explained in the next sections.

5.3. PAYLOAD DESIGN

A basic investigation must be done on what must be included as payload and how this must be accommodated for in the design. The driving aspect of developing an unmanned aircraft system is to conduct a certain mission, which implies that the key purpose of the vehicle is to fly around a certain payload system and let it operate in an optimal way. For NavAid purposes, this payload system consists of a wide range of antennas, sensors, receivers, CPUs and transmitters - to name a few. Accordingly, a clear overview of the payload and its characteristics must be developed, which then forms the primary input for the design of the vehicle. By doing this, the UAV can be designed to facilitate its payload in an optimal way.

Still, it is not advisable to limit the design to one specific application only. It is of vital importance for the success of the system to be versatile as it comes to mission flexibility. Although this section is limited to a description of the payload required for NavAid calibration purposes, a considerable amount of attention is paid to the payload modularity during the development process. This is also reflected in the conceptual designs described later in this chapter.

This section is divided into three parts. First, a description is given of what the payload system entails and which solutions are currently available on the market. It will be discussed how the payload may be integrated in the vehicle. Then, an extensive overview of the payload characteristics is presented. The primary goal of this part is to illustrate key information of various aspects such as weight and size. Finally, it is shown how the payload must be installed in terms of external positioning. This is done on a basic level, i.e. without getting

into the details of signal interference or field of regard. The mere purpose is to describe how the payload must be installed to allow it to perform its function.

5.3.1. GENERAL DESCRIPTION

The central part of the payload is comprised by the flight inspection system (FIS). This system embodies a wide range of avionics, receivers, data transfer links and CPUs. A block diagram of a generic FIS is shown in Figure 5.2. The FIS consists of various elements that are each connected to a central processing body, called the Data Acquisition Unit (DAU) or Signal Processing Unit (SPU), if we have to follow the definition of Airfield Technology, Inc.[1]. The DAU/SPU receives signals from the Avionics Sensor Unit (ASU), which is basically the encompassing term for the various receivers that sense signals from the navigation aids being inspected. As described by Airfield Technology, the NavAid signals are processed by the DAU/SPU, which applies real-time calibration factors from a model that describes the aircraft's own interference profile. This model must be developed on an antenna test flight or may be generated during the calibration flight itself, as described in the Flight Inspection Manual used by the NLR [10]. As such, online corrections can be applied to the antenna gain and pattern. In addition to the payload avionics, the DAU/SPU obtains inputs from fixed aircraft equipment including the radio altimeter, the attitude and heading reference system (AHRS), the air data computer (ADC), and the event marker. Moreover, it gets real-time position reference data from a GPS receiver and a differential GPS (DGPS) datalink, which allows the system to apply very accurate differential corrections and link this information to the NavAid measurements. The DGPS signals are obtained from a ground reference system, which calculates positioning corrections based on raw GPS errors of its own reference position.

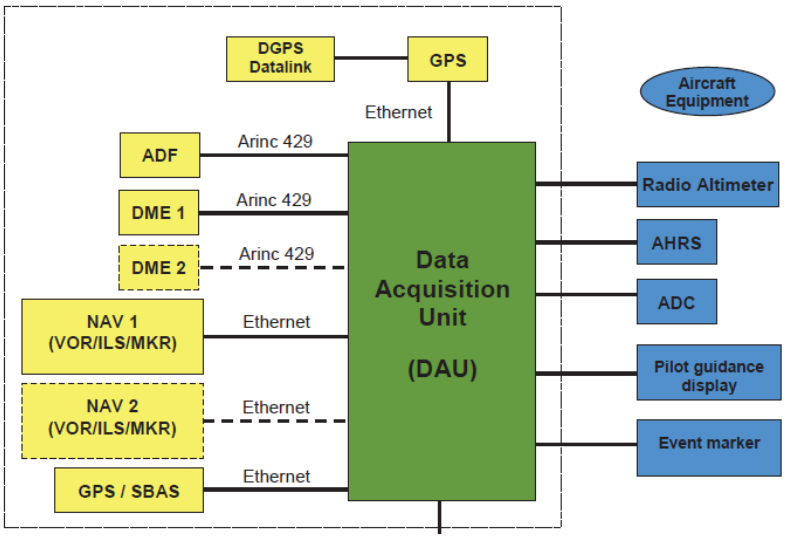

Figure 5.2: Block diagram of a generic flight inspection system; the open link at the bottom side forms the interface with a host computer (source: NLR).

Apart from the ASU and DAU/SPU, the payload consists of a wide range of antennas. The required antennas are completely independent from the primary aircraft antennas, implying that the set is fully duplicated. The antenna types depend completely on the kind of NavAid signals the system is required to measure. From the mission need statement, we can identify that equipment must be installed for the measurement of ILS, DME, VOR, TACAN and NDB signals. Accordingly, the following antennas must be installed, based on the antennas installed on the NLR/TUD Cessna Citation II [10]:

- LOC/VOR antennas
- Glide slope (GS) antennas
- DME/TACAN antennas
- Marker beacon (MB) antennas
- ADF antennas

[1] http://www.icao.int/SAM/Documents/2001/FLIGHT/AIRFIELD.pdf [cited 12 May 2016]

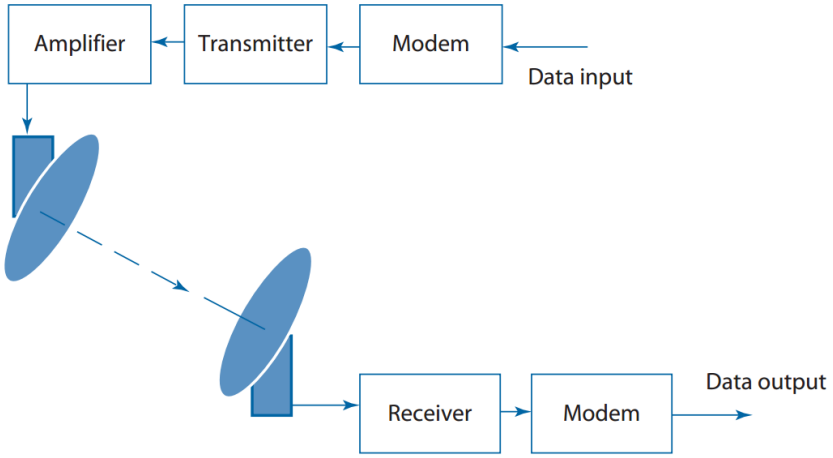

Figure 5.3: Block diagram of a generic telemetry system [7].

In addition to these antennas, the system shall be equipped with WAAS/SBAS GPS antennas, as well as an optical camera that can be used to register PAPI/VASI lights. It is specifically mentioned that the GPS equipment must be WAAS/SBAS-capable. The reason is that this technology provides much better accuracy, integrity and availability compared to conventional GPS technology [2]. This is achieved by correcting raw GPS data, which is made possible by multiple ground stations that are spread over a wide area. These correction signals are uplinked to a set of geostationary satellites and subsequently broadcasted to a WAAS/SBAS-enabled receiver. Accordingly, the augmentation signal has the same structure as the GPS signal sent out by GPS satellites.

Finally, the payload system shall have an interface with its operator. In case of a manned system, the DAU/SPU may be connected directly to a host computer, which can subsequently be used to display measurements as well as the status of various systems including the FIS itself. Also, it may display real-time information about the dynamic state of the aircraft (i.e. its attitude, speed, position, rate of climb, etc.) as well as navigation information [3]. A typical system is assembled into an operator console that may even include seat rail attachments for removal and installation. However, such a conventional system cannot be directly integrated into an unmanned vehicle. Rather, the airborne host computer shall be replaced by a telemetry system that transmits all measurement and aircraft data to the ground. The ground system may then be equipped with a host computer that can display all information to the user. Since the conventional host computer is normally speaking counted as payload, it was decided that the telemetry system it is replaced by also falls under the definition of payload. Therefore, the current stage requires to identify all required telemetry subsystems. Accordingly, a block diagram of a generic telemetry system is shown in Figure 5.3.

As described by Gundlach [7], the key elements that must be installed in the airborne vehicle are the modulator/demodulator (modem), the transmitter, the amplifier, and the antenna. The modem is used to modulate the data signal onto a carrier signal, which usually has a very high frequency (in the order of 2000-2500 MHz). The transmitter than transforms the modulated signal into an electromagnetic wave, which may than be amplified in terms of power by the amplifier. Finally, the RM signal is sent into free space by the antenna. According to Macnamara [11], for telemetry purposes, the type of antennas used most often are omnidirectional blade antennas. Therefore, at the current stage it is assumed that these will be installed on the aircraft, without reverting to a detailed analysis. This implies that it must be decided upon later in the design process which antennas will be used in the final configuration. Therefore, this assumption must be checked upon later.

5.3.2. COMPONENTS

Before the initial sizing of the vehicle can start, it must first be known what the approximate weight and size of the payload is. In order to get useful values for these parameters, a survey must be conducted on typical technologies currently available on the market. By breaking down the system into various modules, a good insight is also obtained into how the weight and size of the payload are built up. The individual elements of the ASU and telemetry system were already discussed in the previous section, as well as the kind of antennas that must be installed. The DAU/SPU will be treated as a single component, partially due to a lack of available information and partially because of the fact that it is not very useful at this point to dive into its technological

[2] https://www.faa.gov/about/office_org/headquarters_offices/ato/service_units/techops/navservices/gnss/waas/ [cited 16 May 2016]
[3] http://www.icao.int/SAM/Documents/2001/FLIGHT/AIRFIELD.pdf [cited 12 May 2016]

details.

A thorough online research was done on the available technologies and their characteristics. Various websites of manufacturers and resellers were researched to get the required information. The full overview is presented in Table A.1 in Appendix A. For most technologies, multiple examples were found. By taking the average of the results found for each element type, the risk of having a too light/small or heavy/large example can be reduced. In the following, some key aspects will be briefly described.

Within the antennas category, it must be mentioned that a single solution for VOR/localiser and GS antennas was found. Some dipole antennas are available on the market that combine these functionalities into one antenna device. As such, the amount of sensors can be reduced with respect to the TUD/NLR Cessna Citation II, as described earlier. It was also found that these antennas may be used to receive GBAS signals from a ground station in the form of VHF Data Broadcast (VDB) data, as described by Heinke and Feuerle [12]. This VHF radiolink is used to provide the aircraft with GPS positioning corrections (amongst others), which are generated by a GBAS ground facility. [4].

For the visual registration of PAPI/VASI lights, a simple solution was found in the form of a small camera that may even be available on the consumer market. The camera may have a live broadcasting functions, thereby transmitting the external view real-time to the operator, or it may store the images offline for later inspection. The primary reasons for considering these types of simple cameras are their small size and weight, as well as the typical low purchase price. For inspecting PAPI/VASI lights, such a simple system might just fit the job because of the low mission demands. That is, the sole task of the system is to make images of the PAPI/VASI system from various positions. The PAPI/VASI inspection function is therefore decoupled from the large and complex camera(s) that provide(s) the ground operator with a real-time cockpit view from the aerial vehicle. It may be decided in a later stage whether the small observation camera is deemed necessary, as it seems that the task may be integrated with the vehicle's main visual system.

Within the avionics category, the conventional set of receivers and interrogators is included. For receiving and decoding GBAS messages, the aircraft must be equipped with a dedicated VDB receiver that can be tuned to the same frequency as the ground system signals [12]. Regarding the DAU/SPU, only very limited information could be find. Only two clear examples were identified. Accordingly, the specifications were estimated based on similar technologies. A large uncertainty is therefore inherent to this element, and the values must be revisited later in the design process once more information becomes available. For the telemetry system, various examples of blade antennas, transmitters and amplifiers could be found. Modems however, are not included in this overview due to the lack of relevant information. Neglecting these systems is justified because of their typical small weight and size. However, a certain level of contingency must be included when determining the final payload weight and size. An overview of all these payload components can be found in Table A.1. Note that although antennas are mentioned in this section, they are in fact part of the avionics, since no duplication is needed in order to perform the mission and navigation simultaneously. Also the camera needed for PAPI/VASI measurements is already part of avionics.

5.3.3. INSTALLATION

Having a detailed payload breakdown and reference database at hand, the sheer number and locations of the full range of technologies can be described. This is done based on reference aircraft used for flight inspection. Each element has its own set of requirements that shall be adhered to when developing the requirements. Accordingly, it is described in ICAO Doc 8071 that "the selection and utilisation of special ground or flight inspection equipment used to determine the validity of navigation information should minimise the uncertainty of the measurement being performed" [13]. This means that detailed attention must be paid to the way the system is installed.

At this point, an initial estimate can be made on the weight and size of the airborne payload installation. The computation is shown in Table 5.2. The individual payload characteristics are estimated as an average from the reference devices presented in Table A.1.

All payload modules combined have a total mass and size of $50kg$ and $72L$, respectively. This does not include any cabling, which has an approximated weight contribution of 10%. Housing equipment is not included, as this is rated to be part of the operational empty weight of the vehicle. By including this additional correction, the combined payload weight is estimated to be around $55kg$. This forms an absolute average which can only

[4] http://www.faa.gov/about/office_org/headquarters_offices/ato/service_units/techops/navservices/gnss/laas/howitworks/ [cited 16 May 2016]

Table 5.2: Payload components with their mass, size and power

Category	Type	Quantity	Mass (kg)	Size (L)	Power (W)
Avionics Sensor Unit					
	VOR/ILS receiver	1	4.55	4.43	35.25
	DME interrogator	1	6.25	5.65	50.00
	TACAN interrogator	1	6.48	9.34	500.00
	MB receiver	1	0.18	0.18	8.25
	ADF receiver	1	3.50	3.62	16.20
	WAAS/SBAS GPS receiver	2	2.73	0.60	32.00
	VDB receiver	1	4.00	9.24	41.40
Signal Processing Unit					
	Data Acquisition Unit	1	10.00	38.50	550
Telemetry System					
	Omnidirectional blade antenna	1	0.11	0.03	0.00
	Telemetry transmitter	1	0.29	0.18	4.67
	Airborne amplifier	1	0.42	0.21	30.00
Corrections					
	Description		MF	MF	MF
	Cabling		1.25	1.05	1.00
	Housing		1.00	1.00	1.40
Total:			**47 kg**	**94 L**	**1295 W**

be used for estimation purposes. When the actual design process of the selected vehicle will be started, however, a contingency factor must be included to account for the probabilistic distribution of the payload weight. Once the design evolves, more definite information will become available and the associated risk of having a certain spread in the potential weight will be reduced.

5.4. COMMUNICATIONS ARCHITECTURE

For unmanned aircraft systems, the communications infrastructure forms the single-most important system element that ensures safe operations and allows the operator to download payload data from the airborne platform. It is often seen on a wide host of unmanned aircraft that the communications system, primarily consisting of multiple antennas and various computers and processors, imposes key requirements on the design of the fuselage. Famous examples of this are the Northrop Grumman RQ-4 Global Hawk and the General Atomics MQ-1 Predator, which have dedicated antenna bays in the front part of the vehicle. The required size of the antennas results in these bays being rather bulgy, illustrating their relevance for the design. Recognising this contributes vitally to the success of the conceptual design phase, in which large design changes can be implemented.

An important tool that is used for preliminary analysis and design of the communication system is the link budget. This analysis is centred around a governing equation that consists of multiple independent design variables, including those related to path losses and gains. By tweaking these variables, one can come up with a configuration that satisfies all governing requirements and constraints. These requirements and constraints are described in Subsection 5.4.1. The reasoning behind and the results of the link budget analysis is specified in Subsection 5.4.2. These results are subsequently used to select, size and position antennas. This is described in Subsection 5.4.3

5.4.1. REQUIREMENTS

For spacecraft communications, a wide host of requirements and constraints apply to the design of the telemetry system. Typical requirements describe the type of signal transmitted, the link capacity in terms of bandwidth and carrier frequency, the coverage area, signal strength and quality, connectivity and availability [14]. These requirements must be satisfied within a set of constraints, which typically includes transmitter power limit, receiver sensitivity, interference, the environment and regulations.

The type of signal transmitted can relate to either the transmission format (analog or digital) or the information to be sent. The transmission format typically depends on the intended application and vehicle size. As described by Gundlach [7], analog transmissions are often employed on small UASs. This is a direct result of the low weight, cost, and required power of analog radios, as well as their small size and ease of integration.

However, analog links require very complex encrypting and do not offer the benefits of multiplexing and digital processing. These drawbacks are resolved by employing a digital link. Accordingly, analog transmissions will be disregarded altogether, and digital links will be opted for in the current design.

The key to having a good understanding of the required capabilities of the communications system is to establish what information must be transmitted, and how these requirements translate to bandwidth and carrier frequencies. Among other considerations to be described later, these last two features stem directly from the required bit rate. In order to do this in a structured manner, an overview must be made of the data to be sent to and by the airborne element. Therefore, a distinction must be made between downlink and uplink. Additionally, data requirements strongly depend on the flight phase. The flight phases that are of relevance here are launch and recovery, en-route, on station and payload control, following the mission breakdown proposed by Dr. Chaput [15]. For each of these phases, a data overview has been created for the current application. The results for uplink and downlink are summarised in tables Table 5.3 and Table 5.4, respectively.

Table 5.3: Data flow overview for uplink communications

	Navigation	Vehicle State	Airspace Ops	Payload	Housekeeping
Launch & Recovery / Climb & Approach	Future flight route updates; climb/ approach procedures; DGPS transmission	Configuration commands	Manual control commands; future automated commands; ATC voice relay	-	-
En Route	Future flight route updates; en route procedures	-	Manual control commands (if necessary); future automated commands; ATC voice relay	Preprogrammed inspection instructions	-
On Station	Future flight route updates; inspection procedures	-	Manual control commands (if necessary); future automated commands; ATC voice relay	Live inspection instructions	-

Table 5.4: Data flow overview for downlink communications

	Navigation	Vehicle State	Airspace Ops	Payload	Housekeeping
Launch & Recovery / Climb & Approach	Current/intended flight path; area awareness; sensor signals	Inertial state; air data information; configuration feedback	HQ external view; nearby traffic; ATC voice relay	PAPI/VASI visuals	GPS signal status; system health status; power usage; system temperatures; warning messages
En Route	Current/intended flight path; area awareness; sensor signals	Fuel used and time remaining; inertial state; air data information	LQ external view; nearby traffic; ATC voice relay	-	GPS signal status; system health status; power usage; system temperatures; warning messages
On Station	Current/intended flight path; area awareness; sensor signals	Fuel used and time remaining; inertial state; air data information; live UA capabilities	LQ external view; nearby traffic; ATC voice relay	Processed flight inspection measurement data	GPS signal status; system health status; power usage; system temperatures; warning messages

The data flow overviews clearly show that, although there is a host of transmission categories that recur throughout the entire flight, there is a significant number of phase-specific transmissions. Accordingly, en route flight is the least demanding stage. For uplink communications, telemetry merely consists of command and control (C2). As described by Gundlach [7], C2 communications typically require low bandwidth, in the range of several tens to hundreds of kbps. Downlink en route communications, however, is very much more demanding, due to the airborne element continuously transmitting flight status information, housekeeping data, real-time navigation data and live video. Live video enhances the situational awareness of the ground operator. However, large resolutions are typically not required, and in order to reduce the required bandwidth, low-quality (LQ)

video can be opted for. Gundlach [7] describes that typical pixel depths for colour videos are 8-14 bits/pixel and typical video frame rates are 15-30 Hz. The colour depth is not that important, since only PAPI lights need to be inspected, but the frame rate is, because the video is used for real-time control. Therefore it is decided that 8 bits/pixel will be satisfactory, while the frame rate will be set to 30 Hz. The resolution and compression ratio of the video are determined later, when more information is available on the link budget and it becomes clear what the options are.

The communication system requires several antennas to fulfil all functions as specified in Section 5.1. First of all, line of sight communication is to be enabled. For this, two antennas will be installed, one in the front and one in the back. This is done to limit the blockage by the UAV itself in all directions, which can pose a serious problem during certain manoeuvres. Due to the fact that line of sight communication provides real-time video that enables manual approaches, the line of sight communication is of vital importance and should be reliable. Therefore two additional line of sight antennas will be used that operate on a different frequency for redundancy. The UAV is also able to operate beyond line of sight, therefore a satellite communication antenna is needed. Due to the limited space available inside the UAV, a dish antenna is considered the optimal solution (omnidirectional antennas will not be able to reach satellites). This satellite communication does not need redundancy, since the UAV is not dependent on it and can be programmed such that it flies back to line of sight if satellite communication is lost.

Next to the above mentioned antennas, also two GPS antennas are needed to provide the UAV with information about location and time, where the second one is used for redundancy. UAVs that share airspace with manned aircraft are often required to be able to communicate with ATC as if it were a manned aircraft. In order to allow for communication between ATC and the GS, two voice relay antennas are installed on the UAV. Again the second one is used for redundancy.

5.4.2. LINK BUDGET

The link budget is used to size the required antennas. A schematic overview of the communication links that are needed is given in Figure 5.4.

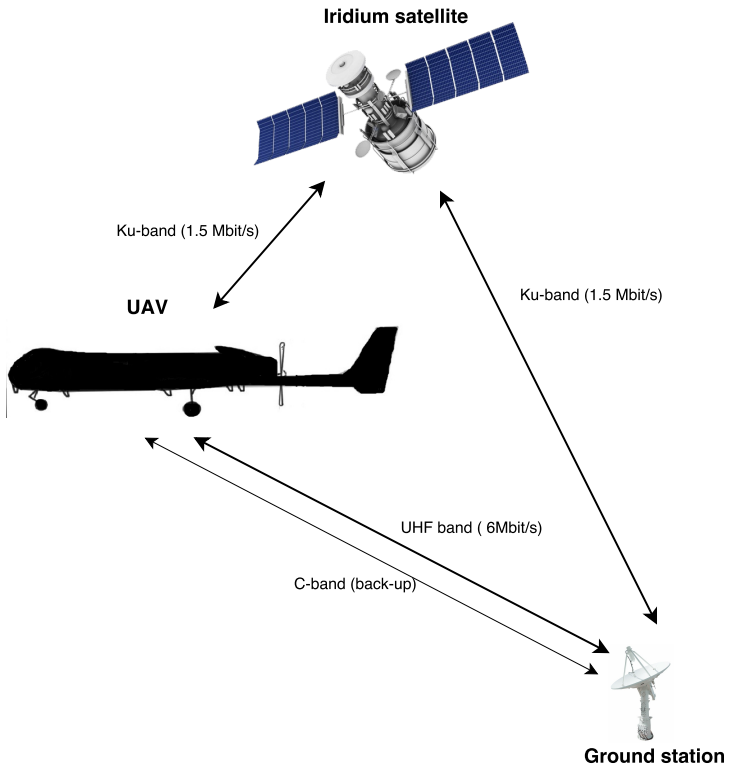

Figure 5.4: Communication architecture between the UAV and the GS.

The antennas used for these links should be large enough to transmit the required data from the UAV to the ground station and vice verse. For this, a sufficient signal-to-noise ratio has to be achieved. In order to determine the signal-to-noise ratio, a link budget is used. This is expressed in Equation 5.1 using the decibel scale [14].

$$\frac{E_b}{N_0} = P_t + G_t + G_r + L_t + L_r + L_a + L_s + L_p + 228.6 - 10log(R) - 10log(T_s) \tag{5.1}$$

In this equation P_t is the transmitter power, G_t is the transmitter gain, G_r is the receiver gain, L_t is the transmitter loss, L_r is the receiver loss, L_a is the atmospheric loss, L_s is the free space loss, L_p is the pointing loss and the 228.6 comes from the Boltzmann's constant, all expressed in [dB]. Then R is the bit rate in [bit/s] and T_s is the ambient temperature in [K].

The required signal to noise ratio is dependent on the energy per bit to noise power spectral density and the data rate to bandwidth ratio, as expressed in Equation 5.2.

$$SNR_{required}[dB] = \frac{E_b}{N_0}[dB] + 10 \cdot log(\frac{R_{data}}{B}) \tag{5.2}$$

The margin between the required SNR and the obtained SNR should at least be 3 dB, but preferably above 10 dB [7]. This is needed to ensure a stable and strong communication link. Three link budgets will be established for the system; one for the link between the UAV and the ground station directly, using line of sight communication, one for the link between the UAV and a satellite, and also one for the link between the ground station and a satellite. An overview of all three links can be seen in Tables 5.5, 5.6 and 5.7. Some of the parameters apply to all three links. These include the transmitter and receiver antenna losses, the ambient temperature, the energy per bit to noise power spectral density and the data rate to bandwidth ratio.

As can be seen in Table 5.5, for LOS communication a frequency of 0.433 GHz will be used, which is part of the UHF range. The gains of both the transmitter and receiver are 1.64, implying they are omnidirectional. These antennas do not require any active pointing mechanism because their pointing loss is negligible. The video bit rate follows from the specifications on the quality of the visual data, using a resolution of 720x1080 pixels, 30 frames per second and a colour depth of 8 bits to provide the ground operator with adequate video quality to perform a manual landing. This is then compressed by a factor of 50 to be able to send all data to the ground station. The actual bit rate (6 Mbit/s) is a little higher so that other data can be send simultaneously. With this data, the maximum distance that can be covered so that the link margin is still sufficient is determined to be 80 km.

The link between the UAV and the satellite uses another frequency, 11.7 GHz, which is part of the Ku-band. The distance between the receiver and transmitter is set to 2200 km, because that is the maximum distance between the UAV and Iridium satellites at 780 km altitude. Due to the large distance the signal has to travel, the allowable bit rate is reduced to 1.5 Mbit/s by decreasing the video resolution to 240x426 pixels. The rest of the bit rate is needed to send all relevant data. In order to be able to close this link, a high gain is needed, implying a pointing mechanism is needed.

The link between the GS and the satellite is fairly similar to the one described above, due to the same distance and frequency. The only difference is that a higher gain can be used here, thus reducing the power needed to send the data.

Table 5.5: Link budget of the LOS communication.

		Line of sight link	**UAV/GS**			
Gains/power	Symbols	Values	dB	**Input parameters:**	UHF	
Transmitted power (W)	P_t	30	14.77	Frequency (GHz)	f	0.433
Transmitter antenna gain	G_t	n.a.	1.64	Distance between the transmitter and receiver (km)	d	80
Wavelength of the carrier signal (m)	λ	0.69	-	Energy per bit to noise power spectral density (dB) (BPSK, 10^-5)	E_b/N_0	10
Receiver antenna gain	G_r	n.a.	1.64	Modulation type (-)	R_{data}/B	0.5
Boltzmann's constant (J/K)	k	$1.38{\cdot}10^{-23}$	228.60	Bit Rate (bits/s)	R	$6.00{\cdot}10^{06}$
				Video bit rate (Mbit/s) (720p, 8 bit colour, 30 fps, CR50)		4.42
Losses	Symbols	Values	dB			
Receiving signal loss from the receiver antenna through the amplifier (-)	L_r	-	1.5			
Atmospheric loss	L_a	-	10.2	**Results**		
Signal loss through the transmitter antenna	L_t	-	1.5	Obtained SNR	17.31	
Antenna pointing loss	L_p	-	0.5	Required SNR p	6.99	
Space loss	L_s	$4.75{\cdot}10^{-13}$	123.23	Net margin	10.3	
Ambient absolute temperature (K)	T	290.00	24.62			
Bit Rate (bits/s)	R	$6.00{\cdot}10^{06}$	67.78			

Table 5.6: Link budget of the SATCOM between the UAV and the satellite.

		SATCOM link	**UAV/SAT**			
Gains/power	Symbols	Values	dB	**Input parameters:**	Ku-band	
Transmitted power (W)	P_t	50	17.0	Frequency (GHz)	f	11.7
Transmitter antenna gain	G_t	n.a.	29.0	Distance between the transmitter and receiver (km)	d	2,200
Wavelength of the carrier signal (m)	λ	0.0256	-	Energy per bit to noise power spectral density (dB) (BPSK, 10^-5)	E_b/N_0	10
Receiver antenna gain	G_r	n.a.	36.0	Modulation type (-)	R_{data}/B	0.5
Boltzmann's constant (J/K)	k	$1.38{\cdot}10^{-23}$	228.60	Bit Rate (bits/s)	R	$1.50{\cdot}10^{06}$
				Video bit rate (Mbit/s) (240p, 8 bit colour, 30 fps, CR50)		0.37
Losses	Symbols	Values	dB			
Receiving signal loss from the receiver antenna through the amplifier (-)	L_r	-	1.5			
Atmospheric loss	L_a	-	22.8	**Results**		
Signal loss through the transmitter antenna	L_t	-	1.5	Obtained SNR	17.1	
Antenna pointing loss	L_p	-	0.5	Required SNR	6.99	
Space loss	L_s	$1.04{\cdot}10^{-18}$	179.83	Net margin	10.1	
Ambient absolute temperature (K)	T	290.00	24.62			
Bit Rate (bits/s)	R	$1.50{\cdot}10^{06}$	61.76			

Table 5.7: Link budget of the SATCOM between the ground station and the satellite.

		SATCOM link	**GS/SAT**
Gains/power	Symbols	Values	dB
Transmitted power (W)	P_t	30	14.77
Transmitter antenna gain	G_t	n.a.	36.0
Wavelength of the carrier signal (m)	λ	0.0256	-
Receiver antenna gain	G_r	n.a.	31.0
Boltzmann's constant (J/K)	k	$1.38{\cdot}10^{-23}$	228.60
Losses	Symbols	Values	dB
Receiving signal loss from the receiver antenna through the amplifier (-)	L_r	-	1.5
Atmospheric loss	L_a	-	22.8
Signal loss through the transmitter antenna	L_t	-	1.5
Antenna pointing loss	L_p	-	0.5
Space loss	L_s	$1.04{\cdot}10^{-18}$	179.83
Ambient absolute temperature (K)	T	290.00	24.62
Bit Rate (bits/s)	R	$1.50{\cdot}10^{06}$	61.76

Input parameters:	Ku-band	
Frequency (GHz)	f	11.7
Distance between the transmitter and receiver (km)	d	2,200
Energy per bit to noise power spectral density (dB) (BPSK, 10^-5)	E_b/N_0	10
Modulation type (-)	R_{data}/B	0.5
Bit Rate (bits/s)	R	$1.50{\cdot}10^{06}$
Video bit rate (Mbit/s) (240p, 8 bit colour, 30 fps, CR50)		0.37

Results	
Obtained SNR	17.9
Required SNR	6.99
Net margin	10.9

5.4.3. SIZING AND SELECTION

With the required antenna gain and signal wavelength, the size of the antennas can be determined, after which, specific antennas will be selected and positioned. For the antenna size, the area and diameter of a parabolic dish antenna are calculated using Equation 5.3 [5] and Equation 5.4.

$$G = 10 \cdot \log_{10}\left(\eta \frac{4\pi}{\lambda} A\right) \tag{5.3}$$

$$d = 2 \cdot \sqrt{\frac{A}{\pi}} \tag{5.4}$$

Here, η is the aperture efficiency of the antenna. For parabolic dish antennas, this value typically ranges from 0.55 to 0.70. For the sizing of the antennas for the avionics system, a aperture efficiency of 0.65 was chosen [6]. Furthermore, G is the antenna gain, λ is the carrier signal wavelength and A is the antenna area.

Here, d is the antenna diameter. These parabolic dish antennas have good characteristics for high gain applications. For the initial link budget, the area calculation is used for validating the feasibility of the chosen data link. For (near)omnidirectional antennas, however, no sizing formula exists. Instead, the dimensions will be determined from actual existing antennas. It is assumed that the dimensions of these antennas are not driving, since omnidirectional antennas are generally quite smaller compared to high gain parabolic dish antennas.

The omnidirectional antennas used for line of sight (LOS) communication between the UAV and the ground station have a gain of $1.64dB$ and are operated on a frequency of $0.433GHz$. The maximum distance for LOS communications is 80 km. The antenna that was found to meet these requirements is the MT-2045/D antenna. It has a height of $0.112m$, length of $0.102m$ and width of $0.055m$ and a mass of $0.31kg$. It uses a power of $30W$ to send and receive the signals.

For communications between the UAV and LEO satellites, a parabolic dish antenna will be used. This antenna has a area of $0.05m^2$ and a diameter of $0.254m$. The antenna gain is $28dB$ at a frequency of $11.7GHz$. The Radiowaves HPLP1-11 has a mass of $7.7kg$ and dimensions of 0.280 x 0.280 x $0.094m$. The placement of this antenna is very important because LEO satellites travel quite fast with respect to the ground compared to GEO

[5] `http://www.qsl.net/n1bwt/chap4.pdf` [cited 2 June 2016]
[6] `http://www.qsl.net/n1bwt/chap4.pdf` [cited 2 June 2016]

satellites. Continuous communication through the satellite link is required, and thus the parabolic dish antenna should be directed to a LEO satellite at all times. For determining the angle required for the antenna, the Iridium satellite constellation is used. This constellation can be found in Figure 5.5 [7]. The constellation consists of 6 polar planes with 11 satellites each, at an altitude of 780 km. By assuming the earth is a perfect sphere, the maximum horizontal distance from a satellite can be calculated to be 2044 km, and from this, the maximum angle from the vertical can be calculated to be 70°. This value can be used for the avionics integration as discussed in Section 5.6.

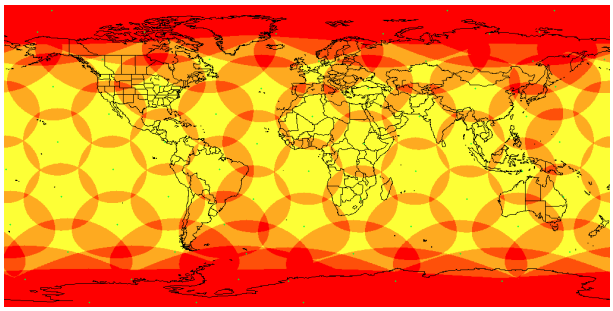

Figure 5.5: Overview of the Iridium satellite constellation.

An additional C-band antenna is used for enabling LOS communications when the regular frequency used for these communications (0.433GHz) is jammed. The omnidirectional antenna that was found to fulfil this job weighs 0.08kg and uses an input power of 10W. Its dimensions are 0.051 x 0.045 x 0.009m.

A GPS antenna is needed for continuous position determination in flight. A regular GPS antenna in not accurate enough, therefore, an antenna with differential GPS (DGPS) capabilities should be used. An example of an adequate antenna weighs 1.13kg, uses 25W and its dimensions are 0.305 x 0.305 x 0.100m.

Finally, a voice relay antenna is used to enable communication with ATC through the UAV to the operator at the ground station. The dimensions of this antenna are 0.142 x 0.127 x 0.251m. It uses an input power of 20W and weighs 5.53kg.

The total mass and power budget of these antennas can be added to the mass an power budget of the avionics system that will be determined in the next section. The final avionics mass and power budget are displayed in Table 5.9. Furthermore, the dimensions of the antennas are used in Section 5.6.

5.5. AVIONICS DESIGN

Avionic systems include communications, navigation and the systems that are fitted to aircraft to perform individual functions. In order to design this system, the requirements first have to be determined. Then, the components are identified and the components are sized to provide a estimation on the avionics size, weight and input power.

5.5.1. REQUIREMENTS

The first step in the design of the avionics system is to determine the precise requirements for the system. The main requirements that have been identified follow from FAR14. For IFR certification, CFR §91.205 determines the required components for the aircraft. However, because these regulations are created for powered civil aircraft, some requirements might not be applicable to a UAV.

The requirements from FAR14 §19.205 that are applicable to UAVs should be met in order to be able to certify the aircraft. These requirements, together with [7], can now be used to determine the required components for the avionics system. This is done in the next subsection.

5.5.2. COMPONENTS

The list of components is presented in Table 5.8. The components required for the avionics are subdivided into seven categories: navigation, air data sensors, lighting, landing aids, management systems and controllers, wiring and sense & avoid systems.

For navigation, several sensors are needed in order to accurately determine the aircraft's position and attitude. First of all, a GPS receiver is used as the main source of the position while the IMU is able to accurately de-

[7] `https://en.wikipedia.org/wiki/Iridium_satellite_constellation` [cited 6 June 2016]

termine the aircraft's attitude. These two sensors are combined in the INS system tow provide the system and operator on the ground a precise picture of the UAV's position in time. Furthermore, an Above Ground Sensor is used to determine the distance between the UAV and the ground, this sensor has to be very accurate in order to be used for precise autonomous landing of the system. Finally, a 3-axis magnetic compass determines the direction of the aircraft with respect to the magnetic poles of the earth.

To provide the UAV with information about the status of the aircraft, several sensors are required. Pitot-static systems are used to determine the airspeed of the vehicle, making use of the difference between the static pressure and the total pressure. In order to measure the angle of attack, vanes will be used. Vanes automatically align themselves with the local airflow, and are capable of measuring the angle with respect to a reference point. Multiple vanes on different locations will be used to account for asymmetric manoeuvres. The altitude of the UAV will be determined using a barometric altimeter, which measures the pressure altitude.

According to Gundlach [7], an unmanned aircraft requires the same lighting systems as a manned aircraft. Therefore, the requirements on lighting for manned aircraft are used. These required lighting systems are (according to the FAA Airplane Flying Handbook [16]): red, green and white position lights, anti-collision strobe lights, anti-collision beacon lights, landing lights and taxi lights.

Very accurate position data is needed to perform both autonomous as well as remote controlled landing. For this, a differential GPS RTK system is used. Such a system is accurate up to the centimetre level and can therefore be used to guide the aircraft to the runway. Furthermore, for remote controlled landing, a landing camera will be used to help the operator see where the aircraft is with respect to the runway. This landing camera should have a low latency to ensure proper controllability of the aircraft. Furthermore, the quality and update rate should be sufficient in order to be able to control the aircraft manually. The resolution is determined to be 720x1080 pixels, the colour scheme is 8 bit which is needed to recognise the PAPI lights, 30 frames per second are needed to provide the operator with an adequate update rate and to keep data rate as low as possible, a compression factor of 50 [8] is applied.

In order to manage the UAV, a UA Management System is required. This system performs important function that enables the UAV to fly and operate. It provides the interface between different subsystems and executes commands. In addition to this, also an autopilot is necessary, since the UAV will not have a pilot on board. This includes a processor with an algorithm. Next to the UA management system, also a Mission Management System is needed that is able to communicate with the payload and manages the up- and down-link. It basically performs all other important function that are not related to the managing of the UAV itself. The UAV that is to be designed does not only fly autonomously, but also manual control should be able. Therefore, a Remote Interface Unit is required, which is the control unit that is used by the ground operator.

UAVs also need an engine controller, which is a unit that controls and monitors the engine(s) of the UAV. This is needed because there are no pilots on-board that can adjust the engine controls [7]. Also a landing position gauge must be installed in case of a retractable landing gear. All data that is measured and received must be distributed appropriately across the UAV subsystems. This is done using a so called data bus, which is the medium of internal data transportation. Relevant flight performance data that is obtained in the UAV is stored in a flight data recorder. This is done to prevent data from getting lost due to a crash, in order to help with the investigation.

Wiring is used to connect all components of the avionics system with each other and with the power source. For a complex avionics system like that of an autonomous flying UAV, the wiring forms a important part of the system in terms of both the weight as well as the volume, therefore it should be included in the initial estimation.

Sense & avoid systems communicate with other aircraft and if necessary initiate avoiding manoeuvres. For this, transponders are used to sent position, heading and airspeed data to other aircraft. Furthermore, a voice relay radio receives spoken commands from ATC and sends these commands back down to the ground system where the operator is able to interpret the commands. Finally, an air traffic detection sensor receives position, heading and airspeed data from other aircraft.

With the provided list of components, an electronic block diagram can be created showing the power distribution system for the avionics. All systems in the aircraft use DC power and therefore no power conversion between DC and AC is required. As can be seen in Figure 5.6, every device in the avionics system has a circuit breaker. The circuit breaker is an automatically operated electrical switch which protects the device from overload or short circuits. Although the circuit breakers can be reset after it has tripped, for safety reason the root

[8] `https://www.videomaker.com/article/f6/9867-video-compression-mpeg-4` [cited 01 June 2016]

Table 5.8: Overview of all components of the avionics system.

Navigation
GPS receiver
Inertial Measurement Unit
INS system (combines GPS and IMU)
Above-ground sensors
Magnetic compass (3-axis)
VOR/ILS/GS receiver
DME/TACAN receiver
MB receiver
ADF receiver

Air data sensors
Pitot-static systems
Vanes
Barometric altimeter

Lighting
Position lights
Anti-collision strobe lights
Anti-collision beacon lights
Landing lights
Taxi lights

Landing aids
Differential GPS RTK
Landing cameras with low latency

Management systems and controllers
UA management system
Mission management system
Engine controllers
Autopilot
Remote interface units
Data bus
Landing gear position indicator
Flight data recorder

Wiring

Sense & avoid systems
Transponder
Voice relay radio
Air traffic detection sensor

cause of the problem must be found before resetting the switch. The avionics has its own power distribution bus separate from the main bus seen in figure 8.8. The equipment in the avionics bay is sensitive and therefore is electronically protected from the engine starter circuit. When the engine is started the electric motor starter will draw a large current from the battery possibly create transient voltage spikes which can enter the avionics bay. When the starter button is pressed the normally closed solenoid (electromagnetic relay) at the top of Figure 5.6 is opened. The power from the main bus is therefore cut off from the avionics equipment as long as the starter engine is used [17]. The CPU is also used to send low voltage control signals to the landing gears system (Figure 9.9) as well as the control surfaces (Figure 9.8). The latter sytems are explained later in this report.

5.5.3. SIZING

After all necessary components are determined in the previous section, commercially available off-the-shelf systems can be found to get a first estimate of the mass, dimensions and power required for the avionics. An explanation of these components is given below and an overview of all components with their characteristics can be found in Table 5.9.

Firstly, the FMC-2000 (flight mission computer) is the most important system that is able to perform the management of both the UAV and the mission. It also has an autopilot included in the system, which means that this device provides fully autonomous flight. The HC-1000 (health control unit) functions as health monitoring device, able to provide the monitoring of engine characteristics, switching of lights and controlling the brakes and landing gear. Then the SP-2000 (sensor pack) is equipped with a GPS, INS, airspeed and altitude pressure sensors, for which a Pitot-static system is needed in addition. This is all that is needed for the navigation of unmanned aircraft. Communication with other aircraft is of vital importance, therefore a Mode S transponder is installed, which is equipped with ADS-B out to inform others about the status of the UAV. In order to be able to sense and avoid other aircraft, the UAV will also be equipped with ADS-B in, for which the TAS 600A will be used.

Accurate measuring of the altitude is done by a radio altimeter (also called above ground sensor), which determines the altitude by measuring the time between sending and receiving a signal that is reflected by the ground. Visual footage is obtained through the AXIS P1224-E camera, which provides 720p resolution with 30 fps and a 145 ° angle of sight. Data distribution is done using the AltaCore 1553 data bus, which uses Ethernet buses. The lighting system consists of three position lights, three anti-collision strobe lights, two anti-collision beacon lights, two landing lights and three taxi lights. The FDR-300 is a small flight data recorder used in fighter aircraft and long range UAVs. Lastly, it is estimated that the wiring of all avionics weighs 10 % of the total equipment

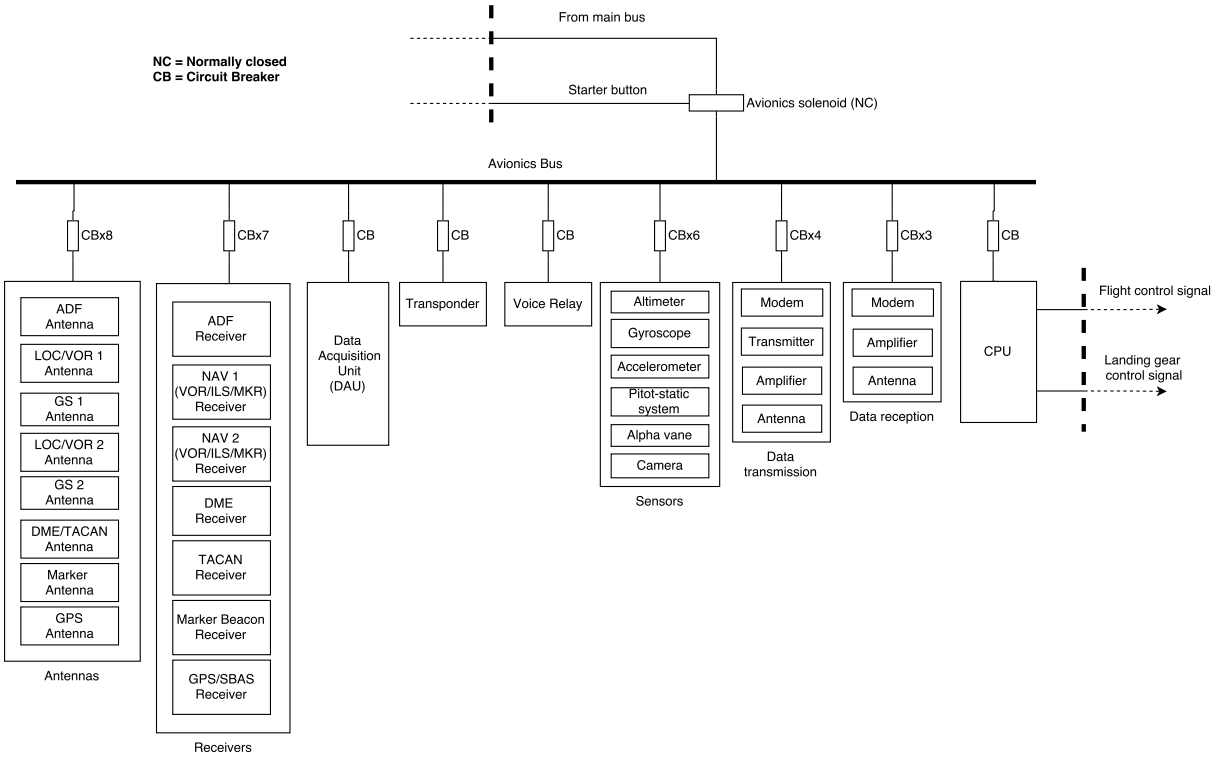

Figure 5.6: Electronic block diagram of the avionics system.

weight.

Redundancy is incorporated into the avionics system to ensure a high reliability and safety of the aircraft. Possible failure of components should not result in loss of property or people. The exact number of components that is installed depends on multiple factors. these factors are, amongst other, the cost of a certain component, the chance of component failure, the effect of a certain component's failure. For a simplex system, the loss of the system will result in loss of the system's functionality, this system does not have redundancy, but is obviously lighter and more cost effective.

In order to create optimal redundancy, a triplex system can be used. Triplex systems are able to handle the loss of one string because there are two backups. It is also able to detect invalid input from strings by voting between the three systems. If one system deviates from the other two, it is considered to be an invalid value. The voting scheme is no longer possible once the system is down to two strings [7].

Duplex systems are used less compared to simplex and triplex systems. The duplex system lacks the possibility to detect invalid input. It does however incorporate redundancy since the second system is able to take over the functionality when the first fails.

[9] http://www.tellumat.com/defence-and-security_unmmaned-systems/ [cited 31 May 2016]
[10] http://www.trig-avionics.com/library/TT2xBrochureUK.pdf [cited 31 May 2016]
[11] http://www.avidyne.com/products/tas-a/index.html [cited 31 May 2016]
[12] http://www.freeflightsystems.com/products/radar-altimeters/altimeters/ra-4000 [cited 31 May 2016]
[13] http://www.axis.com/global/en/products/axis-p1224-e/support-and-documentation [cited 31 May 2016]
[14] http://www.uavfactory.com/product/12 [cited 31 May 2016]
[15] http://www.altadt.com/products/mil-std-1553/ [cited 31 May 2016]
[16] http://www.whelen.com/pb/Aviation/Catalog%20Price%20Lists%20and%20Manuals/General_Aviation_Catalog.pdf [cited 31 May 2016]
[17] http://www.etiservicesinc.com/products/fdr-300.html [cited 31 May 2016]
[18] http://www.mtiwe.com/?CategoryID=252&ArticleID=370 [cited 2 June 2016]
[19] http://www.cobham.com/communications-and-connectivity/antenna-systems/antennas-for-communication-and-navigation/gps-navigation-antennas/gpsxm-antennas/comant-ci-428-410-datasheet/ [cited 2 June 2016]
[20] https://www.rockwellcollins.com/~/media/Files/Unsecure/Products/Product%20Brochures/Communcation%20and%20Networks/Communication%20Radios/ARC-210%20Gen5%20brochure.aspx [cited 2 June 2016]
[21] http://www.pharad.com/uhf-to-c-band-uav-antenna.html# [cited 2 June 2016]
[22] http://www.radiowaves.com/en/product/hplp1-11 [cited 2 June 2016]

Table 5.9: List of avionics components with the mass, dimensions and power.

Component	Quantity	Mass (kg)	Dimensions (m)	Power (W)
Air system				
FMC-2000 [9]	3	1.30	0.220 x 0.125 x 0.080	25.0
HC-1000 [9]	1	0.20	0.120 x 0.075 x 0.024	14.4
SP-2000 [9]	3	0.40	0.130 x 0.086 x 0.040	14.4
Mode S transponder [10]	2	0.44	0.048 x 0.068 x 0.160	250.0
TAS 600 A (avidyne) [11]	1	0.77	0.082 x 0.070 x 0.131	40.0
Radio altimeter [12]	1	1.20	0.078 x 0.080 x 0.172	11.2
AXIS P1224-E Camera [13]	1	0.36	0.052 x 0.020 x 0.020	6.5
Pitot-static system [14]	3	0.04	0.230 x 0.024 x 0.027	0.0
Data bus AltaCore 1553 [15]	1	0.03	0.142 x 0.070 x 0.035	7.0
Lighting set[16]	1	2.45	N.A.	180.0
FDR-300 Flight data recorder [17]	1	2.50	0.100 x 0.163 x 0.267	30.0
Omnidirectional antenna [18]	2	0.31	0.102 x 0.055 x 0.112	30.0
GPS antenna [19]	2	0.18	0.200 x 0.100 x 0.050	3.0
Voice Relay antenna [20]	2	5.53	0.142 x 0.127 x 0.251	20.0
Additional C-band antenna [21]	2	0.08	0.051 x 0.045 x 0.010	10.0
Dish antenna HPLP1-11 [22]	1	7.70	0.280 x 0.280 x 0.094	50.0
VOR antenna	1	0.27	0.406 x 0.002 x 0.100	28.5
DME/TACAN antenna	1	0.09	0.128 x 0.040 x 0.078	50.0
MB antenna	1	0.27	0.055 x 0.055 x 0.015	10.0
ADF antenna	1	1.20	0.265 x 0.192 x 0.024	16.2
Wiring factor	1	1.1	1.1	1.0
Total:	**31**	**39.1 kg**		**1188 Watt**

5.6. PAYLOAD & AVIONICS INTEGRATION

It is important to determine not only the weight of the payload & avionics and the power that is needed, but also the dimensions, so that all payload & avionics can be fit inside the fuselage. This means that if some subsystems are large, they can be driving in the fuselage design. Therefore, in this section the dimensions of all payload & avionics are analysed and it is determined whether the subsystems need to be accounted for in the design of the fuselage.

Proper antenna placement is one of the key means to ensure the correctness of the validation measurements. On the TUD/NLR Cessna Citation II, in total ten antennas are installed for flight inspection purposes: two LOC/VOR antennas, two GS antennas, one DME/TACAN antenna, one Marker antenna, one ADF antenna, one GPS antenna, one VHF antenna for communications, and one UHF antenna for the reception of DGPS signals [10]. However, it was described before that the LOC/VOR and GS antennas may be combined into one single device, while the DME/TACAN antenna may also be used for receiving GBAS signals. Therefore, the total number of antennas can be reduced by two.

The VOR/LOC/GS antennas must be positioned at the top or front of the fuselage, as well as on the upper side of the vertical tailplane. It is of key importance here that the antennas are not positioned in the proximity of the engine and are kept away from surfaces having large curvatures [23]. Antennas that must be positioned on the bottom side of the vehicle include those for DME/TACAN, marker beacon and ADF. This also applies to telemetry antennas, which must have a direct view to the ground.

Special attention must be paid to GPS antennas. Although only a single example is installed on the TUD/NLR Cessna Citation II, it is described by Heinke and Feuerle [12] that a second GPS antenna must be installed when conducting flight inspections of GBAS procedures. This additional antenna must be downward looking and therefore mounted on the bottom side of the aircraft, such that it can register the signal interference from the ground. Accordingly, Heinke and Feuerle describe that a second GPS receiver may be installed for redundancy purposes. All other payload elements, including the remaining avionics, the DAU/SPU and the measurement telemetry system, may be singly installed. Again, this only applies to those systems that are part

[23] `https://www.cobham.com/media/5045/antennainstallationguide.pdf` [cited 16 May 2016]

of the NavAid calibration payload, and not to flight-critical systems. The payload avionics and DAU/SPU may be installed on any convenient location in the aircraft, as long as the experienced vibration levels and signal loss are minimised. The telemetry antenna must be positioned at the bottom of the aircraft to minimise signal interference from the vehicle. In fact, this is similar to the position of the VHF communication antenna on the TUD/NLR Cessna Citation II.

5.7. COMMUNICATION FLOW

A communication flow is an important tool to visualise the different subsystems and their communication links inside the aircraft. The communication flow diagram is displayed in Figure 5.7. As can be seen, the signals that are received by the antennas are first sent to their respective receivers. Subsequently, all data is processed and sent to the DAU. From here on, the data flows to the CPU, where also all other measured data and transponder data is sent to. This is the core of the UAV system, since all data is processed here. From here on, the UAV is controlled by determining the settings of the rudder, ailerons, elevator and engine. Next to all the internal data, the CPU also communicates with the ground station via modems and antennas. The CPU of the UAV is indirectly connected to the CPU of the GS. The CPU of the ground station processes all data obtained from the UAV and displays this in useful format to the operator, who observes, makes decisions and if necessary, inputs commands.

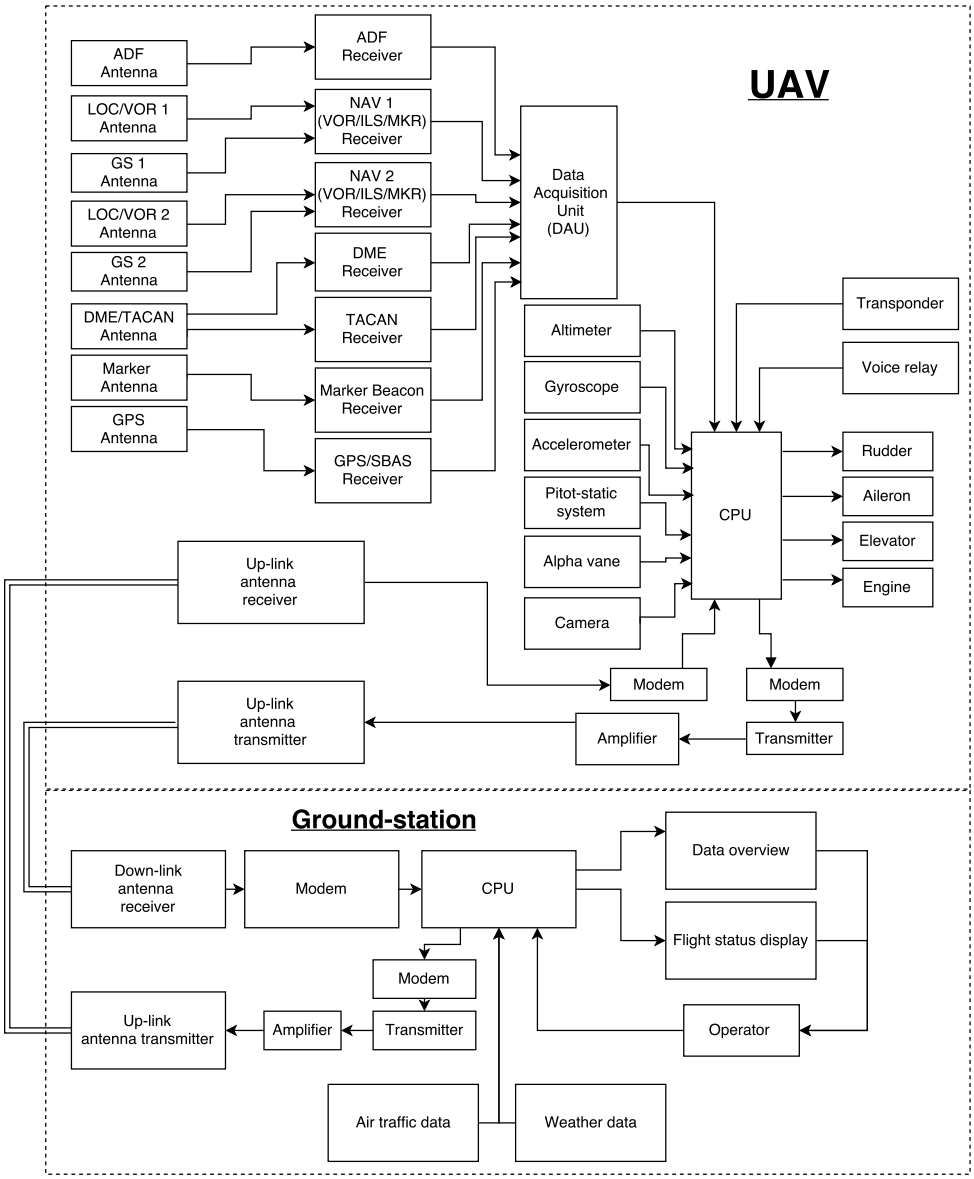

Figure 5.7: Communication flow diagram.

5.8. DATA HANDLING ARCHITECTURE

Next to the communication flow diagram, a data handling architecture is created to show the different flows within the aircraft subsystems. The data handling architecture shows the different data flows and the required data rates which are influenced by the frequency and data size. The data handling diagram is displayed in Figure 5.8.

From the data handling diagram, it can be seen that the maximum down-link data rate is equal to 6 Mbit/s, while the maximum up-link data rate equals 1.5 Mbit/s. This large difference mainly comes from the live video down-link. Furthermore, it can be seen that the CPU of the UAV consists of four systems; the flight management computer, health monitoring unit, sensor pack and a data bus. These systems are all interconnected.

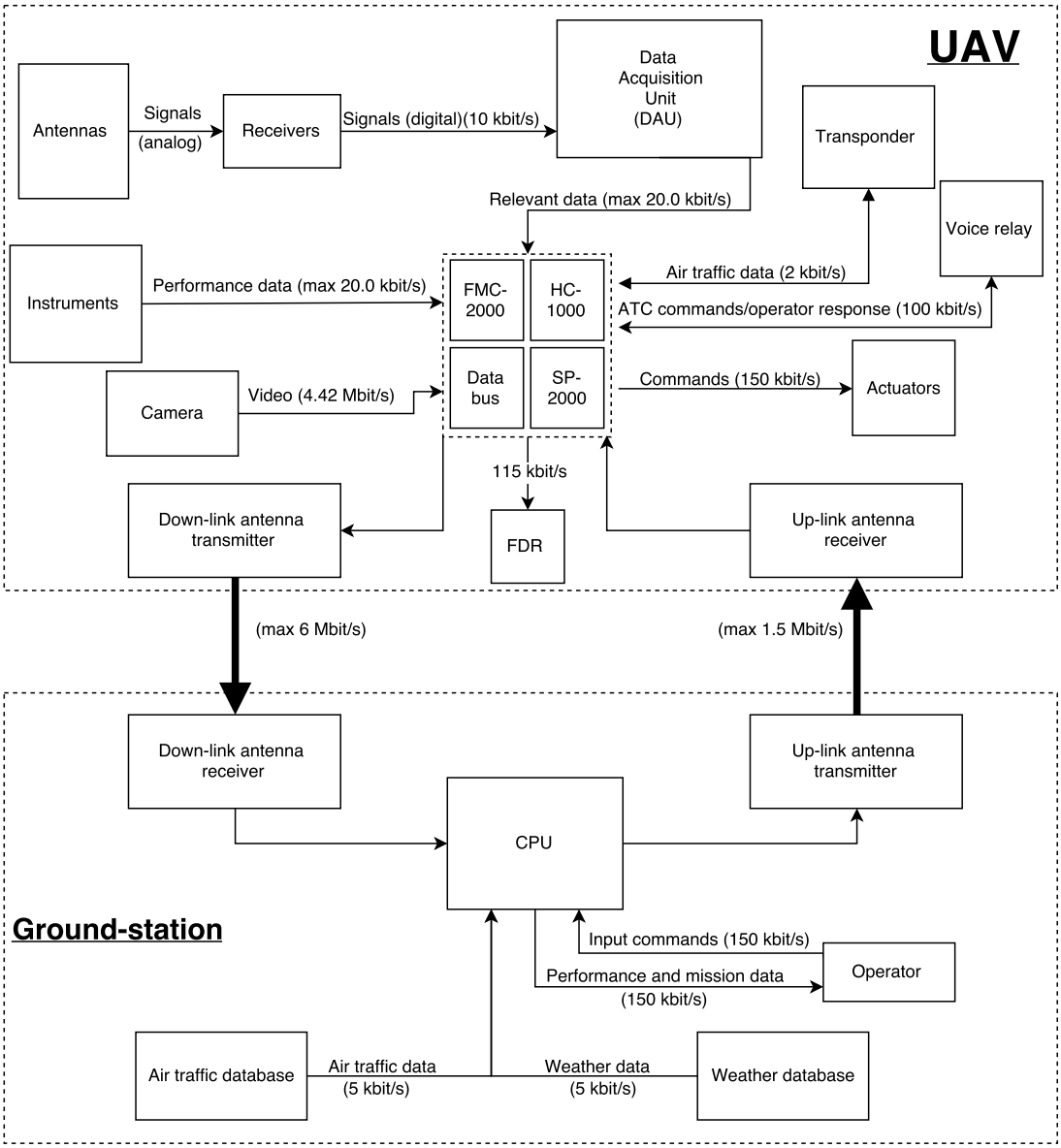

Figure 5.8: Data handling diagram.

5.9. VERIFICATION & VALIDATION

In addition to searching for specifications of individual payload elements, two examples of complete FIS systems, excluding antennas and operator console, were found for which relevant information could be obtained. These are shown in Table 5.10. The specifications were found from the websites of the respective manufacturers. The weight and size of these systems form a good benchmark to check the payload weight computed in Section 5.3.

Table 5.10: Specifications of example FIS systems, excluding antennas and operator console.

Type	Product name	Manufacturer	Size [L]	Mass [kg]
Operator console	AD-AFIS 130	Aerodata AG	400	42.5
Mobile FIS	Carnac MS	Safran Sagem	170	60

Only one tool has been used in the design of the payload & avionics subsystem. This tool calculated the link budget for satellite and line-of-sight communications. The tool can be verified by making use of known values from existing aircraft. In this case, the link budget of the General Atomics MQ-1 Predator [24] was used. Table 5.11 shows the link budget as calculated with the known values from the Predator. It can be seen that the tool calculates a signal-to-noise ratio just above 10 dB, which is the minimum required for a closed link between the UAV and the satellite. It would mean an optimal design (i.e. not over-designed) of the communication link of the Predator. The tool that has been used is therefore assumed to be correctly calculating the link budget.

Table 5.11: Link budget of the SATCOM between the General Atomics MQ-1 Predator and a geostationary satellite.

		SATCOM link	**UAV/SAT**			
Gains/power	Symbols	Values	dB	**Input parameters:**	Ku-band	
Transmitted power (W)	P_t	50	17.0	Frequency (GHz)	f	11.7
Transmitter antenna gain	G_t	n.a.	37.5	Distance between the transmitter and receiver (km)	d	36000
Wavelength of the carrier signal (m)	λ	0.0256	-	Energy per bit to noise power spectral density (dB) (BPSK, 10^-5)	E_b/N_0	10
Receiver antenna gain	G_r	n.a.	31.0	Modulation type (-)	R_{data}/B	0.5
Boltzmann's constant (J/K)	k	$1.38{\cdot}10^{-23}$	228.60	Bit Rate (bits/s)	R	$2.00{\cdot}10^{05}$
Losses	Symbols	Values	dB			
Receiving signal loss from the receiver antenna through the amplifier (-)	L_r	-	1.5			
Atmospheric loss	L_a	-	10.8	**Results**		
Signal loss through the transmitter antenna	L_t	-	1.5	Obtained SNR	17.2	
Antenna pointing loss	L_p	-	0.5	Required SNR	6.99	
Space loss	L_s	$3.21{\cdot}10^{-21}$	204.93	Net margin	10.2	
Ambient absolute temperature (K)	T	290.00	24.62			
Bit Rate (bits/s)	R	$2.00{\cdot}10^{05}$	53.01			

5.10. COMPLIANCE MATRIX

After the payload & avionics subsystem is determined and verification and validation is performed, the final design can be reviewed. The requirements the subsystem has to fulfil have been determined before in Section 5.2. The compliance with these requirements can now be checked. In order to do this, a compliance matrix is created in Table 5.12. This table shows the list of requirements for the payload & avionics subsystem again, along with a check for compliance and a comment explaining why a certain requirement is or is not fulfilled.

[24] `http://privat.bahnhof.se/wb907234/pics/specs.pdf` [cited 06 June 2016]

Table 5.12: Compliance matrix for the payload and avionics subsystem requirements.

ID	Requirement	Comp.	Comment
NVD-Syst-02	The system shall be able to navigate through Class A, B, C, D, E, F, G airspace.	✓	
NVD-Syst-02-01	The system shall be IFR certified.	✓	The design of the avionics was based on the FAA requirements for IFR flight.
NVD-Syst-02-02	The system shall be able to determine its flight path between two generic locations that are fixed in space.	✓	
NVD-Syst-02-02-01	The system shall have the adequate systems installed to compute its path through the air, independent of Class, using the information it extracts from its sensors.	✓	The path can be calculated by the autopilot installed in the FMC.
NVD-Syst-02-02-02	The system shall have access to a navigation database, from which navigation information can be extracted.	✓	The navigation database is installed in the FMC and updateable via the GS communications.
NVD-Syst-02-02-03	The system shall have real-time knowledge of the three-dimensional position of the airborne element.	✓	The (D)GPS antenna provides real-time knowledge of the aircraft's position.
NVD-Syst-02-02-04	At all times, the system shall have full knowledge about a destination for the airborne element.	✓	Multiple communication systems are installed for continuous contact between UAV and GS
NVD-Syst-08	The system shall enable for operations on the ground.	✓	
NVD-Syst-08-02	The system shall allow for ground support of the airborne element, in the form of system monitoring and maintenance.	✓	
NVD-Syst-08-02-01	The operator shall be able to monitor key system parameters from the ground system during all phases of the mission.	✓	The communication links enable constant monitoring of the key system parameters.
NVD-Syst-08-02-02	All system elements must be maintainable.	✓	Because of the use of COTS components, the system is easily maintainable
NVD-Syst-08-04	The system shall have a set-up time of no longer than 1 hour.	**?**	This can not be guaranteed at this stage of the design. However, it can be assumed that it is possible.
NVD-Syst-08-05	The payload shall be readily accessible.	✓	This is enabled by the integration of the payload in the fuselage.
NVD-Syst-09	The system shall comply with all technical constraints.	✓	
NVD-Syst-09-02	The airborne element shall be able to operate in diverse environments.	✓	
NVD-Syst-09-02-02	The airborne element shall be operable under all temperatures ranging from -30 degrees to +50 degrees Celsius.	✓	All chosen components are certified to operate at these temperatures.
NVD-Syst-09-02-03	At all times during the mission, the system shall have access to weather reports.	✓	Weather updates can be communicated to the UAV through one of the communication links (LOS, SATCOM, C-band)

6 Weight Estimation

In aircraft design the weight estimation is determinative for the budgeting in component design, the wing design of the aircraft, the stability and controllability characteristics of the aircraft and all other design steps. In this section the Class II weight estimation is explained. The methodology and verification is discussed. At last, the results of the estimation are given and compared with the requirements.

6.1. Functional Analysis

In order to start with the establishment of the tool, the functional analysis has to be done, to make sure all requirements will be fulfilled by the estimation. As most of the designed components are based on the Functional Breakdown Structure (FBS), the weight is based on technical constraints. Those constraints do not influence functions directly, however they limit the design, mostly determined by stakeholders.

6.2. Requirements

Only one requirement determined in the Baseline report [3] is used for the weight estimation. With this requirement, the class I estimation was done, and is still leading for the class II estimation.

Table 6.1: Requirements for weight estimation [3].

ID	Requirement
NVD-Client-09-01-04	The airborne element shall have a maximum take-off mass less than 500 kg.

6.3. Weight Estimation Tool

In the concept design during the mid-term phase, a class I weight estimation had been done. [2] In this weight estimation reference aircraft were used to approximate the Operating Empty Weight (OEW). Using mission profile analysis, the fuel fractions could be estimated and so was the Maximum Fuel Weight (MFW). A Maximum Payload Weight (MPW) of $55kg$ was computed in the Mid-term Report [2], resulting in a Maximum Take-off Weight (MTOW) of $480kg$. This results are leading for the class II weight estimation, where there should be aimed for the same weights.

6.3.1. Methodology

For aircraft design, different weight estimation methods can be used. The Society of Allied Weight Engineers has multiple ways to estimate the component weights of different aircraft. [1] To be accurate in estimation, methods should not be combined. However, in this case there is no other choice because of lack of methods. In Gundlach [7] UAV design methods, a weight estimation for UAVs is described. However, this estimation method is based on sailplanes. The aspect ratio is far out of range of the reference aircraft. For this reason, all general UAV components were estimated by the Gundlach method, while the other components (mostly structural) are based on general aviation aircraft. For this estimation, the Raymer method is used. The following assumptions are used in the estimation:

- **General aviation weight estimation methods are used** for the design of the wing and fuselage. The effect of this is that mainly the fuselage weight will be different on the built aircraft.
- The **nacelle weight is zero** on the aircraft. Because the engine is fully integrated in the fuselage, a nacelle is not needed. The effect of the assumption is that there is no weight compensation for the air inlet of the engine.
- The **fuselage is not pressurised**. The payload does not need pressurisation and so the aircraft does not need a pressurised cabin. Depending on the estimation method, the estimation should therefore be reconsidered and assumed to be different from the assembled weight.
- The **electrical system weight** is equal to the battery weight.The weight contribution of the wiring is very low compared to the battery. The effect is that the estimated weight will be slightly lower.

The tool has the aerodynamic characteristics, class I weight estimation, propulsion characteristics and performance characteristics as input, used for computing the component weights. During the iterative process, new input values will be put in the tool, which than estimates new weight budgets, that are used for new aerodynamic design and stability and controllability analysis.

6.4. COMPLIANCE MATRIX

To verify the weight estimation with the requirements, a compliance matrix is used. For the weight estimation only one requirement has to be verified.

Table 6.2: Compliance matrix for the weight estimation requirements.

ID	Requirement	Compliance	Comment
NVD-Client-09-01-04	The airborne element shall have a maximum take-off mass less than $500kg$.	✓	The MTOW is estimated to be $484kg$.

[1] `https://www.sawe.org` [cited 1 June 2016]

7 AERODYNAMICS

In this chapter the aerodynamic analysis and design of the UAV is described. The wing design of the aircraft will play a major role at this stage of the design. Many other subsystems are influenced by its characteristics. Not only by the performance of the wings but also by the overall geometry of the wings. To start of with the design first a clear basis has to be set. First in the functional analysis the functions this subsystem has to perform are defined after which the requirements that are derived from these function are discussed. With the requirements and functions clearly stated, the wing design can take place. This will cover the largest part of this chapter.

7.1. FUNCTIONAL ANALYSIS

During this phase of the design, the aerodynamics department will focus on the function *perform flight* and especially the sub-function of *provide lift*. The perform flight function is shown in Figure 7.1. As can be seen this specific function is comprised out of several other functions that combined serve perform flight function. For aerodynamics the *provide lift* function is of main concern since it will drive the overall design of the aircraft to a large extent. The stability and control functions are closely related to the aerodynamics department, however, the aerodynamics involved for these functions will not lead to large changes in the overall design and is therefore not evaluated by aero during the preliminary design.

The functional flow diagram as shown in Figure 2.5 shows other functions that are related to the *provide lift* function. These include: lift-off, climb, fly (cruise) and land. These functions combined with other non-aero related function and constraints will set the requirements that have to be met by the aerodynamics department. These will be reviewed in the next section.

7.2. REQUIREMENTS

Most system requirements have already been generated during the baseline report [3] and are derivatives from the functions the system has to perform. Some of these requirements, such as the maximum recovery and launch distance, served as input for the matching plots that were generated during the concept development phase of the Mid Term Report [2]. The output of the matching plots determine the technical requirement the wings should comply with such that together with the other aircraft parameters the aircraft meets its performance requirements. These requirements together with applicable system requirements are shown in Table 7.1. The last three requirements are derived from the matching plots. For example, NVD-Syst-01-01-01 is a new requirement that is derived from the Mid term report where the decision was made that the UAV would feature a fixed wing configuration.

7.3. WING DESIGN

In this section the process to get to the wing design is described. This process is set up in such a way that it is applied in the iteration loop. This process is shown in Figure 7.2. As can be seen, the process includes 4 steps to

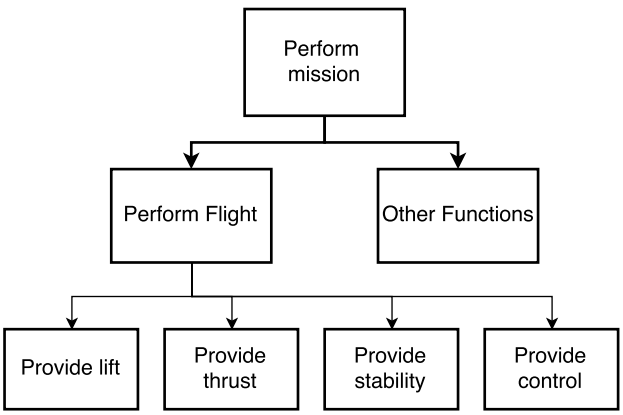

Figure 7.1: Perform flight function.

Table 7.1: Requirements to be monitored and complied with by the aerodynamics department.

ID	Requirements
NVD-Client-01	The system shall include an unmanned airborne element (UAV).
NVD-Syst-01-01	The UAV shall be aerodynamically efficient.
NVD-Syst-01-01-01	The UAV shall feature a conventional fixed wing configuration
NVD-Syst-01-02	The airborne element of the system shall be able to lift-off from the ground surface.
NVD-Syst-01-03	The UAV shall be able to climb to cruise altitude within reasonable time.
NVD-Syst-01-05	The UAV shall be able to decent to recovery altitude.
NVD-Syst-08	The system shall enable for operations on the ground.
NVD-Client-08-01-02	The full system shall fit in a standard LD6 aviation container
NVD-client-09-01-01	The airborne element shall have cervice ceiling of at least 10,000 ft
NVD-client-09-01-02	The airborne element shall have a maximum speed of at least 200 knots
NVD-Syst-09-01-03	The airborne element shall have optimized performance for inspection speeds.
NVD-Syst-01-01-02	The UAV shall have a highest $C_{L_{max}}$ of at least 1.57
NVD-Syst-01-01-03	The UAV shall have a maximum wing loading of 726 N/m^2
NVD-Syst-09-01-03-01	The wings shall be designed so that the drag throughout a complete mission is minimized.

develop the wing. First the wing placement is considered and determined, this process stands very much alone from the other 3 steps and for the first iteration is based on literature study only. The second step is the airfoil selection, which is done in 2 trade-off steps one quantitative and one qualitative. Next the from the airfoil, the 3D wing can be sized where specific attention is given to drag reduction. After the finite wing is designed the high lift devices are sized if necessary to meet the $C_{L_{max}}$ requirement.

7.3.1. WING PLACEMENT

This section will describe the process to determine the vertical wing position with respect to the fuselage. At the current stage of the design, this design choice mainly influences the stability and control of the aircraft. However, later in the design the position will also influence aerodynamics and structure. This will become more clear in the following trade-off decision. First, the advantages and the disadvantages of the possible options will be reviewed. These pros and cons are derived from empirical data from literature since the available information of the current aircraft design at this stage is insufficient to choose a configuration. The trade-off process in then conducted based on the method of Saaty [18].

There are four main configurations distinguished in literature: the high wing, the low wing, the mid wing and the parasol wing [19].

HIGH WING

The high wing configuration features a wing on the top of the fuselage. Main advantages of high wing aircraft are [19]:

1. High accessibility to fuselage belly near to the ground. This makes loading and unloading of the payload system easier.
2. The wing allows for easier engine placement since the engine clearance from the ground is higher compared to lower wing configurations.
3. High wings facilitate the installation of tension struts to provide a load path from the wings to the fuselage. Struts in low wing aircraft are loaded in compression which is less weight efficient.
4. The dihedral effect is increased which makes the aircraft laterally more stable.
5. The wings produce more lift compared to mid- and low wing configurations.
6. Because of the previous reason, the stall speed also decreases.
7. The engines are less vulnerable to sand and other debris entering and damaging the engine and/or prop.
8. The aerodynamic shape of the fuselage belly can be smoother.
9. There is more space inside the fuselage for the payload.

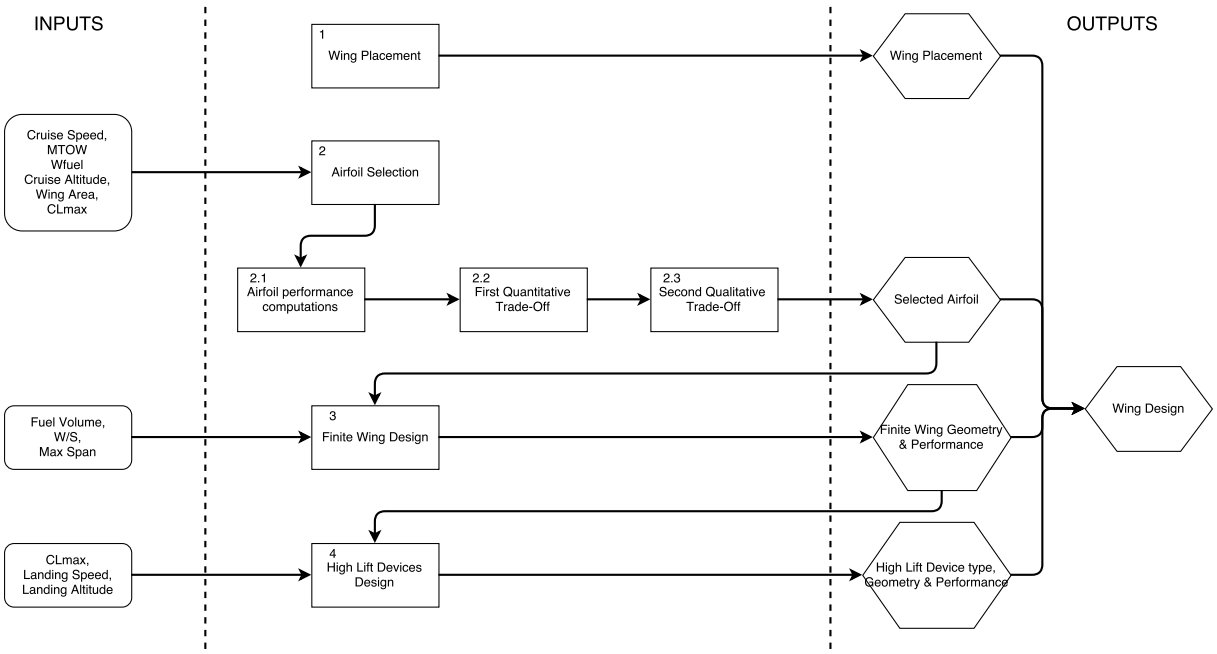

Figure 7.2: Wing design process.

Main disadvantages are[19]:

1. The aircraft tends to have a larger frontal area compared to mid-wing aircraft.
2. The ground effect during take off and landing is lower because larger ground clearance. This will increase the required take off and landing distance.
3. Landing gear may be heavier if it is connected to the wing.
4. If the landing gear is connected to the fuselage, the fuselage may have to be enlarged if there is opted for a retractable gear.
5. The wing produces more drag due to the higher lift coefficient compared to low- and mid wing aircraft.
6. The horizontal tail of high wing aircraft is generally about 20% larger than for other configurations because of the tail experiencing more downwash from the main wing
7. The structure is about 20 % heavier than other configurations
8. Gear retraction inside the wing is often not an option because of the long landing gear struts.
9. The aircraft is laterally more stable so less control able.

LOW WING

The low wing configuration features a wing that on the bottom of the fuselage. Main advantages for low wing aircraft are [19]:

1. Due to the ground effect, the take-off performance is better than high wing aircraft.
2. Gear retraction inside the wing is easier.
3. If the landing gear is connected to the wing, the landing gear struts are shorter and therefore lighter.
4. The total aircraft weight is lighter compared to high wing aircraft.
5. The aircraft frontal area is less.
6. Low wing aircraft produce less drag.
7. Less lateral stability
8. The tail can be sized smaller because there is less downwash from the wing on the tail.
9. The tail is lighter compared to a high wing configuration

Table 7.2: Overview of the pairwise comparison of wing configuration the trade-off criteria and their final weights.

	Stability	Control	Cost	Drag	Weight	Producibility	Operational	Sum	Weight factors
Stability	**1.00**	1.00	0.50	0.25	0.33	0.50	0.33	3.92	5.00%
Control	1.00	**1.00**	0.50	0.25	0.33	0.50	0.33	3.92	5.00%
Cost	2.00	2.00	**1.00**	0.20	0.50	1.00	0.33	7.03	9.00%
Drag	4.00	4.00	3.00	**1.00**	4.00	4.00	4.00	24.00	31.00%
Weight	3.00	3.00	2.00	0.25	**1.00**	2.00	0.20	11.45	15.00%
Producibility	2.00	2.00	1.00	0.25	0.50	**1.00**	0.20	6.95	9.00%
Operational	3.00	3.00	3.00	0.25	5.00	5.00	**1.00**	20.25	26.00%
							Total	77.52	

10. The wing drag produces a nose-down pitching moment which is longitudinally stabilising.

Main disadvantages are:

1. The wing generates less lift compared to high wing configurations, because the wing consist out of two different sections.
2. The wing has a higher stall speed because of the previous statement.
3. The wing has a lower contribution on the aircraft's dihedral effect so the aircraft is less laterally stable.

MID WING

For mid wing aircraft the aerodynamic characteristics stand somewhere in between the high wing and low wing aircraft. However, there are significant differences with respect to the wing structure and the fuselage space. Because the fuselage lies in the way of the wing, either the wings spars need to be cut in half or if the spar travels through the fuselage this will lead to occupied space of the fuselage that cannot be used for other storage. This will than either:

- Make the aircraft structure heavier, because of the wing root reinforcements where the wing intersects the with the fuselage and thus,
- More material is used, the aircraft structure will be more expensive.
- Or, the available space in the fuselage is decreased and so it cannot be used to store payload or other aircraft systems.

PARASOL WING

The parasol wing configuration shares a lot of the same advantages and disadvantages with high wing aircraft. The structure of parasol wings is generally larger and therefore heavier compared to high wing aircraft.

With the characteristics of the different configurations known, a trade-off procedure can take place comparing the configurations with each other within various criteria. These criteria include: stability, controllability, cost, drag, weight, producibility and operationability. Because some criteria are more important than others, they will get weights assigned during the trade-off. The determination of weight values is done via another table as can be seen in Table 7.2, in which a pairwise comparison is done between the criteria. The comparison is done by looking at the which criterion is more driving in the design of the overall aircraft.

During the trade-off, the four wing considerations that are under consideration are given scores from 1 to 4. Where 1 means that a configuration scores badly on a specific criterion and 4 means that it performs excellent in a specific criterion. The trade-off can be seen in Table 7.3.

Table 7.3 shows that the low wing configuration scores the highest and is therefore the winner of this trade-off. It is important to note that this trade-off is based on empirical data from literature because there is at this stage not enough information available from the design to make a decision based on calculations. During the iterations of the preliminary design, more information will become available which may causes this choice to be changed again.

7.3.2. AIRFOIL SELECTION

As can be seen from Figure 7.2 the airfoil selection is comprised out of 3 parts. First, the performance of the airfoil is computed in step 2.1. This includes calculation as for example the cruise design C_l, operating Reynolds number, Mach number etc. The second step, step 2.2, is were the quantitative characteristics of a large selection

Table 7.3: Wing position Trade-off.

Criteria	Weight (%)	High wing	Low wing	Mid-wing	Parasol wing
Stability	5.05%	3	2	3	3
Control	5.05%	3	4	3	3
Cost	9.07%	3	3	3	3
Drag	30.96%	2	4	3	2
Weight	14.77%	2	4	2	2
Producibility	8.97%	4	4	3	4
Operational	26.12%	4	2	3	3
Total score		0.3241	0.3703	0.3009	0.0047

Table 7.4: Flight Regime Characteristics.

	Alt [ft]	Alt [m]	TAS [kts]	TAS [m/s]	Re [-]	M [-]
FR 1	0	0	61	31.4	$1.5 \cdot 10^6$	0.092
FR 2	10000	3048	200	103	$6 \cdot 10^6$	0.31

of airfoils are evaluated and a trade-off is made based on these specific characteristics. These characteristics include for example the $\left(\frac{C_l^3}{C_d^2}\right)_{max}$ and the $\left(\frac{C_l}{C_d}\right)_{max}$. The third and last step of the airfoil selection process, step 2.3 is where the winners of the first trade-off are evaluated based on their qualitative characteristics. This includes for example the drag bucket dimensions and the manufacturability. Because these characteristics are difficult to determine via an automated computerised manner, this is done manually via visual inspection of the gathered data. This is why the first iteration step, 2.2 is introduced in the first place because it is impossible to compare around 300 airfoils with each other manually. The first trade-off thus serves as a filter that leaves only a limited number of airfoils to evaluate manually.

Before the step the airfoil selection process can be started some research has been done into airfoils for general aviation with emphasis on climb and turn performance. This resulted in a few airfoil series to be of primary importance. The series are the Eppler, NACA low speed airfoil series and 6 series. The majority of airfoils tested came from these series. In addition to these, the standard NACA 4 and 5 series were tested, as well as some other lesser known airfoils to a lesser extent. The airfoil coordinate data was retrieved from the University of Illinois Urbana-Champaign airfoil database[1]. 304 airfoils in total were processed using a MATLAB script with an interface with XFOIL[2].

AIRFOIL PERFORMANCE COMPUTATIONS

Before the evaluation of the airfoils can begin, the performance that they have to show and in which flight regime have to be determined. The flight regime is defined by the Mach numbers and Reynolds numbers at which the aircraft has to operate. The Mach numbers for the different phases of flight are computed using the international standard atmosphere together with the performance characteristics that are determined with the matching plots. The Reynolds number is also a function of the operating altitude and the chord length of the airfoil which has been determined in the matching plots as well. These flight regimes that are computed $FR1$ and $FR2$ are the limit cases for the mission profile. $FR1$ is the flight regime at an altitude of zero feet while flying a true airspeed of 61 kts. This situation occurs in the flight when the aircraft is in landing configuration and is coming in to land. The second flight manoeuvre that is evaluated, $FR2$, is when the aircraft is cruising at an altitude of 10,000 feet with a true airspeed of 200 kts. Table 7.4 shows the Reynolds and Mach number for both situations. It is important to note that in $FR2$, the Mach number is 0.31, meaning that the UAV is flying at the limit of what can be assumed to be incompressible flow.

The airfoil performance characteristics that are computed in this case are the cruise design C_l. and the $C_{l_{max}}$. Starting of with the cruise design C_l, this airfoil parameter is important during the two trade-offs when comparing the $\left(\frac{C_l}{C_d}\right)_{max}$ and drag bucket dimensions of different airfoils. The $C_{l_{cruise}}$ is computed in 3 steps. The first step is computing the aircraft C_{L_A}, next the wing C_{L_W} is computed after which in the third step the airfoil $C_{l_{cruise}}$ can be calculated. The C_{L_A} is computed with the use of Equation 7.1. This equation is derived from the equations of motions of the aircraft assuming steady and horizontal flight. This holds for cruise flight and is

[1] http://m-selig.ae.illinois.edu/ads/coord_database.html
[2] http://web.mit.edu/drela/Public/web/xfoil/

Table 7.5: Weights for 1^{st} trade-off.

	Cl^3 / Cd^2	Cl / Cd	C_m	Area	Structural stiffness	Sum	Weight factors
Cl^3 / Cd^2	1	0.5	7	3	6	17.5	35.0%
Cl / Cd	2	1	7	3	6	19	38.0%
C_m	0.14	0.14	1	0.5	0.33	2.1	4.2%
Area	0.33	0.33	2	1	0.33	4	8.0%
Structural stiffness	0.16	0.16	3	3	1	7.3	14.7%
					Total	49.9	

therefore used in the where the aircraft is flying at 10,000 ft at 200 KTAS. The weight $\bar{W}$ in this equation is the average gross weight of the aircraft during a flight. The gross weight of this aircraft is only dependend on the fuel burned during flight and the average can therefore be estimated with Equation 7.2. Where W_fuel is the weight of the total fuel capacity onboard the aircraft.

To get from the aircraft C_{L_A} to the wing C_{L_W} the lift force generated by the wing has to be corrected for the lift (either positive or negative) generated by other parts of the aircraft such as the horizontal tail surface and the fuselage. To correct for these effects Equation 7.3 by [19] can be used to determine the C_{L_W}. Equation 7.3 is method based on statistics and is therefore very useful if there is limited information available of the current design, however, after the first iteration loop, the components that generate effect have been properly sized. That means that for example the actual horizontal tail surface can be used to estimate the down force created by the tail as will be explained in Section 9.2.

The final step to get to the $C_{l_{cruise}}$ is to correct for the 3D effects of the wing. This is done via Equation 7.4 proposed by [19].

$$C_{L_A} = \frac{2\bar{W}}{\rho \cdot S \cdot V^2} \tag{7.1}$$

$$\bar{W} = \frac{2MTOW - W_{fuel}}{2} \tag{7.2}$$

$$C_{L_W} = \frac{C_{L_A}}{0.95} \tag{7.3}$$

$$C_{l_{cruise}} = \frac{C_{L_W}}{0.9} \tag{7.4}$$

The other airfoil performance characteristic, the $C_{l_{max}}$, is computed via a similar way. The only differences are that a stall speed of 61 KTAS is used in stead of 200 KTAS and that the MTOW is used in stead of the average gross weight.

1^{st} TRADE-OFF

As mentioned before the first trade-off serves as a filter to limit the airfoils to be reviewed manually in during the second trade-off and will shrink the number of airfoils under consideration from 304 to 15 airfoils. This involves looking at the relevant performance specifications of the airfoils for the mission profile and, in addition, determining the relevant magnitudes for the mission profile and the aircraft given the preliminary specifications.

Criteria & Weights

The criteria that are deemed to be important for the mission are the turning and climbing performance $\left(\frac{C_l^3}{C_d^2}\right)_{max}$ for ILS calibration performance and cruise performance $\left(\frac{C_l}{C_d}\right)_{max}$ for the VOR orbits at 20 NM. Other considerations that are considered relevant for the aircraft design are the structural stiffness of the profile (determined by the Steiner terms), the internal wing area for landing gear and fuel storage and to a lesser extent the moment coefficient of the profile which impacts the trim drag during cruise. These are all quantitative airfoil characteristics that can be automatically numerically determined using MATLAB.

Because not all criteria are equally as important, they should be weighted during the trade-off. The weights are determined using the analytical hierarchy process by Saaty. These weights were checked with the client and modified accordingly. This resulted in the weights in Table 7.5. The climb/turn and cruise performance are the most critical to mission performance, especially the cruise performance at maximum cruise speed as the power over weight ratio determined by the match plot is the most demanding requirement in the matching plot.

2^{nd} TRADE-OFF

The second trade-off was based on more qualitative traits of the 15 airfoils that were left from the first trade-off and took into consideration the $C_l - \alpha$ as a whole, the $C_l - C_d$ curve, the $C_{l_{max}}$ and the manufacturability of

Table 7.6: Weights for the 2^{nd} trade-off.

	$C_l - \alpha$	Manufacturability	$C_l - C_d$	$C_{l_{max}}$	Sum	Weight factors
$C_l - \alpha$	1	4	0.5	0.33	5.8	23.2%
Manufacturability	0.25	1	0.5	0.33	2.1	8.3%
$C_l - C_d$	2	2	1	5	10	39.8%
$C_{l_{max}}$	3	3	0.2	1	7.2	28.7%
				Total	25.1	

the airfoil. Taken into consideration during this analysis are also the different flight regimes $FR1$ and $FR2$ that were discussed in Subsection 7.3.2.

Criteria & Weights

The $C_{l_{max}}$ is one of the most important airfoil characteristic that will be evaluated during this trade-off. This specific airfoil attribute cannot be analysed by a program such as XFOIL and thus this has to be evaluated with the use of experimental data from literature such as [20] and [21]. Because the $C_{l_{max}}$ largely influences the stall speed of the aircraft, it is analysed at a Reynolds number from $FR1$.

It is however very well possible to analyse the lift curve in XFOIL up until the AoA where flow separation on the airfoil starts to take place. For this criterion the C_{l_α}, C_{l_0} and the α_0 are analysed in both $FR1$ and $FR2$.

Another airfoil attribute that can be assessed by XFOIL is the $C_l - C_d$ curve. This characteristic is used to see if the airfoil features a drag bucket and if so, what the specific dimensions are. The drag bucket is used to determine the efficiency of the aircraft during the various phases of the mission. The lower the C_d during the design C_ls the more efficient the wing is. When optimising for cruise, the $C_{l_{cruise}}$ should be located in the middle of the drag bucket where the airfoil shows the lowest drag ($C_{d_{min}}$). For example, the installation angle is generally chosen close to the optimum cruise angle of attack to minimise drag during this phase; however, if the lift-slope is small, relatively large rotation angles are required. This is a major consideration as the propulsion system is located in the rear of the aircraft and thus the propeller blades must maintain ground clearance during landing and take-off. Furthermore, the maximum lift-coefficient is important to determine whether high-lift devices are required to satisfy requirements and how much additional lift needs to be generated.

The last criterion that is assesed during the second trade-off is the manufacturabillity of the airfoil. Here the focus lies specifically on the trailing edge and how thin the trailing edge is and if the edge leads to a cusp. This characteristic is important for of course the manufacturability of the wing but also for the possibility to implement high lift devices to the trailing edge. This inspection is performeded visually.

Because not all criteria are equally as important, they should be weighted during the trade-off. The weights are determined using the analytical hierarchy process by Saaty. These weights were checked with the client and modified accordingly. This resulted in the weights in Table 7.6. The climb/turn and cruise performance are the most critical to mission performance, especially the cruise performance at maximum cruise speed as the power over weight ratio determined by the match plot is the most demanding requirement in the matching plot.

VERIFICATION & VALIDATION OF THE AIRFOIL SELECTION PROCEDURE

For the verification and the validation of the airfoil selection procedure, only the validation of the XFOIL program is considered. This is done by comparing experimental windtunnel data from eppler [20] of the airfoil E953 (Figure 7.3) with XFOIL data (Figure 7.4) at the same Reynolds number, both in incompressible flow. As can be seen in both figures that the curves match nicely with the exception of the stall behaviour. The $C_l - \alpha$ in the experimental plot shows far at a much lower C_l than XFOIL does. This agrees with the disision that was made earlier to only rely on experimental data when looking at the $C_{l_{max}}$ and the α_{max}

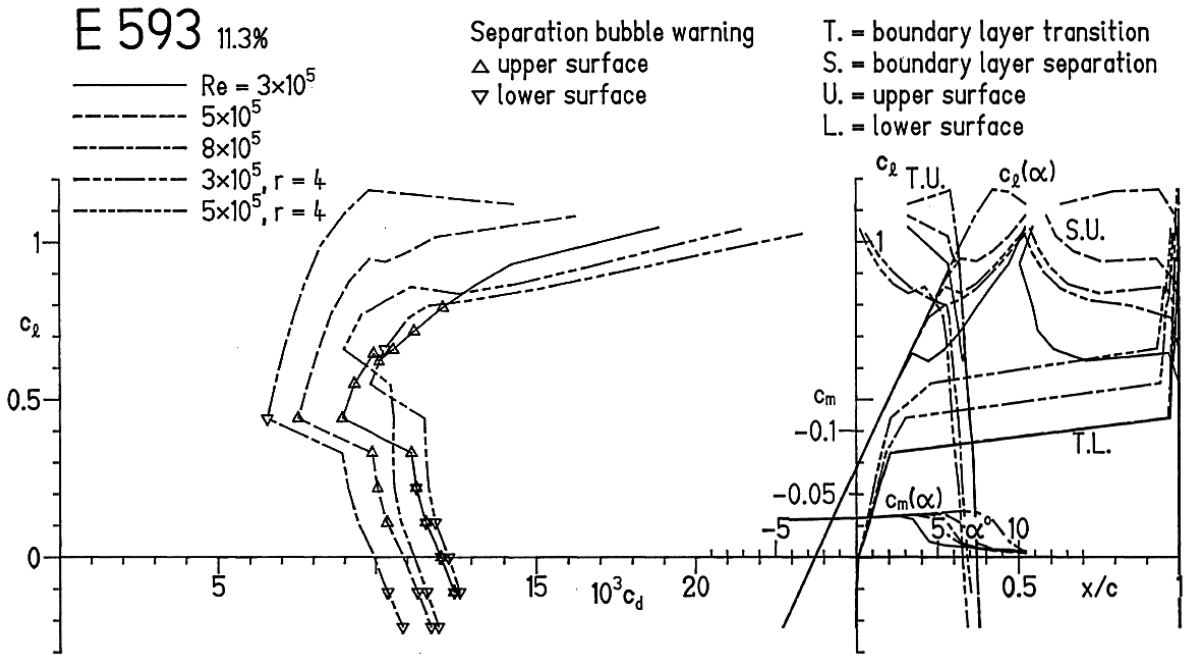

Figure 7.3: Experimental data of the E539 airfoil by Eppler [20].

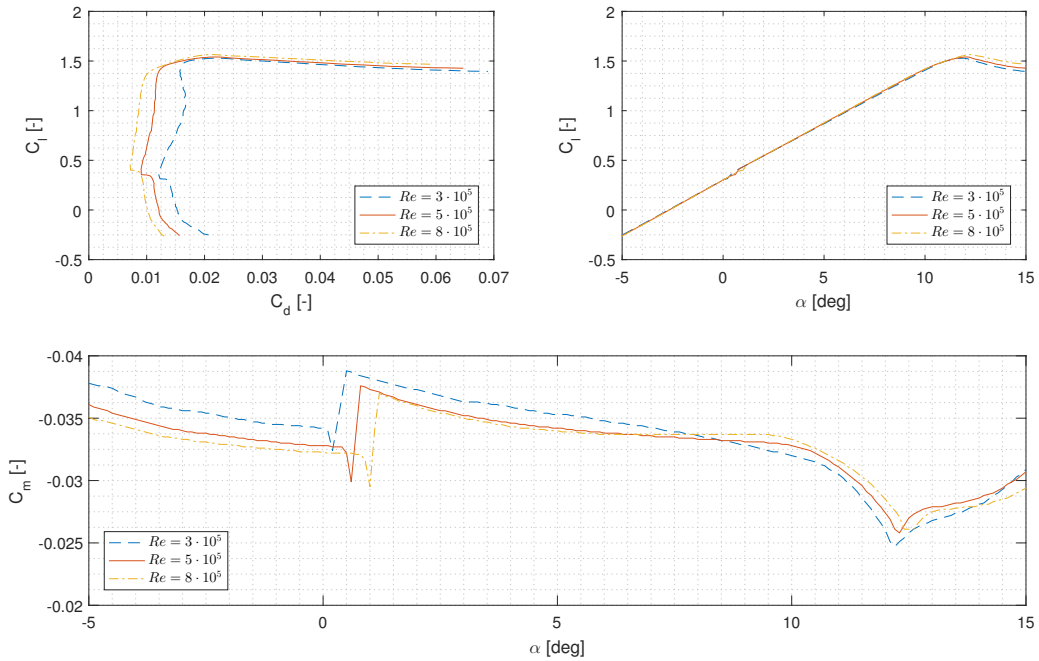

Figure 7.4: XFOIL results of the E539.

7.3.3. FINITE WING DESIGN

Subsequently to the selection of the airfoil the aerodynamic performance of the finite wing is analysed. This is necessary to evaluate the aerodynamic characteristics in more detail. Aerodynamic effects such as tip vortices can only be accessed in a three dimensional model. During that process the general planform of the wing is determined and optimised. The goal is to maximise the lift over drag of the wing while meeting several constrains, as shown in Equation 7.5 and Equation 7.6. Where V_{Fuel} is the fuel volume, $C_{L_{wing}}$ is the 3D wing lift coefficient, $\frac{W}{S}$ the wing loading and S is the wing area.

$$\max_{\bar{x}} f(\bar{x}) = \begin{cases} V_{Fuel} \geq k_1 \\ C_{L_{wing}} \geq k_2 \\ \frac{W}{S} \leq k_3 \\ S = k_4 \end{cases} \tag{7.5}$$

$$f(\bar{x}) = \left(\frac{L}{D}\right)_{wing} \tag{7.6}$$

$$\bar{x} = \begin{bmatrix} b \\ \Lambda \\ \Gamma_{LE} \\ c_{root} \\ \lambda \\ \alpha \end{bmatrix} \tag{7.7}$$

Where the k_1, k_2, k_3 and k_4 are constants derived from requirements or from previous computations. The independent variables are contained in the design vector $\bar{x}$, as in Equation 7.7. They define the general geometry of the wing.

The design vector lists the wing span b, dihedral Λ, leading edge sweep Γ_{LE}, root chord length c_{root}, taper ratio λ, and angle of attack α. As previously stated, the goal is to optimise the lift over drag of the wing. In fact, the wing should comply with the constrains, while generating sufficient lift to sustain cruise at minimum drag. The angle of attack is therefore included as parameter, to access the preferable cruise angle of attack. This information is then used to determine the wings incidence angle.

7.3.4. OBJECTIVE FUNCTION

To conduct any optimisation it is necessary to define the underlying objective function. In this case a function, which determines the aerodynamic characteristics of the wing, given its shape and surrounding as input. Generally high fidelity computational fluid dynamics methods are utilised to determine the primary aerodynamic forces of the wing. However these usually accompany high computational costs. Given the relative narrow time budget and restricted access to computational power, it is vital to select a fast and accurate model. Therefore it was chosen to implement a quasi-three-dimensional (Q3D) aerodynamic solver as developed by Mariens, Elham and Van Tooren [22] as underlying objective function.

7.3.5. DESIGN CONSTRAINS

Before conducting any optimisation it is important to define constrains in our design space, since the wing has to comply with more requirements besides its aerodynamic performance. Four major constrains as in Equation 7.5 are defined. The first constrain requires the wing design to meet a minimum fuel tank volume set by the propulsion and power department. For the computation of the fuel tank volume it is assumed that the fuel tank is accommodated between ten to sixty percent of the chord length, along the wing. The fuel tank volume V_{Fuel} is estimated as proposed by La Rocca[23]. The second constrain the wing has to meet is a minimum lift coefficient during cruise $C_{L_{wing}}$. This constrain is derived as proposed by Heinke and Feuerle[19], where the aircraft average mass during cruise dictates the required lift coefficient of the aircraft, which in turn yields the required lift coefficient of the wing. The constrains on a maximum wing loading $\frac{W}{S}$ and wing surface area S originate from the matching plots as discussed in Chapter 4. Additionally to the constrains defined in Equation 7.5, bounds on the design space are set. Bounds can originate from mathematical constrains to additional design requirements. For example the wingspan has a lower bound of zero, since a negative wingspan obviously can not exist . The upper bound for the wingspan is simply eight meters. This is due to the fact that the wing is required to fit in a LD6 container, as discussed in Chapter 14. The bounds for the other design parameters are set in a similar manner. Last but not least some 'simplification' of the design space is necessary. The wing is assumed to consist of one type of airfoil only. Furthermore the the twist angle is chosen to be zero. The main reason to restrict the design space is to reduce computational cost. Furthermore, parameters whose effect can not be described by the solver are constrained, such as the wing twist. It mainly affects the stall behaviour of the wing, which is not modelled by the solver. Therefore the complexity is reduced by excluding it from the design vector.

7.3.6. OPTIMISATION

Subsequently to setting up the objective function and its constrains, the objective function is implemented in an optimisation routine. It is chosen to apply a sequential quadratic programming (SQP) algorithm to determine local optima. The adoption of other optimisation algorithms such as local optima smoothing (LOC) would allow for the determination of the global optimum, but would require extensively more computational time. Furthermore the SQP algorithm is effective for large nonlinear engineering problems, as discussed by Yang[24]. The optimisation algorithm is developed using MATLAB. The code can be provided upon request.The objective function Q3D can be set to utilise a viscous or inviscid model. Ideally the optimisation is run employing the viscous model. However, due to limited time it was required to apply the inviscid model during the optimisation. Once the optimal design vector is acquired, a viscous aerodynamic evaluation of the wing is conducted, to acquire realistic aerodynamic characteristics of the wing. The main difference between the viscous

and the inviscid model, is found in the results for the drag coefficient. The consequences of using the inviscid model during the optimisation is discussed below.

7.3.7. VERIFICATION

Verification is necessary to ensure that the model is executed correctly and is able to provide plausible results. This is usually accomplished by comparing it to a simplified model. Methods such as Prandtls lifting line theory can be utilised to approximate the incompressible flow around a finite elliptical wing, as discussed in [25]. Equation 7.8, Equation 7.10 and Equation 7.9 describe the aerodynamic characteristics of a finite wing as a function of the wing planform and the aerodynamic characteristics of the two dimensional airfoil. They serve as the simplified model.

$$C_D = C_d + \frac{C_L^2}{\pi A R e_w} \tag{7.8}$$

$$\frac{dC_L}{d\alpha} = \frac{a_0}{1 + \frac{a_0}{\pi A R e_w}} \tag{7.9}$$

$$C_L = \alpha \frac{dC_L}{d\alpha} + C_{l_0} \tag{7.10}$$

$$e_w = 1.78(1 - 0.045 AR^{0.68}) - 0.64 \tag{7.11}$$

As test case an unswept, rectangular wing is chosen (with $AR = 6$) as well as a NACA0018 airfoil. The aerodynamic characteristics of the NACA0018 airfoil are determined using XFOIL. The span efficiency factor e_w is approximated using Equation 7.11, as suggested by [26].

Our simplified model for a three dimensional wing is acquired by substituting the two dimensional airfoil data into the previous equations. The same wing is analysed with the Q3D solver. Figure 7.5 illustrates the results of the simplified model, the Q3D solver, and the two dimensional airfoil data.

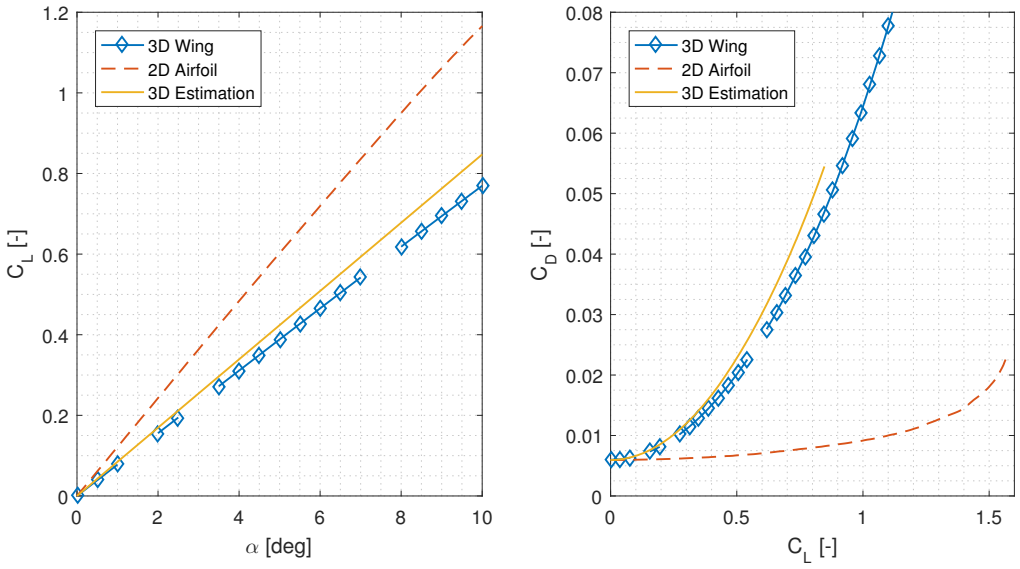

Figure 7.5: Aerodynamic polars; $M = 0.31$ and $Re = 6E6$.

The average error between the simplified model and the Q3D solver is 6%. Therefore the implementation of the Q3D solver is considered verified.

7.3.8. VALIDATION

To ensure that the results produced by the algorithm are representative of experimental results, the algorithm is validated. This is achieved by validating the underlying objective function. Unfortunately, it is difficult to conduct an independent validation of the Q3D solver. This is primarily because of the restricted access to experimental data of finite wings, and since the code of the Q3D solver is protected. However, a thorough validation of the Q3D solver has been conducted by [22], where the Q3D solver is validated for both subsonic and transonic regimes. This is achieved by comparing the results from the Q3D solver to results from a higher-fidelity solver named MATRICS-V, which is based on fully conservative full potential outer flow in quasi-simultaneous interaction with an integral boundary layer method on the wing. The MATRICS-V solver is a well established solver that has been validated by wind tunnel and flight test data [27]. In [22] the Q3D solver is compared to the MATRICS-V solver by using the Fokker 50 wing as test case. An negligible average error of one percent in

the total drag values is observed by [22]. Additionally the computational time needed for the subsonic regime is about eighty-nine percent lower. The superior computational time combined with accurate results makes Q3D the optimal objective function for this application.

7.3.9. HIGH-LIFT DEVICES

After the design of the full 3D wing the $C_{L_{max}}$ is checked at low speed and low altitude, i.e. $FR1$. This value is than compared to the required $C_{L_{max}}$ determined by the matching plots as explained in Table 4. If the $C_{L_{max}}$ matches the one from the matching plots, no high lift devices are needed. However, if the $C_{L_{max}}$ of the wing is less than required by the matching plots, high lift devices should be considered. Because it difficult to determine the $C_{L_{max}}$ of the wing from programs such as XFOIL and XFLR5, the DATCOM method is used to get from the $C_{l_{max}}$ of the airfoil to the $C_{L_{max}}$ of the 3D wing.

DETERMINE $C_{L_{max}}$ BASED ON THE AIRFOIL

The DATCOM method proposes 2 different approaches to get from the airfoil to the 3D wing. One for high and low aspect ratio wings. For high aspect ratio wings, the characteristics of the airfoils have stronger impact on the wing behaviour, than for low aspet ratio wings, where 3D effects are dominant [28]. To check whether the current 3D wing is a high or low aspect ratio wing, the following equation is used: Equation 7.12. Where C_1 is determined by using the plot shown in Figure 7.6. If the aspect ratio is higher than the right part of the inequality than the wing is a high aspect ratio wing and if it is lower than the the wing is a low aspect ratio wing. Where $\left[\frac{C_{L_{max}}}{C_{l_{max}}}\right]$ is determined via Figure 7.7 and $\Delta C_{L_{max}}$ is a term that accounts for the effect of Mach numbers higher than 0.2. But, because the $C_{L_{max}}$ when designing for high lift devices is evaluated at $FR1$ for landing and take off at a Mach number of 0.09 this correction term is set zero.

$$A > \frac{4}{(C_1 + 1) \cdot cos(\Lambda_{LE})} \tag{7.12}$$

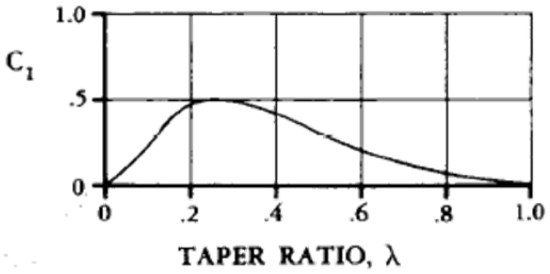

Figure 7.6: C_1 vs taper ratio [28].

If the wing has a high aspect ratio, the DATCOM methods suggests using the relationship as described in Equation 7.13. Where $\left[\frac{C_{L_{max}}}{C_{l_{max}}}\right]$ is determined via the plot shown in Figure 7.7 and $\Delta C_{L_{max}}$ is a term that accounts for the effect of Mach numbers higher than 0.2. But, because the $C_{L_{max}}$ when designing for high lift devices is evaluated at $FR1$, for landing and take off at a Mach number of 0.09, this correction term is set zero.

$$C_{L_{max}} = \left[\frac{C_{L_{max}}}{C_{l_{max}}}\right] \cdot C_{l_{max}} + \Delta C_{L_{max}} \tag{7.13}$$

For low aspect ratio wings Equation 7.14 is used. Where the $(C_{L_{max}})_{base}$ is determined from the plot shown in Figure 7.7. As with the high aspect ratio wing, the $\Delta C_{L_{max}}$ is set zero because the $C_{L_{max}}$ is only evaluated at $FR1$ which has a low Mach number.

$$C_{L_{max}} = (C_{L_{max}})_{base} + \Delta C_{L_{max}} \tag{7.14}$$

SIZING OF THE HIGH LIFT DEVICES

There are a lot of different types of high lift devices of which trailing edge flaps the most widely used. But still withing this specific familiy of high lift devices there are a lot of different types to choose from and a lot consideration to be made when choosing for a certain solution. The performance of HLDs usually goes up when

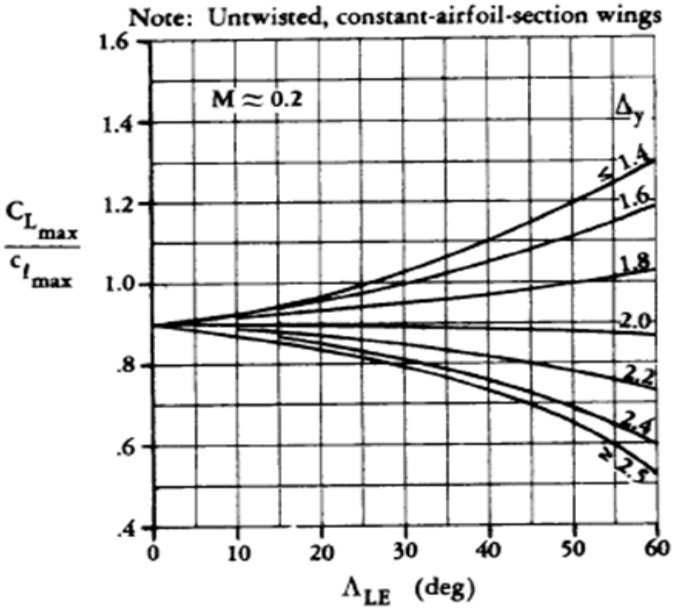

Figure 7.7: $\left[\frac{C_{Lmax}}{C_{l_{max}}}\right]$ vs Λ_{LE}[28].

complexity increases [19][28]. For example, when looking at a triple slotted flap vs a plain flap in Figure 7.8 to Figure 7.11, the amount of mechanisms and moving parts of the triple slotted flap system is larger than for the simple plain flap design. But a triple slotted flap system increases the wing area and the slots in between the flaps create a better flow that lowers the risk of flow separation when flying at higher angles of attack. Plain flap systems do not increase the wing area and also do not feature a slot to increase the quality of the flow over the flapped surface. This makes the plain flap often perform less with respect to aerodynamics, i.e. lower $\Delta C_{L_{max}}$ and $\Delta\alpha_{max}$, and higher Δ_{C_D}[28].

In the current design phase the computational capacity and aerodynamic knowledge is limited. This basically means that no advanced CFD software can be used other than XFOIL, XFLR5 etc. However, the analysis of the performance of more complex flap systems, requires more than these programs. This is why at this stage it is chosen that current design will feature a plan flap system, because of its simplicity when evaluating its performance. As mentioned before, plain flap systems do not show the best aerodynamic performance and the choice of choosing this system will make the results show a bit conservative [28], [19].

Since the C_{L_max} of the wing is now known the from Equation 7.14 or Equation 7.13 the difference, between this value and the $C_{L_{max}}$ that is required is known, the $\Delta C_{L_{max}}$. With this value known the size of the flap system can be determined as shown in Equation 7.15. In this equation S_{wf} is the effected wing area by the high lift devices, $\Delta C_{l_{max}}$ is the change in $C_{l_{max}}$ by applying full flap at a chosen hinge line, $\Lambda_{hingeline}$ is the local sweep at the hinge line of the flap. The parameters that can be changed to meet the certain $\Delta C_{Ll_{max}}$ are the hinge line and maximum deployment angle.

Figure 7.8: Triple slotted flap [28].

Figure 7.9: Plain flap [28].

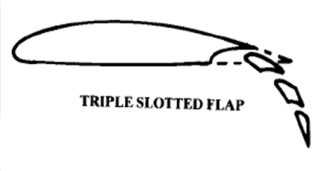

Figure 7.10: Triple slotted flap [28].

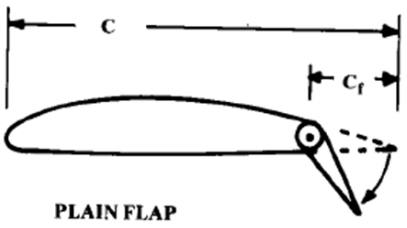

Figure 7.11: Plain flap [28].

$$S_{wf} = \frac{\Delta C_{L_{max}} \cdot S}{0.9\Delta C_{l_{max}} \cdot cos(\Lambda_{hingeline})} \tag{7.15}$$

7.3.10. AIRCRAFT AERODYNAMICS

The aircraft aerodynamics is modelled using the 2-term drag-polar representation (Equation 7.16). This has been selected as the minimum C_D for the wing does indeed occur at the point of zero-lift.

$$C_D = C_{D_0} + \frac{C_L^2}{\pi Ae} \tag{7.16}$$

$$C_{D_0} = \frac{S_w}{S_{ref}} \cdot C_{fe} \tag{7.17}$$

The first step is to determine the zero-lift drag of the aircraft, which is estimated using an empirical relationship relating the aircraft's wetted area to its skin-friction contribution. This approximation is reasonable for low-speed subsonic aircraft as skin-friction drag is the governing contribution to this term. The empirical formulation is based on manned light single-engined aircraft which means that the estimation would be conservative as windows, for example, are not required. The empirical equation is given in Equation 7.17. The skin-friction coefficient used is 0.0055[26] and the reference surface area is that of the wing.

The next step is to estimate the aircraft's lift coefficient. This is calculated using two simultaneous equations involving the tail to determine the down-force or up-force generated by the tail. This allows for the tail's contribution to the aircraft's lift to be included. From the stability analysis, it is found that the tail must provide a down-force during cruise to counteract the moment caused by the lift of the wing about the centre of gravity. This translates to reduced aircraft lift compared to that of the wing on its own. Solving Equation 7.18 and Equation 7.19 simultaneously, the total lift due to the tail and the wing can be determined. The aircraft lift coefficient is then given by Equation 7.20.

$$W = L_w + L_h \tag{7.18}$$

$$0 = M_{ac} - L_w(x_{ac}) - L_h(x_h) + W(x_{cg}) \tag{7.19}$$

$$C_{L,aircraft} = \frac{L_w + L_h}{q \cdot S} \tag{7.20}$$

In actuality, the high-wing configuration locally increases the lift of the wing. This means that the tail-force required by the tail to counteract the moment generated by the lift during cruise would be larger. This local effect also has an impact on the fuselage aerodynamics; however, these impacts can only be analysed through a CFD simulation or experimental data. Furthermore, the pitching-moment contribution due to this interference is negligible as the wing is not very swept; however, effects due to sideslip will not be negligible.[29] In addition, the lift generated by the fuselage can be assumed to be the same as that generated by the wing section within the fuselage.[29] Finally, since the aircraft lift and drag has been calculated for static cases, the actual loads experienced by the tail will differ during dynamic loading.

In closing, all the unknowns in Equation 7.16 have been determined and an estimate for the aircraft lift and drag can now be made and can be seen in Figure 7.12.

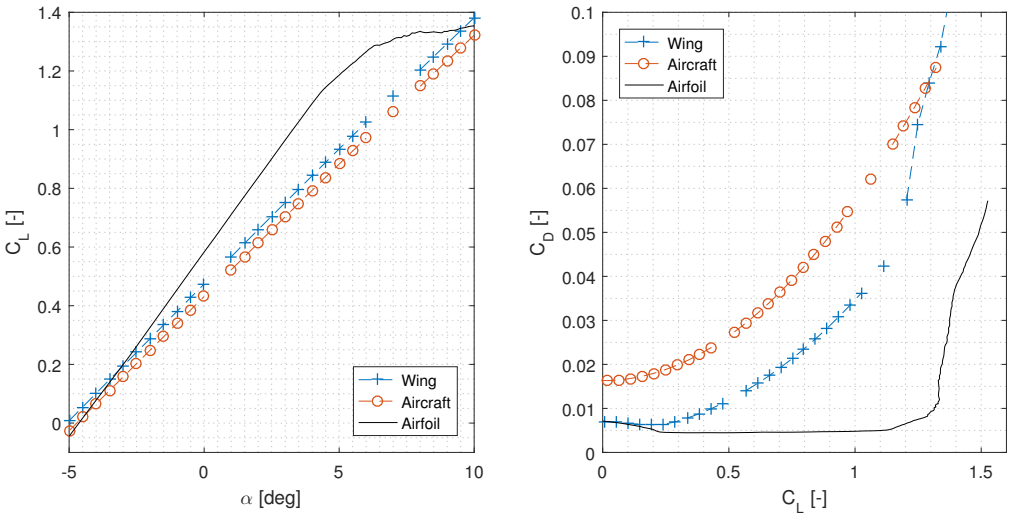

Figure 7.12: Drag polar for the aircraft including the tail contribution but excluding the fuselage.

7.3.11. COMPLIANCE MATRIX

Table 7.7: Compliance matrix for aerodynamic department.

ID	Requirements	Comp.	Comments
NVD-Client-01	The system shall include an unmanned airborne element (UAV).	✓	
NVD-Syst-01-01	The UAV shall be aerodynamically efficient.	✓	
NVD-Syst-01-01-01	The UAV shall feature a conventional fixed wing configuration	✓	
NVD-Syst-01-02	The airborne element of the system shall be able to lift-off from the ground surface.	✓	
NVD-Syst-01-03	The UAV shall be able to climb to cruise altitude within reasonable time.	✓	In fact the aircraft needs about 4.8 minutes to reach cruising altitude.
NVD-Syst-01-05	The UAV shall be able to decent to recovery altitude.	✓	
NVD-Syst-08	The system shall enable for operations on the ground.	✓	
NVD-Client-08-01-02	The full system shall fit in a standard LD6 aviation container	✓	Details about the transportation of the system is discussed in Section 14.2
NVD-client-09-01-01	The airborne element shall have service ceiling of at least 10 000 ft	✓	The actual service ceiling of the aircraft is 19 000 ft.
NVD-client-09-01-02	The airborne element shall have a maximum speed of at least 200 knots	✓	The maximum level speed at 10,000 feet is about 204 kts, as discussed in Chapter 11.
NVD-Syst-09-01-03	The airborne element shall have optimised performance for inspection speeds.	✓	
NVD-Syst-01-01-02	The UAV shall have a highest $C_{L_{max}}$ of at least 1.57	✓	
NVD-Syst-01-01-03	The UAV shall have a maximum wing loading of 789 $\frac{N}{m^2}$	✓	
NVD-Syst-09-01-03-01	The wings shall be designed so that the drag throughout a complete mission is minimised.	✓	

8 PROPULSION & POWER

In this chapter, the propulsion system of the UAV is chosen and the design process of the propeller is explained. The propulsion system is one of the most important parts of the UAV and must be chosen carefully. From the Mid-term Report [2], a piston fixed-wing aircraft was chosen, but it was decided to reperform the trade-off between a piston and turboprop engine. First, the functions and requirements relevant to the propulsion and power are discussed. Subsequently, the engine descriptions and trade-off is conducted, after which the propeller design process and initial result are presented. Finally, the power supply and the engine electric power system is explained.

8.1. ITERATIVE PROCESS

Aircraft design is a dynamic and iterative process. Therefore many of the assumptions mentioned in this chapter are mostly first estimates. Several iterations have been performed, which have refined these assumptions. When applicable, initial assumptions will be outlined during the chapter. Moreover, the iteration process for the entire aircraft with the final values for each department is presented in Chapter 4.

8.2. FUNCTIONAL ANALYSIS

Before a start can be made with the design of the power systems, a good understanding of the functions it should perform is required. In the Baseline Report [3], a complete functional breakdown is derived, of which the parts regarding Propulsion & Power are shown in Figure 8.1.

The major function the propulsion system should perform is to propel the aircraft. The biggest component of the energy taken on board will be expended on this. The other part is to provide electrical power for the payload and communication subsystems, which will be a much smaller component of the total energy. To provide propulsion an engine must be chosen that fits within the system, performs its functions sufficiently, and within financial and weight limits as specified by the requirements. In the Mid-term Report [2], it was determined that turbojet and turbofan engines are not viable options for this concept. Henceforth, the choice is between turbine-powered propellers and piston-powered propellers. The engines will also include an electrical generator, which will deliver electrical power to the subsystems.

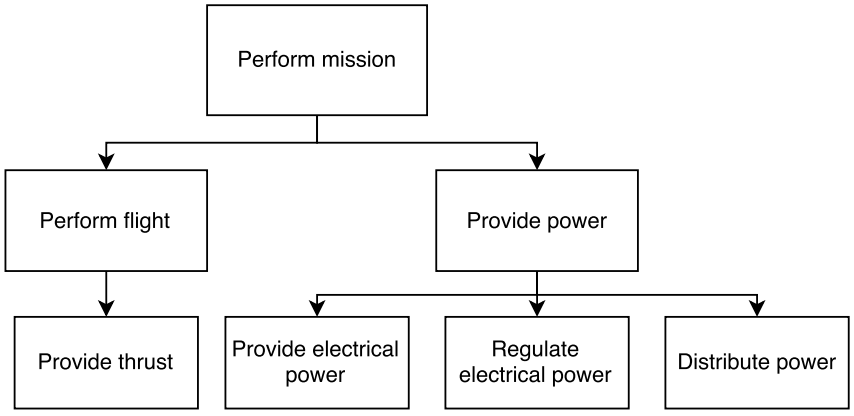

Figure 8.1: Functional Breakdown structure for Power and Propulsion.

8.3. REQUIREMENTS

The requirements listed in Table 8.1 are the requirements that apply to this particular subsystem from the complete list as presented in the Baseline Report [3].

Table 8.1: Requirements for the propulsion and power subsystem.

ID	Requirement
NVD-Syst-01-03	The UAV shall be able to climb to cruise altitude within reasonable time.
NVD-Syst-01-04	The UAV shall be able to maintain a constant altitude.
NVD-Syst-03	The full system shall be equipped with a power system that allows it to perform all mission actions.
NVD-Syst-03-01	The airborne element shall be equipped with a propulsion system that allows it to accelerate, in a controlled manner, to its maximum air speed.
NVD-Syst-03-02	The system shall be equipped with a power system that provides electrical power to all mission-related devices.
NVD-Syst-03-02-01	The power system on-board the airborne element shall generate sufficient electrical power, to allow the system to complete all mission-related actions.
NVD-Syst-03-02-02	Under all nominal flight conditions, the electrical power supply for all on-board systems shall be stable.
NVD-Syst-08-02-01	The operator shall be able to monitor key system parameters from the ground system during all phases of the mission.
NVD-Syst-08-02-02	All system elements must be maintainable.
NVD-Syst-08-02-02-01	The motor(s) of the airborne element shall be replaceable.
NVD-Syst-08-04	The system shall have a set-up time of no longer than 1 hour.
NVD-client-09-01-01	The airborne element shall have service ceiling of at least 10,000 ft
NVD-client-09-01-02	The airborne element shall have a maximum speed of at least 200 knots
NVD-client-09-01-04	The airborne element shall have a maximum take-off mass less than 500 kg.
NVD-client-09-01-05	The airborne element shall have a maximum range of more than 800 nm.
NVD-client-09-01-06	The airborne element shall have an endurance of at least 4 hours.
NVD-Syst-09-02-01	The airborne element shall be fit for ground operations on tarmac, grass and gravel.
NVD-Syst-09-02-02	The airborne element shall be operable under all temperatures ranging from -30 degrees to +50 degrees Celsius.
NVD-Syst-09-02-04	The system shall be able to operate in war zones.

8.4. COMPARISON OF PISTON & TURBOPROP ENGINES

To be able to conduct an engine trade-off, the characteristics of the engines must be discussed. It has been decided to only look into piston and turboprop engines as these are the most prevalent in general aviation at low-speed flight. Characteristics regarding altitude changes, speed changes, temperature changes, fuel consumption, pricing and noise are detailed in this section. The power estimate used here is the final estimated power from the mid-term report [2]. This is the starting point for the iterations. The final results of the iterations are presented in Chapter 4

8.4.1. SPECIFIC FUEL CONSUMPTION

The specific fuel consumption (SFC) of a power plant is an important parameter describing how well chemical energy is converted into mechanical energy. Within a certain group of power plants, the SFC range is small. However, between different types of engines there is a large difference. From chapter Chapter 4, the initial estimation for the required power for the UAV was determined to be 90.5 kW from the matching plot. From collected data, the specific fuel consumption of 4-stroke piston engines, around the 100 kW power range, are generally lower than that for turboprop engines. A piston engine in this power range has a typical SFC of 175-305 g/kWh. There is a very limited number of commercially available turboprops at this power rating. However, turboprops from 380-2000 kW have a SFC from 275-365 g/kWh according to Gudmundsson [30]. Therefore, depending on the chosen engines the SFC difference can be minimal. However, the SFC of a certain engine increases sharply with decreasing engine power [15]. This is assumed to be because of the difficulty of achieving high pressure ratios with smaller diameter engines. The PBS TP100 Turboprop engine[1] has a power of 180 kW with a SFC at max continuous power of 525 g/kWh, which when compared to piston engines is considerable worse [2]. Piston engines also have an increase in SFC with decreasing engine size due to reduced heat losses[3].

[1] http://www.pbsvb.com/customer-industries/aerospace/aircraft-engines/tp-100-turboprop-engine [cited 20 May 2016]

[2] http://www.pbsaerospace.com/getattachment/008208e0-be93-4e4f-af89-ccd7f663de80/TP-100-Turboprop-Engine.aspx [cited 23 May 2016]

[3] http://www.iitg.ernet.in/scifac/qip/public_html/cd_cell/chapters/uk_saha_internal_combustion_engine/qip-ice-05-engine%20efficiencies.pdf [cited 3 June 2016]

Although the SFC is dependent on altitude and velocity, the variation can be neglected for both piston and turboprop engines[4].

8.4.2. POWER-TO-WEIGHT RATIO

The power-to-weight ratio of a specific engine can assist in contrasting engines in the same category. It can also be used to contrast different types of engines. Table 8.2 shows the power-to-weight ratio of piston and turboprop engines from different sources. With an initial power requirement of 90.5 kW, as derived from the matching plots Chapter 4 the weight of the powertrain can be estimated. Table 8.3 shows the estimated powertrain mass based on the power-to-weight ratio and the estimated required power. The turboprop is advantageous as it in theory can be in the range from half to four times the weight of an equivalent piston engine.

Table 8.2: Power-to-weight ratio of piston and turboprop from different sources.

Engine	Gudmundsson[30]	Sadraey[19]	Gundlach [7]	Unit
Piston	0.82-1.64	1.1	-	kW/kg
Turboprop	3.78-4.44	4.11	3.45-4-77	kW/kg

Table 8.3: Estimated powertrain mass based on power-to-weight ratio.

Engine	Gudmundsson	Sadraey	Gundlach	Unit
Piston	55-110	82	-	kg
Turboprop	20-24	22	19-26	kg

8.4.3. AVAILABILITY

The availability of the piston and turboprop engines in the desired power class of around 90-105 kW class is also an important factor. Piston engines are available in sizes suitable for small radio controlled (RC) aircraft to large general aviation aircraft. Turboprops on the other hand are usually available from around 650 kW and up. As stated by Gundlach [7], perhaps the single greatest reason turboprops are not used in UAVs is the lack of engines in the desired power class. Therefore finding a commercial turboprop engine of around 100 kW with an estimated weight of around 25 kg, as shown in Subsection 8.4.2, is not possible. Table 8.4 shows collected data on piston and turboprop engines around the desired power class. There is, to the design teams knowledge, no commercially available turboprop smaller than the listed PBS TP100. This engine considerably exceeds the power required by the UAV while simultaneously weighing less than the piston options.

Table 8.4: List of piston and turboprop engines around the needed power class.

Engine	**Type**	**Dry weight [kg]**	**Power max. cont. [kW] (hp)**	**RPM**	**Gear ratio**	**BSFC [g/kWh] @ max cont. power**	**Dimensions (lxwxh) [m]**	**Volume [m^3]**
Rotax 914	Piston	75.5	74 (99)	5500	2.43	276	0.665x0.576x0.531	0.203
Rotax 912	Piston	69.4	69 (95)	5500	2.43	285	0.589x0.576x0.394	0.134
D-Motor LF39	Piston	78.0	90 (121)	3000		-	0.649x0.556x0.424	0.153
Hirth F-30ES	Piston	58.5	82 (110)	6200	Multiple	-	0.380x0.660x0.355	0.084
Jabiru 3300	Piston	81.0	79.8 (107)	2750	-	225	0.671x0.582x0.445	0.174
ULPower ul350iS	Piston	66.1	92 (123)	2800	-	288	0.553x0.736x0.472	0.192
Sauer S 2500 ULT	Piston	83.0	84 (114)	2700	-	148	0.550x0.780x0.500	0.215
Continental OI-240	Piston	108.9	93 (125)	2800	-	317	0.757x0.801x0.667	0.404
Continental IO-360-ES	Piston	138.4	157 (210)	2800	-	289	0.864x0.797x0.569	0.392
Lycoming O-235	Piston	113.0	93 (125)	2800	-	285	0.749x0.813x0.569	0.346
PBS TP100	Turboprop	61.6	160 (214)	2158	26.04	523	0.330x0.398x0.887	0.116

8.4.4. PRICE

Piston engines are easier to design and manufacture than the turboprop counterparts. Therefore the acquisition price of reciprocating engines is lower. However, due to the far fewer moving parts of the turboprop engines, as well as their smooth running nature, the TBO is longer for turboprop engines[5]: typically 1,500 to 2,000 hours for naturally-aspirated pistons, between 1,000 and 1,500 hours for turbocharged pistons, compared to

[4] `http://soliton.ae.gatech.edu/people/dschrage/AE3310/3310%20Chapter%203.pdf` [cited 3 June 2016]

[5] `http://www.shorelineaviation.net/news---events/bid/50442/Piston-Engine-Aircraft-vs-Turboprop-Engine-Aircraft` [cited 3 June 2016]

the 3,000 to 4,000 hours for turboprop engines.[31] For the engine purchase cost, a few piston engine prices are displayed in Table 8.5. No prices could be found for the TP100 turboprop, but it is expected to be considerably more expensive than the listed engines.

Table 8.5: Engine purchase prices.

D-Motor LF39	: 18 800 €
Rotax 914	: 25 350 €
Rotax 912	: 18 000 €
Hirth 30ES	: 9 000 €

8.4.5. TEMPERATURE EFFECTS

For a piston engine, the power increases with decreasing air temperature according to Equation 8.1.[30] The power increases because of the increase in air density with lower temperatures. "OAT" is the outside air temperature while "std" is the standard power and temperature as defined by ISA.

$$P = P_{std}\sqrt{\frac{T_{std}}{T_{OAT}}} \tag{8.1}$$

Turboprop engines have similar characteristics, but tend to be more sensitive to temperature variations than piston engines [32]

8.4.6. ALTITUDE EFFECTS

Piston engines and turbine engines might deal differently with altitude changes. The effect will be discussed in the next two parts.

PISTON PROPELLER

The power output of reciprocating engines depends on the amount of oxygen in the cylinder before combustion occurs. The amount of oxygen is directly related to the pressure and density inside the cylinder. That pressure and density are at the start of the compression stroke equal to the ambient pressure and density. As altitude increases, the density decreases resulting in a lower shaft power. To increase the power output, the pressure can be naturally or artificially increased: by using ram air pressure or by using a turbo- or supercharger. A simple relation between sea-level power and altitude power is given in Equation 8.2, where P is the power output, ρ the density and the subscript $_{SL}$ means at sea-level. The equation only holds for naturally-aspirated engines.

As an example, at 10 000 ft assuming P_{SL}=100 kW and a density of ρ = 0.9048. The power is 73.8 kW. That means that naturally-aspirated engines lose 26.1% power at the required cruise altitude of 10 000 ft.

Turbo-charging, turbo-normalisation and super-charging forces more air into the cylinders. Normalising turbos are meant to maintain the sea-level conditions up to higher altitudes, while turbo-charging and supercharging boosts the manifold pressure beyond the ambient sea-level pressure. Therefore, these systems diminish most of the altitude effects up to a certain design altitude, and reduces effects above that altitude.

$$P = P_{SL}\left(\frac{\rho}{\rho_{SL}}\right) \tag{8.2}$$

$$P = P_{SL}\left(\frac{\rho}{\rho_{SL}}\right)^{n} \tag{8.3}$$

TURBOPROP

The turboprop engine has a similar characteristic to the piston engine. Because of the decrease in air density the shaft power decreases with altitude. Using Equation 8.3, the power for the same scenario as the piston engine can be calculated to be 79.7 kW. n is taken to be 0.75 for the troposphere.[32]

Figure 8.2 quantitatively shows the effect of altitude on shaft power, thrust and SFC for a generic turboprop engine. The thrust will only be slightly affected by altitude while the SFC on the other hand will decrease slightly resulting in more fuel-efficient operations. However, the thrust and SFC can be approximated as constant [32].

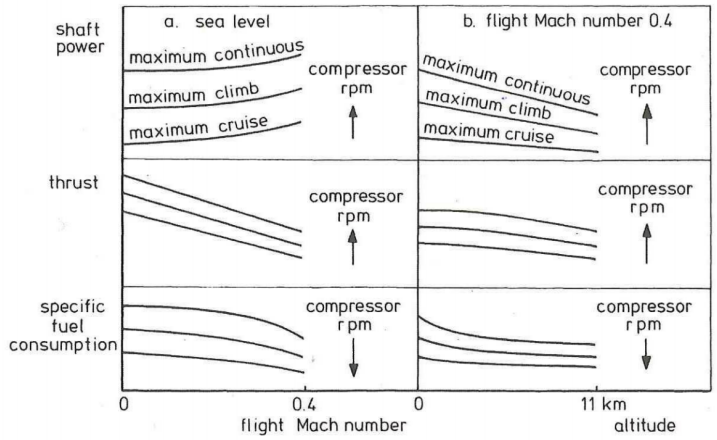

Figure 8.2: Speed and altitude effects on a turboprop engine [32].

8.4.7. SPEED EFFECTS

Piston Propeller The effects of velocity on the power output and SFC of a piston engine can be approximated as constant [30]. Power is a function of total volume displaced, mean effective pressure and RPM of the engine. Increasing the RPM increases the power output proportionally[6].

Turboprop From Figure 8.2, the SFC of a turboprop can be seen to have a slight improvement of SFC with velocity. It is therefore valid to approximate the SFC as constant with velocity. On the other hand the thrust can be seen to decrease linearly with increasing velocity. Lastly the shaft power has a slight increase in power with higher velocity, but can be assumed constant.

8.4.8. NOISE

The major source of noise in a piston engine is the movement of numerous parts, especially the reciprocating pistons. These vibrations can be reduced by some vibration-damping solutions, but it is still significant. Turbine engines make less machinery noise, due to the simple single-motion of the parts. The higher exhaust velocity of the turboprop also adds to the noise level, more so than a piston prop. A few ways to reduce propeller noise are to reduce the tip speed or reduce the pressure difference over the propeller. But overall, a turbine-powered aircraft is quieter than a piston-powered one.[31]

8.4.9. FUEL ESTIMATION

The power-to-weight ratio of a turboprop engine is considerably better than a piston engine. However, one must consider the entire weight of the propulsion system to be able to conduct a trade-off. The fuel weight is in that regard the most important factor to consider. The SFC of a turboprop can be comparable to a piston engine, but as presented in Subsection 8.4.1, the engine size has a large influence on the SFC. The only turboprop engine applicable for the intended mission is the PBS TP100[7], which has around twice the SFC than a piston engine in the desired power class. Therefore there is a possibility that the higher engine weight of the piston can be offset by a lower needed fuel weight. Therefore a fuel estimation simulation has been created to determine the fuel weight required to meet all the requirements. Only a basic simulation has been created for estimating the fuel. However, a detailed fuel estimation was later created for estimating the flight performance and is presented in Chapter 11

The fuel weight can be estimated from the SFC and power used over a certain time step. First, the fuel flow can be calculated (Equation 8.4) and, subsequently, the fuel used for the chosen time step (Equation 8.5. Here, P represents the power.

$$\Delta \dot{m}_{fuel} = SFC \times P \tag{8.4}$$

$$\Delta m_{fuel} = \Delta \dot{m}_{fuel} \times \Delta t \tag{8.5}$$

The total fuel can be calculated by summing the fuel used for each time step (Equation 8.6).

$$\sum_{t=0}^{t=final} = \Delta m_{fuel} \tag{8.6}$$

$$ROC = \frac{P_a - P_r}{W} \tag{8.7}$$

[6] http://soliton.ae.gatech.edu/people/dschrage/AE3310/3310%20Chapter%203.pdf [cited 3 June 2016]

[7] http://www.pbsaerospace.com/getattachment/008208e0-be93-4e4f-af89-ccd7f663de80/TP-100-Turboprop-Engine.aspx [cited 3 June 2016]

The power will be different for each flight phase and altitude. Three phases have been defined, a climb, a cruise and a descent phase. For the climb and decent phase, steady symmetric climb and descent is assumed, where the rate of climb (ROC) (or rate of descent, ROD) is defined in Equation 8.7. Assuming a constant ROC, the available power (P_a) can be solved for as a function of ROC and power required (p_r) shown in Equation 8.8. Where the power required is calculated from Equation 8.9.

$$P_a = ROC \times W + P_r \tag{8.8}$$

$$p_r = DV \tag{8.9}$$

For the cruise phase, a velocity of 200 knots is assumed, which is the requirement for the maximum cruise speed. The power used during cruise is therefore equal to the power required. Consequently, an estimation for the drag is needed. Assuming a parabolic lift-drag polar (Equation 8.10),ing that L=W during cruise and that $L = \frac{1}{2}\rho V^2 C_L S$, the final form of the drag can be calculated (Equation 8.11).

$$C_D = C_{D_0} + \frac{C_L^2}{\pi Ae} \tag{8.10}$$

$$D = C_{D_0}\frac{1}{2}\rho V^2 S + \frac{W^2}{\pi Ae \frac{1}{2}\rho V^2 S} \tag{8.11}$$

The initial values for the simulation are presented in Table 8.6. Be aware that the final values used are presented in Chapter 4 as many of these values depend on the iterations. The ROC and ROD will later be taken from the actual aircraft performance presented in Chapter 11. The rate of climb, rate of descent, climb velocity, descent velocity and base altitude are all estimated from the ILS mission profile presented in the Mid-term report [2]. The cruise altitude and velcoity are both taken from the requirements (NVD-client-09-01-01 and NVD-client-09-01-02). The Specific fuel consumption of 280 for piston engines and 523 for the PBS TP100 turboprop engine are estimated from Table 8.4.

Table 8.6: Parameters used for fuel estimation.

Parameter	**Value**	**Unit**
Mass (m)	450	kg
Specific fuel consumption (SFC)	280 & 523	$\frac{g}{kWh}$
Aspect ratio (AR)	10.88	-
Wing area (S)	5.885	m^2
Oswlad factor (e)	0.734	-
Zero-lift drag coeffcient C_{D_0}	0.015	-
Rate of climb (ROC)	14	$\frac{m}{s}$
Rate of descent (ROD)	-5	$\frac{m}{s}$
Cruise velocity (V_{cruise})	200	kts
Climb velocity (V_{climb})	150	kts
Descent velocity ($V_{descent}$)	165	kts
Cruise Duration (ILS Profile)	300	s
Base altitude	1 500	ft
Cruise altitude	10 000	ft
Propeller efficiency cruise ($\eta_{p_{cruise}}$)	0.82	-
Propeller efficiency climb ($\eta_{p_{climb}}$)	0.74	-

The fuel which is needed for the mission using a representative SFC for a piston engine and the PBS TP100 turboprop will be compared. The SFC for a representative piston engine is taken as 280 while for the turboprop a value of 523 is used. Two simplified mission profiles will be considered. The mission which is most fuel intensive will be used to size the fuel tank and therefore the maximum fuel which the UAV can carry. The mission profiles are presented in Figure 8.3 and Figure 8.4. Profile 1 (Figure 8.3) is a simplified ILS calibration profile similar to the profile presented in the mid-term report [2]. It consist of 15 climb, cruise, and descent cycles. The second profile is a cruise profile with only one climb, cruise and descent cycle. Table 8.7 shows the fuel mass and volume results for the two profiles. The total fuel mass is the calculated fuel mass with 5% of the MTOW added to account for reserve fuel. The total fuel volume is calculated using the total fuel mass. The tank volume adds 2% to the fuel volume to account for the thermal expansion of the fuel as mandated by FAR Part § 25.969 [8]. For the turboprop SFC the fuel is assumed to be JET A fuel and for the piston Avgas is used.

[8] `https://www.gpo.gov/fdsys/granule/CFR-1999-title14-vol1/CFR-1999-title14-vol1-sec25-969/content-detail.html` [cited 3 June 2016]

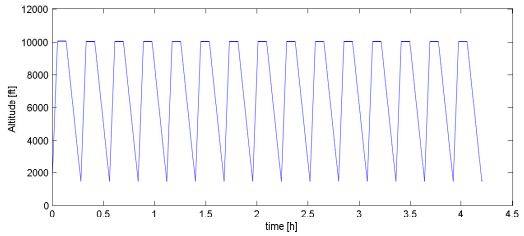

Figure 8.3: Profile 1: Simplified ILS flight profile.

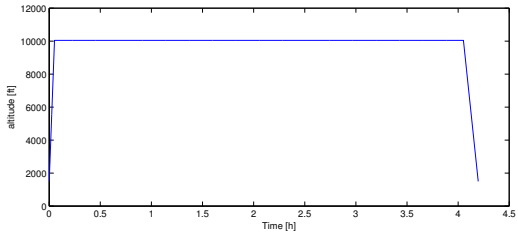

Figure 8.4: Profile 2: Cruise flight profile.

Table 8.7: Fuel mass and volume for different profiles.

	SFC [g/kWh]	Cal. fuel mass [kg]	Total fuel mass [kg]	Total fuel volume [L]	Tank volume [L]
Profile 1	280	50.80	73.30	102.09	104.13
	523	94.12	116.62	138.43	141.61
Profile 2	280	63.45	85.95	119.71	122.11
	523	117.93	140.43	167.17	170.52

Comparing the results it can be observed that the fuel mass for profile 2 is the more critical profile. This is be because the descent has a low fuel flow which offsets the higher fuel flow during climb. During the iteration phase the it was seen that profile 2 was still the most critical profile.

To compare the mass of a piston and turboprop both the fuel and engine mass have been taken into account. From Table 8.3 the estimated piston engine weight is taken as 82kg while the turboprop engine mass is 61.6kg from the PBS TP100. The combined fuel and engine mass for the piston is 167.95kg while the turboprop has a combined mass of 202.03kg. That is a difference of 34.08kg between the piston and turboprop.

8.5. ENGINE TYPE TRADE-OFF

Which kind of engine will power the propeller is not determined yet. After careful research in Section 8.4 a Trade-Off can be made. That is shown in this section.

As trading criteria are chosen: Noise, Initial cost, Maintenance cost, Engine weight, Total fuel weight and Operational cost. Most of them have been covered in the aforementioned section. Availability was of great concern to the design team, since there is only one turboprop engine available in the required size. The availability of piston engines however is much better. It is not included in the trade-off table however, because the only having one choice for a turboprop engine is considered a constraint.

In Table 8.8 the weight factors are shown. Fuel weight is the most important factor here, right after engine weight. These two factors determine a big part of the UAV weight, also influencing structural weight. Costs are all rated as medium important, and noise is of least concern. The main cause of that is that differences between turbo or piston engines are not very big, but still present (Subsection 8.4.8).

Since only two options, turboprop or pistonprop, are available, it was not possible to create a baseline. Therefore the two options are compared to each other, only defining which option is better in every category. The opposing option is then multiplied with -1.

The trade-off results can be found in Table 8.9, concluding that a piston engine as powerplant is the best option. Therefore this option is chosen.

As can be seen in Figure 8.5 a sensitivity analysis is done on the engine trade-off. As baseline the trade-off as shown in Table 8.9 is used. Then the weight of respectively Noise, Initial cost, Maintenance cost, Engine weight, Fuel weight and Operational cost are increased by one percent point, while the others are decreased by one

Table 8.8: The Trade-off weights.

	Noise	Initial cost	Maintenance cost	Engine weight	Total fuel weight	Operational cost	Sum	Weight factor
Noise	**1.0**	0.5	0.5	1.0	0.3	0.7	4.0	9.5%
Initial cost	2.0	**1.0**	1.0	0.5	0.3	0.5	5.3	12.7%
Maintenance cost	2.0	1.0	**1.0**	0.5	0.5	1.0	6.0	14.3%
Engine weight	1.0	2.0	2.0	**1.0**	1.0	1.0	8.0	19.1%
Total fuel weight	3.0	3.0	2.0	1.0	**1.0**	0.7	10.7	25.5%
Operational cost	1.5	2.0	1.0	1.0	1.4	**1.0**	7.9	18.8%
						Total	41.9	

Table 8.9: Weighted trade-off criteria.

	Noise	Initial cost	Maintenance cost	Engine weight	Total fuel weight	Availability	Sum
Turboprop	1	-1	1	1	-1	-1	
Pistonprop	-1	1	-1	-1	1	1	
Weighted Turboprop	0.095	-0.127	0.143	0.191	-0.255	-0.188	-0.142
Weighted Pistonprop	-0.095	0.127	-0.143	-0.191	0.255	0.188	0.142

fifth percent point. In the baseline a piston-prop is 14.2% better than a turboprop, and with increasing weight factors the difference increases between both choices regarding Operational cost, Fuel weight and Initial cost, but decreases the difference regarding Engine weight, Maintenance cost and Noise. As van be seen. With one percent change in the weight piston propeller still wins the trade-off.

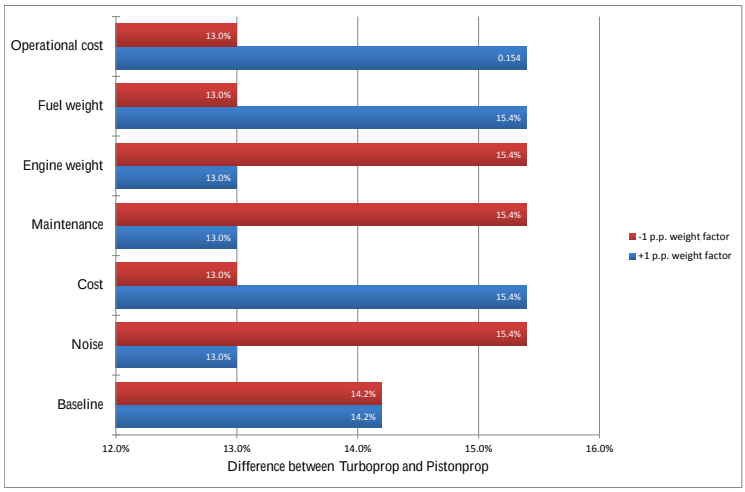

Figure 8.5: Sensitivity analysis of the engine trade-off.

8.6. PROPELLER DESIGN

To generate thrust a pusher propeller will be used. First the advantages and disadvantages of ducted propellers will be discussed. A first estimation of the propeller efficiency and diameter will be done by using the actuator disk propeller analysis method. Also a discussion about using ducted propeller is presented.

8.6.1. PROPELLER TYPE

The type of propeller is important for the performance of the UAV. With a piston engine there are several options for the type of propeller. The simplest one is the fixed-pitch propeller (FPP). They have propeller blades set at a constant, predefined fixed pitch. Their blade pitch can not be changed prior to flight or during flight. The propeller does not require any control input in flight. Rather, the engine RPM is changed to achieve more or less thrust. The propellers are designed to be the most efficient at one rotational and forward speed [17]. Therefore any deviations from the design point means less efficient operation. For example, the propeller used on the first few Spitfire Mk I's[33] was optimally designed for top speed only, which inherently meant very poor take-off and climb performance. These type of propellers are generally used in aircraft with low power, range, altitude or speed [17].

The other main type of propellers are variable-pitch propellers (VPP) and constant-speed propellers (CSP). These propellers can change their blade pitch for different flight phases, like the name variable-pitch tells. These propellers have a near constant efficiency for almost any part of the mission. A CSP also has variable-pitch blades, but blade changes are done automatically by a constant-speed unit (CSU), or propeller governor. The CSU is made to change the blade pitch in such a way that the propeller RPM remains constant. That can be done hydraulically or electro-mechanically. Three settings must can be controlled either by the pilot or the control system: the throttle (manifold pressure), desired RPM and fuel/air mixture. The RPM setting is connected to the governor, and if the engine can produce enough power, will keep the constant RPM. If more thrust is wanted the throttle is increased, which will try to increase the RPM of the engine, but the governor will then increase the propeller pitch. The increased pitch creates a larger torque on the propeller which will decrease the RPM to the desired value. The opposite hold true for a throttle down situation.

Although the variable and constant-pitch propellers have an improved performance they have also increased weight and cost as compared to the fixed-pitch propeller. The pitching mechanism is vulnerable to wear and tear and therefore also maintenance-intensive, adding to the maintenance costs.

A possible disadvantage of the FPP is either the reduced take-off and climb performance, or the reduced top speed. The requirement of having a maximum top speed of at least 200 kts with a low MTOW will result in a propeller which is designed for top speed.

An advantage of the CSP was that it reduces the pilots workload. However, in a UAV there is no pilot, so other measures has to be taken to control the pitch anyways.

Since the mission profile of the UAV both consist of repeated climbing as well as more typical cruising missions, there is no single phase where the propeller can be optimised ($\eta_{p,max}$). Therefore a constant-speed propeller will be used. As mentioned before, for changing the pitch angle an electrical or hydraulic system can be used. The hydraulic system is more expensive but for constant speed it seems to respond better to changes in RPM. This is why an hydraulic governor will be used. There is also no need to install a separate hydraulic system. The engine itself uses its own engine oil pressure to control the pitch of the blades.

8.6.2. DUCTED PROPELLER

Ducted propellers can be an interesting addition to the UAV. There are some possible improvements in terms of efficiency, noise and safety. However the potential performance increase may come with some downsides.

To make the decision to use, or not to use a ducted propeller, the advantages and disadvantages, retrieved from [34], are listed below.

Advantages

- Eliminates tip vortecies. As already mentioned, a propeller blade uses the same basic principle as a normal wing. In front (on top of the blade) of the blade there will arise a low pressure zone, while behind the propeller (under the blade) there will arise a high pressure zone. On a normal open propeller the high pressure will roll over the tip due to the pressure difference. This phenomenon will generate tip vortices and therefore also generate induced drag. The duct will prevent the pressure transition and for that reason also reduce the drag produced by this phenomena.

- When the propeller is spinning, it becomes invisible to the naked eye. When the UAV is on the ground and the propeller is spinning, ground crew need to realise not to come too close to the rotating propeller. If the propeller hits a crew member it can cause serious injuries of even death. Using a duct will reduce this risk and is thus an advantage related to safety. Another risk is a blade coming loose or braking off. Due to centrifugal forces the blade can fly far and can hit employees, other people or other items. Using a duct will potentially keep the propeller from flying away.
- Allows various acoustic treatments to absorb noise before spreading further from the aircraft. This can for example be done by a noise damping sandwich panels or via active noise cancellation.
- The duct itself has the shape of an airfoil, this will give a little bit extra lift/thrust. As the duct shape is offering improved static conditions and low speed thrust, the climb performance becomes better.

Disadvantages
To understand the disadvantages better, some equations are shown below. Equation 8.12 shows the propeller efficiency when also considering a duct [34].

$$\eta_p = \frac{\dot{m} \cdot \Delta V \cdot V_0}{\frac{1}{2} \cdot \dot{m} \cdot \Delta V \cdot (V_4 - V_0)} = \frac{2 \cdot V_0}{V_4 - V_0} \tag{8.12}$$

$$V_4 = \frac{T}{\dot{m}} + V_0 \tag{8.13}$$

$$V_0 = \frac{\dot{m}}{\rho \cdot A_0} \tag{8.14}$$

$$\eta_p = \frac{2 \cdot \dot{m}^2}{\rho \cdot A_0 \cdot T} \tag{8.15}$$

Where η_p is the combined propulsive efficiency, $\dot{m}$ the mass flow, V_0 the inlet speed, V_4 the exit speed, ΔV the change in velocity, T the thrust, ρ the density and A_0 the inlet area. When the three equations are combined, the equation is as follows:

- From Equation 8.15 it can be seen that for a fixed inlet area, there is only one optimum speed to get the the highest efficiency. This means that a duct only can be efficient for a certain velocity. If you do have a large speed range, the inlet and exit must be provided with variable area to get a satisfactory design, or in other words to keep the efficiency constant.
- If a variable area system is required a major drawback is the significant weight increase. The mechanical system will also be complex and difficult to design, adding to the overall cost of the system.

Although there are potential performance, noise and safety improvements with using a ducted propeller, there are also major disadvantages. Most importantly a variable inlet area which would be needed for the calibration mission as the there is no single speed which is typical for the mission. This complexity and added weight were too large factors to ignore in the decision and therefore a ducted fan will not be designed.

8.6.3. BLADE SHAPE

A propeller blade works exactly the same as a normal wing. The difference in air flow velocity before and behind the propeller will create thrust and torque (lift and drag in case of a wing).

The lift generated by the wing is dependant on the True airspeed (TAS), while the thrust generated by the propeller is dependent on the TAS of the aircraft and the rotational speed of the propeller. These two components combined is called "the total inflow". It is clear that the further a way from the centre, the higher the tangential velocity will be. The vectorial component of these velocities is the what the propeller sees. Due to air compressibility law's and aerodynamic forces reached at high velocities, the propeller diameter is limited. The maximum tip speed allowed (which is the maximum speed reached on the blade, normally on the blade tip) is dependant on the material which the propeller is constructed of, and is listed in Table 8.10.

Table 8.10: Tip speed limit for different propeller types [19].

Tip speed limit [m/s]	Propeller type
310	Metal high-performance prop
270	Metal regular prop
250	Composite prop
210	Wooden prop
150	Plastic prop for RC model aircraft

To work effectively, airfoils are set at a small angle of attack (AOA). The angle between the chord line and the plane of rotation is called the blade angle or pitch. The rotational velocity at the tip is higher then at the hub.

If the pitch would remain constant along the radius, the AOA would increase towards the tip. This will increase the probability of propeller stall and make the propeller work at an inefficient high AOA. To prevent this, the blades are twisted in such a way that the AOA remains constant.

8.6.4. PROPELLER POWER ABSORPTION

Propellers must be able to absorb the power from the engine, otherwise it will just spin faster with zero effect. To absorb the engine power, the airfoil surface needs to be increased. There are two ways to do this. One is to increase the diameter, which result in an efficient high aspect ratio. But it will increase the tip velocity as mentioned before.

The other solution of increasing the airfoil surface, is the increase in chord length. this method will reduce the aspect ratio and therefore also the efficiency. To create an efficient propeller which will not exceeds the tip speed limit and is able to absorb the engine power, extra blades can be installed.

8.6.5. CONCEPTIONAL PROPELLER DESIGN

To get a first estimate of the propeller efficiency some preliminary calculations are done. Some assumptions were made which are shown in Table 8.11. To estimate the drag during cruise Equation 8.11 is used with first iteration estimates of Table 8.6.

Table 8.11: Preliminary propeller design inputs.

Parameter	Value	Unit
Cruise speed (V)	200	[kts]
Propeller type	Metal regular propeller	[-]
Density (ρ)	1.07 (4500ft)	[kg/m^3]
Airframe drag	500	[N]
Propeller rotation speed	4500	[RPM]

All the following equations are based on the actuator disk propeller analysis method and were collected from [7]. In cruise, the thrust is assumed equal to drag. Thrust generated by the propeller can be calculated using Equation 8.16. Delta V is the velocity difference before and after the propeller and A_P is the propeller area (Equation 8.17) where D is the propeller diameter. For the preliminary design, the propeller diameter is calculated using the tip speed limit from Table 8.10 and the assumed rotational speed. Further in the design process the propeller diameter will be restricted because of landing gear and tail boom restrictions.

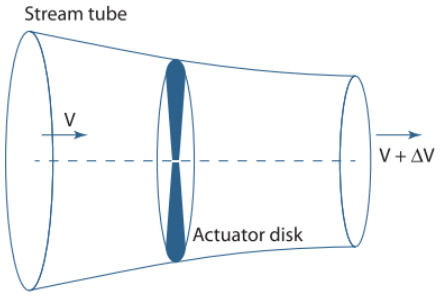

Figure 8.6: Propeller disk actuator flow properties.

$$T = \frac{1}{2}\rho \cdot A_p \cdot \Delta V \cdot (2V + \Delta V) \quad (8.16) \qquad A_p = \frac{\pi}{4} \cdot D^2 \quad (8.17)$$

Next the change in velocity before and after the propeller can be written (Equation 8.18).

$$\Delta V = V_e - V \quad (8.18) \qquad \Delta V = \sqrt{V^2 + \frac{2T}{\rho \cdot A_p}} - V \quad (8.19)$$

In this equation, V_e is the average velocity of the air acted upon by the propeller, far downstream. Equation 8.16 can be solved for the velocity difference (Equation 8.19).

Now the theoretical propeller efficiency can be calculated. Using actuator disk theory the ideal efficiency can be described by Equation 8.20.

$$\eta_{p_{ideal}} = \frac{2V}{V_e - V} = \frac{1}{\Delta V/2V + 1} \tag{8.20}$$

$$\eta_P = \eta_{p_{ideal}} \cdot \eta_{p_{nonideal}} \tag{8.21}$$

The ideal efficiency is computed iteratively by changing the diameter and setting the tip speed constrained at 270 m/s. In the actuator disk model, inescapable practical inefficiencies are neglected. To take these deficiency into account, a non-ideal efficiency factor is added. The total propeller efficiency can be written as follows:

The non-ideal efficiency varies form 85% to 95% based on comparisons with Blade Element Momentum (BEM) theory. For now, a nominal value of 90% is used.

The last parameter which is important for the propeller design is the shaft power. The relation between the shaft power and efficiency is shown in Equation 8.22.

$$\mathrm{P}_{\mathrm{Shaft}_{\mathrm{Prop}}} = \frac{P_{Thrust}}{\eta_p} = \frac{T \cdot V}{\eta_p} \tag{8.22}$$

$$\mathrm{P}_{\mathrm{Shaft}_{\mathrm{Prop}}} = \frac{T}{\eta_{p_{nonideal}}} \left(V + \frac{1}{2} \Delta V \right) \tag{8.23}$$

For this equation, the propeller efficiency is undefined when the free stream velocity is equal to zero. A more general form of the actuator disk model relating power to thrust is Equation 8.23.

If the shaft power for a static thrust case (V = 0) is needed, Equation 8.24 can be used.

$$\mathrm{P}_{\mathrm{Shaft}_{\mathrm{Prop}}} = \frac{T^{3/2}}{\sqrt{2\rho \cdot A_p} \cdot \eta_{p_{nonideal}}} \tag{8.24}$$

For the detailed design phase, propeller design program PorpCalc is used for the propeller design as explained in Subsection 8.6.6. Iterations has mainly been done in this section as part of the overall iterative design process of the UAV. The results of the preliminary propeller sizing is listed in Table 8.12

Table 8.12: Results of the preliminary design.

Parameter	Value	Unit
Diameter (D)	0.954	[m]
Propeller efficiency (η_p)	0.874	[-]
Shaft power cruise	58.9	[kW]

8.6.6. DETAILED PROPELLER DESIGN

As mentioned before, designing a propeller by hand is very difficult. This is basically caused due to different flow speed over the entire propeller radius. Figure 8.7 gives a good illustration of how the propeller design is done.

From aerodynamics, the power required over the hole mission is defined and stated in the flight preference chapter. Based on that power required a proper propeller configuration is selected with help of the PropCalc software[9]. In this software parameters such as propeller diameters, RPM, airfoil, chord thicknesses and blade angels on different percentages of the radius and pitch angles can be defined. The propeller diameter is defined based on the distance between the booms and the length of the landing gear and is set constant during the design process. From Table 8.10 the maximum tip speed is set to 270m/s and knowing the propeller radius the RPM has been defined.

Next, for different airfoils the maximum efficiency for the operational velocity range is investigated. Note that from Subsection 8.6.1 the decision was made to use a constant speed propeller, which means that the maximum efficiency is almost constant for almost the entire flight speed range.

When the blade configuration is determined the amount of blades has to be analysed. The amount of blades is dependent on the thrust that the propeller needs to develop. The larger the the blade area, the higher the thrust produced will be. Similar to a wing, the efficiency becomes higher with increased aspect ratio. The ideal blade shape would be an infinite long blade with zero chord length, but this is of course not possible. Therefore the solution will be to increase the chord to increase the area and thus increase in thrust. But as explained before, the aspect ratio becomes smaller meaning the propeller becomes less efficient. The final solution for increasing the total blade area and not decrease the aspect ratio is to add an extra blade.

[9] `http://www.drivecalc.de/PropCalc/PCHelp/Help.html` [cited 08 June 2016]

In Section 10.2 the final blade shape, the amount of blades and rotational speed (RPM) are presented.

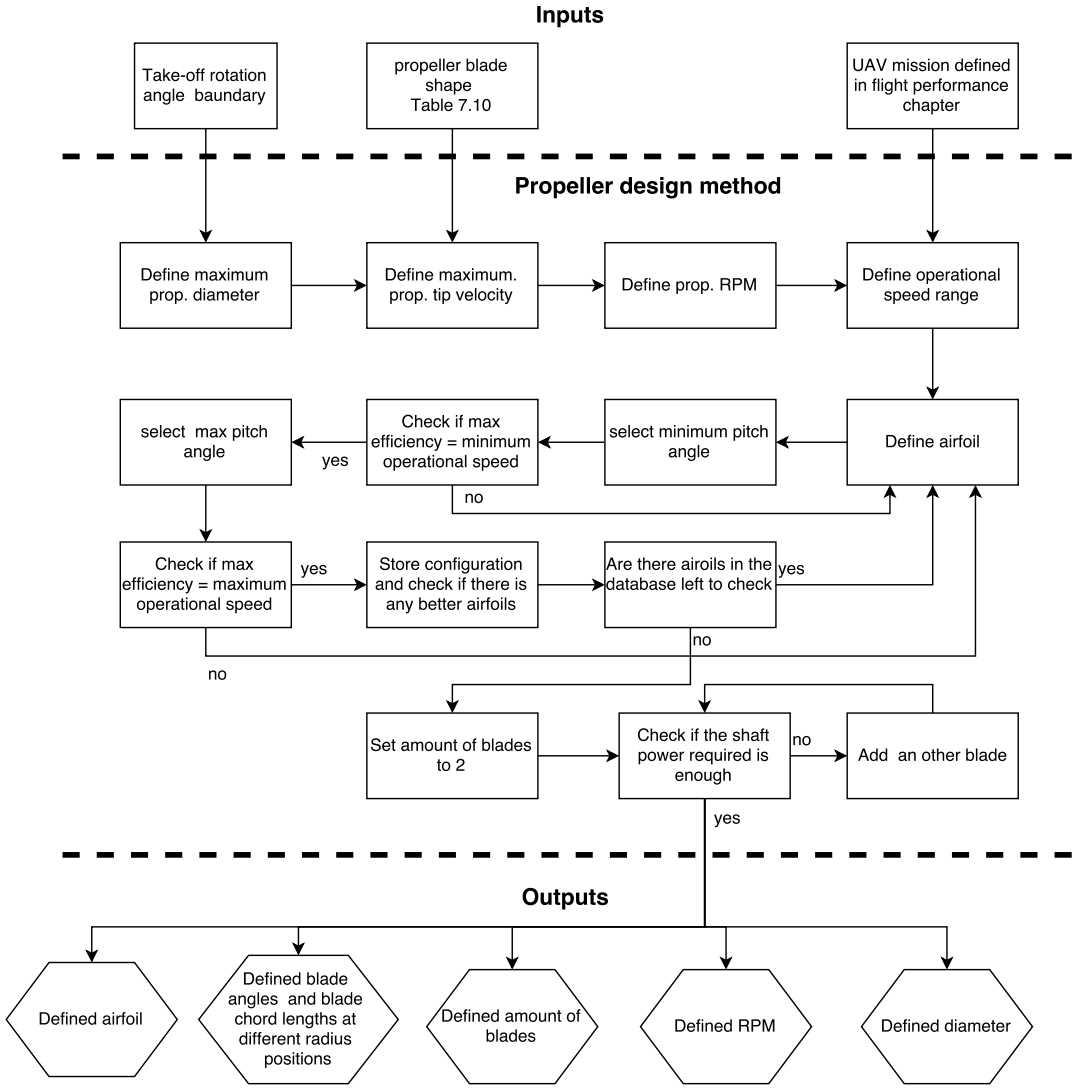

Figure 8.7: Propeller design iteration process.

8.7. AVIONICS AND PAYLOAD POWER SUPPLY

The payload needs power for the sensors, computers and antennas; the avionics also need power to operate. Therefore a power-supply is necessary. A few options are available: take the energy on board before the mission starts, or acquire the energy during the mission. The last solution might be done using e.g. solar cells, but the first option has more choices. Here a division can be made in energy converted during the mission, or stored electrical energy by means of some kind of capacitor.

In case of an engine-out situation the UAV must still be controllable. Therefore, in the design the choice was made to use both of last options: a battery is used, in combination with the generator power supply of the engine.

Most aircraft engines these days are already equipped with a generator or alternator of sufficient power to power the fuel pump, avionics, the payload and to charge the battery. The battery is used for engine starts, control in emergency situations and to flatten out temporary power fluctuations. As for the weight estimation a range of batteries is looked at from the manufacturer Concorde Battery Corporation.[10]

Following from the first estimations of the Payload & Avionics Department, during normal operations approximately 3 kW of power is needed for the operation of the payload and the avionics. Also power for flight control

[10] `http://www.concordebattery.com/aviationbattery.php` [cited 2 June 2016]

actuators, landing gear actuators and lights is needed. The engine's generator is powerful enough to supply power for these applications. However, during engine failure the generator will not provide any power anymore. During this event all mission-related systems are turned off. The battery in this case will provide power for all absolutely necessary flight systems to perform a safe landing. It is estimated that the battery has to provide 1.1 kW during half an hour. The approximate battery size and volume can be found in Table 8.13. These values are based on statistics[10]. Most aircraft battery suppliers have the option to choose between 12V and 24V battery systems. The 12V is estimated to be lighter and smaller for the same capacity. Therefore the 12V battery is chosen. A disadvantage is that for the same power the current is higher, therefore power cables might be a slightly thicker.

Table 8.13: Battery weight and size.

	12V	**24V**
Mass [kg]	19.6	21.9
Volume [L]	7.91	12.6

8.8. ELECTRIC POWER SYSTEM

The electrical power system has three main functions: generate power, store energy and distribute the power to all systems in the UAV. Power conversion can normally also be an important function, however all systems will use DC power and therefore conversion to and from DC and AC power is not necessary, after a single conversion from the engine's alternator AC to DC. Figure 8.8 shows the engine starter circuit and the UAV battery. The main bus distributes power to the engine components, landing gear motors, and control surface motors. The power comes from two sources, the battery and alternator. The alternator is part of the engine and can be used to power some components or charge the battery. A master switch on the ground station is used to separate the battery from the circuit using a solenoid (electromagnetic relay). An electric starter motor is needed for the engine. When a button is presses on the ground station a solenoid switches such that the motor can draw current from the battery. When the starter button is presses the power to the avionics is disconnected for the duration the motor starter is drawing a current from the battery. This is further explained in Subsection 5.5.2.

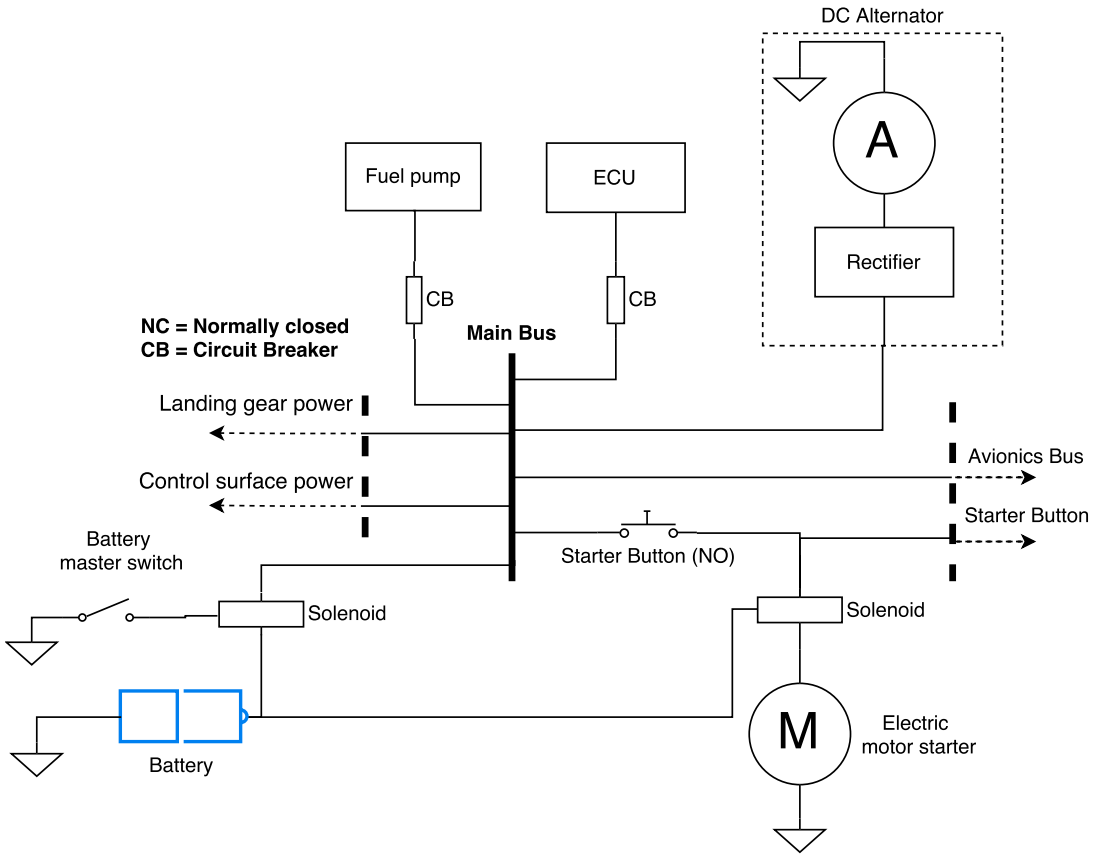

Figure 8.8: Electric starter circuit.

8.9. COMPLIANCE MATRIX

Table 8.14: Compliance matrix for the propulsion and power subsystem.

ID	Requirement	Comp.	Comment
NVD-Syst-01-03	The UAV shall be able to climb to cruise altitude within reasonable time.		
NVD-Syst-01-04	The UAV shall be able to maintain a constant altitude.	✓	The engine was chosen on power required for constant speed, constant altitude flight.
NVD-Syst-03	The full system shall be equipped with a power system that allows it to perform all mission actions.	✓	Electrical generator is also included, together with a battery.
NVD-Syst-03-01	The airborne element shall be equipped with a propulsion system that allows it to accelerate, in a controlled manner, to its maximum air speed.	✓	Combination of engine and control system.
NVD-Syst-03-02	The system shall be equipped with a power system that provides electrical power to all mission-related devices.	✓	Engine-integrated generator with sufficient capacity.
NVD-Syst-03-02-01	The power system on-board the airborne element shall generate sufficient electrical power, to allow the system to complete all mission-related actions.	✓	
NVD-Syst-03-02-02	Under all nominal flight conditions, the electrical power supply for all on-board systems shall be stable.	✓	Fluctuations are levelled using the battery.
NVD-Syst-08-02-01	The operator shall be able to monitor key system parameters from the ground system during all phases of the mission.	✓	The engine parameters will be relayed to the ground station.
NVD-client-09-01-01	The airborne element shall have service ceiling of at least 10,000 ft	✓	Accounted for in engine choice.
NVD-client-09-01-02	The airborne element shall have a maximum speed of at least 200 knots	✓	Accounted for in engine choice.
NVD-client-09-01-05	The airborne element shall have a maximum range of more than 800 nm.	✓	Accounted for in engine choice in combination with fuel system.
NVD-client-09-01-06	The airborne element shall have an endurance of at least 4 hours.	✓	Checked with the fuel system.
NVD-Syst-09-02-02	The airborne element shall be operable under all temperatures ranging from -30 degrees to +50 degrees Celsius.	✓	The engine components allow it to operate in these conditions.
NVD-Syst-09-02-04	The system shall be able to operate in war zones.	✓	Engine does not limit operations in war zones

9 Stability & Control

Since the aircraft needs to be able to fly a certain mission, stability and control is very important to ensure manoeuvrability and safety. Therefore, this chapter first describes the longitudinal stability tool which has been created. After this, the landing gear configuration is defined and finally, a detailed stability & control analysis is performed in order to size the control surfaces and determine the stability derivatives. The chapter finishes with a compliance matrix showing the compliance of the system with the requirements.

9.1. Longitudinal Stability

For the longitudinal stability, the first step is to analyse the functions associated with it. After this, the requirements applicable to the longitudinal stability can be determined and a tool can be created to assess the stability characteristics.

9.1.1. Functional Analysis

The functions for stability and controllability were determined in the Baseline Report [3]. Both functions ("provide stability" & "provide control") are related to aircraft functions, namely the "perform flight" function in the Functional Breakdown Structure (FBS).

The stability of the aircraft is determined by multiple factors. Firstly, the moments should be in equilibrium in a certain steady flight attitude, also called the trim condition. This condition should be achieved within the entire airspeed range. Secondly, the aircraft's behaviour around the trim condition is defining the stability. This means that after a disturbance, the equilibrium is restored in original condition, without large oscillations, or in other words, a adequately damped oscillation. Some forms of instability are, however, tolerated in case the pilot or flight computer has sufficient options to recover. The controllability of the aircraft is defined as being able to change the aircraft's equilibrium on demand by changing the forces around the centre of gravity.

9.1.2. Requirements

in Table 9.1, the requirements for the stability and controllability are given, based on the functions as determined in the previous subsection. Using these requirements, the stability and controllability tool can be made as discussed in Subsection 9.1.3.

Table 9.1: Requirements for the stability & control system.

ID	Requirement
NVD-Syst-04	The airborne element shall be stable and controllable during the entire mission.
NVD-Syst-04-01	The airborne element shall be stable for the entirety of the mission
NVD-Syst-04-01-01	In all flight conditions, the airborne element shall be dynamically and statically stable.
NVD-Syst-04-01-02	The airborne element shall be stable when operating on ground.
NVD-Syst-04-02	In all phases of the mission, the airborne element shall be actively controllable.

9.1.3. Stability and Controllability Tool

In this section the tool that is used for the stability and control analysis is discussed, starting off with the methodology that is used. After that, the verification and validation methods are explained.

In Chapter 6 the component weights were determined. A typical way to analyse the stability is to first determine the centre of gravity (c.g.) of the OEW. All variable weights, in this case the payload and fuel, are added in order to see how the c.g. shifts. Doing this for multiple configurations, the optimal wing position and tail size is found. In order to do this, however, some bounds and initial values have to be set first.

Centre of gravity

In the weight estimation, a total of eight component weights for the OEW were determined. In order to find the optimal wing position with respect to centre of gravity range, the components are divided in a fuselage group and a wing group. All components that move with the wing are added to this last group, e.g. wing mounted engines, main gear and fuel tanks. After that, for both components the centre of gravity location is calculated by Equation 9.1.

$$x_{cg} = \frac{\Sigma_{i=1}^{N}(W_i \cdot x_{cg,i})}{\Sigma_{i=1}^{N} W_i} \tag{9.1}$$

Because of stability criteria, the centre of gravity needs to be in front of the neutral point. The centre of gravity is measured with a datum at the wing. The leading edge mean aerodynamic chord (LEMAC) is used as reference. All distances are expressed as a percentage of the Mean Aerodynamic Chord (MAC).

Loading diagram
After the components' c.g. were determined, the variable weights are added. For the UAV, these weights are the payload and fuel weight, which can be loaded or unloaded in two different orders. Not only for stability the range is important, but also for landing gear design. For longitudinal stability, the main gear should be after the c.g., however, the c.g. should not be too forward with respect to the main gear to be able to rotate during take-off while the nose gear still carries weight to enable steering. This loading diagram is done for three different LEMAC positions, the initial estimate and one forward and one aft of that position. Mostly, 10% of the fuselage length is used. A safety margin of 2% is used on the minima and maxima. This loading diagram now provides an overview on the most aft and forward locations of the aircraft's c.g. during loading and is essential for the complete stability analysis.

Stability
The next step in the analysis is comparing the centre of gravity range of the loading diagram with the neutral point position for stability. This neutral point position is plotted against S_h/S which represents the tail volume. With the centre of gravity placed on the neutral point, the aircraft will be neutral statically stable. In order to be positive statically stable, a safety margin (S.M.) is added. In Equation 9.2 the stability curve is given. This curve determines the most aft c.g. location as function of the tail volume.

As can be seen, it is dependent on the lift slope of the wing and the total aircraft, the tail volume, the downwash ratio and the airspeed ratio.

$$\bar{x}_{cg} = \bar{x}_{ac} + \frac{C_{L\alpha_h}}{C_{L\alpha}}\left(1 - \frac{d\epsilon}{d\alpha}\right)\frac{S_h l_h}{S\bar{c}}\left(\frac{V_h}{V}\right)^2 - S.M. \tag{9.2}$$

$$\bar{x}_{cg} = \bar{x}_{ac} - \frac{C_{m_{ac}}}{C_{L_{A-h}}} + \frac{C_{L_h}}{C_{L_{A-h}}}\frac{S_h l_h}{S\bar{c}}\left(\frac{V_h}{V}\right)^2 \tag{9.3}$$

Control
The controllability of the aircraft is mainly determined by the tail size. Increasing the horizontal tail area, decreases the minimum centre of gravity position.

This controllability is dependent on the location of the aerodynamic centre, the moment coefficient, wing lift coefficient, tail lift coefficient, tail volume and speed ratio.

Centre of gravity range
The range of the centre of gravity can now be determined by plotting the centre of gravity range plot with the stability and controllability plot. The position where the range is equal for both cases determines the S_h/S ratio (the tail volume) and the $LEMAC/L_f$ ratio (the wing position relative to the fuselage length), what in the end gives the wing position and the horizontal tail surface. The plot is shown in Figure 10.15.

Centre of gravity envelope diagram
Now the wing position is known, a more specific analysis on the c.g. shift due to fuel consumption can be performed. Multiple fuel tanks can be used, which influences the centre of gravity location during the flight phases. It is off course important that the centre of gravity location stays in between the c.g. range during the entire flight.

During the iteration process, some parameters can change. The computed tail size, fuel tank allocation, aerodynamic characteristics, weight estimation and fuel fractions can be put in the first centre of gravity calculations, in order to start an iterative design process, until an optimal stability and control design is established. The final results are given in Section 10.4. In order to visualise this process, a flow diagram has been made. This flow diagram is shown in Figure 9.1.

9.2. DETAILED STABILITY ANALYSIS METHOD

After the initial wing and c.g. calculations, a start has been made to optimise the design from a stability- and control perspective. After some research, the decision was made to use XFLR5 V6.14 [1] as the tool for further

[1] `http://www.xflr5.com/xflr5.htm` [cited 13 June 2016]

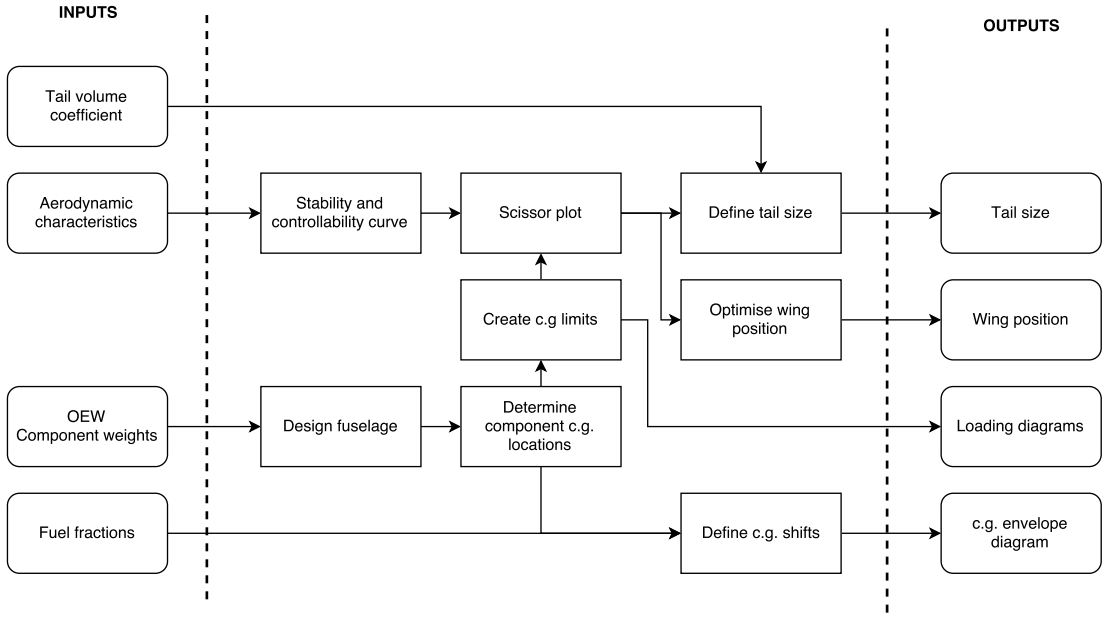

Figure 9.1: Longitudinal stability analysis tool.

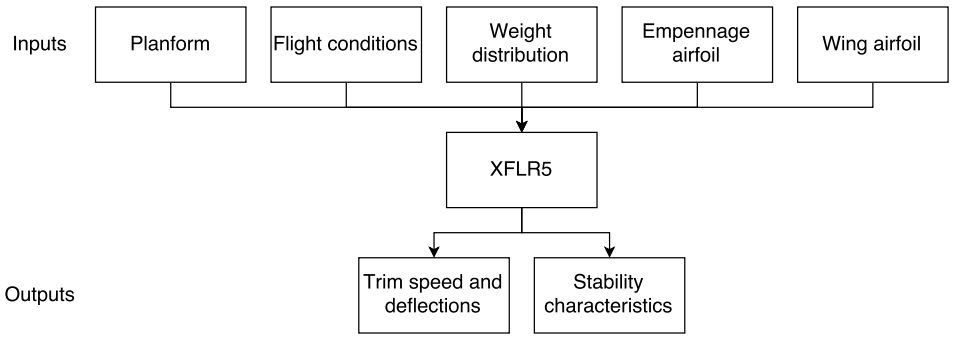

Figure 9.2: Inputs and outputs of XFLR5.

stability analysis. The most important reasons for this choice where the fact that it is free, that there is good documentation available and that it has an active community which can help with questions. The in- and outputs of the program are shown in Figure 9.2.

The arrangement of elements in the state-matrices is a little different from what is taught in the TUD Flight Dynamics AE3202 course, since the program is based on course 16.61 Aerospace Dynamics by Jonathan How from MIT[2].

When input values are know, the entire aircraft is analysed on its stability. This analysis is also part of the iteration process, and input parameters will change during the design. Analysis is done in four longitudinal modes (Lo1 - Lo4) and four lateral modes (La1 - La4). The different modes can be seen in Table 9.2. The periodic modes have a complex conjugate in order to be periodic. The eigenfrequency and damping ratio of these two modes are therefore the same. Final results can be found in Chapter 10.

[2] `http://ocw.mit.edu/courses/aeronautics-and-astronautics/16-61-aerospace-dynamics-spring-2003/lecture-notes/Lecture17.pdf` [cited 13 June 2016]

Table 9.2: Definitions stability modes.

Lo1	Short period
Lo2	Short period conjugate
Lo3	Phugoid
Lo4	Phugoid conjugate
La1	Roll damping
La2	Dutch roll
La3	Dutch roll conjugate
La4	Spiral

9.3. LANDING GEAR

Besides the stability in air, the aircraft should also be stable and controllable on the ground. In this section the design of the landing gear is explained. The requirements are shown and the section after that elaborates on the design methodology.

9.3.1. FUNCTIONAL ANALYSIS

As mentioned before, the stability and controllability functions were defined in the Baseline report [3]. In addition to providing control and stability, the landing gear on its own functions as presented in Figure 9.3.

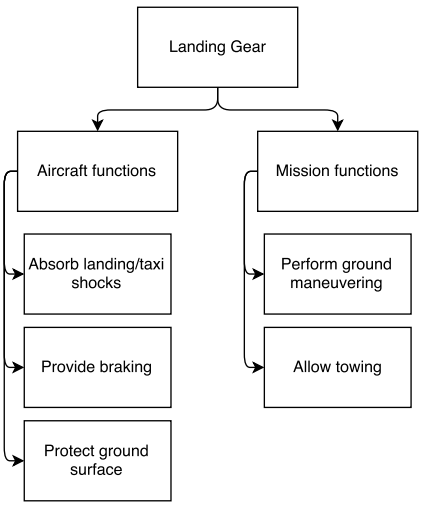

Figure 9.3: Overview of the functions for the landing gear system.[35]

During landing an taxi, shocks are introduced to the aircraft. In order to protect the aircraft and the payload from these vibrations, the landing gear should absorb them. On the other hand, the ground surface should be protected from the UAV during ground movements. Mission related, the system should be able to perform stable ground manoeuvring, this includes that the UAV can not tip-over. In order to get the aircraft from assembly site to airport, it should also be able to be towed. In other words, it should absorb vertical touchdown loads, longitudinal loads from spin-up, braking and rolling, and lateral forces from crosswind landings and turns.

9.3.2. REQUIREMENTS

In Table 9.3 the requirements for the landing gear are given. Partly,the requirements were set in the Baseline Report [3] and others were set during the design phase. During the design of the landing gear, all steps will be taken accounting for the requirements.

Table 9.3: Requirements for providing stability & control [3].

ID	Requirement
NVD-Syst-01-06	The airborne element of the system shall be recoverable without getting dam- aged.
NVD-Syst-01-06-01	The UAV shall be able to perform a full-stop recovery within a distance of 610 meters.
NVD-Syst-04-01-02	The airborne element shall be stable when operating on ground.
NVD-Syst-04-01-02-01	The airborne element shall meet the ground clearance requirements.
NVD-Syst-04-01-02-02	The airborne element shall satisfy the tip-over criteria.
NVD-Syst-06	The airborne element shall be able to support all loads experienced during its lifetime, multiplied by a safety factor of 1.5, without failure.
NVD-Syst-06-01	The airborne element shall be able to support all static loads experienced during its lifetime
NVD-Syst-06-01-02	The airborne element shall support all loads related to recovery throughout its lifetime.
NVD-Syst-06-01-02-01	The structural attachment points of the landing gear shall not require the introduction of significant additional structure.
NVD-Syst-06-01-02-02	The landing gear shall be retractable without interfering with other aircraft components.
NVD-Syst-06-01-02-02-01	The landing gear retraction kinematics shall be feasible and do not require excessive actuator forces to retract or lower.
NVD-Syst-09-02-01	The airborne element shall be suitable for ground operations on tarmac, grass and gravel.
NVD-Syst-09-02-01-01	The landing gear tires shall not cause any spray on wet or slushy runways that can enter the engine inlets.

9.3.3. CONFIGURATION

This section discusses the landing gear configuration of the UAV. The configuration choice consists of trade-offs for retractable or fixed landing gear and for the positioning of the gear with respect to the centre of gravity.

The trade-off characteristics for the retraction of the landing gear are shown in Table 9.4. Included are, aerodynamic drag, weight, complexity and cost and maintenance cost. Although that the costs, complexity and weight are important factors, the aerodynamic drag criterion is driving in this trade-off. Requirement *NVD-Client-09-01-02* [3] states that the aircraft shall have a maximum cruise speed of $200 kts$. Within this speeds range, the drag penalty is too high to design for fixed gear. Furthermore, the aerodynamic force on the landing gear would introduce a high moment in the structure, which means that the structural weight of the wing has to be increased [35].

Table 9.4: Summary of pros and cons of fixed versus retractable landing gears [35].

Characteristic	Fixed gear	Retractable gear
Aerodynamic drag	High	Minimal
Weight	Low	High
Complexity and cost	Low	High
Maintenance cost	Insignificant	Significant

Now the decision has been made to use retractable landing gears, the configuration of the gear can be chosen. Because of development risk and costs, the trade-off is done for the three most conventional configurations, namely the tricycle, bicycle and tail wheel configuration. Criteria for the configuration are ground loop behaviour, floor attitude, weight, steering and take-off behaviour. The criteria including gradings are shown in Table 9.5. The tricycle has as advantage that it is very stable on ground operations, what is preferred when the aircraft needs to be controlled remotely. The bicycle landing gear is found on aircraft that need the middle of the fuselage for other purposes, e.g. bombers. A tail wheel configuration is often found on aircraft that need to operate on rough ground surfaces, however, their stability is very poor. Considering all these configurations, the nose gear tricycle configuration is the best option. At first, the gear provides lateral ground loop stability

and stable steering. Secondly, the take-off rotation is easy performed and controlled. At last, the straight, or slightly forward-tilted fuselage attitude is beneficial for the pushing propeller ground clearance.

Table 9.5: Summary of pros and cons for three gear types [35]

Characteristics	Tricycle	Bicycle	Tail wheel
Ground loop behaviour	Stable (+)	Stability dependent on c.g. location (-)	Unstable (-)
Floor attitude on the ground	Level (+)	Can be level (+)	Not level (-)
Weight	Medium (+)	High (-)	Low (+)
Steering after touchdown	Good (+)	Good (+)	Poor (-)
Steering while taxiing	Good (+)	Good (+)	Poor (-)
Take-off rotation	Good (+)	Marginal (-)	Good (+)

9.3.4. POSITIONING

The position of the gear is determined by its configuration and the location of the centre of gravity. For calculating static loads, equilibrium mechanics equations were used. For the front gear, the most forward centre of gravity position is used, and for the main gear the most aft position is used. In order to keep control of the aircraft on the ground, the nose gear needs to be loaded with at least 8% of the MTOW. However, too high loads on the nose gear mean that the rotation during take-off is more difficult. The stability angles are shown in Figure 9.4 and Figure 9.5. longitudinal tip-over stability angle needs to be 15° and lateral tip-over stability angle shall be 55°. Besides the stability tip-over criteria, there are criteria on ground clearance. The lateral ground clearance should be 5°, this is to prevent from touching the ground with the wingtip during crosswind landings. The longitudinal ground clearance shall be 15° to be able to increase the angle of attack during take-off and landing.

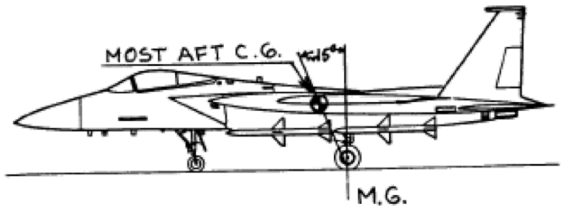

Figure 9.4: Longitudinal tip-over criterion [35]

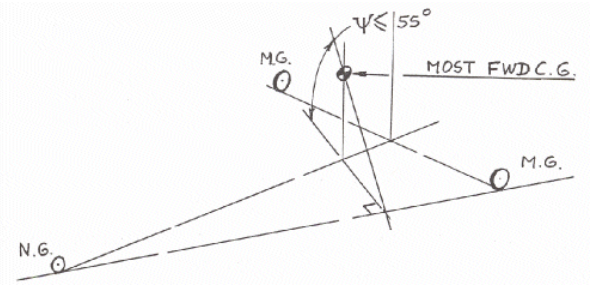

Figure 9.5: Lateral tip-over criterion [35]

After calculating the location of the c.g. in Chapter 6, the landing gear is positioned complying with the stability criteria. In Table 9.6 the final position parameters of the landing gear are mentioned. Because the Roskam estimation [35] was used, all units are imperial, and are converted to SI units. Since the configuration of the aircraft consists of a twin-boom tail configuration, the main landing gear can be stored into the nacelles where the booms are connected onto the wing. Note that the dimensions in the table are for landing limits, hence the gear height is determined for the landing gear length with the shock absorbers compressed.

Table 9.6: Landing gear positioning

Definition	Symbol	Value	Imp. Unit	Value	SI Unit
Max. static nose gear load	$F_{nosegear}$	598.4	lbs	2662.7	N
Nose gear position w.r.t. a/c nose	$x_{nosegear}$	0.98	ft	0.3	m
Max. static main gear load	$F_{maingear}$	473.9	lbs	2108.7	N
Main gear position w.r.t. a/c nose	$x_{maingear}$	9.51	ft	2.9	m
Spacing between nosegear	$\Delta_{y_{maingear}}$	6.34	ft	1.94	m
Gear height	h_{gear}	2.72	ft	0.83	m
Longitudinal tip-over angle	θ	-	-	34.2	°
Longitudinal ground clearance angle	θ	-	-	15.6	°
Lateral tip-over angle	ϕ	-	-	34.4	°
Lateral ground clearance angle	ψ	-	-	15.3	°

9.3.5. TIRE SIZING

Now the configuration has been chosen, the tire sizing is done. The tires are the providing the only contact between the ground and the aerial system, so they need to be designed to withstand all surfaces that the aircraft is designed for, all loads the aircraft introduces during ground operations and have a certain wear life-cycle. Ground surfaces are divided in three different types by Roskam [35]; The type I unprepared simple surface, Type II flexible pavement surfaces and Type III rigid pavement surfaces. As requirement *NVD-Syst-09-02-01* [3] states, the aircraft needs operate on tarmac (Type II), grass (Type I) and gravel (Type I), so the tires will be designed for Type I surfaces.

According to Roskam, the tire pressure for grass surface (softest surface) shall be in the range of $3.2-4.2 kg/m^2$. With the mass range of the aircraft, a single wheel configuration per gear is sufficient to carry the loads. Using air pressure, landing velocity and maximum loading, the tire is sized.

After using the trade-off table by Roskam [35], a tubed tire was chosen for both main and nose gear with a diameter of $0.34m$, $0.13m$ width, maximum loading of $5340N$, unloaded pressure of $379kPa$ and a maximum speed of $104kts$.The weight per tire will be $24.5N$. An overview is given in Table 9.7. Important in the tire sizing is the attachment design. The wheel well clearance after retraction, the tire strut and the tire-to-tire clearance should be achieved. During the life of the tire the diameter increases due to centrifugal forces and wear. Every cycle, the tire grows due to heating and forces by 4% in width and 10% in diameter.

Table 9.7: Tire sizing of the landing gear.

Definition	Symbol	Nose gear		Main gear	
Diameter	D_0	336.55	mm	336.55	mm
Width	w_0	128.27	mm	128.27	mm
Max. loading	P	5339.7	N	5339.7	N
Unloaded inflation pressure	UIP	379	kPa	379	kPa
Max. speed	V_L	104	kts	104	kts
Weight	W	24.47	N	24.47	N

9.3.6. STRUT SIZING

For the strut design the dynamics of the aircraft are analysed. During the landing phase, all kinetic energy needs to be absorbed by the landing gear in order to prevent the aircraft and ground from damaging. A part of the energy is absorbed by the tires, however, the main contribution on energy absorption is done by the strut. Trading off the different shock absorbers from Table 9.8, the oil-damped metal spring is the absorber that is going to be used, since this unit has the best efficiency for its cost. Furthermore, in equation Equation 9.4 [35] the stroke length of the shock absorber is defined.

Table 9.8: Energy shock absorber efficiency [35].

Shock absorber	Energy absorption efficiency
Air springs	0.60-0.65
Oil damped metal springs	0.70
Liquid springs	0.75-0.85
Oleo-pneumatic	0.80
Cantilever spring	0.50

$$s_{s_{design}} = \frac{0.5\left(\frac{W_L}{g}\right)\left(w_t\right)^2}{n_s P_m N_g} - \eta_t s_t + \frac{1}{12} \tag{9.4}$$

$$P_{n_{dyn_t}} = \frac{MTOW\left(l_m + \frac{a_x}{g}\left(h_{cg}\right)\right)}{n_t\left(l_m + l_n\right)} \tag{9.5}$$

In the equation above W_L is the MLW in lbs, g is the gravitational acceleration in ft/s^2, w_t is the descent speed in ft/s, n_s the number of struts, P_m the main gear static load in lbs, N_g is the landing gear load factor, η_t is the tire efficiency, s_t is the allowable tire deflection in ft and η_s is the strut energy absorption efficiency. An safety margin is added of 1 inch for the design. For nose gear stroke length, the MLW is replaced by the nose gear static loading, the static loading is replaced by the nose gear dynamic load, which is defined in Equation 9.5[35] and $N_s = 1.0$.

In the equation all units are imperial. a_x/g is the braking acceleration factor, $h_c g$ the landing gear height, n_t the number of tires and l_m and l_n the distances of the gears with respect to the c.g. The stroke diameter in ft

is defined by Equation 9.6[35].

$$d_s = 0.041 + 0.0025\left(P_m\right)^{0.5} \tag{9.6}$$

In Table 9.9 the dimensions of the shock absorbers are shown in both imperial and the converted SI units.

Table 9.9: Shock absorber sizing for the UAV landing gear.

Definition	Symbol	Value	Imp. unit	Value	SI unit
Nose gear strut length	$s_{s_{nosegear}}$	0.489	ft	149	mm
Nose gear strut diameter	$d_{s_{maingear}}$	0.056	ft	17	mm
Main gear strut length	$s_{s_{maingear}}$	0.791	ft	241	mm
Main gear strut diameter	$d_{s_{maingear}}$	0.089	ft	27	mm

9.3.7. BRAKING SYSTEM

The braking system in the landing gear is decisive for stopping the aircraft after landing, after an aborted take-off or during taxiing. Furthermore it can help the aircraft to steer by differential braking, hold the aircraft while parking and controls the taxi speed.

The way the aircraft is decelerated is done by disc brakes, which convert kinetic energy into heat. The heat needs to be transferred to the wheels, tires and surrounding air. Depending on the type of brake, the deceleration is determined. According to Roskam [35], most used brakes are conventional and carbon brakes, divided into regular and anti-skid. Carbon brakes are lighter and more efficient, but also more expensive. For conventional brakes, it can be assumed that the maximum deceleration is $0.35g$.[35] With a landing speed of $V_L = 61kts$ the landing distance with braking is calculated.

$$t = \frac{V}{a} = \frac{1.2V_L}{0.35g} = 10.97s \tag{9.7}$$

$$s = \frac{1}{2}at^2 = \frac{1}{2}\cdot 0.35g \cdot 8.99 = 207m \tag{9.8}$$

So with conventional brakes the requirement for landing distance is met, and no carbon or anti-skid system is necessary. In normal landing conditions this braking deceleration is not used because of wear of the brakes and the tires. On wet or slushy runways the landing distance is increased and braking systems might become useless.

9.3.8. RETRACTION KINEMATICS

The kinematics of the of the landing gear are determined by the weight of the gear, the size of struts, the size of the wheel and the force that is needed to retract. The main gear can retract straight forward into the wing pod. In the nose, the well is shorter but can be increased in height. The mechanism of the retraction is shown in Figure 9.6 and Figure 9.7. The nose gear uses a retraction actuator with folding main strut. The main gear is a forward retraction gear with horizontal slot.[35] important in the design are the reinforcements on the mains strut. Near the shock absorber a torque link is added to prevent the wheel from turning. The diagonal struts are, besides the fact they are used for retraction, also used for longitudinal strength. For lateral strength the options are limited, because the gear is retracting in longitudinal direction. However, the upper members of the gear are increased in width.

9.3.9. ELECTRONIC BLOCK DIAGRAM

The power system of the control surfaces are shown in Figure 9.8. They all use elctric DC motors for actuation. Control signals from the CPU closes a solenoid which the motors recieve power from the main bus.

The landing gear electronic power system is shown in Figure 9.9. There are two circuits which are used to actuate the motors, a low current control circuit and high current circuit providing power to the motor. The low current circuit receives a signal from the CPU shown in the top right corner. This signal goes to a terminal which splits the signal into six parallel lines which are connected to limit switches. Each of the three gears has a two limit switches, one for gear up and one for gear down position. When the gear is not fully retracted or extended their will be a signal sent to either terminal two or three depending on if the gear is retracting or extending. From there a signal is sent to the appropriate solenoid which closes its circuit to draw power from the high current circuit. If for example the gear is going down, all three gears must have reached to fully extended position and activated the three limit switch before the landing gear motors stop receiving power. When the gear is fully extended three lights light up on the ground station giving feedback to the operator that the gear is successfully extended as seen in the middle of the figure. If the gear is neither fully extended or retracted warning lights will be turned on at the ground station sown the at the bottom of the figure. Moreover,

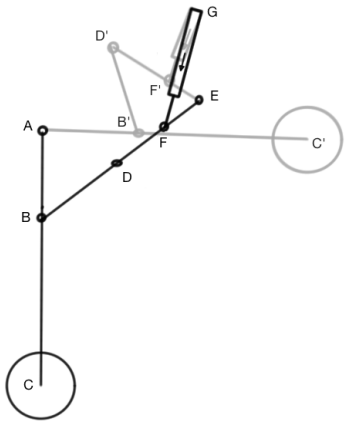

Figure 9.6: Stick diagram of the nose gear retraction kinematics.

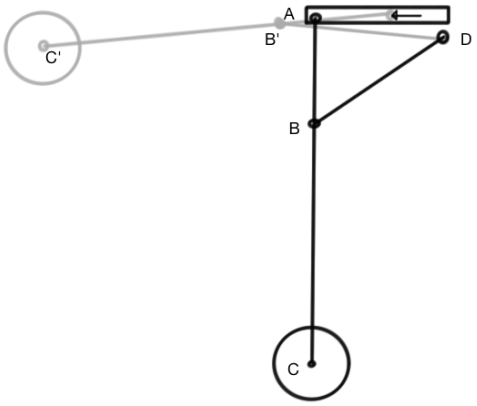

Figure 9.7: Stick diagram of the main gear retraction kinematics.

after terminal two a switch is used in case the operator tries to retract the landing gears while the aircraft is standing on ground. This is called a squat switch and uses a force sensor to detect of the aircraft is on the ground [17].

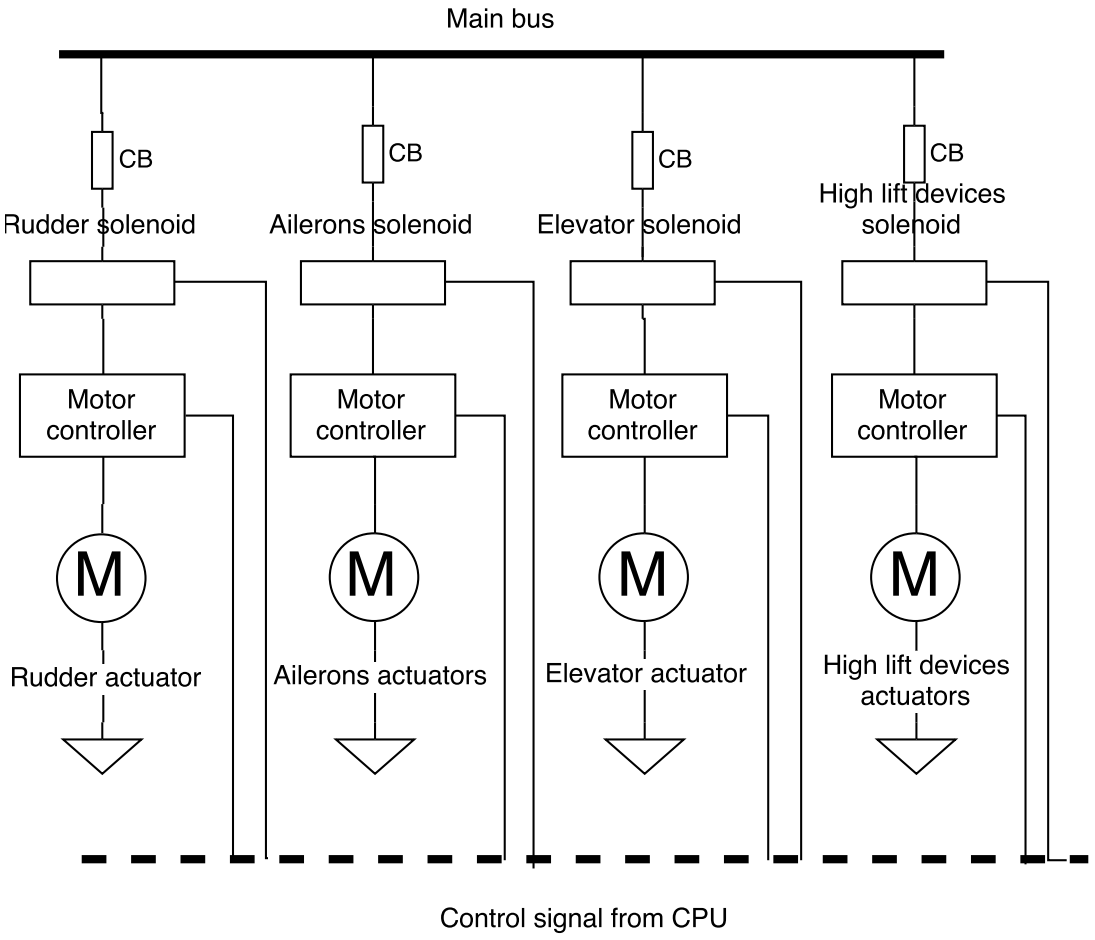

Figure 9.8: Electrical power system control surfaces

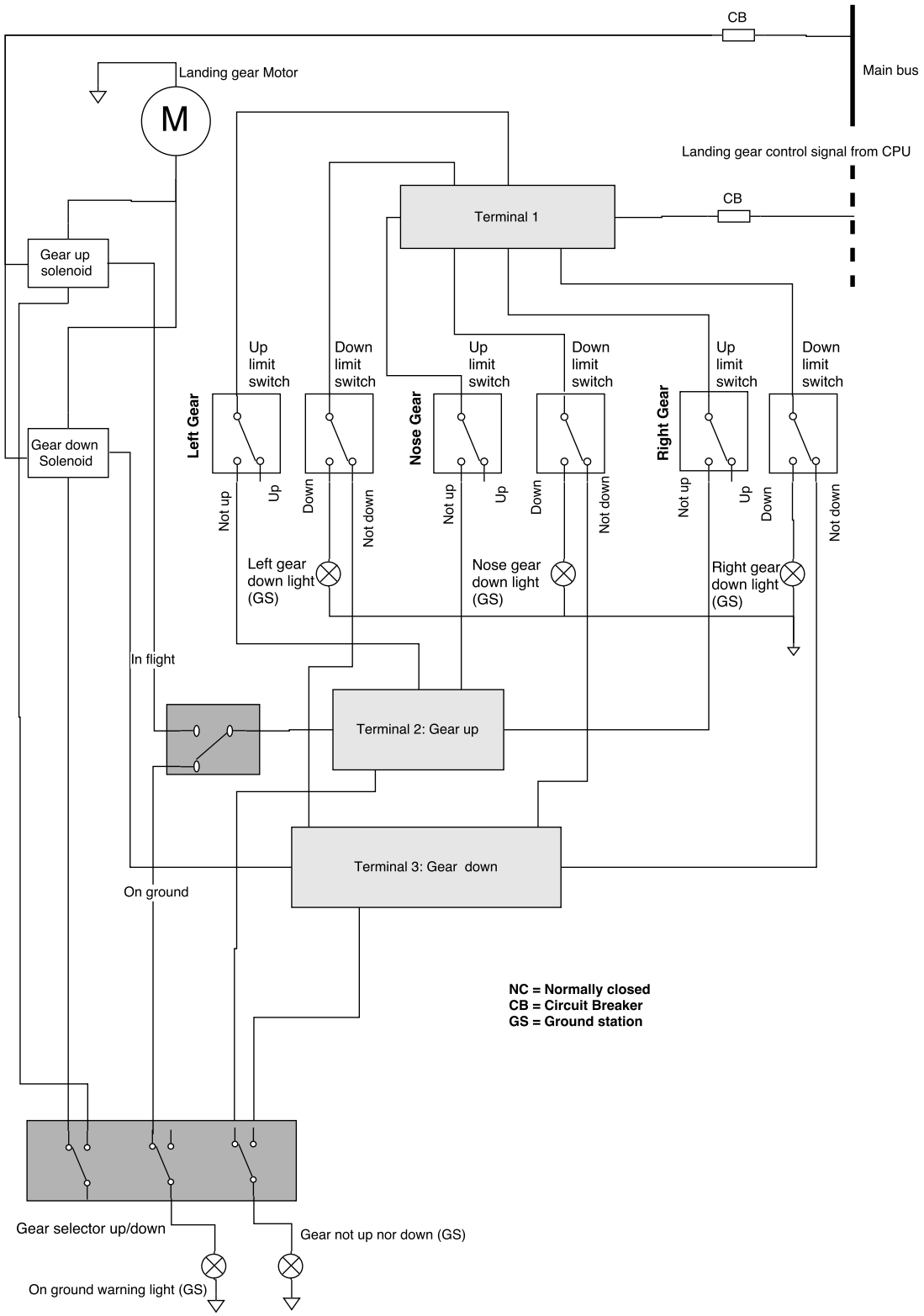

Figure 9.9: Electrical power system landing gears

9.4. COMPLIANCE MATRIX

In the compliance matrix in Table 9.10 the requirements are shown again. This is done in order to give an overview if all the requirements are met.

Table 9.10: Compliance matrix for the stability and controllability.

ID	Requirement	Comp.	Comment
NVD-Syst-04	The airborne element shall be stable and controllable during the entire mission.	✓	
NVD-Syst-04-01	The airborne element shall be stable for the entirety of the mission.	✓	
NVD-Syst-04-01-01	In all flight conditions, the airborne element shall be dynamically and statically stable.	✓	
NVD-Syst-04-01-02	The airborne element shall be stable when operating on ground.	✓	
NVD-Syst-04-02	In all phases of the mission, the airborne element shall be actively controllable.	✓	
NVD-Syst-01-06	The airborne element of the system shall be recoverable without getting damaged.	✓	A landing gear is added to the aircraft.
NVD-Syst-01-06-01	The UAV shall be able to perform a full-stop recovery within a distance of 610 meters.	✓	A landing distance of $139m$ is computed.
NVD-Syst-04-01-02	The airborne element shall be stable when operating on ground.	✓	Stability by tricycle landing gear.
NVD-Syst-04-01-02-01	The airborne element shall meet the ground clearance requirements.	✓	
NVD-Syst-04-01-02-02	The airborne element shall satisfy the tip-over criteria.	✓	
NVD-Syst-06	The airborne element shall be able to support all loads experienced during its lifetime, multiplied by a safety factor of 1.5, without failure.	✓	The landing gear structure
NVD-Syst-06-01	The airborne element shall be able to support all static loads experienced during its lifetime.	✓	
NVD-Syst-06-01-02	The airborne element shall support all loads related to recovery throughout its lifetime.	✓	All recovery loads are taken by the landing gear and transferred to the connection points
NVD-Syst-06-01-02-01	The structural attachment points of the landing gear shall not require the introduction of significant additional structure.	✓	
NVD-Syst-06-01-02-02	The landing gear shall be retractable without interfering with other aircraft components.	✓	
NVD-Syst-06-01-02-02-01	The landing gear retraction kinematics shall be feasible and do not require excessive actuator forces to retract or lower.	✓	
NVD-Syst-09-02-01	The airborne element shall be suitable for ground operations on tarmac, grass and gravel.	✓	The gear is designed for Type I ground surfaces
NVD-Syst-09-02-01-01	The landing gear tires shall not cause any spray on wet or slushy runways that can enter the engine inlets.	✓	The engine air inlet is on top of the fuselage.

10 Final Results

After the iteration loop, as described in Chapter 4, had been performed five times, the iteration was stopped and the final results of the preliminary design were frozen. This chapter describes the final results after the last iteration was performed for each chapter. Figure 10.1 shows the final parameters from all departments.

Final iteration							
9-6-2016	10-6-2016			P [kW]	90,2	D_prop [m]	0,95
15:00	19:30			Onboard P [kW]	2,423	W_F [kg]	91,02
INPUT	-	*OUTPUT*	-	Propulsion & Power		Prop syst type	Piston
vs0 [kts] (SL)	56	W/S [N/m^2]	789			N_engines [-]	1
vs1 [kts] (SL)	65	W/P [N/W]	0,0527			V_tank [L]	129,3
CLmax_clean [-]	1,17	Class I Matching Plots				l_engine [m]	0,649
CLmax_flapped [-]	1,57					w_engine [m]	0,556
CD_0 [-]	0,0163					h_engine [m]	0,424
eta_p cruise [-]	0,874					Selected engine	D-motor LF39
eta_p climb [-]	0,836					BSFC [g/kWh]	280
nmax [-]	3,8					V Battery [L]	7,81
Vnmax [kts]	156			W_Av [kg]	39,1	MTOW [kg]	484,0
S_to [m]	598			S_f wet [m^2]	6,100	OEW [kg]	342,0
TOP [-]	29,4			l_f [m]	3,2	Wing weight [kg]	51,47
S_l [m]	610			D_f [m]	0,65	Fuselage weight [kg]	26,67
W_L/W_TO [-]	1			l_tail [m]	2,97	Landing gear weight [kg]	19,19
V_c max [kts]	200			W_PL [kg]	47,0	Empennage weight [kg]	28,97
h_c [ft]	10000			Class II Weight Estimation		Fuel tank weight [kg]	13,54
P_set [-]	0,95					Propulsion weight [kg]	147,97
W_fr [-]	0,85					Engine weight [kg]	134,43
HLDs	Plain					Electr. Syst. Weight [kg]	25
W_PL [kg]	47					FCS weight [kg]	1,44
W_F [kg]	91,2	Airfoil R	e1098			Hydraulics/pneumatics [kg]	0,48
Re	6000000	Airfoil T	e1098			Paint weight [kg]	1,82
M [-]	0,31	t/c R [-]	0,189			Vert. tail surface [m^2]	0,734
C_L wing cr [-]	0,1713	t/c L [-]	0,189			Vert. tail sweep [deg]	30
		L/D visc [-] (AOA = X)	30.83 (-3.0)			Vert. tail taper [-]	0,7
		R twist [deg]	0	Payload CG [m]	1,37	LEMAC [m]	2,24
		T twist [rad]	0	Avionics CG [m]	2,12	Main LG CG [m]	2,62
		b	8,00	Engine CG [m]	2,88	S_tail hor [m^2]	0,9848
		A	10,56	Empennage CG [m]	4,01	S_tail ver [m^2]	0,733976
		e	0,742	Fuel CG [m]	2,53	Tail pos [m]	5,2
		Dihedral [deg]	0	x_ac LEMAC [%MAC]	2,23	Tail layout	Horizontal unit
		c_r [m]	0,98	W_dish [kg]	8,5	l_boom [m]	2,96
		taper [-]	0,55	Dish + front LG CG [m]	0,65	x_limAFTLEMAC/MAC	0,4287
Aerodynamics		LE sweep [deg]	2,05	W_av bay [kg]	30,6	x_limFWDLEMAC/MAC	0,1998
		S [m^2]	6,06	Electr. CG [m]	1,95	CG LEMAC/MAC OEW	2,54
		c_t [m]	0,539	S_flap/S [-]	0,74	MAC [m]	0,781
		dC_L/da [/deg]	0,0925	HLDs	Flaperons	b_Htail [m]	1,94
		dC_m/da [/deg]	-0,0303	Stability & Control			
		Cm_ac airfoil [-]	-0,123	Loc. Prop [m]	3,4	Loc. Nose gear [m]	0,62
		x_ac airfoil [x/c]	0,25	Landing Gear Positioning		Loc Main gear [m]	3,15
		Wing position	High			H Nose gear compr. [m]	0,83
		CL_cruise [-]	0,1948			H Main gear compr. [m]	0,83
		AOA_cruise [deg]	-3			Lat Pos main gear [m]	0,97

Figure 10.1: final parameters of the iteration

10.1. Aerodynamics

The results for aerodynamics have been split into four parts. First the vertical wing placement is explained, then the selected airfoil after which the 3D wing and the high-lift devices will be discussed. The procedure that was used during the iterations, as shown in Figure 7.2 and explained in Section 7.3, was followed for every loop.

WING PLACEMENT

The wing placement has experienced one change since the first trade-off that was performed in Section 7.3. At first, the wing configuration was set low, but, as explained in Chapter 4, was changed to a high wing configuration.

AIRFOIL SELECTION

The airfoil trade off, as discussed in Chapter 7 yields an selected airfoil. The resulting airfoil is the Eppler 1098, as illustrated in Figure 10.2. As discussed in Chapter 7, important attributes for the airfoil were the enclosed area of the airfoil, which is a large indicator of the available space to store fuel inside the wing. Also for structural considerations it was opted to choose for an airfoil that was a little bit thicker than the airfoil that won the trade off in Section 7.3. The performance of the airfoil modelled by XFOIL, at a Re of $6 \cdot 10^6$ and a Mach number of $M = 0.31$, are shown in Figure 10.4. The important airfoil performance characteristics are shown in Table 10.1.

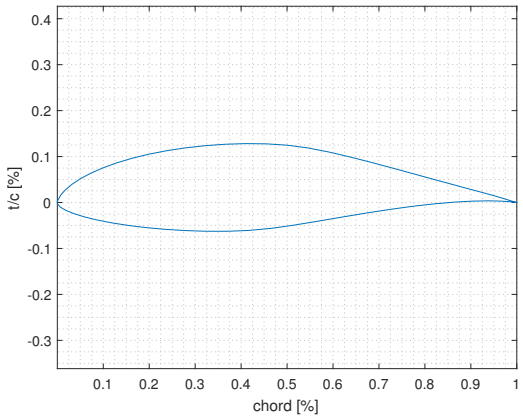

Figure 10.2: Airfoil shape - Eppler 1098

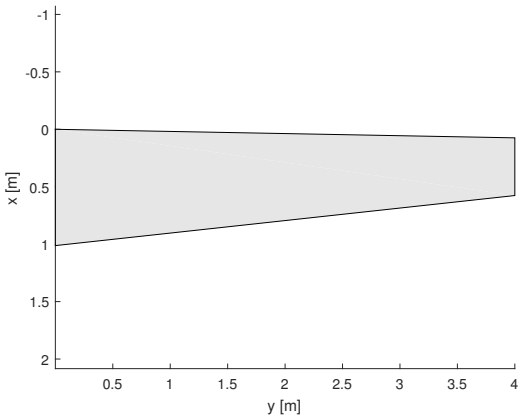

Figure 10.3: Wing planform

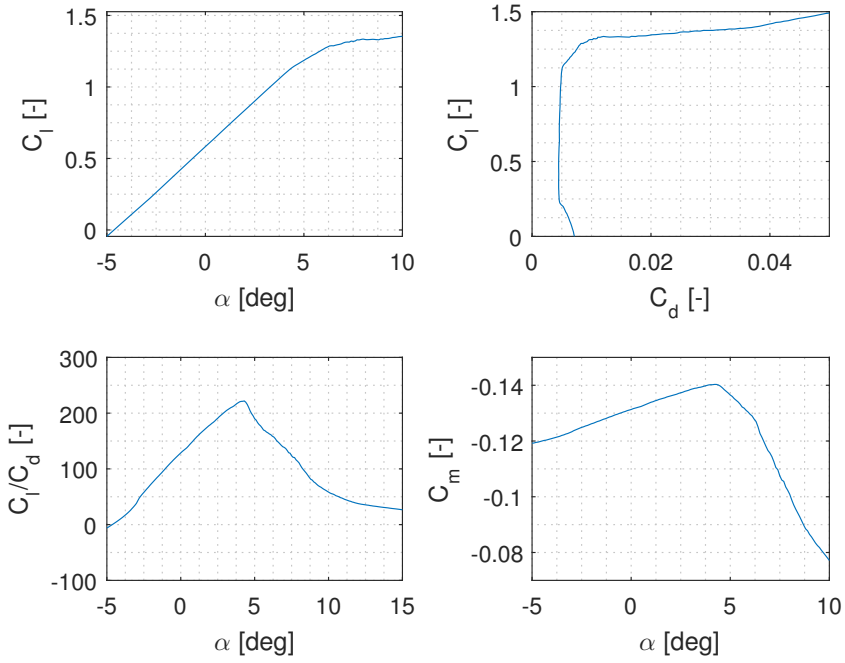

Figure 10.4: Airfoil polars - Eppler 1098; $Re = 6 \cdot 10^6$ and $M = 0.31$

Table 10.1: Airfoil e1098 parameters; $Re = 6 \cdot 10^6 and M = 0.31$

Parameter	**Value**	**Unit**	**Source**	Comments
C_{l_α}	0.13	$[\frac{1}{deg}]$	XFOIL	
$(\frac{C_l}{C_d})_{max}$	221.85	$[-]$	XFOIL	
$(\frac{C_l^3}{C_d^2})_{max}$	$5.54 \cdot 10^4$	$[-]$	XFOIL	
$C_{d_{min}}$	$4.5 \cdot 10^{-3}$	$[-]$	XFOIL	
C_{m_α}	$-2.40 \cdot 10^{-3}$	$[\frac{1}{deg}]$	XFOIL	
$C_{l_{max}}$	1.5	$[-]$	Eppler [20]	@ $Re = 1.5 \cdot 10^6$ [20]

FINITE WING DESIGN

The final geometric parameters of the wing planform are tabulated in Table 10.2. It is a high wing installed at an incidence angle of -3 [deg], to minimise the drag produced by the fuselage during cruise. Figure 10.3 illustrates the general geometry of the wing. Figure 10.5 depicts the aerodynamic characteristics of the wing. Table 10.2 tabulates the major aerodynamic parameters of the wing. Furthermore the wings size allows to easily accommodate a fuel tank of about 130 litres.

Table 10.2: Geometric parameters of the wing

Parameter	Value	Unit
Wing span b	8.00	$[m]$
Taper ratio λ	0.50	$[-]$
Root chord length c_{root}	1.01	$[m]$
Leading edge sweep Λ_{LE}	1.07	$[deg]$
Dihedral Γ	0.00	$[deg]$
Incidence angle i_w	-3.00	$[deg]$
Twist ϵ	0.00	$[deg]$
Area S	6.06	$[m^2]$
Aspect ratio AR	10.56	$[-]$
Wing span efficiency e_w	0.74	$[-]$

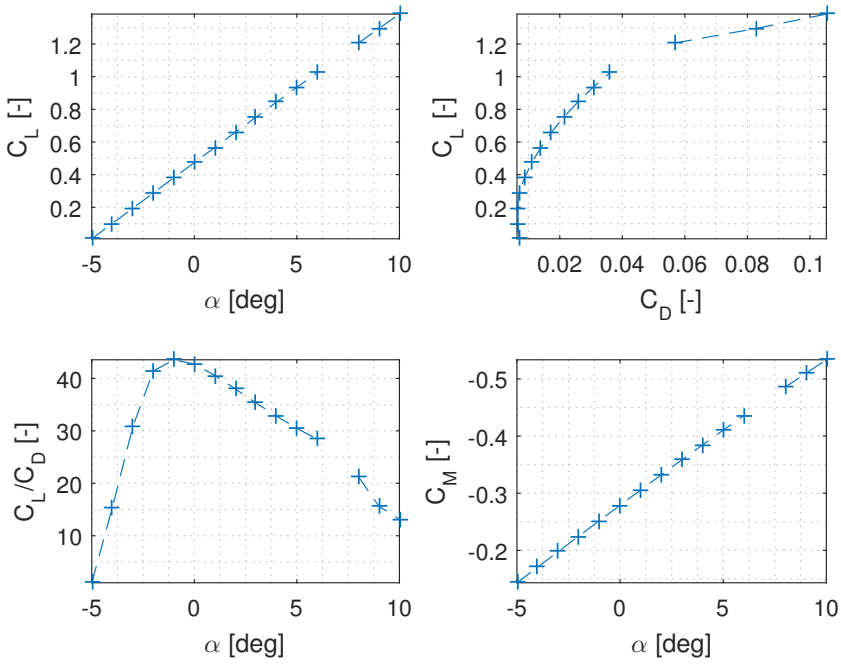

Figure 10.5: Wing polars; $Re = 6 \cdot 10^6$ and $M = 0.31$

Table 10.3: High Lift Device Parameters

Parameter	Value	Unit
$\frac{dC_L}{d\alpha}$	0.0922	$[\frac{1}{deg}]$
$C_{D_{min}}$	0.0063	[−]
$(\frac{C_L}{C_D})_{max}$	43.55	[−]

HIGH LIFT DEVICES

For the HLDs it was chosen to use a plain flap as was explained in Subsection 7.3.9 with hinge line at 75% of the chord. The other dimensions and performance specification are shown in Table 10.4

Table 10.4: Aerodynamic performance and size of the flaps

Parameter	Value	Unit
$\Delta C_{L_{max}}$	0.4	[−]
Hinge line location	75	[%] of chord
$\Delta C_{l_{max}}$	0.6	[−]
$C_{L_{max}}$ @ full flaps	1.57	[−]
Max flap deflection angle	40	$[deg]$
S_{fw}	4.5	$[m^2]$
b	6.2	$[m]$

10.2. PROPULSION & POWER

In Chapter 8 it was chosen that a piston engine will be used as the propulsion system. Based on the power need of 90.2 kW as seen in Figure 10.1 an engine has been chosen which meets this power criteria. From Chapter 8 a list of possible engines which meet the power requirement are given in Table 10.5. Continental Motors and Lycoming are traditional engine manufacturers which have been in the business for decades. On the other hand D-motor was founded in 2009 while ULPower in 2006. They represent the new era of aircraft piston engines focusing on light weight, but powerful engines. Their specific fuel consumption are all similar which is normal for propulsion systems within the same type. However, the time between overhauls (TBO) has a significant difference between the engines. The newer engines have a TBO of a 1000h for the ULPower and 1500h for the D-motor. The Continental and Lycoming both have 2000h. They can therefore be used for a much longer period before major overhaul must be conducted. Another large difference between all motors are their dimensions and volume. The Continental and Lycoming are relatively large motors especially in the length (flying direction) and more importantly the width (across the fuselage) direction. The latter dimension turned out to be a challenge as the aft fuselage needed to be significantly widened to fit the engine. Therefore the width and height of the engine has been a limiting factor for the engine choice. Because of the high weight and large dimensions the Continental and Lycoming engines were not chosen even though they provide a better TBO. The D-motor LF39 has been chosen for the UAV. as it offers a relatively low weight with the best dimensions in width and height.

Table 10.5: List of piston and turboprop engines around the needed power class

Engine	**Type**	**Installed weight [kg]**	**Power max. cont. [kW] (hp)**	**RPM**	**Gear ratio**	**BSFC [g/kWh] @ max cont. power**	**Dimensions (LxWxH) [m]**	**Volume [m^3]**	**TBO h**
D-Motor LF39	Piston	85	90 (121)	3000		280 (estimated)	0.649x0.556x0.424	0.153	1500
ULPower ul350iS	Piston	78.4	92 (123)	2800	-	288	0.553x0.736x0.472	0.192	1000
Continental OI-240	Piston	108.9	93 (125)	2800	-	317	0.757x0.801x0.667	0.404	2000
Lycoming O-235	Piston	113.0	93 (125)	2800	-	285	0.749x0.813x0.569	0.346	2000

A CAD model of the D-motor LF39 is shown in Figure 10.6. Table 10.6 shows the most important parameters of the motor. [1]

[1] http://www.d-motorusa.com/wp-content/uploads/2013/07/D-Motor-LF39-6_cylinder-3900cc_drawing.jpg

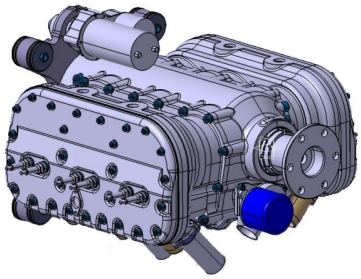

Figure 10.6: The D-motor LF39 [1]

Table 10.6: D-motor LF39 specifications

Engine	6 cylinder, 4 stroke
Displacement	3993 cc
Stroke	79 mm
Compression ratio	8/1
Cooling	liquid
Max power	93.2 kW (125hp)
Max cont. power	90.2 kW (121hp)
Fuel	91, 93, 95 oct. 98 oct. or avgas
Maximum torque	285Nm at 2500RPM
Intake	Multipoint sequential fuel injection
Alternator	25 Amp
Electric Starter	1.1 kW
Price	€18,000

The final fuel mass and volume as explained in Chapter 8 is presented in Table 10.7. The cruise mission is more fuel intensive than the ILS mission. The final fuel mass is therefore 91.02kg while the total fuel tank volume is 129.30 litres. Total fuel and engine mass is therefore 176kg. The PBS TP100 turboprop engine has a weight of 61.6kg and from table Table 10.7, a fuel weight of 145.35 with a total mass of 207kg. There is therefore a difference of 31kg between the piston and turboprop option.

Table 10.7: Fuel mass and volume for different profiles.

	SFC [g/kWh]	Cal. fuel mass [kg]	Total fuel mass [kg]	Total fuel volume [L]	Tank volume [L]
Profile 1	280	54.79	78.99	110.01	112.21
	523	101.54	125.74	149.69	152.68
Profile 2	280	66.82	91.02	126.77	129.30
	523	124.15	148.35	176.60	180.14

10.2.1. PROPELLER DESIGN

In Subsection 8.6.6 the process to select the right propeller is defined. After doing analyses on different propeller types and shapes, the decision is made to use a 'Taipan 8" x 6"'. Based on the landing gear size the the diameter is set to 0.9m and since the blades will be produced out of regular metal, the maximum tip speed is 270m/s (Table 8.10). Whit this given, the rotational speed is set to 5250 RPM (based on Subsection 8.6.3).

The dimensions of the propeller blade are illustrated in Figure 10.7 and the propeller performance is shown in Figure 10.8 which both comes from the PropCalc software.

10.3. WEIGHT

In this section the results from the weight estimation are shown. In Figure 10.9 and Figure 10.10 the two weight estimation results are shown and can be easily compared. As can be seen, the fuel weight decreased due to iterations in performance and propulsion, which will be explained later in Chapter 8. Also the payload weight

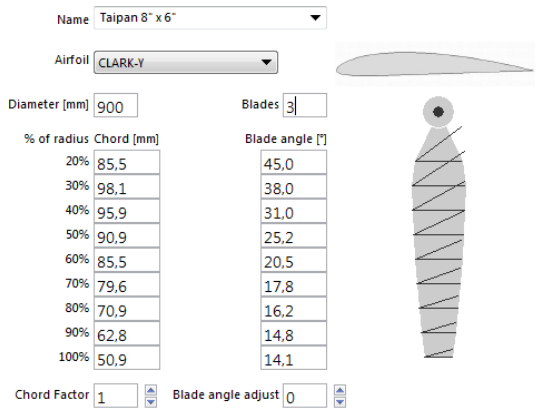

Figure 10.7: Propeller blade configuration

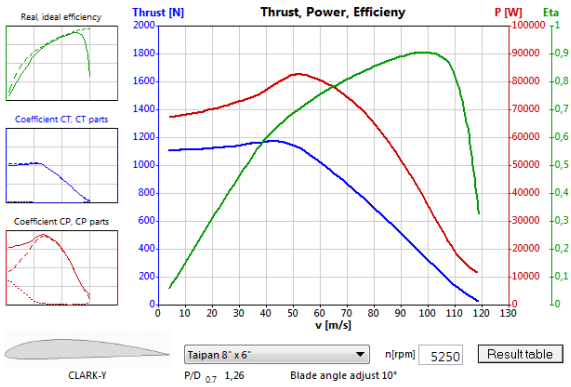

Figure 10.8: Propeller performance at 10° pitch angle

decreased, because some systems became lighter, and others had to move to the fixed avionics weight, as explained in Chapter 5.

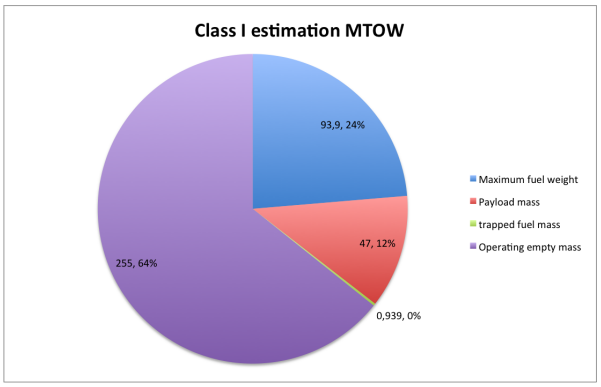

Figure 10.9: Class I weight estimation.

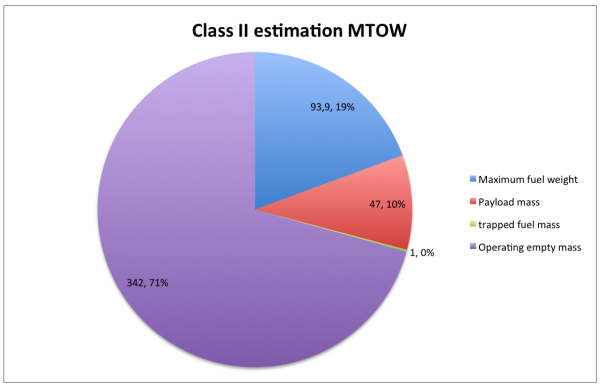

Figure 10.10: Class II weight estimation.

In Table 10.8 the weight components are given, including their estimation method, mass, and weight fraction W/OEW. This is visualised in Figure 10.11.

Verification In order to verify the estimation method that is used for the UAV, the weight fractions are compared with those of reference aircraft. In Table 10.9 the weight fractions of manned light aircraft are given, the same reference aircraft as on which the Raymer weight estimation is based. Example aircraft in this reference list are the Cessna 172 and the Beachcraft G50.

The wing weight fraction is within the range of light aircraft. The fuselage weight fraction is one the lower side of the range of reference aircraft. The fuselage estimation is based on fuselages which are sized to carry pilots. Giving the relative low UAV dimensions as input for the estimation method will decrease the weight too much. The empennage weight is completely out of range compared with light manned aircraft. All reference aircraft are tractor piston aircraft with tailplanes attached to the fuselage. For the tail estimation, a method is used that is accounting for booms. With the loads created by the tailplanes, the structural weight of the booms increases the empennage weight significantly. The landing gear is in the range. The flight controls are in range of the reference aircraft statistics.

Now the weight components are verified, the total OEW is compared with the class I estimated OEW. The new estimated value is 34% larger. This can be clarified by the fact that the reference aircraft, used in the class I estimation, differed to much from the UAV design. The mission of this UAV is rare, where most of the pushing propeller aircraft are designed for long range, high altitude, low airspeed flight, is this UAV designed for short endurance, low altitude and high airspeed. This results in a relative low fuel weight and a greater OEW, because of the structural loads and high engine weight.

As a conclusion, the fuselage was estimated to light and will be heavier in the assembled aircraft. Other weights will be closer to the estimated values, however, there is still a probability of changes. The operating empty

Table 10.8: Weight components, estimated by class II estimation.

Component		Symbol	Estimation method	Mass [kg]	Fraction [%]
Structural	Wing weight	W_w	Raymer	51	15
	Fuselage weight	W_f	Raymer	27	8
	Landing gear weight	W_{lg}	Gundlach	19	6
	Empennage weight	W_{emp}	Gundlach	29	8
Propulsion	Engine weight	W_{en}	Raymer	134	39
	Fuel tank weight	W_{ft}	Raymer	14	4
Fixed equipement	Avionics weight	W_{avion}	Gundlach	39	11
	Electrical system weight	W_{elec}	Gundlach	25	7
	Flight control system	W_{FCS}	Raymer	1	<1
	Hydraulics/pneumatics weight	W_{hyd}	Gundlach	<1	<1
	Paint weight	W_{paint}	Gundlach	2	1
Total		*OEW*		**342**	

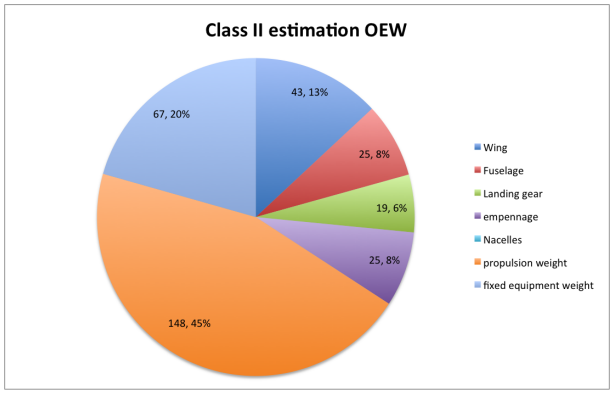

Figure 10.11: Class II component weight estimation.

weight estimation is larger than the class I OEW estimation, but the MTOW is not exceeded. During the development of the aircraft, a weight growth of 2-5% should be accounted for because of structural reinforcements, avionics changes, etc.

10.4. STABILITY & CONTROL

In this section the results of the stability and controllability of the UAV is explained. The tool as explained in Chapter 9 is used to compute all values.

10.4.1. LOADING DIAGRAMS

Below in Figure 10.12, Figure 10.13 and Figure 10.14 the loading diagrams are shown for three different wing positions. All plots start at the same OEW. The diagram is shaped by first loading the payload and than the fuel, and the other way around.The mass is expressed in kg and the centre of gravity in $\%MAC$ with the LEMAC as datum. Note that the LEMAC is moving with respect to the nose when the wing is shifted.

As can be seen in the figures, the more forward the wing is placed, the further the c.g. is located after the wing. With a tricycle landing gear this can create ground instability during loading and unloading. For the most aft position, the total c.g. change is close to zero. Since the LEMAC position is a part of the iteration process, the zero offset diagram is the actual loading diagram of the UAV. The combination of the three plots is used in computing the scissorplot.

10.4.2. SCISSOR PLOT

The scissor plot is shown in Figure 10.15. The CG range and the scissor plot are on the same X_{cg} axis. At the left the tail-surface over wing surface ratio is shown. On the right axis the LEMAC position on the fuselage length is plotted. The plots need to be shifted until the space between the two plot lines are equal, or in other words, the centre of gravity range is equal. At this position, the two intersection points should be horizontally aligned in the plot. The result of this is a horizontal tail surface area and a wing position.

In the figure, the loading diagram ranges are plotted diagonally from the topleft to the bottom right. The stabil-

Table 10.9: Weight fractions for light manned aircraft [31].

Component	Fraction range [%]
Wing	8-15
Fuselage	6.5-12
Tail	1.5-2.0
Landing gear	4.0-7.5
Flight controls	1.0-2.5

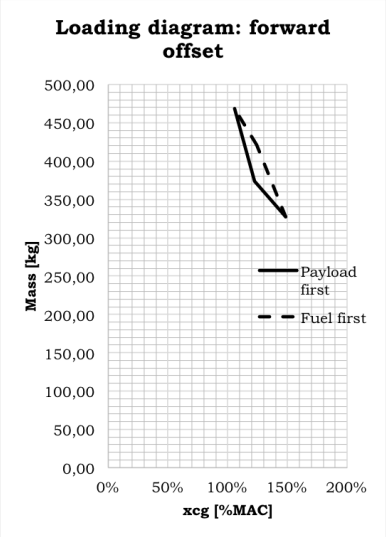

Figure 10.12: Loading diagram forward wing position.

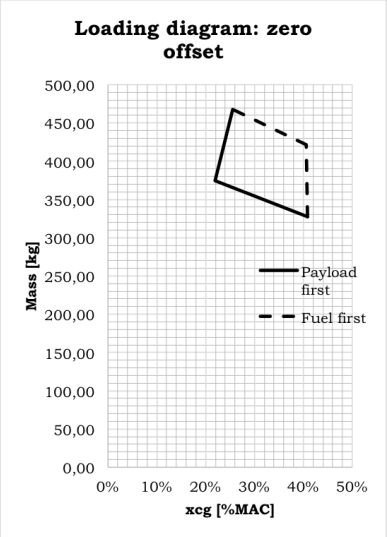

Figure 10.13: Loading diagram mid wing position.

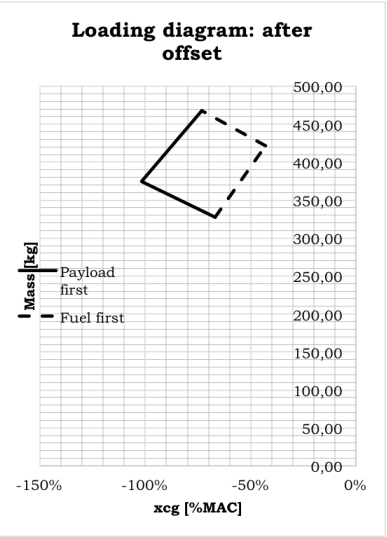

Figure 10.14: Loading diagram after wing position.

ity and controllability curves are convergent. Due to this, an equal c.g. range is found. The LEMAC is positioned at 70% of the fuselage length, so at 2.23m from the nose datum. The S_h/S ratio is found to be 0.168, making the horizontal tail surface have an area of 0.9848m^2. Using the tail volume coefficient determined in the Midterm report [2] of 0.631, the tail length (from 25% wing MAC to 25% tail MAC) is 2.97m.

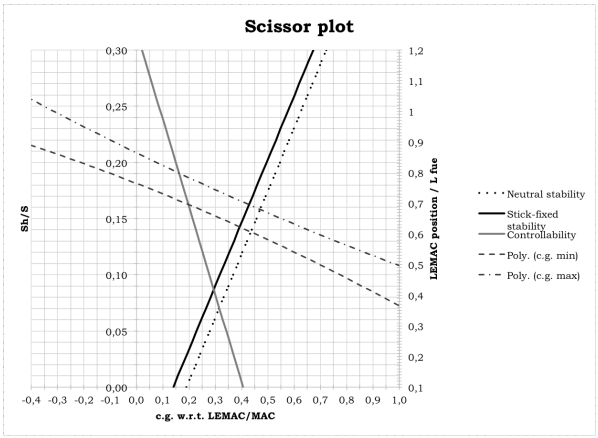

Figure 10.15: Stability & controllability scissor plot.

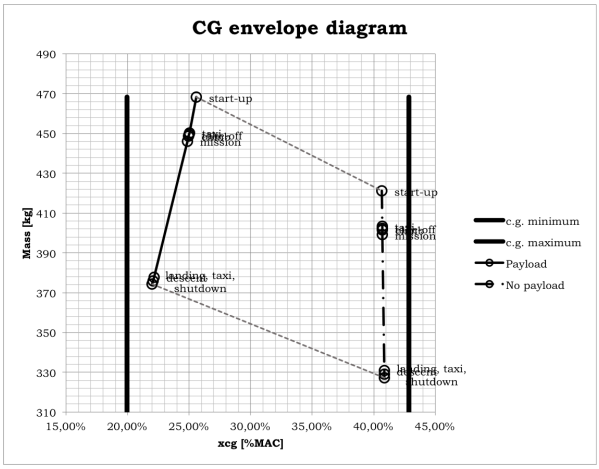

Figure 10.16: Centre of gravity envelope diagram of the UAV.

10.4.3. C.G. ENVELOPE DIAGRAM

In Figure 10.16 the CG envelope is shown. The CG minimum and maximum from the previous section are set, and the centre of gravity shift, influenced by the fuel flow, should be always between the limits, with or without payload. In this plot the CG location is expressed in $\%MAC$ with the LEMAC as datum. The mass is expressed in kg.

In the figure, all fuel shifts stay in between the boundaries of the c.g. In fact, the c.g. envelope diagram is in this

Table 10.10: Moments of inertia calculated by XFLR5.

Axis of inertia	$[kg \cdot m^2]$
Stability reference frame	
$I_{s_{xx}}$	474.0
$I_{s_{yy}}$	407.8
$I_{s_{zz}}$	837.5
$I_{s_{xz}}$	-56.38
Body reference frame	
$I_{b_{xx}}$	466.6
$I_{b_{yy}}$	407.8
$I_{b_{zz}}$	844.9
$I_{b_{xz}}$	-20.91

case the same as Figure 10.13, besides the flight phase points.

10.4.4. DETAILED STABILITY AND CONTROL ANALYSIS

In this section a more detailed analysis on stability and control is done as explained in Section 9.2. Airfoil Eppler 593 was analysed first. However, due to structural efficiency, fuel tank volume and flap attachment, it was changed to Eppler 1098. For the fin and elevator, NACA 0012 is used. These airfoils are all analysed in a batch for ranges of $-15 \leq \alpha \leq 16$ and $100{,}000 \leq Re \leq 7{,}000{,}000$. After that the wing as defined by the aerodynamics department is modelled, including wing flaps, elevator flap and ailerons. It is decided to combine the flaps and ailerons to flaperons. This will make the wing structurally less complex, because less linkages and actuators are needed.

STABILITY

In Table 10.11 the eigenfrequencies (F), damped eigenfruequencies (F_D), damping ratios (ζ), time constants (τ) and time-to-double amplitude or time-to-half amplitude (t_2) are given for different configurations and speeds. The aircraft's stability is analysed for deployed flaps, from 0° deflection to 40° deflection with an interval of 5°, of which only results of 0°, 20° and 40° are shown; and for different elevator deflections of which −5° and +4° are shown. The elevator is trimmed by a trim-tab. Further explanation about controllability is shown in Table 10.4.4.

It is important to note that resulting values are rough estimates and cannot directly be used without validation though CFD or flight testing. A major part that contributes to the uncertainty is that the moment of inertia is underestimated. Most masses are added as point masses, without an inertia. This yields a correct c.g., but the total inertia is not well estimated. For the used values see Table 10.10. The difference between the stability reference frame and the body reference frame is that in the stability reference frame the X_S-axis is aligned with the projection of speed vector V on the plane of symmetry. In short, the system is tilted by α over Y.

It is seen that the dutch roll, roll damping, short period and phugoid are always stable, of which the roll damping is overdamped and does not have an eigenfrequency. The spiral mode is not stable, which can be corrected in further studies. Besides the influence of flap and elevator deflection, also stability of the aileron-part of the flaperon is checked, as well as combinations of flap and elevator deflections. Both cases were stable. However, with decreasing speed, t_2 decreases. That means that during take-off and landing phases the spiral mode can be dangerous, corrective action should be taken quickly. This can be a problem when the operator tries to land manually, due to the lag of pilot reaction, the ground station, transmission and reception and FCS on board the UAV. This means that a part of the FCS on board the UAV shall be autonomous controlling the roll angle, assisting the pilot in case of manual flying. Also, the dutch roll mode at low speed sees a very strong damping, getting overdamped at very low speeds. On the bode-plot that means that the imaginary part of the complex conjugates are approaching zero, after which they diverge on the real axis, getting an unstable mode. But the effect of this is not fully known yet and more research has still to be performed.

A feature of XFLR5 is that it shows the control and stability derivative estimates. For standard clean configuration the derivatives can be found in Table 10.12. Just like with the stability modes, these values are very rough estimates and their value can differ significantly from real values. As validation the values are compared with what can be found in Appendix D of Flight Dynamics Lecture Notes[29]. Subsequently the conclusion is drawn that the estimates generally have the correct sign and are of the same order of magnitude as given reference values. It gives the team a good faith belief that the aircraft will be stable.

Table 10.11: Results of the stability analysis

Condition	Mode	F	F_D	ζ	t_2	τ
Standard (clean)	Lo1 & Lo2	1.196	1.079	0.477	-	-
$V_{trim} = 47.4\,m/s$	Lo3 & Lo4	0.043	0.043	0.018	-	-
	La1	-	-	-	0.104	0.150
	La2 & La3	0.505	0.499	0.151	-	-
	La4	-	-	-	12.673	-
Elevator deflection −5°	Lo1 & Lo2	0.823	0.763	0.407	-	-
$V_{trim} = 41.7\,m/s$	Lo3 & Lo4	0.050	0.050	0.003	-	-
	La1	-	-	-	0.122	0.175
	La2 & La3	0.174	0.170	0.211	-	-
	La4	-	-	-	8.967	-
Elevator deflection +4°	Lo1 & Lo2	1.877	1.708	0.456	-	-
$V_{trim} = 102.9\,m/s$	Lo3 & Lo4	0.020	0.020	0.002	-	-
	La1	-	-	-	0.047	0.068
	La2 & La3	0.724	0.721	0.094	-	-
	La4	-	-	-	88.420	-
Flap deflection +20°	Lo1 & Lo2	1.020	0.928	0.455	-	-
$V_{trim} = 39.3\,m/s$	Lo3 & Lo4	0.053	0.053	0.020	-	-
	La1	-	-	-	0.134	0.193
	La2 & La3	0.454	0.446	0.188	-	-
	La4	-	-	-	5.604	-
Flap deflection +40°	Lo1 & Lo2	0.869	0.795	0.441	-	-
$V_{trim} = 33.4\,m/s$	Lo3 & Lo4	0.062	0.062	0.061	-	-
	La1	-	-	-	0.174	0.251
	La2 & La3	0.429	0.417	0.240	-	-
	La4	-	-	-	3.279	-

CONTROLLABILITY

For control of an aircraft also control surfaces are needed. Usually primary three-axis control is done by three different control surfaces: elevator, aileron and rudder. In our design part of the flaps and ailerons are combined to flaperons, part is just flaps: the inboard portion (between fuselage and pod) is flap, the outboard portion (between pod and wingtip) is flaperon. Due to the double fin design, the aircraft features two rudders, which adds to the redundancy of the system. The horizontal stabiliser is positioned in between the two fins, attached to the booms. The elevator is then part of the horizontal stabiliser, spanning the entire width of the stabiliser and using the aft 20% of the chord. The maximum elevator deflection is ±15°. In addition, the horizontal stabiliser has an installation angle of −5° to maintain moment equilibrium during the flight while limiting constant control forces during cruise.

The flaps have a chord of 25% of the main wing local chord and span from 0.29 m to 0.80 m span-wise location on both wings. The maximum flap deflection is 40°. From 1.13 m to 3.75 m the flaperons are located, also 25% of the chord, having a maximum of 25° flap deflection and ±15° aileron deflection. During normal horizontal turns the flaperons will deflect like normal ailerons, while during landing phases the flaps will deflect in stages to 40°, the flaperons to 25° and if a rolling moment is required the flaperons will deflect asymmetrically, adding deflection on one side and subtracting deflection on the other side. The flaperons consists of two separate sections on each wing, which are actuated separately. This is for redundancy, but also if better landing performance is required part of the outboard flaperons can be permanently deflected to 35°, using only the outboard part as ailerons.

Regarding the rudder, it is symmetric for both vertical tails. The rudder surface starts at 20% chord of the fin and has a maximum deflection angle of ±20°. Using these control surfaces the UAV is suspected to be stable and controllable.

10.5. RESOURCE ALLOCATION

The technical resources are estimates that are done during the design process and are therefore uncertainties. During the design process, technical resources tend to always grow in an undesired and unfavourable direction.

Table 10.12: Derivatives in clean configuration

Longitudinal derivatives			
X_u	-6.3304	C_{x_u}	-0.035905
X_w	76.073	C_{x_α}	0.43147
Z_u	-197.71	C_{z_u}	-0.00011827
Z_w	-1034.4	C_{L_α}	5.8667
Z_q	-962.84	C_{L_q}	13.980
M_u	-0.34133	C_{m_u}	-0.0024780
M_w	-423.26	C_{m_α}	-3.0728
M_q	-1753.3	C_{m_q}	-32.585
Lateral derivatives			
Y_b	-64.991	C_{Y_b}	-0.36861
Y_p	-11.108	C_{Y_p}	-0.015751
Y_r	202.96	C_{Y_r}	0.28778
L_b	-14.469	C_{l_b}	-0.010258
L_p	-3166.3	C_{l_p}	-0.56121
L_r	911.71	C_{l_r}	0.16159
N_b	170.15	C_{n_b}	0.12063
N_p	-432.17	C_{n_p}	-0.076598
N_r	-528.38	C_{n_r}	-0.093652
Control derivatives			
X_{δ_e}	-811.16	$C_{X_{\delta_e}}$	-0.09706
Y_{δ_e}	0	$C_{Y_{\delta_e}}$	0
Z_{δ_e}	-1976.9	$C_{Z_{\delta_e}}$	-0.23655
L_{δ_e}	0	$C_{L_{\delta_e}}$	0
M_{δ_e}	-6499.9	$C_{M_{\delta_e}}$	-0.99552
N_{δ_e}	0	$C_{N_{\delta_e}}$	0

In order to compensate for this, a contingency plan needs to be constructed in which a contingency allowance will be determined. The contingency value needs to be monitored and action is necessary when the values are exceeded. If this is not done, over-designed subsystems can be created. The values are dependent on the type of system and the design progress. In the baseline report [3] the contingency uncertainties were set. When one of the design parameters in the iterative design is not meeting the contingency allowance, the focus should be kept on this parameter to lower it as far as possible. In case this could not be achieved, the uncertainty can be broadened, in order to increase the allowance. As last option, resources can be allocated in a way that certain subsystems get more budget constraints than others.

Table 10.13: Contingency allowance of several technical resources determined for the different design phases [3].

Design maturity	Mass	Costs	Dimensions	Endurance	Range	Sound exposure level
Baseline	20%	20%	20%	20%	20%	20%
Mid Term	15%	15%	15%	15%	15%	15%
Final design	5%	5%	5%	5%	5%	5%

In Table 10.14 the budgets, estimations and deviations are given.

- **Mass** Designing for mass is done in Chapter 6. Here the budgets for the subsystems are estimated by the Class II estimation. Those budgets are estimated to be higher in the final concept, by 5%. The total weight can be compared with the budget that was set in the start of the project. as shown in Table 10.14, the weight is off by 3.3%. This is out of the 5% boundary, however it could not get closer to the budget during iteration, so the contingency allowance must be increased to the 3.3%.
- **Cost** The cost is estimated to be €1.27M. This is 508% more expensive than the requirement set. This is explained by the requirement that is out of range for cost values of reference aircraft.
- **Dimensions** The dimensions are off by 7.6%. This requirement is set to not be larger in volume than a LD6. The system can increase by more than 5% while still fitting in the container. So the allowance does

Table 10.14: The allocated technical resources and estimations for NavAid calibration and testing.

Resource	Budget	Estimation	Error
Mass	$\leq 500kg$	$484kg$	3.3%
Production cost per unit	≤ €250.000	€1.200.000	380%
Dimensions (lxbxh)/Volume	$4.06x1.53x1.62m/9.8m^3$	$4.06x1.53x1.62m/9.1m^3$	7.6%
Endurance	$> 4hrs$	$18hrs$	350%
Range	$> 800NM$	$1738NM$	117%
Sound exposure level	$\leq 87dBA$	$45dBA$	68%

not need to be changed and the estimation is acceptable.

- **Endurance** The endurance of the aerial vehicle is designed to be much higher than the budget value. The estimation is done for cruise at the service ceiling, where straight flight is performed. Because the UAV mission needs to ascent and descent continuously, the endurance will decrease drastically. After production, the endurance will decrease because of fuel deficiencies, engine wear or increased drag because of added material, such as antennas and rivets.
- **Range** For the range the same reasoning is feasible as for the endurance budget. The intensive mission decreases the range.
- **Sound exposure level** The sound of the UAV is 15dBA less than the noise pollution of the Cessna Citation 550. This means that the sound of the citation is 68% louder than the requirement.

10.6. LAY-OUT

In this section, the lay-out of the UAV is presented in several figures to give the reader an idea of the design.

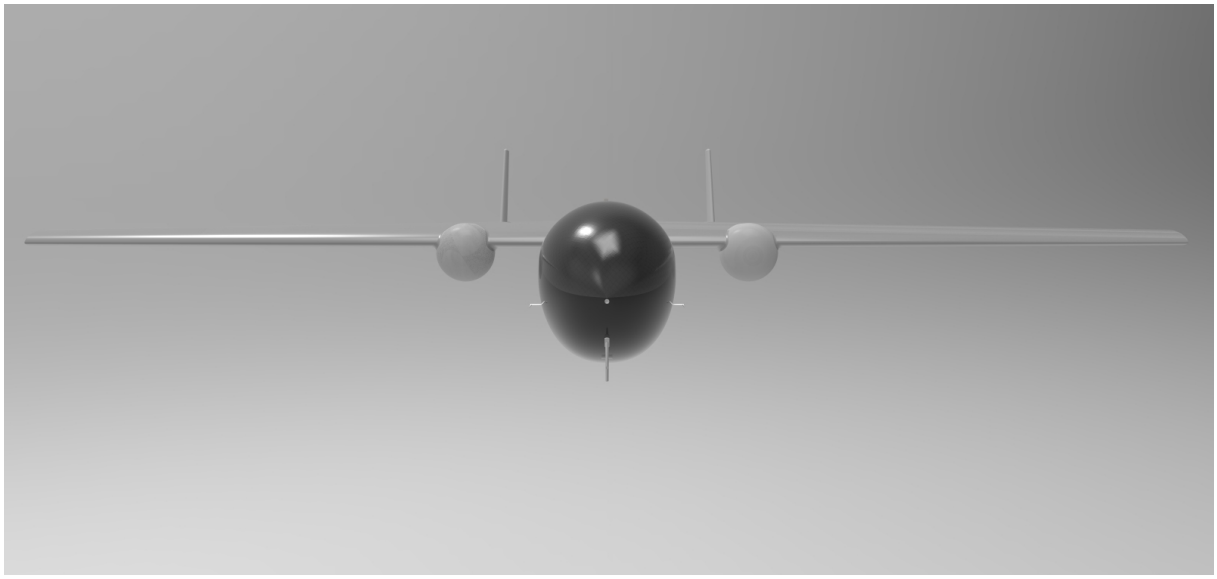

Figure 10.17: Front view of the aircraft

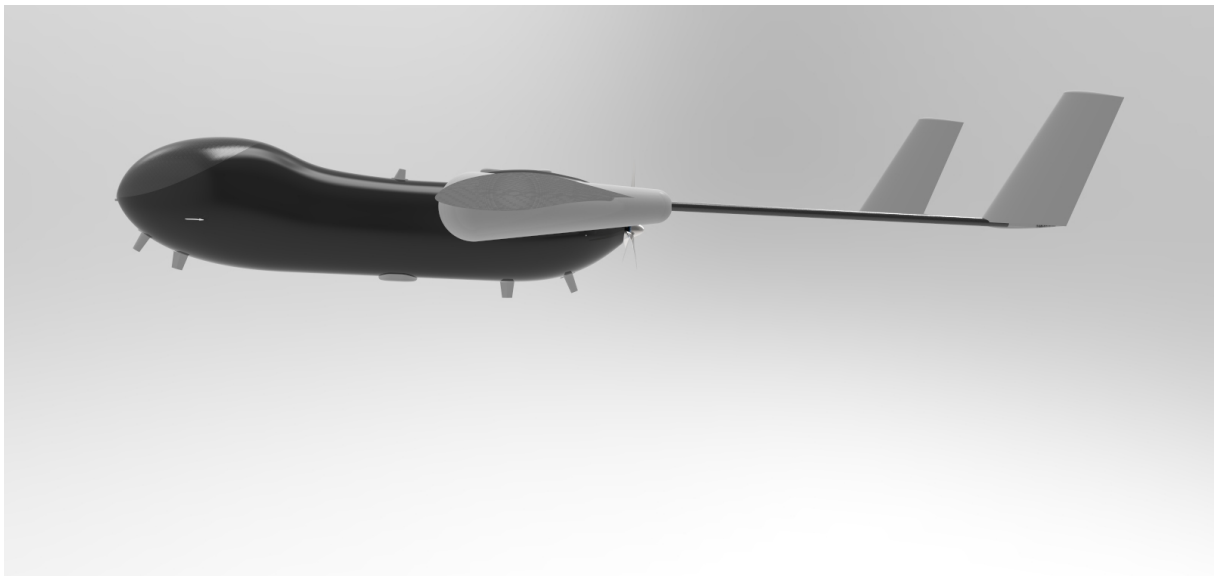

Figure 10.18: Side view of the aircraft

Figure 10.19: Top view of the aircraft

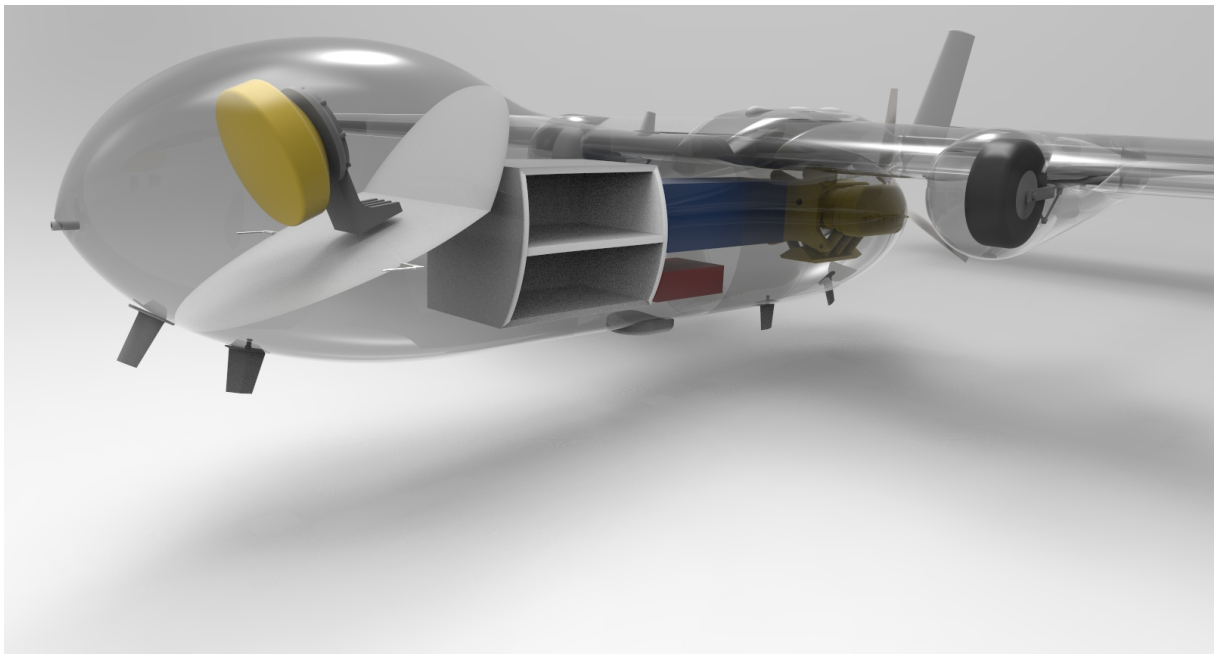

Figure 10.20: Inside view of the aircraft

11 Flight Performance

This chapter will describe the performance of the aircraft during various flight profiles. First, the climb and descent performance of the aircraft will be estimated from the performance diagrams. Next, a fuel estimation will be determined based on a simulated mission profile, then standard performance metrics will be analysed based on this fuel weight estimation. As can be seen in Figure 4.1, Flight Performance calculations are not part of the iteration process. However, if the performance does not suffice, a step back is necessary. Like a fail-pass test, redesign is required if the performance is insufficient.

11.1. Climb & Descent

The mission statement places a focus on mitigation of aerodrome interference and, as a result, the climb and descent performance for all flight profiles will be analysed at a state that minimises this.

The climb is performed at maximum excess power to ensure the biggest climb rate and get the aircraft at mission altitude within the minimum amount of time. The optimum true airspeed for climbing changes with altitude; however, is constant with equivalent airspeed. This means that the aircraft must accelerate during the climbing phase to achieve optimal climb performance, yet this means that excess power needs to be used to accelerate the aircraft. Optimal climb performance is calculated at discrete height intervals of 100 m to determine if this approach is satisfactory. The speed gradient (dV/dH) in the kinetic energy correction factor given by Equation 11.1 must be checked to determine whether or not this assumption has a negligible impact. The average speed gradient between 0 and 10,000 ft is equal to 6E-4 which makes the unsteady ROC approximately equal to what would be obtained using the energy method. The climb tool was verified by comparing the plot to those found in [32]. It was also checked to see if the maximum ROC remains constant with equivalent airspeed. See Figure 11.1 for power at different altitudes, and for Rate of Climb at different altitudes see Figure 11.2.

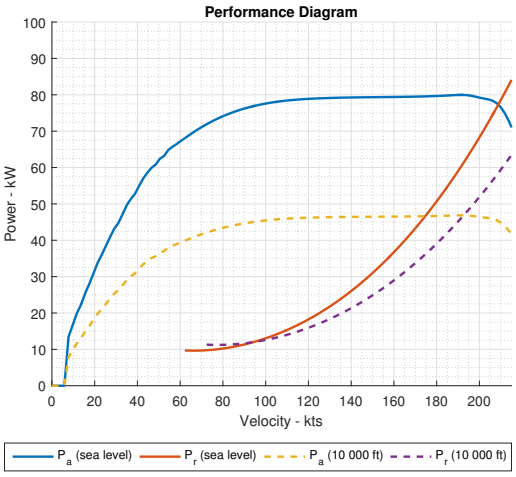

Figure 11.1: Performance diagram at different altitudes.

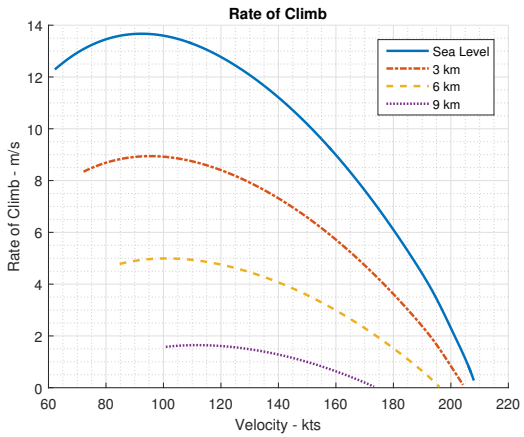

Figure 11.2: Variation of rate of climb at various altitudes as a function of true airspeed.

$$K_e = 1 + \frac{V}{g_0}\frac{dV}{dH} \tag{11.1}$$

The descent must be performed using a 3° glide-slope and it will be performed using a powered-descent to mitigate interference. The reference mission flies this approach at 165 kts, but in order to have better performance, the UAV will fly this approach at 185 kts. The gliding performance of the aircraft is given below, assuming the weight is equal to the MTOW and that no fuel is being jettisoned. This performance is obtained at the maximum lift to drag ratio and is of importance for engine failure performance.

- Rate of descent = 2.35 m/s

- Glide distance at service ceiling = 114.5 km
- Glide angle = 3°

11.1.1. FUEL ESTIMATION

The fuel estimation for the ILS mission is based on the profile showed in Subsection 8.4.9. The simulated mission profile does not directly take into account the increased power required by the turning manoeuvres during the mission but this is compensated for by flying additional climbs and descents. The climbs are performed at the same power and performance parameter (C_L^3/C_D^2); however, this approach is conservative as the duration of climbing flight is much longer than a standard turn (order of minutes vs seconds). Furthermore, cruise, for all profiles, is flown at a constant CL/CD ratio and altitude. This is favourable for fuel consumption but negatively impacts mission time. This approach is favourable to ATC as your altitude does not vary as much. This approach was opted for as the mission is flown in close proximity to the airport. It is important to note that for propeller aircraft the continuous climb cruise profile and the constant CL/CD at constant altitude profile produce identical ranges[32]. Descent is omitted in the standard profiles as gliding can be used for the descent. The fuel consumption for descents is often approximately the same as that used by climb.

Table 11.1: Flight performance during different flight profiles, excluding 25 kg of reserve fuel. *Descent is not included in the analysis. **Flown at a constant CL/CD ratio and altitude with reduced throttle. ***HD video streaming limited to 50 NM; however, SATCOM has global coverage.

Flight Profile	Mean Cruise Speed (kts)	Range (NM)	Endurance (hrs)	Fuel Consumed Cruise (kg)	Fuel Consumed Climb (kg)	Fuel Consumed Descent (kg)
Mission Profile (ILS)	200	286	2.9	29.2	9.6	9.4
Range (200 kts)	193**	607	3.2	64.3	1.7	0*
Range (optimum cruise)	100	1740	17.5	64.3	1.7	0*
Endurance	76	1440	19	64.3	1.7	0*

11.1.2. RANGE

The range of the aircraft is determined using a stepwise integration of the velocity following a flight at constant CL/CD at constant altitude. This expression produces the same range as the constant cruise and climb profile for propeller aircraft but the average airspeed for the chosen approach is lower[32]. This is because the fuel consumption for propeller aircraft is independent of altitude and both are flown at the same performance parameter. Verification was done by using the Breguet range equation (Equation 11.2), which is an approximate analytical expression for propeller aircraft. The maximum range was calculated at the point of minimum drag $(C_L/C_D)_{max}$.

The payload-range diagram for the final configuration is shown in Figure 11.4. The range differs by about 400 NM from the initial payload-range diagram. The most significant reason for this deviation is the initial approximation used for the the lift and drag. The current maximum lift-drag ratio is 19.4 whereas the initial assumption assumed a ratio of 11. This is primarily due to the initial estimation of C_{D_0} for the aircraft, which has decreased by 60 points.

$$R = \int_{W_2}^{W_1} \frac{\eta_j \cdot C_L \cdot dW}{c_p \cdot C_D \cdot W} \tag{11.2}$$

$$E = \int_{W_2}^{W_1} \frac{\eta_j \cdot dW}{c_p \cdot W \sqrt{\frac{W \cdot 2 \cdot C_D^2}{S \cdot \rho \cdot C_L^3}}} \tag{11.3}$$

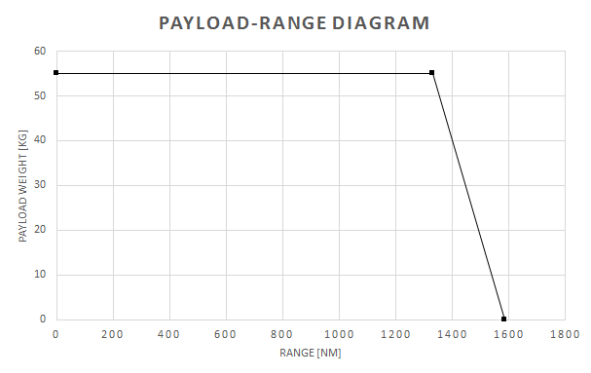

Figure 11.3: Payload-range diagram from midterm review.

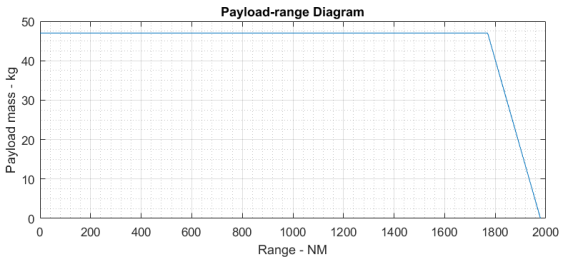

Figure 11.4: Final payload-range diagram

11.1.3. ENDURANCE

The endurance of the aircraft is approximated analytically using Equation 11.3. This approximation assumes that altitude is constant and the throttle is reduced to maintain optimum endurance as the weight decreases. A further check was performed by contrasting the achieved endurance with that of the reference aircraft from the Class I weight estimation. The optimum endurance is obtained at the point of minimum power required. This corresponds to the point of maximum C_L^3/C_D^2. Speed stability at this point is not of concern, as mentioned in Subsection 11.2.1, but the clean configuration stall is in close proximity to this region.

11.2. AIRFIELD

This section will delineate the performance of the aircraft within the proximity to the airfield. This includes the stall characteristics, and the take-off and landing distances.

11.2.1. STALL

The stall speed of the aircraft is given by Equation 11.4 and must be lower than 61 kts to satisfy system requirement *NVD-Syst-01-06-01* which is derived from CS23.49[36].

$$V_{stall} = \sqrt{\frac{W \cdot 2 \cdot 1}{S \cdot \rho \cdot C_{L_{max}}}} \tag{11.4}$$

The $C_{L_{max}}$ necessary for the selected design point is 1.6. The final aircraft has a $C_{L_{max}}$ of 1.57, which is within bounds as wing area increased reducing the stall speed to 56 kts. This value is preliminary as flight tests must be performed to determine the accuracy of this value and for certification. It is important to note that usually flight speed is slightly higher at 1.1-1.2 times the stall speed to operate in the minimum comfortable airspeed region to ensure the aircraft is still controllable on the back side of the power curve. In the case of the UAV system under consideration, the reversed command region is almost nonexistent. However, this means that the aircraft is often operating near the condition of stall. Furthermore, the increased drag due to the landing gears increase the speed stability in this region.

11.2.2. TAKE-OFF

The take-off performance of the aircraft is approximated using an analytical approximation. The main assumptions are:

- Constant angle of attack
- Constant weight
- Rotation is instant
- $V_{LOF} = 1.05 V_{min_{take-off}}$
- $V_{LOF} = 1.2 V_{min_{take-off}}$

Furthermore, average values of thrust, drag, lift and acceleration are approximated during the ground and airborne phase. The average values during the ground roll are calculated at a velocity equal to $V_{LOF}/\sqrt{2}$.[32] The average acceleration in Equation 11.5 is given by Equation 11.6. The impact of ground effect is found to have a minimal impact on the aircraft's take-off and landing performance but the impact is an increased lift slope and reduced induced drag as shown in Figure 11.5.

$$S_g = \frac{V_{LOF}^2}{2\bar{a}} = 123m \tag{11.5}$$

$$\bar{a} = \frac{g}{W}(\bar{T} - \bar{D} - \mu(W - \bar{L})) \tag{11.6}$$

During the airborne phase, the average velocity is assumed to be that at the screen height.[32] The airborne distance travelled is then given by the analytical equation in Equation 11.7 where the screen height is determined by CS23[36] to be 15 m. The climb angle is then determined by substituting the average thrust, drag and weight into Equation 11.8.

$$S_a = \frac{\frac{1}{2g}(V_{scr}^2 - V_{LOF}^2) + h_{scr}}{\sin(\gamma_{scr})} = 111m \tag{11.7}$$

$$\sin(\gamma_{scr}) = \frac{\bar{T} - \bar{D}}{W} \tag{11.8}$$

The tool used was verified at each calculation with a reference aircraft problem to which the solution was known.

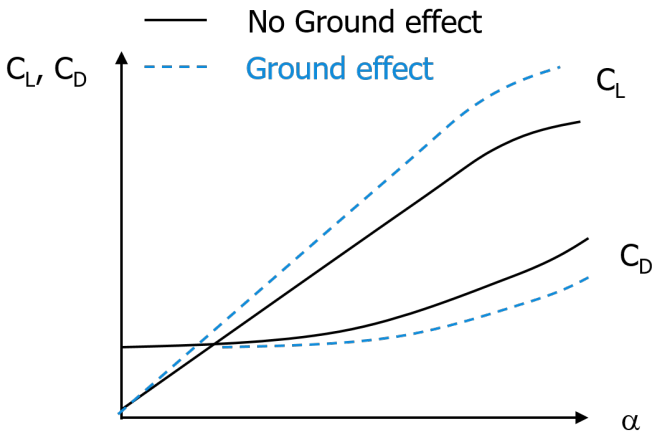

Figure 11.5: Impact of induced drag on ground performance.

11.2.3. LANDING

In addition to the assumptions in Subsection 11.2.2, the assumptions for landing are:

- $V_{touchdown} = 1.15 V_{min_{landing}}$
- $V_{approach} = 1.3 V_{min_{landing}}$

First the airborne distance must be calculated and then the ground roll distance. During landing, the glide-slope is assumed to be the standard 3°, as used by most ILS systems.

$$S_a = \frac{\frac{1}{2g}(V_A^2 - V_T^2) + h_{scr}}{\frac{1}{2}\left(sin(\gamma_A) + \left(\frac{C_D}{C_L}\right)_T\right)} = 318m \quad (11.9) \qquad S_g = \frac{W}{2g}\frac{W}{S}\frac{2}{rho}\frac{1.15^2}{C_{L_{max}}}\frac{1}{\bar{D}+\bar{D_g}} = 207m \quad (11.10)$$

The ground roll distance is then calculated using Equation 11.10, where the average values are computed at $V_T/\sqrt{2}$. D_g is the friction contribution as a result of tyre friction with the runway.

The tool used for the landing was verified at each calculation with a reference aircraft problem to which the solution was known.

11.3. V-N DIAGRAM

The V-n diagram is part of the flight envelope. It illustrates the aircraft limit load factor as a function of equivalent airspeed. The maximum positive and negative limit load factor is extracted and of great importance for the structural design of the aircraft. In fact the V-n diagram consist out of two diagrams; a manoeuvre diagram and a gust diagram. The manoeuvre diagram illustrates the variation in the load factor with the equivalent airspeed for manoeuvres, where as the gust diagram displays the loads associated with vertical gusts encountered during different flight phases. Figure 11.7 illustrates the resulting V-n diagram.

Manoeuvre loading

First, the manoeuvring curve is established. The line from the origin to point A is constrained by the maximum lift coefficient of the aircraft. The aircraft is not able to experience higher loads at that speed range, since it will stall before that. The speed at point A is the design manoeuvring speed V_A of 119.3 knots (also referred to as the corner speed). The corresponding maximum manoeuvring load is 3.8, as determined by CS 23.337 for the normal aeroplanes category [36]. The design dive speed V_D (240.6 knots) is determined by the requirements of CS 23.335 [36], compared to the design cruise speed V_C [36] of 200 knots. The negative limit manoeuvring load factor (-1.52) is established from CS 23.337 [36]. It can be observed that the stall speed V_S of the aircraft corresponds to a load factor of one.

The manoeuvring loads are limited aerodynamically up to 118 kts and then the limit is structurally imposed until 186 kts and only thereafter is it limited by the propulsion system. This means that the corner velocity (V_A in Figure 11.7) results in the maximum turning rate. Furthermore, this turning rate can be sustained as it is not limited by the propulsion system. Higher instantaneous (unsustained) turns cannot be performed due to the aerodynamic and structural limitations imposed on the aircraft system. Finally, it can be seen from Figure 11.6 that there is only a marginal difference between the structural and propulsive limits prior to 186 kts.

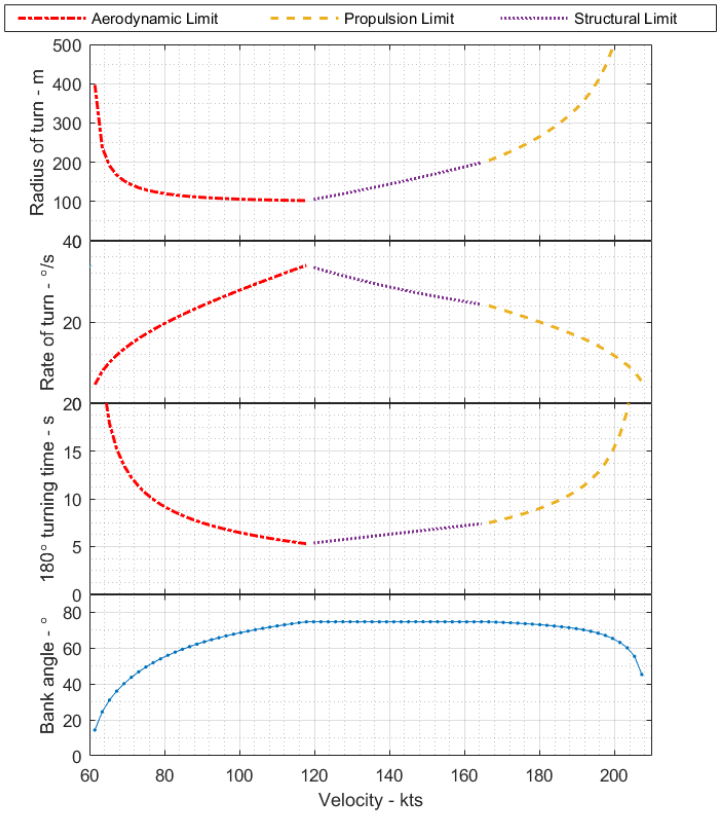

Figure 11.6: The aircraft's turning performance at sea level.

Gust loading

Gusts are one of the phenomena of a dynamic atmosphere that are encountered, especially at high altitude flights. When an aircraft flies through a gust, it will experience an immediate increase or decrease in angle of attack. The gust loads experienced by the aircraft may exceed the manoeuvring loads and should therefore be considered carefully. There are many publications on modelling of gust loads. For this aircraft, the requirements as established in CS 23.333 and CS 23.341 [36] are utilised. The resulting limit load factor for two conditions are determined. Positive and negative gusts of fifty feet per second during cruise, and positive and negative gusts of 25 feet per second at the design dive speed V_D. These requirements set by CS23[36] are depended on altitude. The values previously described correspond to the altitude range from sea level to 20,000 feet. The gust loads are computed with the formulae as specified in CS23[36].

Once both the manoeuvring and gust diagrams have been created, they are combined into a load envelope. From Figure 11.7, it can be observed that the loads for this aircraft are limited by gust. This behaviour is expected for this aircraft, since sensitivity to gusts is correlated with a large lift slope and a low wing loading. By superimposing the manoeuvre and gust diagrams the maximum and minimum limit load factors are determined to be 5.34 and -3.34, respectively. The design load factor required for the structural design of the aircraft is determined by multiplying the limit load factors by a safety factor of 1.5, resulting in maximum and minimum design load factors of 8.01 and -5.01, respectively.

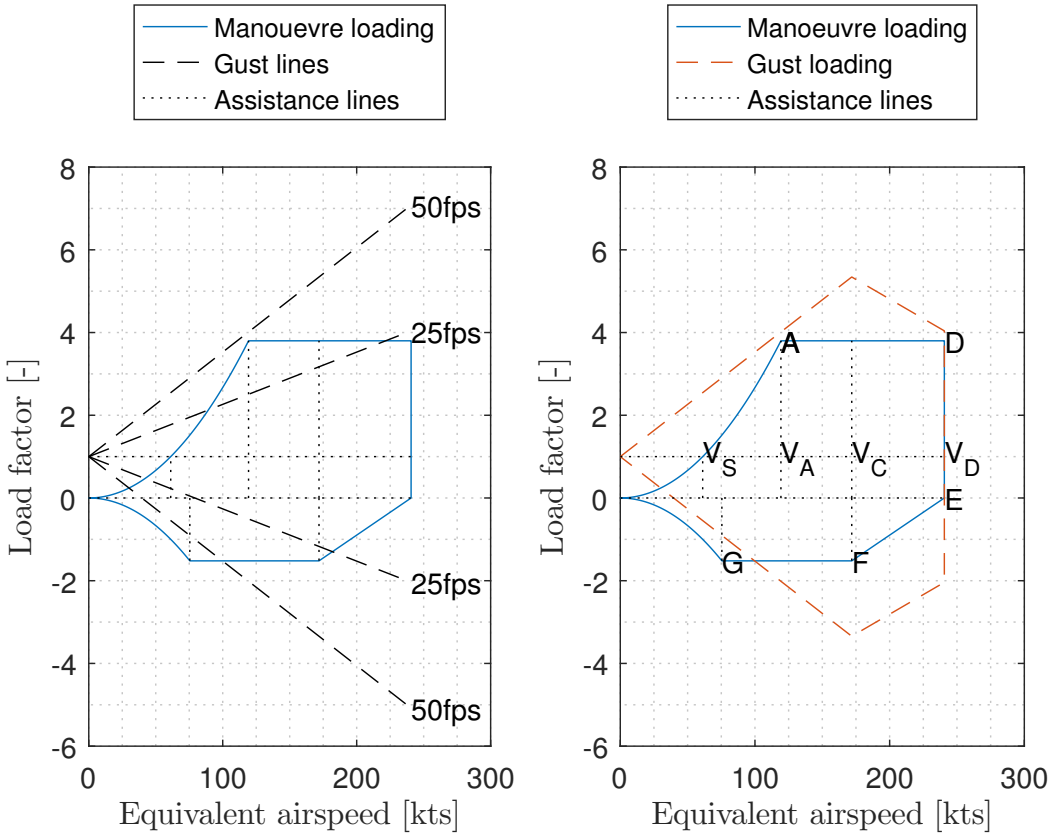

Figure 11.7: Load diagram

11.4. FLIGHT ENVELOPE

The service ceiling is defined as the maximum altitude at which a rate of climb of 5 m/s can be achieved. Altitudes higher than this can be achieved; however, these altitudes take a much longer time to reach as the rate of climb starts to act like an asymptote. This is the reason for the significant difference between the theoretical and the service ceiling. The model used to model the altitude effects on the piston engines performance is the Gagg and Ferrar equation (Equation 11.11). σ is the density ratio between the flight altitude and that at sea level.

$$P = P_{SL} \cdot (1.132\sigma - 0.132) \tag{11.11}$$

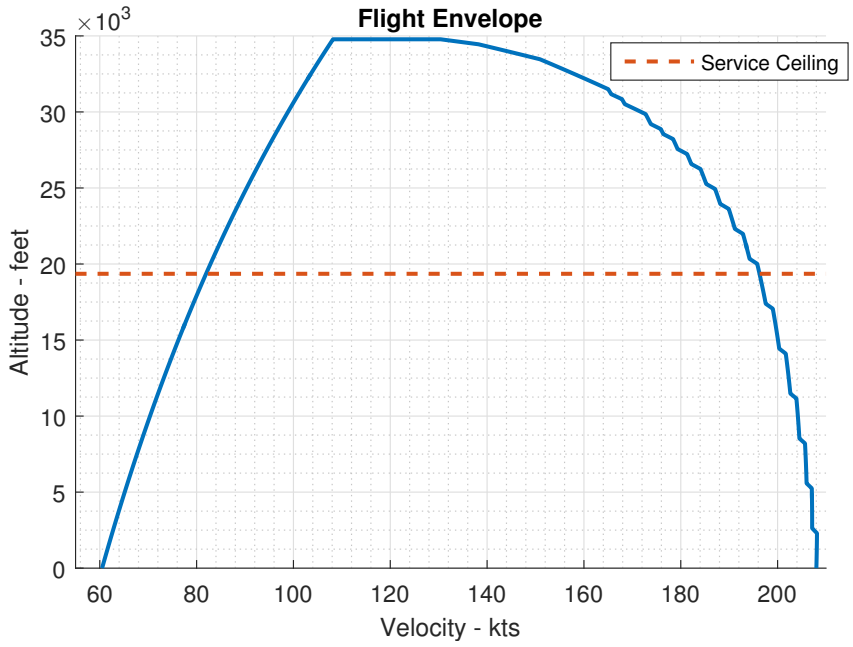

Figure 11.8: Flight envelope for the clean configuration aircraft.

11.5. SENSITIVITY ANALYSIS

The sensitivity analysis was performed by varying the inputs to the tool and contrasting the outputs. This is a simplified approach as there is often coupling between different parameters, which is evident from the drag-polar analysis. The parameters that have been found to have the most impact on flight performance are:

- $C_{L_{max}}$
- Drag-polar
  - C_{D0}
  - $\left(\frac{C_L}{C_D}\right)_{max}$
  - Aspect ratio
- Propeller efficiency during each phase
- Surface area
- MTOW

The aspect ratio (+10% change) has the largest impact on the range (+10%) and endurance (+8.4%) performance parameters as it impacts $\left(\frac{C_L}{C_D}\right)_{max}$ the most. Take-off and landing is not significantly impacted. The wing surface area (+15% change) also impacts the endurance (+5.2%) but the range is not as affected; however, the optimum flight speed does decrease and the fuel consumption increases. The most notable impact of surface area is in the take-off (-18.8%) and landing (-9%) performance where small changes can have a large impact on the required distances. $C_{L_{max}}$ has a noteworthy impact and is the value to which most the design is the most sensitive as a lot of performance parameters, such as the turn performance and stall, are calculated at these limits. It is also the most difficult to get an estimation for this parameter, as it is only accurately found from experimental data or flight tests. MTOW (3.2%) increases the landing slightly; however, its most significant impact is seen in the endurance (-4.7%) and take-off distance(+9.4%) of the aircraft. Climb performance is also decreased resulting in more fuel required for climb. The take-off is very sensitive to propeller efficiency as it determines the available thrust that the aircraft can generate. This also has an impact on the service ceiling and the maximum speed; however, the propeller is usually designed to have constant efficiency over almost the entire flight regime. If a fixed-pitch propeller was opted for then the climb or cruise performance would be significantly impacted, depending on which one the design is optimised for. This can also impact the maximum achievable flight speed as currently the propeller and aerodynamics are the limiting factors.

12 Structural Analysis & Design

The feasibility of the proposed design must be verified by analysing the structural integrity of the vehicle. A preliminary design of the primary structural elements must be generated in order to get a feeling of the load carrying characteristics of the aircraft. The main goal is to verify whether the vehicle is able to survive all limit loads that may be expected during its lifetime, within the assigned weight budgets. Accordingly, the structural analysis and design of the NavAid UAV represents a feasibility check of the proposed configuration, as described in Chapter 4. Because of the limited time available, the efficiency of this verification process can be enlarged by analysing the most critical structural parts of the aircraft. Accordingly, the sizing of two elements will be described in this chapter, including the structural configurations of the main wing and the tail booms. However, since the analysis of the fuselage and empennage structures will not be considered, the feasibility of the complete vehicle is verified only to a limited extend.

This chapter starts with an analysis of the functions of the structure (Section 12.1) and an overview of the requirements (Section 12.2). First, in Section 12.3, the wing loads are determined and from this, the proposed structure of the wing can be analysed. Then the booms are analysed and sized in Section 12.4. After this, the verification and validation is shown in Section 12.5 and lastly, the compliance matrix is shown in Section 12.6.

12.1. Functional Analysis

The start of the structural analysis & design is defining all functions that the structure has to fulfil. An overview of these functions is given in Figure 12.1. These are derived from the FBS as presented in the Baseline Report [3]. There is only a small amount of functions to be performed by the structure, but the structure is a critical part in the design. Providing structural integrity is a vital function that is applicable to multiple situations, such as ground operations, heavy manoeuvres in flight, bird strikes, etc.

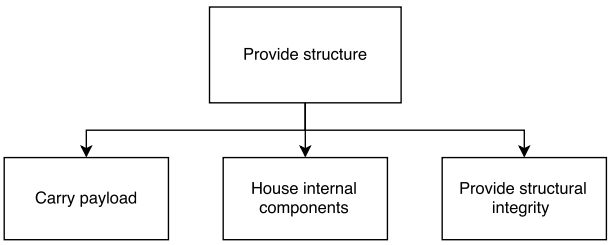

Figure 12.1: Function of the structure.

12.2. Requirements

In the Baseline Report [3], all requirements were determined. From this entire list, a selection is made that is applicable to the functions that are mentioned in the previous section. This selection can be found in Table 12.1.

12.3. Wing Analysis

The main wings of an aircraft generally carry the highest loads and should therefore be carefully analysed. Besides aircraft weight, these loads dependent on a multitude of parameters. As explained in the previous chapter, the converged vehicle configuration seems to be highly sensitive to gust loads, increasing the load factors the vehicle must be design for. In addition to aerodynamic loads, the wing is also the primary attachment structure for other aircraft systems such as the main landing gear, the fuel tanks and the tail structure. These systems locally introduce additional loads that must be properly accounted for in the analysis. The approach to wing box analysis and design starts with identifying the critical design loads. These loads will be used to analyse the structural behaviour of the preliminary system geometry, and recommendations are made for how the system may be designed in more detail in the future. By doing so, any future design challenges and focus points may be addressed.

Table 12.1: Requirement table for the payload and avionics subsystem.

ID	Requirement
NVD-Syst-01-06	The airborne element of the system shall be recoverable without getting damaged.
NVD-Syst-06	The airborne element shall be able to support all loads experienced during its lifetime, multiplied by a safety factor of 1.5 without failure.
NVD-Syst-06-01	The airborne element shall be able to support all static loads experienced during its lifetime.
NVD-Syst-06-01-01	The airborne element shall support all propulsion loads throughout its lifetime.
NVD-Syst-06-01-02	The airborne element shall support all loads related to recovery throughout its lifetime.
NVD-Syst-06-01-03	The airborne element shall support all aerodynamic loads throughout its lifetime.
NVD-Syst-06-01-04	The airborne element shall be able to withstand minor impact loads.
NVD-Syst-06-02	The airborne element shall be able to support all dynamic loads experienced during its lifetime.
NVD-Syst-06-02-01	The airborne element shall not fail due to fatigue throughout its lifetime.
NVD-Syst-06-02-02	The airborne element shall not be damaged as a result of flutter throughout its lifetime.
NVD-Syst-07-02-05-04-01	The payload shall be protected against aggressive environments, including wide temperature ranges, precipitation and radiation.
NVD-Syst-07-02-05-04-02	The payload shall experience low vibration and oscillation levels.
NVD-Syst-07-02-05-04-03	The airborne element shall be robust to flight-path related disturbances during measurements.
NVD-Syst-08-02-02	All system elements must be maintainable.
NVD-Syst-08-02-02-01	The motor(s) of the airborne element shall be replaceable.
NVD-Syst-08-02-02-02	All key subsystems shall be accessible for maintenance purposes ,without compromising the structural integrity of the system.
NVD-Syst-09-02-02	The airborne element shall be operable under all temperatures ranging from -30 degrees to +50 degrees Celsius.
NVD-Syst-10-03	The system shall have a minimum life time of 5,000 flight cycles.
NVD-Syst-11-06-01	All systems that are critical for flight safety shall be equipped with sufficient redundancy.

12.3.1. DESIGN LOAD CASES

There are three critical load cases identified which might be experienced by the UAV. The first two are determined from regulations and are the standard ultimate load case that is caused by manoeuvres and the negative limit manoeuvring load case. The third one is landing, which results in a different combination of loads.

Ultimate load factor

To start off, the loads during flight will be investigated that generate the ultimate load factor, which is set to 8.0. This number is obtained by multiplying the limit manoeuvring load factor from CS23 [36] (which is 5.3) by 1.5. With this load factor, a lift distribution can be determined using the tool that is generated in Chapter 7 about the aerodynamics of the UAV. This lift distribution is illustrated in Figure 12.2.

While the lift is acting upwards, the weight of various components acts downwards. The weight can be divided in the wing weight, the fuel weight, the main landing gear weight, the pod weight and the tail weight. The weight of the wing is assumed to be scaling with the cross-sectional area of the airfoil, since the shape of the airfoil is constant of the wingspan (the chord decreases, but so does the thickness, since the thickness to chord ratio is constant). Therefore the cross-sectional area of the airfoil decreases quadratically over the wingspan from the root to the tip, and thus also the weight of the wing decreases quadratically towards the tip, which is expressed quantitatively in Equation 12.1. The density used in this equation is determined by dividing the total weight of the wings by the total volume of the wings.

$$\text{Weight per metre span} = \rho_{wing} \cdot (A_{root} - (A_{root} - A_{tip}) \cdot (\frac{x}{b})^2) \tag{12.1}$$

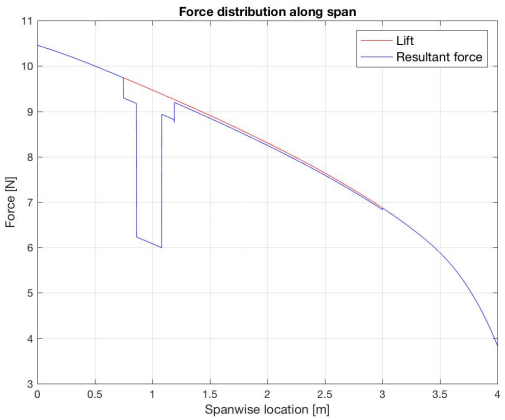

Figure 12.2: Lift and resultant force distribution along the wingspan for the ultimate load case of n=8.0.

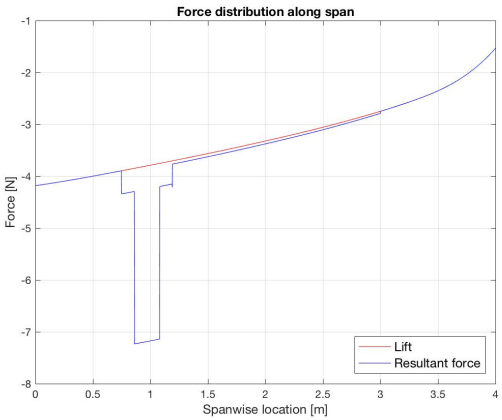

Figure 12.3: Lift and resultant force distribution along the wingspan for the ultimate load case of n=-5.0.

Since the lift force acting on the wings is much larger than the weight of the wings, or any of the other weight components, the resulting forces on the wing will point upwards for this case. The weight of the fuel varies over the duration of the flight, and less fuel will result in less weight, so initially it seems that this results in a more upwards force. But with a full fuel tank, the total lift force is also increases because the ultimate lift force is determined by multiplying the weight of the aircraft with the ultimate load factor. Therefore the critical case is when the fuel weight is assumed at its maximum. This fuel weight is distributed quadratically with the chord length of the wing section, similar to the distribution of the weight of the wing, however, for the fuel, only a part of the span and chord length is used for fuel storage.

The weight of the main landing gears, the pods and the connection for the tails is assumed to be evenly distributed over their widths, which does not require more calculations. Then summing this all up, the force distribution over the span of the wing can be determined and is illustrated in Figure 12.2.

Negative limit load case

Another load case to be analysed is the negative limit manoeuvring load case. Like the ultimate load factor, this load case is also dictated by CS23 regulations [36] and is equal to a load factor of -40% of the ultimate load factor (which is -3.3) multiplied by a safety factor of 1.5.

Since the load factor for this case is negative, the lift and weight point in the same direction (downwards) and add up to the total resultant force. The total resultant force on the wing in this case is thus also negative (pointing downwards). The distribution of the different weights is again assumed similar as in the ultimate load factor case. The spanwise lift and resultant force distribution for this load case is presented in Figure 12.3.

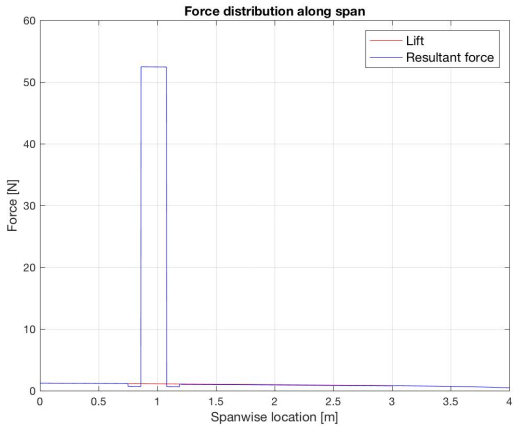

Figure 12.4: Lift and resultant force distribution along the wingspan during landing for an ultimate load case of n=0.67.

Loads during landing

Another critical load case is landing. According to CS23 [36], the maximum vertical speed at touch down should

be 10 ft/s or 3.048 m/s. The length of the landing gear stroke is already known, and assuming constant deceleration, the average deceleration can be calculated using Equation 12.2. Multiplying this deceleration with the weight during landing results in the vertical force experienced during landing. Figure 12.4

$$a = \frac{V_v^2}{2 \cdot l_{stroke}} \tag{12.2}$$

12.3.2. STRUCTURAL DESIGN

The most common solution for providing the wing with structural integrity is an integrated box that consists of spars, ribs, stringers, stiffeners, and the upper and lower wing skin. The flexible nature of a wing box allows the structural design to be accurately tailored to a specific design case by adjusting thicknesses, spacings, and lengths. The key objective for the wing box design is threefold. First, it must be proven that the wing must have sufficient strength to survive all expected limit loads multiplied by a safety factor of 1.5. Second, the wing must be sufficiently stiff in order to prevent too large deflections. However, a too high stiffness is also not desirable, as some degree of wing flexibility helps alleviating sudden aerodynamic loads. An example of this is a gust load. While in theory such a load would be modelled as an impulsive force, its more gradual nature in reality gives the structure some time to deform. However, this load alleviation will be limited if the stiffness of the wing is too high. Therefore, a trade-off has to be made. Third, the structural weight of the wing must remain within the assigned limits. The converged results listed in Chapter 4 show that the total wing weight was estimated at 51.6 kg, including the flaperon system. For a half-wing this translates to a weight budget of 25.8 kg. However, this weight budget applies to the combined weight of the primary and secondary wing structures. According to Torenbeek [37], the secondary structure consists of the leading and trailing edge structure, high-lift devices, and control surfaces, and typically contributes between 25-30% of the total wing weight. Since the current vehicle will only feature trailing edge high lift devices, it seems reasonable to keep the secondary wing structure weight at 25%, leaving a total wing box weight of 19.3 kg. However, another 4% must be subtracted from this result for contingency purposes, as was described in Section 10.5. This results in a design weight of 18.6 kg for the entire wing box. In combination with the strength and stiffness considerations and the semi-span of 4 meters, this very low design weight poses significant challenges for the structural design of the wing.

The structural analysis and design of the wing is centred around the application of the engineering program *FEMAP*. This software, developed by Siemens PLM, is used to build a finite element model of the primary wing structure. FEMAP is a pre- and post-processor that allows for the preparation and meshing of geometry, which may be imported as a CAD model, and lets the user investigate FEA results. The actual solving of the FEA problem is done by the *NX Nastran* solver, which uses the mesh and boundary conditions defined in the FEMAP environment. The primary reasons for choosing this software are (1) its high algorithmic power, making it possible to get highly detailed results that cannot be obtained with standard structures theory, and (2) the fact that it is a fully validated tool. These two advantages therefore allow for more detailed results in less time. In order to limit the modelling complexity, the wing box has been modelled as consisting of five different structural elements. These include the forward and aft spars, the upper and lower wing skins, longitudinal stringers, spar stiffeners and ribs. Attachment fittings, such as rib connections or landing gear supports, were not explicitly included in the model. The details behind the FEM model will be explained later.

The first step is to define a preliminary wing box geometry that meets the weight requirements and forms a good starting point for the optimisation process. Structural analysis and design of an aircraft structure is an iterative process that aims at getting the best structural properties at the lowest possible weight. Although the iteration process falls outside the scope of the current report, a well-defined initial wing box geometry can give some good first insights into what may have to be done during the optimisation cycle. Accordingly, preliminary decisions must be made on thicknesses, spar positioning, and the location and number of stringers and ribs, as well as their cross-sectional geometry. For the initial layout, this has been done based on qualitative engineering judgement, with the primary aim of meeting the weight requirements. An overview of the preliminary layout is shown in Table 12.2. A CAD render of the preliminary wing box is shown in Figure 12.5.

The preliminary wing model geometry was built up logically. The spars are located at 10% and 60% of the local cross-section, which are typical values. The rib spacing decreases along the span, as the bending and shear loads get smaller when moving away from the wing root. It is expected that this approach will prevent skin buckling along the entire span, while allowing for a lower structural weight. Regarding stringers, each skin is featured with four stringers running along the entire span, with the top skin featuring two additional stringers running from the root to the fifth rib. This will enhance the load carrying capability at the upper root, at which the stresses will be the highest. Spar stiffeners were installed to increase the shear resistance of the structure.

Table 12.2: Preliminary wing box parameters

Material	Al7075	Stringer thickness, top	1.4 mm
Forward/aft spar position	10%/60%	Stringer thickness, web	1.4 mm
Spar thickness	1.7 mm	# Spar stiffeners	16
# Ribs	8	Stiffener profile	T-section
Rib thickness	2-2.3 mm	Stiffener height	15 mm
Skin thickness	0.75 mm	Stiffener width	20 mm
# Stringers, top	6	Stiffener thickness, top	1.7 mm
# Stringers, bottom	4	Stiffener thickness, web	1.7 mm
Stringer profile	T-section	Model weight	17.3 kg
Stringer height	15 mm	Rib connection weight	0.9 kg
Stringer width	20 mm	Wing box weight	18.2 kg

For all parts, it was chosen to use Al7075 as structural material. This allows the requirement of 80% recyclability to be met.

The preliminary wing box is imported into FEMAP and the identified load cases are applied. The wing box was given a fixed constraint, which approximates it as a cantilevered structure. This does not fully represent correctly the way the wing is installed in reality, as it is typically clamped by a set of bolds over a certain range. However, it is expected that the modelled constraint will not lead to very large deviations from reality. Three load cases are considered, including maximum wing load factor, minimum wing load factor and hard landing. The result for maximum wing load factor will be discussed first. It was shown in Chapter 11 that the design load factor for maximum positive loads equals 8.01, due to the vehicle's high sensitivity to gust loading. Therefore, the aerodynamic wing load distribution associated with standard cruise flight must be multiplied with this factor. Other loads that are imposed on the wing structure are the tail shear and bending loads, which are propagated through the empennage booms, the landing gear and pod weight, and the weight of the wing itself. Also, the gravity load due to fuel weight was included. Although adding the fuel weight in the analysis relieves the bending moments along the span, the additional lift generation it requires due to its weight contribution means that the case of a filled fuel tank is more critical. The results of the static analysis are shown in Figure 12.6 and Figure 12.7.

The conclusion of the static analysis of the maximum positive loading case is that the wing box must be reinforced locally to be able to cope with all the loads. There are two main elements of attention. First, there is the wing root that experiences stresses above the material's yield stress of 503 MPa. This is due to the nature of the loading condition, but also to how the wing root has been constrained in the model. Right at the edge of where the skins and stringer have been fixed in space, very high stress concentrations occur. The second high stress

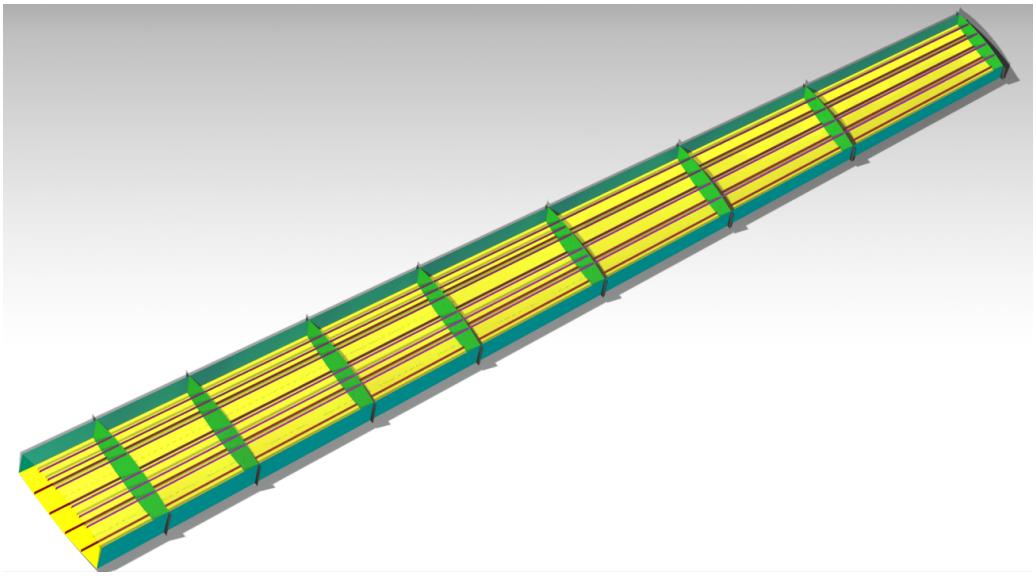

Figure 12.5: Three-dimensional view of the preliminary wing box used for finite element analysis. The stringers and stiffeners shown in this view do not feature the correct cross-sections, and all surfaces have zero thickness.

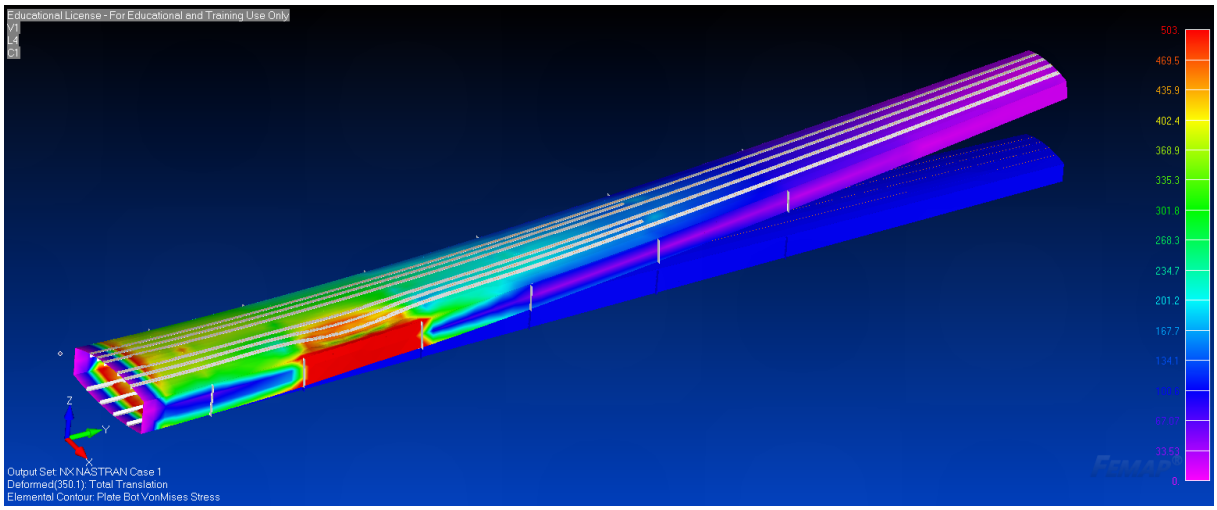

Figure 12.6: Contour display of the plate Von Mises stress in MPa. The actual deformation can be compared with the undeformed model, shown in blue.

area is the connection between the rear spar and the tail boom. This region must be heavily reinforced in order for the load to be fully carried. As a consequence of the large deformations in this area, the Von Mises stresses in the nearby stringer parts are also seen to be very high, as seen in Figure 12.7. If the local deformations would be limited by installing a properly designed spar reinforcement, the stringers are expected to be able to carry the loads. In short, it is expected that with the installation of these root and rear spar reinforcements, the wig box must be able to meet the load requirements. However, this will be at the expense of a higher weight.

The maximum negative loading case shows similar results as the positive loading case, although the stress magnitudes are smaller due to the small load magnitudes. As was discussed in Chapter 11, the maximum negative load factor equals -5.01. This load was used in addition with all other loads described for the maximum positive loading case. Although the results of the static analysis were similar, from buckling analysis it resulted that the amount of stringers installed on the root of the lower skin must be increased. It was seen that the lower wing skin would already buckle at a value of 6% of the total applied load, illustrating the need for additional stringers in this region.

The case of a hard landing shows very large stress concentrations at the attachment point of the main landing gear. The effect is similar to the situation illustrated in fig:fem1, although the landing gear load is pointed upwards. In addition to the impact shear load, the large offset of the main landing gear strut with respect to the rear spar also leads to a very high additional bending moment. Also here, a proper reinforcement must be designed to cope with the large landing loads.

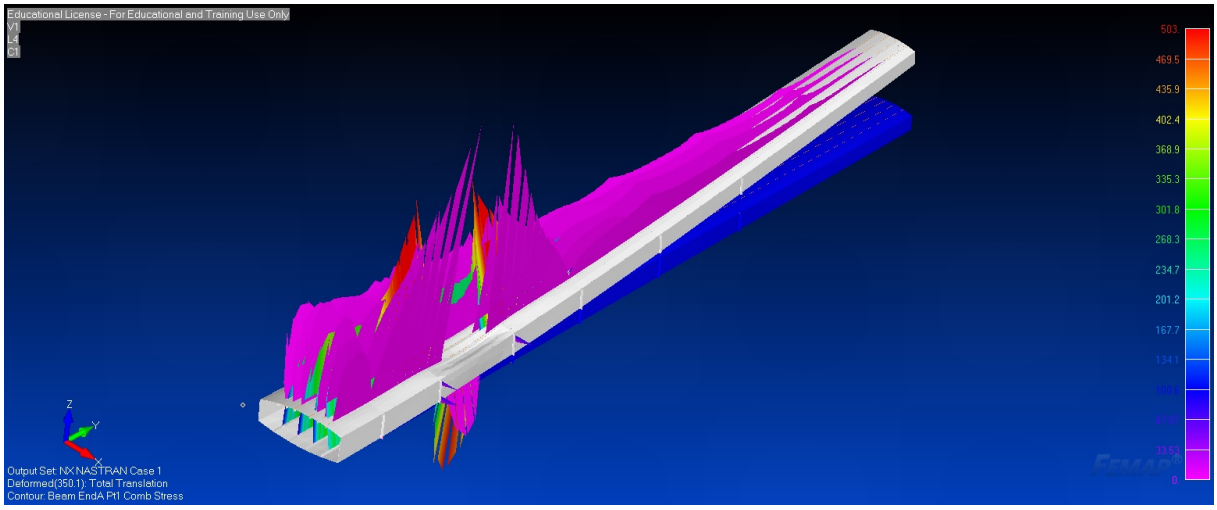

Figure 12.7: Beam diagrams of the Von Mises stress in the stringers

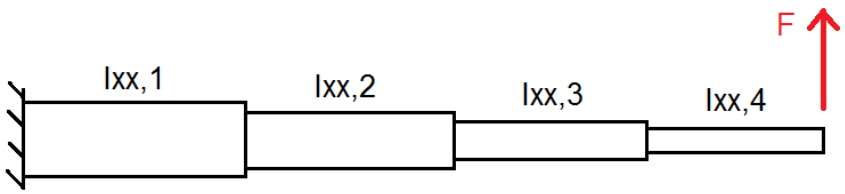

Figure 12.8: Analytical model of the wing bending problem

12.3.3. SOLUTION VERIFICATION

Although FEMAP and NX Nastran are both validated software packages, the FEA model must still be verified with another calculation. It was decided to verify the model with an upward point load of 10 kN at the position of the wing tip. Accordingly, an analytical solution of a cantilevered beam was used to verify the deflections along the wing span. The reason for verifying the models by comparing deflections rather than stresses stems from the fact that the FEA model computes stresses once it has solved the displacement vector of the model. Using the geometry mesh and the assigned material characteristics, NX Nastan generates a stiffness matrix $\mathbf{K}$ which it uses to compute the node displacements with the matrix equation $\mathbf{u} = \mathbf{K}^{-1} \cdot \mathbf{f}$. Accordingly, if the displacements computed with the two methods are comparable, the FEA model is verified.

The analytical model used for verification consists of a simple cantilevered beam with multiple inertia segments along the span. An overview of the model is shown in Figure 12.8. The deflection of the wing can be calculated as follows:

$$\delta_{tip} = \frac{F}{3E}\left\{\frac{L_1^3}{I_{xx,1}} + \frac{L_2^3}{I_{xx,2}} - \frac{L_1^3}{I_{xx,2}} + \frac{L_3^3}{I_{xx,3}} - \frac{L_2^3}{I_{xx,3}} + \frac{L_4^3}{I_{xx,4}} - \frac{L_3^3}{I_{xx,4}}\right\} \tag{12.3}$$

The derivation of this equation is shown in a document of Purdue University [1]. The moments of inertia of each section are approximated as the average inertias of the boundaries of the individual bays. The results are plotted in Figure 12.9, together with the wing deflections under the 10 kN tip load computed with the FEA model. It can be seen that the results differ significantly from each other, with the analytical solution giving a tip deflection of twice the magnitude of the FEA output. It is believed that the primary cause is the non-tapered representation of the wing box in the analytical solution. By introducing taper, part of the bending load translates to direct membrane stresses which do not contribute to the out-of-plane deflections. For better verification, it is recommended that a tapered wing model is used for the analytical computations.

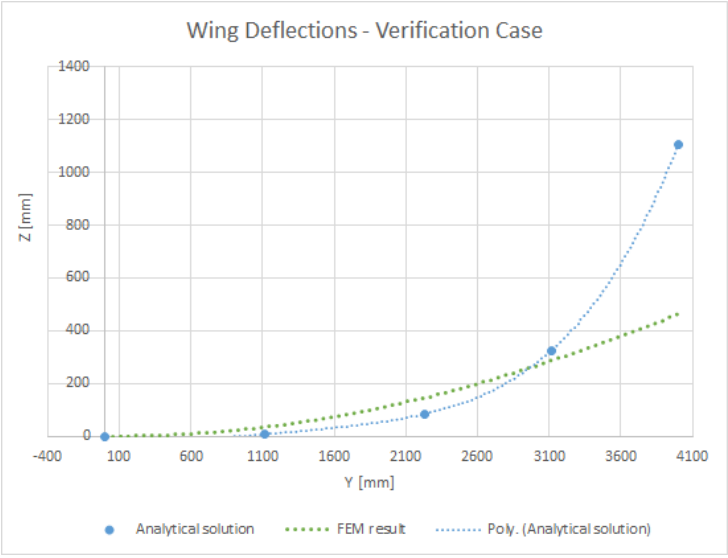

Figure 12.9: Results of the analytical deflection computations versus the FEA results

[1] https://engineering.purdue.edu/~ce474/Docs/Beam_Examples01.pdf

12.4. TAIL STRUCTURE ANALYSIS

Another critical part of the UAV's structure is the tail. The tail start at the connection between the booms supporting the tail surfaces and the pod located on the wing. For the structural analysis of the tail structure, the first step is once again to determine the loads acting on the structure in the critical cases and then to design the structure.

12.4.1. LOADS DETERMINATION

The loads on the tail structure consist of three major parts; first of all the weight of the boom connecting the pods to the tail surfaces, secondly the weight of the tail surfaces itself and finally the lift (or downforce for that matter) of the horizontal tail surface.

The critical case for the tail structure is taken at the maximum force of the horizontal tail surface, since this maximum force is way larger than the forces induced by the weight. This maximum aerodynamic force of the horizontal tail surface is equal to $-500N$ and is thus pointing downwards. For the structural weights, since the tail provides a negative lift, the aircraft will pitch up and will experience a higher gravitational load. This precise gravitational load has been estimated on the maximum manoeuvring load of $3g$.

Assuming a constant cross-sectional area, the total weight of the boom can simply be divided by the boom length in order to create a constant distributed load along the boom. The same is done for the tail structure; the total tail weight is divided by two (since the tail is supported by two booms) and constantly distributed along the chord length of the horizontal tail surface. Finally for the aerodynamic force of the horizontal tail surface, a sinusoidal distribution is assumed. This is done since no real force distribution could be created using the aerodynamic tool from Chapter 7. This is off course a very rough assumption, but since more force is located further away from the root (the connection of the boom and the pods), it will lead to an overdesigned rather than a underdesigned structure and is therefore used in this analysis. The loads as determined are plotted along the tail structure length in Figure 12.10.

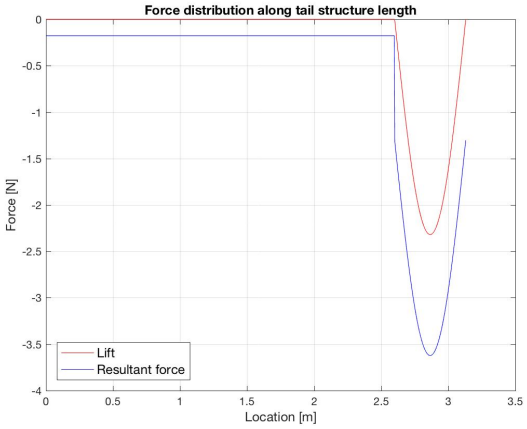

Figure 12.10: Lift and resultant force distribution along the length of the tail structure.

12.4.2. STRUCTURAL DESIGN

From the estimated empennage weight described in Chapter 10, the booms were allocated a maximum weight of 5 kg. Similar to the wing box structure, a boom structure must be designed that can carry the tail loads while remaining within the assigned weight budget. As a preliminary configuration, a circular cross-section was selected. Two FEA models were created, including one beam model using Al7075, and one surface model using carbon fiber. It was seen that the metal boom model could not handle the applied tail loads, with the maximum stress being equal to 650 MPa. Compared to the material's yield stress of 503 MPa, an aluminum boom is not feasible. The carbon fiber model however, with carbon fiber having a maximum tensile stress of 1300 MPa, showed a maximum stress of only 341 MPa. The reason for the maximum stress being lower in the composite model is the fact that the composite model can feature an extensive layup consisting of 14 plies, while still meeting the maximum weight budget of 5 kg. The layup was defined such that the majority of the fibers would lie in the 0 direction, i.e. along the main axis of the boom, and a large part in the 45/-45 direction in order to cope with torsion. The FEA result is shown in Figure 12.11.

Although the composite boom meets the strength requirements, it can also be seen from the figure that the

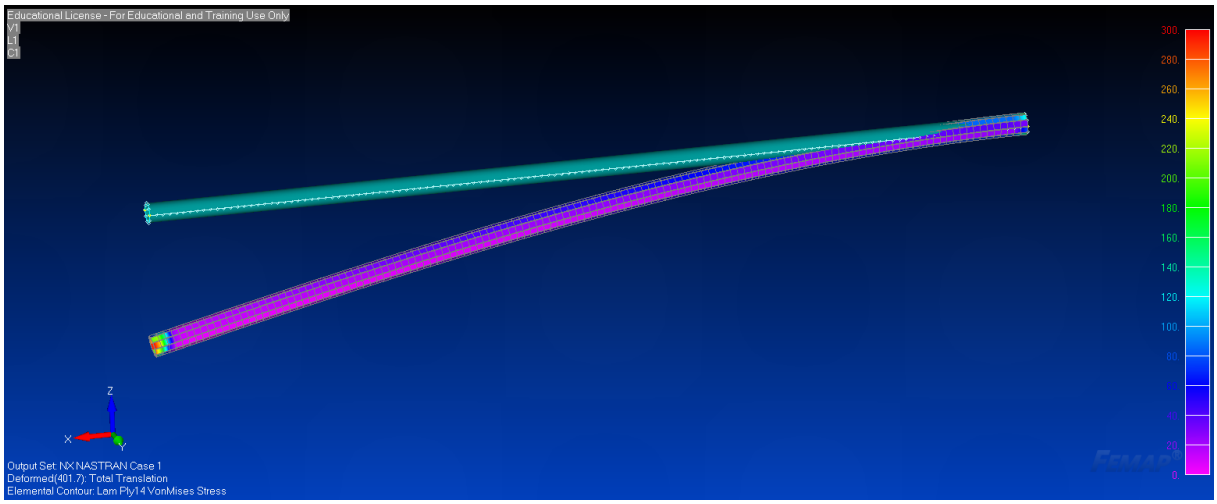

Figure 12.11: FEA results of the boom analysis

current design lacks sufficient stiffness. It is seen that with the current model, which is fixed at one end, the maximum boom deflection equals about 41 cm at the tip. Compared to the boom length of 2.6 meters, this is a very significant deflection. This will lead to significant difficulties in terms of aeroelasticity, as the vehicle cannot be seen as a rigid body anymore. This will also have consequences for the effectiveness of the horizontal tail. Therefore, it is recommended that the boom design is changed to an oval shape, with the highest inertia in the direction of tail bending. Also, it is advised to taper the boom a little towards the root. Another solution can be to specifically tailor the carbon fiber layup by very accurately stitching the fibers in their most effective directions. However, this would result in an increase of production complexity.

12.5. VERIFICATION & VALIDATION

For the load determination as discussed in this chapter, a Matlab tool has been created and used to calculate the loads acting on the main wing and tail boom. Before this tool can be used to implement the load distributions in a FEM analysis program, the tools should be verified.

The wing tool imports the non-viscous lift distribution from the aerodynamic tool used in Chapter 7. The lift distribution is then used to calculate the total lift per segment along the span. The total lift along the span can now be compared with the lift as calculated by the 3D viscous tool. For the calculation with 2000 segments, the total lift as calculated by the tool is equal to 5.656 kN (at a load factor of 5.7) while the 3D viscous tool calculates a lift of 5.666 kN. This is a deviation of less than 0.2%.

The tail structure tool only plots the distributed weight of the boom and tail together with the aerodynamic force created by the horizontal tail surface. With this, it calculates the distributed resultant force along the tail structure length. Since no lift distribution is available for the horizontal tail surface, a sinusoidal distribution is assumed. The sum of this distribution is within 0.1% of the actual maximum lift created by the horizontal tail surface (250 versus 249.9976N).

One can only determine whether a tool is working properly after also validating the tool. In order to do this, however, real life test data is needed to compare the outcome of the tool with a real life application and with this, check the assumptions made. This can thus only be done after the production phase of the system.

12.6. COMPLIANCE MATRIX

After the structure of the UAV is determined from the load cases and the tools have been verified, it should be checked whether the design meets the requirements in an adequate manner. For this, a compliance matrix has been constructed in which can be seen if a certain requirement is met and if needed, an explanation is given. The compliance matrix can be seen in Table 12.3.

Table 12.3: Compliance matrix for the requirements of the structure of the UAV.

ID	Requirement	Comp.	Comment
NVD-Syst-01-06	The airborne element of the system shall be recoverable without getting damaged.	✓	The structure is designed such that it can cope with all loads during landing without getting damaged
NVD-Syst-06	The airborne element shall be able to support all loads experienced during its lifetime, multiplied by a safety factor of 1.5 without failure.	✓	
NVD-Syst-06-01	The airborne element shall be able to support all static loads experienced during its lifetime.	✓	The structure of the UAV is designed such that it can withstand maximum loads that might be experienced, multiplied by a safety factor of 1.5.
NVD-Syst-06-01-01	The airborne element shall support all propulsion loads throughout its lifetime.	✓	
NVD-Syst-06-01-02	The airborne element shall support all loads related to recovery throughout its lifetime.	✓	
NVD-Syst-06-01-03	The airborne element shall support all aerodynamic loads throughout its lifetime.	✓	
NVD-Syst-06-01-04	The airborne element shall be able to withstand minor impact loads.	✓	
NVD-Syst-06-02	The airborne element shall be able to support all dynamic loads experienced during its lifetime.	?	Within the time of this project, dynamic loads could not be analysed.
NVD-Syst-06-02-01	The airborne element shall not fail due to fatigue throughout its lifetime.	?	Within the time of this project, fatigue could not be analysed.
NVD-Syst-06-02-02	The airborne element shall not be damaged as a result of flutter throughout its lifetime.	?	Within the time of this project, flutter could not be analysed.
NVD-Syst-07-02-05-04-01	The payload shall be protected against aggressive environments, including wide temperature ranges, precipitation and radiation.	✓	The payload bay is located inside the UAV and therefore it is protected against aggressive environments.
NVD-Syst-07-02-05-04-02	The payload shall experience low vibration and oscillation levels.	✓	
NVD-Syst-07-02-05-04-03	The airborne element shall be robust to flight-path related disturbances during measurements.	✓	The structure of the UAV is designed such that it can withstand maximum loads that might be experienced, multiplied by a safety factor of 1.5.
NVD-Syst-08-02-02	All system elements must be maintainable.	✓	All parts are maintainable.
NVD-Syst-08-02-02-01	The engine of the airborne element shall be replaceable.	✓	The engine is located at the very end of the fuselage and therefore easily replaceable.
NVD-Syst-08-02-02-02	All key subsystems shall be accessible for maintenance purposes, without compromising the structural integrity of the system.	✓	The structure of the UAV is designed such that maintenance can be done without compromising the structural integrity.
NVD-Syst-09-02-02	The airborne element shall be operable under all temperatures ranging from -30 degrees to +50 degrees Celsius.	✓	All elements used in the UAV are operable under all temperatures ranging from -30 degrees to +50 degrees Celsius.
NVD-Syst-10-03	The system shall have a minimum life time of 5,000 flight cycles.	?	The life time of the structures could not be analysed at this time of the project.
NVD-Syst-11-06-01	All systems that are critical for flight safety shall be equipped with sufficient redundancy.	✓	

13 Aircraft System Characteristics

In this chapter, the layout of the fuel system, actuator controls and landing safety system are briefly described. How the actuators will function on given inputs (assisted by the ground station or the flight computer unit) is based on written software and is a task that has to be done after the DSE. Also, a more detailed design of the landing safety system will be conducted at a later stage.

13.1. Fuel System Layout

The volume of the wings is large enough to store all the fuel needed during the calibration mission. There is thus no need to place an extra fuel tank in the fuselage. The fuel tank is split into two times three sections by the ribs in the wing and linked to each other by fuel lines. The sectioning of the fuel tank is advantageous since the fuel in each section can be extracted individually, which is beneficial in case of a leak; Or regarding the stability of the aircraft, since the fuel can be pumped to other sections to alter the c.g. location.

13.2. Control Actuators

It is already known that the UAV is controlled by the common control surfaces such as ailerons, elevator and rudders. To deflect those surfaces, a system has to be installed. There are three main control systems that can do the job.

First, there is the mechanical system [1] (Figure 13.1), which mainly uses cables and pulleys. This system in not necessarily useful for the UAV since the control surface inputs will be sent remotely to the aircraft (digital).

Next, a hydraulic actuator system [2] (Figure 13.2) can be employed. This system uses (hydraulic) fluid to rotate or translate a part, for example, a cylinder. Since the fluid is essentially incompressible, larger forces can be produced by such a system, which becomes necessary when the aerodynamic forces become larger on the control surfaces. At the other hand, hydraulic actuators have some drawbacks. A hydraulic system has to be introduced (hydraulic-lines, -pump, -reservoir, etc.). Additionally, a backup circuit needs to be introduced in case of a leak in the primary circuit, which will increase the weight.

Last, the control surfaces can be controlled by an electromechanical actuator [3] (Figure 13.3). This actuator uses electrical signals and translates those in a mechanical motion, which can be rotational or translational. In this system no fluids are used, so there is no danger of leaks. There is still a chance that the actuator fails, or that the electrical cable to the actuator fails, but making this redundant will relate to a smaller weight increase compared to the hydraulic solution.

As there is no need to use hydraulics on board, it will be better to use electromechanical actuators for the control of the control surfaces and landing gear retraction system.

13.3. Landing Gear Safety System

In Subsection 9.3.8 the retraction/extension mechanism of the landing gear is described. This mechanism is only working if the actuators and other (landing gear retraction/extension) components are working properly. In the case of a malfunction in one of the landing gear components, the landing gear should still be able to extend and lock into position. In the case of a problem, the mission would be aborted. Hence, an emergency retraction system is not necessary.

In general aviation, there are two common emergency extension systems [38], which are integrated into the NavAid calibration UAV.

First, a backup system will be linked to the lock-up linkage, which holds the landing gear retracted during the flight. When the emergency lever is lowered in the ground station, a signal is sent to the lock-up linkage and the landing gear will extend due to its weight (gravity extension).

[1] https://pritamashutosh.wordpress.com/2012/11/17/flight-control-system/ [cited 14 June 2016]
[2] https://upload.wikimedia.org/wikipedia/commons/f/fd/Hydraulic_circuit_directional_control.png [cited 14 June 2016]
[3] http://www.moog.com/literature/Space_Defense/Technical_Bulletins/Electromechanical_Actuation_for_Launch_Vehicles.pdf [cited 14 June 2016]

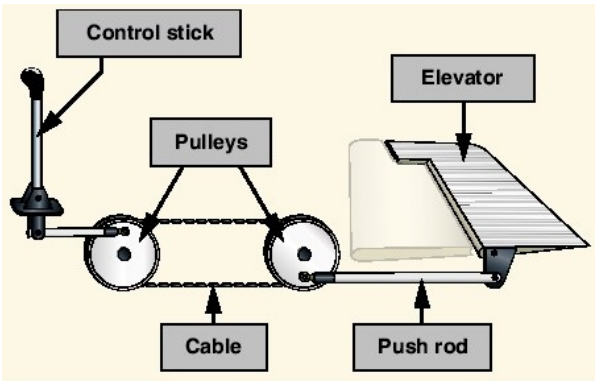

Figure 13.1: Manual Control Example

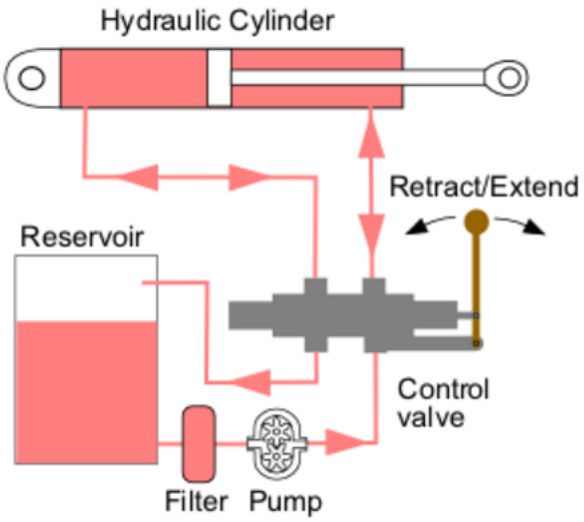

Figure 13.2: Hydraulic Actuator System

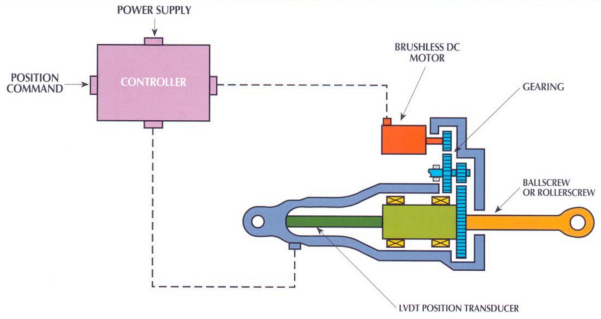

Figure 13.3: Electromechanical Actuator System

Another system that is used is a landing gear extension due to air pressure. On each gear, a small compressed air reservoir will be installed which can generate an additional force to extend the landing gear into position.

Note that not only direct linked systems can cause a malfunction of the landing gear. If there is, for example, a malfunction in the pitot tubes, the flight computer may fail in interpreting the flight speed. When this happens, the flight computer unit can not know if the UAV is flying below the maximum landing gear extension speed. In that case, the landing gear will also be extended with the emergency procedure.

14 Operations & Logistics

In the Midterm Report [2], a start has been made on describing the operations & logistics (O&L) of the system. For this, a first operations & logistics flow diagram was made. At this stage of the design process, the O&L can be further described. This is done by first determining the ground system architecture. Then, the transport procedures and system procedures can be developed. With this newly gained information, a more detailed O&L flow diagram will be created.

14.1. Ground Station Architecture

A vital part of any UAV system is the ground station. This ground station should be able to communicate with the UAV in order to receive flight or mission data from the UAV and to send new commands to the UAV. In some cases, the UAV should even be controllable by a pilot from the ground station.

Because of these communication links, the most important part of the ground station is the telemetry system. As was already defined in Chapter 5, the aircraft makes use of three separate systems for continuous communication between the aircraft and the ground station. The first communication link is a direct (LOS) UHF link. This link enables constant communication including live video feed from the UAV to the ground station at a maximum distance of 80 km. In order to close the link, a helical antenna with a length of 15.3 cm will be used. This antenna length can be calculated with Equation 14.1 for the gain of a helical antenna [1].

$$G_{max}\,(dB) = 10.25 + 1.22\,(L/\lambda) - 0.0726\,(L/\lambda)^2 \tag{14.1}$$

The second link is an indirect (SATCOM) link. This link is used beyond LOS and is used to send and receive data via a LEO satellite. The ground station should therefore have an antenna that is able to communicate with these LEO satellites.The antenna has a required gain of 31 dB, which is best achieved by using a parabolic dish antenna with a diameter of 0.36 m. The final link is a direct link used as a backup system in case the UHF frequency gets jammed or fails. It uses the C-band frequency (6 GHz) for communication. The antenna needed at the ground station for this communication link is a helical antenna with a length of 30 cm.

Next to the communication antennas, the ground station should have a control unit that is able to interpret the data received from the UAV and display them on a screen. The operator can now check the calibration results and, if necessary, send new commands to the UAV. Finally, the operator should be able to control the aircraft manually with the control unit. For this, the OCU-1000 (operator control unit) was selected [2]. This system is a portable solution for controlling and managing UAVs. The system comprises of one or more operator control units and together with an antenna positioner and the antennas itself, it forms the complete ground station solution.

14.2. Transport Procedures

According to requirement *NVD-Client-08-01-02*: "The full system shall fit in a standard LD6 aviation container." However, since the outer dimensions of the UAV are too large to fit into such an LD6 container right away, some transport procedures are necessary to enable this. Other procedures might be necessary to enable safe transport for both the system and the environment.

The dimensions of a standard LD6 aircraft container are given in Figure 14.1 [3]. The total volume of the container can be calculated from these dimensions, which is determined to be 9.8m^3. From the maximum length of the LD6 (4.064m) it becomes clear that the aircraft, with a wing span of 8m, will not fit in the container without any modifications. In order to fit the entire system into the LD6, the following dismantling procedures will be executed:

1. The vertical and horizontal tail structure consists of two booms connecting the tail surfaces to the aircraft and the actual tail surfaces. The booms are dismounted from the pods, and the horizontal tail is taken

[1] https://theses.lib.vt.edu/theses/available/etd-02102000-19330046/unrestricted/07chapter2.PDF [cited 7 June 2016]
[2] http://www.tellumat.com/defence-and-security_unmmaned-systems/ [cited 7 June 2016]
[3] https://www.searates.com/reference/ld6/ [cited 19 May 2016]

from between the two vertical planes. In total the tail has a size of $2102x785x2045mm$, including booms, vertical tail and horizontal tail.

2. The wings are detached at the side of the fuselage. The fairing at this location is $56cm$ wide, which leaves the wing parts to be $3.72m$. Before dismantling, the fuel is drained from the wings. The controls are connected by rods from the fuselage and will be put in sockets inside the wing. After dismounting, the wing has a size of $3720x1155x400mm$ which will fit easily in the LD6.
3. The propeller is a fragile part of the aircraft. Dismounting them enables for safe, compact storage. The $1200x300x100mm$ sized propeller will be protected by covers to minimise damage.
4. At this point, the main wings, tail and propellers are detached from the fuselage. The remaining system is put into the fuselage with retracted gear. All fragile parts as antennas and tubes will be covered. The size of this is $680x870x3200mm$.
5. The ground station consist of a operator control unit case and three antennas mounted on a tripod (two helical antennas and a parabolic dish antenna). The operator control unit case's dimensions are $1170x535x245mm$. The antenna stand and antennas fit in a case with the same dimensions. The total ground station will therefore fit in two cases measuring 1170mm x 535mm x 245mm.

Table 14.1: All dismantled system parts width their outer dimensions.

Part	Quantity	Length (m)	Width (m)	Height (m)	Volume (m^3)
Wing	2	3.720	1.155	0.400	1.729
Tail	1	2.102	0.785	2.045	3.374
Propellers	1	1.200	0.300	0.100	0.036
Fuselage	1	3.200	0.680	0.870	1.893
Ground station	2	1.170	0.535	0.245	0.153

The result of this dismantling procedure is nine boxes in total with the dimensions as presented in Table 14.1. These parts can now be fit into the LD6 in order to finish the transport procedures. The drawings displaying the internal layout of the container can be found in Figure 14.2. Here the wings are placed on the sides and the fuselage is placed in the bottom middle. The ground system is located in the back. The propeller is hinged on the top of the LD6, and the tail is placed in the centre. The entire system now fits inside a single LD6 container and is ready to be transported.

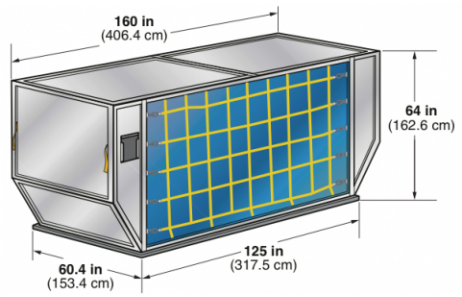

Figure 14.1: Universal loading device LD6 dimensions.

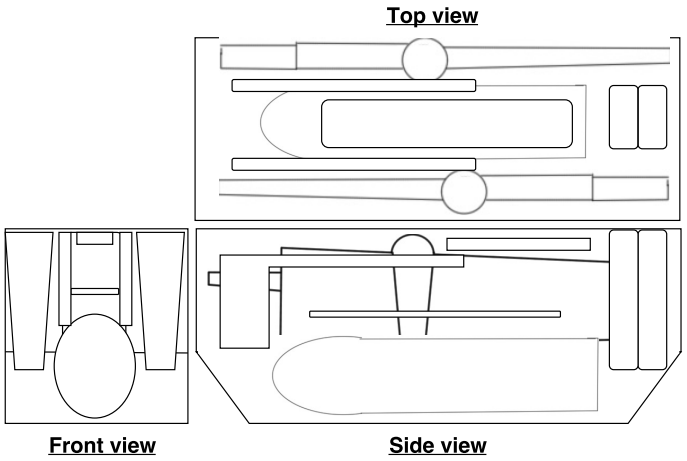

Figure 14.2: Schematic overview of the internal layout of the LD6 container for transport.

It is important to note that during transport of the UAV, the transport of a vehicle in a LD6 on an aircraft has its restrictions regarding dangerous goods. Dangerous goods are divided into multiple HAZMAT (hazardous materials) classes, e.g. explosives, flammable materials or radioactive materials. Vehicles are included in Class 9, miscellaneous dangerous goods. Those goods are not covered by the other classes, meaning they can be environmentally dangerous, there are products that are transported at extreme temperatures or, in this case, products may contain trapped oils, magnetics etc. Consequences of the dangerous goods in air transport are

that it needs to be stored carefully with intensified monitoring and environmental control on airports, as far as necessary, and may not be loaded in the aircraft next to vulnerable loads such as animals.

14.3. System Setup Procedures

The system setup procedures describe how the system will be made operable. There are two different procedures, one where the system is already used at the airport and another one where the system has been transported to another airport before use. In the latter case, some extra tasks need to be performed before the actual start of the system setup.

If the system has been transported to another airport before use, the system setup starts with unpacking the seven boxes comprising the entire system from the LD6 container. After this is done, the antennas have to be assembled on the antenna mounts, the OCU has to be started and the UAV has to be assembled. The procedure for assembling consists of the following tasks:

1. First, the ground station consisting of the control unit and the antenna tower has to be unpacked and set up. The control unit should be connected to a 200V AC power source.
2. At this point, the UAV can be assembled. To do this, the fuselage is first put on its landing gear to be able to mount the other systems. Also, the antennas and other fragile external systems have to be mounted on the fuselage.
3. The propellers can now be mounted to the rear of the fuselage where the engine is located.
4. After the propellers are attached, the main wings can be installed on the sides of the fuselage.
5. Finally, the booms are connected to the pods located under the main wings and the vertical and horizontal tail surfaces are attached to the booms.

All connections should be checked and approved before moving on the the next phase of the system setup procedure. When the previous tasks have been performed, or the system has not been transported before use, the next part of the system setup procedure can be initiated.

First of all, the mission should be determined and uploaded to the UAV's CPU. The mission describes to manoeuvres to fly at what locations, airspeed etc. If everything goes according to plan, the UAV will fly this predefined mission without any further input from the operator.

After this, the fuel and all systems should be checked. If the fuel level is not sufficient, fuel will be added to the fuel tank. For the a lot of systems, simple ground checks should be performed to check if everything is functioning properly. The engine should be started to see if it is running properly at all required power and rpm ranges. The control surface actuators should be operated to see if they function and reach the required deflection angles. Furthermore, the avionics systems that should be checked include the following subsystems:

- Navigational aids
- Air data sensors
- Aircraft lighting
- Landing aids
- Sense & avoid systems
- Communication links

Finally, the system can be started and the UAV is ready to taxi to the runway for take-off. Before this can be done, however, ATC has to be contacted to get clearance for a certain runway in order to actually take off.

14.4. Operations & Logistics Diagram

The O&L diagram illustrates the use or support (e.g. maintenance, ground support) of the system. As can be seen in Figure 14.3, the activities needed to perform the mission can be divided into four main parts: maintenance, fuel provision, operation and assembly.

- Maintaining: First of all, a hangar is needed to perform the maintenance tasks. Furthermore, spare parts might be needed to replace broken or defect system parts and finally, maintenance staff is required to perform the checks and possible repairs.

- Fuelling: For refuelling the aircraft, fuel has to be bought and delivered to the airport. After the fuel is delivered, it should be stored until it will be used and finally, if required the fuel should be loaded onto the UAV.
- Operating: Operating the system requires a flight inspector to asses the calibration and control the UAV, if necessary. It also requires ATC to control the airspace and avoid collisions with other aircraft. Finally, an operations centre is needed from where the system can be controlled.
- Assembling: For assembly of the system after transport, the system has to be unloaded from the container first. It can then be assembled and the system can be checked to function properly. This is all done according to the procedures as described in the previous sections.

When all conditions are satisfied, the mission can be performed. After the mission, the aircraft should be able to be disassembled and transported to a different location, if necessary. It is interesting to notice that all sub-parts of the activities imply costs: fuel costs, transport costs, personnel costs, spare parts costs, etc.

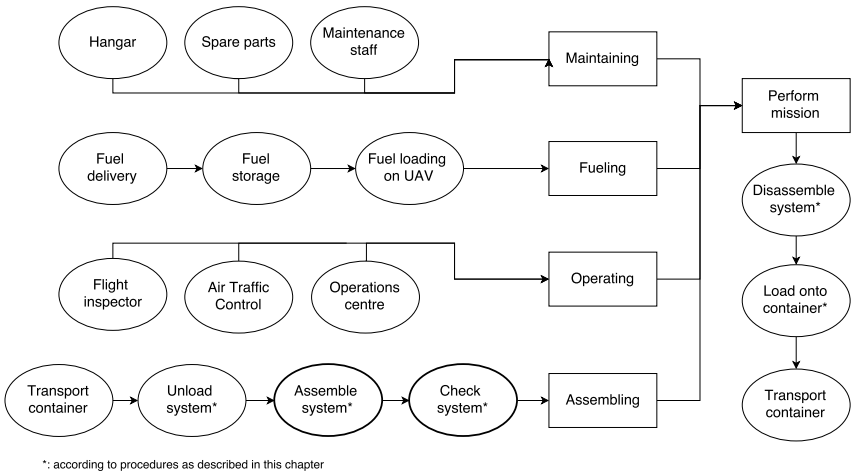

Figure 14.3: Operations and logistics flow diagram

15 System Synthesis

At this point the conceptual design of the system is finalised, providing the possibility to analyse the system on some vital characteristics. The requirements as presented in the Baseline Report [3] state the following characteristics.

- NVD-Client-10-01-01: The system shall have a unit cost of no more than € 250,000.-
- NVD-Client-10-02-02: The airborne element shall have at least a 20 dBA lower noise exposure level than a Cessna Citation II on a 3-degree glideslope landing.
- NVD-Syst-10-02-03: The airborne element shall adhere to the maximum emissions specified by ICAO Annex 16.
- NVD-Client-10-02-01: The operating empty weight of the system shall be at least 80% recyclable.
- NVD-Syst-11-06-02: The airborne element shall have a crash rate of less than 1 per 10 million flight hours

In this chapter a noise analysis is conducted in Section 15.1, to check the compliance with these requirements. Followed by the emission characteristics of the system in Section 15.2. After this, Section 15.3 determines the sustainability of the system and finally the RAMS characteristics is discussed in Section 15.4. Finally, a cost estimation is made from which will be used to calculate the return on investment in Section 15.6.

15.1. Noise Analysis

One of the requirements of the UAV is that it shall produce 20 dBA less noise than a Cessna 550. To evaluate the noise characteristics of the UAV, a analysis of its noise contour is done. It must be noted that the most important part of the noise contour is the one around airports since this is where aircraft are flying at their lowest altitude. Also, this is the region where most complaints originate. Since many airports have restrictions on aerodrome operations due to noise, it is of vital importance of the feasibility of this project to know what the impact of the UAV will be on noise. To analyse this, the Integrated Noise Model (INM), developed by the FAA, will be used, which is capable of determining the noise contours for a given set of aircraft parameters, procedural profiles (landing and take-off procedures) and mission profiles at airports. The software already contains data of some aircraft, which includes procedural flight profiles as well. The aircraft with which the UAV is compared, the Cessna 550, is also included in the database.

Before any calculation is made, the runway needs to be defined on which the take-off and landing take place. For this, Newark Liberty International Airport (EWR) runway 04L has been selected. The choice of airport and runway is stated now, so that the calculations can be reproduced afterwards. To generate a noise contour that is large enough, i.e. they are clearly visible, 300 landings and take-offs per day are analysed and added cumulatively. The tracks that are flown are just straight landings and take-offs. Note that these parameters are not of high influence on the results, but it is essential that parameters are consistent for the comparison of noise contours.

Subsequently, the aircraft parameters and procedural profiles need to be determined. The model contains information on those aspects for the Cessna 550, however not for the UAV. Therefore, they are added manually. Some top-level parameters are the take-off weight and landing weight, the max landing distance, engine type, number of engines and the static thrust. Followed by specific information about the UAV, starting with the propeller thrust coefficient. Next to that, the flap coefficients are needed. This entails, for each flap setting, the drag over lift ratio and velocity. From this configuration, the procedural profiles can be determined. Since these are not known yet, they are copied from the smallest aircraft in the database, which is the Cessna 172. An overview of the inserted parameters for the UAV can be found in Table 15.1.

Table 15.1: Overview of parameters for the UAV.

Flap coefficients	Drag over Lift (-)	Velocity (m/s)
Take-off (clean)	0.06	35
Landing (clean)	0.059	47
Landing (flaps out)	0.09	39

Propeller coefficients	
Propeller efficiency	0.79
Net power (hp)	100

The noise contour of the Cessna 172 is also determined, to ensure that copying of the procedural profiles does not have a significant effect on the results. At the same time, this serves as a verification of the results. The Cessna 172 is a lot lighter than the Cessna 550 and also flies slower, so the noise contour should be smaller. However, the UAV is even lighter and has a smaller engine, so this noise contour should be even smaller. If this development is recognised in the noise contours, it may be assumed that the tool is verified. The results can be seen in Figures 15.1 to 15.3.

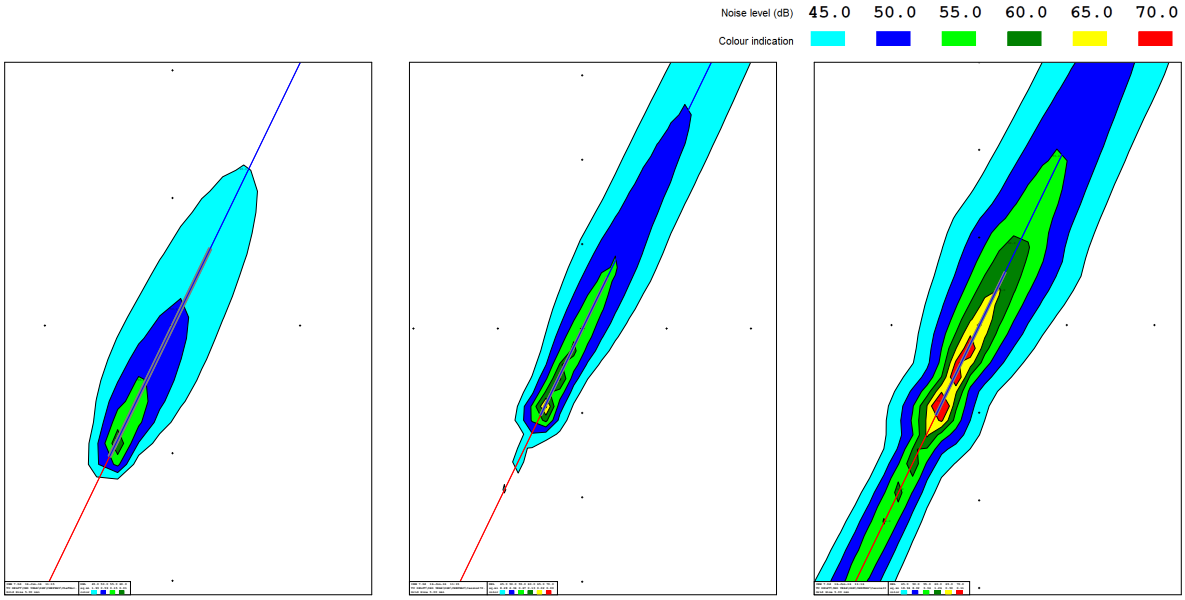

Figure 15.1: Noise contour of the UAV. Figure 15.2: Noise contour of the Cessna 172. Figure 15.3: Noise contour of the Cessna 550.

As can be seen in the figures, the noise contours are as expected and therefore verified. Validation is not necessary since the tool is already deemed valid, as stated in the User's Guide [1]. The Cessna 550 produces 70 dBA at its maximum point, whereas the UAV only produces 60 dBA on a effected area that is a lot smaller than that of the Cessna 550. Furthermore, in the region where the UAV produces 45 dB, the Cessna 550 produces 60 dBA. Indicating that, despite the requirement not entirely being met, the UAV produces significantly less noise (-15 dBA). 20 dBA seemed to be too ambitious, as confirmed by the customer after a consultation. Considering that the model overestimates the UAV (a bigger engine is used, and the flight profile is not optimised yet), the customer agreed with the results.

15.2. EMISSION CHARACTERISTICS

The selected engine is a D-motor LF39, a relatively new, naturally aspirated engine. Unfortunately, limited information on the engine is available, especially regarding its emissions. For aircraft engines, in general, it is difficult to find any data about their emissions. Therefore, a different approach is chosen: the D-motor LF39 engine is very comparable to a naturally aspirated, high displacement, low power automotive petrol engine. A big difference, however, is the fact that an aircraft engine runs at a higher constant power setting, usually around 75%. Compared to car engines it burns almost five times as much fuel per hour. The fuel usage of the engine at 75% is known, namely 19 $L/hour$. That converts[2] to 44 kg of CO_2-emissions per hour. Emissions are given in terms of carbon dioxide CO_2, carbon mono-oxide CO, hydrocarbon HC, mono-nitrogen oxides NO_x and particulate matter PM.

The current Euro VI norms in g/km are: 1.00 CO, 0.10 HC, 0.06 NO_x and 0.005 PM. Assuming a car running at 80 km/h burning 0.04 L/km and just meeting the standard, will emit 25 CO, 2.5 HC, 1.5 NO_x and 0.125 PM gram per burned litre of petrol. Converting that to gram per hour at a fuel burn rate of 19 litre per hour for the UAV yields 475 CO, 47.5 HC, 28.5 NO_x and 2.38 PM gram emissions per hour of fight.

[1] https://www.faa.gov/about/office_org/headquarters_offices/apl/research/models/inm_model/inm7_0c/media/INM_7.0_User_Guide.pdf [cited 16 June 2016]
[2] http://www.ecoscore.be/info/ecoscore/co2?locale=nl

15.3. SUSTAINABILITY CHARACTERISTICS

In Section 2.3, a sustainable development strategy has already been developed. Now, after the design of the entire system, it is time to review this strategy and to analyse the sustainability characteristics. As presented in Figure 2.6, the sustainable development strategy has been divided into three parts: design, production and operation of the system.

For the design phase of the system, the main considerations were the use of recyclable materials and using techniques that simplify the dismantling process at the end of life. This is mainly driven by the top-level requirement (*NVD-Client-10-02-01*) that "at least 80% of the operating empty weight of the system shall be recyclable". In order to assess the recyclability of the system, several definitions can be used [3].

- the EOL Recycling Rate (EOL-RR, %) determines how much of the available material at end-of-life has been recycled. This definition measures the recycling relative to the end-of-life availability.
- the Recycled Content (RC, %) determines the share of recycled material to the total material input in refining. This definition measures the recycling relative to the primary production.
- the Old Scrap Ratio (OSR, %) determines the ratio of old scrap to the total scrap (old + new). More old scrap (recycled material) over new scrap (production waste) indicates a better-recycled material.

Since the RC and OSR are too much dependent on the current production magnitude and processes, the EOL-RR rate will be assessed in this sustainability analysis. In typical aircraft, and also this UAV, three different material types are most used: metals, rare-earth elements and fibre-reinforced plastics.

Metals

Most commonly used engineering metal have a quite high EOL-RR. Mainly because of the simple techniques required for recycling which makes the energy savings for recycled material compared to virgin material very high [1] and thus an economically favourable option.

Table 15.2: Overview of energy saving for recycled material production versus virgin material for most commonly used metals.

Metal	Energy saving (%)
Aluminium	95
Copper	85
Steel	75

The most commonly used metal in aircraft is aluminium because of its relatively low density and high strength. Because of the high energy savings, the EOL-RR of aluminium ranges from 85% to 95% [39]. The EOL-RR of other materials are generally lower ranging from 80% for steel [4] and 75% for lead [5] to just above 40% for copper [6].

Plastics

Plastics are used in numerous applications, mostly as packaging. Today, the EOL-RR of plastic packaging sits around 66%, while the overall EOL-RR of plastics is a little lower at 59% in Europe [7].

Rare-earth elements

The rare-earth elements are a group of 17 chemically similar metallic elements (15 lanthanides, plus scandium and yttrium). They are becoming increasingly important in the transition to a green, low-carbon economy. Due to their essential role in permanent magnets, batteries, catalysts and other applications. The EOL-RR of these elements is generally below 1% [40], mostly because of their low volume use in appliances and difficult recycling techniques. The use of these elements should thus be minimised but might be inevitable in some cases.

Fibre-reinforced plastics

Fibre-reinforced plastic (FRPs) have a large advantage over traditional engineering materials. Their corrosion

[3] https://blackboard.tudelft.nl/bbcswebdav/pid-2641745-dt-content-rid-8955112_2/courses/35882-151602/MS4151-2015%20Lecture%201_%20Introduction%20to%20materials%20recycling.pdf [cited 15 June 2016]

[4] http://www.recycle-steel.org/~/media/Files/SRI/Releases/Steel%20Recycling%20Rates%20Sheet.pdf?la=en [cited 16 June 2016]

[5] http://www.ila-lead.org/UserFiles/File/ILA9927%20FS_Recycling_V08.pdf [cited 15 June 2016]

[6] http://copperalliance.org/wordpress/wp-content/uploads/2013/03/ica-copper-recycling-1405-A4-low-res.pdf [cited 15 June 2016]

[7] http://www.plasticseurope.org/plastics-sustainability-14017/zero-plastics-to-landfill/plastics-waste---recycling-and-recovery-in-europe.aspx [cited 16 June 2016]

resistance, weight and high strength give them an advantage over traditional materials, but the long life of polymeric composites poses serious environmental problems. FRPs, in general, are difficult to recycle due to their multiphase nature, typically containing three or more components: fibre reinforcement, resin matrix and fillers.

Recycling of thermoset FRPs presents an especially difficult challenge because once the inherent nature of thermosets, they can not be melted or reformed. Therefore, the structure has to be shredded and both the fibres, as well as the resin, can not be re-used for structural applications. Thermoplastic resin FRPs can be remelted. Recycling these composites is, therefore, easier and thus more economical.

Overall, recycling of composites at the moment is almost 0% [8]. However, composite granulate is being used as filler in non-structural applications. Because this is a downgraded product, it does not count towards the recycling rate but does off course add to a sustainable future.

Overall recycling rate
After the determination of the recycling rate for the most used materials, the overall recycling rate can be calculated. For this, the weight content of each of these materials in the OEW has to be determined. In Table 15.3 the calculation of the recycled weight over OEW is shown. It shows the most used materials in the UAV and their EOL-RR. With this, the recycled weight is calculated.

Table 15.3: Calculation of overall EOL-RR based on the OEW.

Material	EOL-RR	Weight [kg]	Recycled weight [kg]
Aluminium	95	263.1	249.9
Steel	80	19.2	15,36
Lead	75	2	1.5
Plastics	59	20	10
REEs	1	1	0.01
FRPs	0	36.7	0
Total:		342.0	276.8

The steel portion of the OEW originates from the landing gear, which is almost entirely made of steel. The lead-acid battery installed in the propulsion and power subsystem accounts for the lead portion of the system. Plastics appear in the system in the battery, as well as the payload & avionics. These systems also feature some Rare Earth Elements (REEs). However, the use of these elements is limited. Finally, the booms connecting the tail and the wings as well as the fuselage are made out of FRPs (both carbon fibre as well as glass fibre). The rest of the aircraft (mainly the engine, wings, tail structure) is made out of aluminium.

$$EOL-RR = \frac{W_{recycled}}{OEW} \cdot 100\% = \frac{276.8}{342.0} \cdot 100\% = 80.9\% \tag{15.1}$$

The EOL-RR or recyclability of the OEW can now be calculated using Equation 15.1. It can be seen that the complete system satisfies requirement *NVD-Client-10-02-01* with a EOL-RR of 80.9%.

15.4. RAMS ANALYSIS

Now that the final concept is designed, a final analysis on Reliability, Availability, Maintainability and Safety (RAMS) is conducted. The RAMS analysis is used to estimate the quality characteristics of the product. The following four elements are explained:

Reliability
The reliability of the system is the probability or ability to perform the calibration of navigational aid equipment without failure. Important factors for reliability are the complexity of the system, the redundancy of subsystems and the operations of the system.

The conventional aircraft configuration is very reliable since much research has been done on this specific design solution. Another important role in the reliability is the amount of moving/rotating equipment. The high wing makes the aircraft statically and dynamically stable in case a part of the controls fail.

[8] https://blackboard.tudelft.nl/bbcswebdav/pid-2650079-dt-content-rid-9026628_2/xid-9026628_2 [cited 16 June 2016]

The reciprocating propulsion system is not very complex comparing with other aircraft propulsion systems. The engine is designed safe life and in case it fails, the aircraft can still glide for landing.

The carriage of measurement elements is more complex than the avionics connection. All payload measurement systems are separated and not connected to the avionics, so if the payload fails, the aircraft will always be able to continue the flying. The communication with the ground is a redundant system since a satellite-based Ku-band, a direct C-band and a direct UHF-band is used.

Besides all aircraft performance and system effectiveness, the reliability of the aerial system is less than manned systems. Mainly because unmanned systems are designed to be cheaper and therefore have a smaller development budget. Levels of redundancy are lower, and less testing is conducted compared to manned aircraft. [7] Reliability is a manner of public confidence in the system and is of great importance, especially for missions in populated areas.

Reliability is commonly expressed as a percentage of flight hours where the system does not fail, based on the probability of failure of each component. When components are dependent on other systems, the reliability is calculated in series. Otherwise, it is calculated in parallel, for example for redundant systems. The equations are shown in Equation 15.2 and Equation 15.3. Input values for the parameters are Mean Time Between Failure and the flight hours. All values are based on statistics. [41].

$$R = \prod_{i=1}^{N} R_i = \prod_{i=1}^{N} e^{\left(\frac{-t}{MTBF_i}\right)} \tag{15.2}$$

$$R = 1 - \prod_{i=1}^{N} \left(1 - R_i\right) = 1 - \prod_{i=1}^{N} \left(1 - e^{\left(\frac{-t}{MTBF_i}\right)}\right) \tag{15.3}$$

In Figure 15.4 the reliability of the components is shown for the number of flight hours. The airframe component is the most reliable, whereas the avionics are most likely to fail. Because of the high velocity and high loads the UAV experiences, the airframe reliability will be worse with respect to reference aircraft. Reliability is increased by overhauling aircraft components during its lifetime.

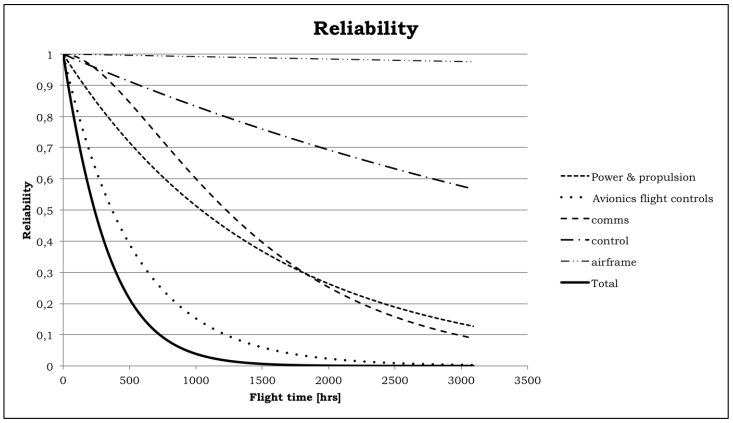

Figure 15.4: Reliability of the system

Availability
The availability of the system is dependent on the reliability and maintainability, but also on the set-up times, production time and transport time.

The set-up time of the system is dependent on the allocation of the aircraft. When the aircraft needs to be transported to a certain airport to perform calibration flights, the availability is dependent on air transport and needs to be assembled and checked before flight. When an aerodrome has a dedicated UAV for calibration, it can be stored in a hangar and does not need to be mounted before flight. The refuelling is a matter of minutes. Transport time is dependent on the location and airport logistics, as the LD6 is transported by air cargo. According to Table 15.4, the availability is most dependent on the flight crew, which needs to rest or be shifted after 10 hours.

Maintainability
The maintainability is defined by the ease and accuracy of of repairing and maintaining the aircraft. Refuelling is also included here. Maintainability is not only driven by the pace at which maintaining and repairing can be performed, but also by the complexity of those actions.

The aircraft is designed for fast flying and high resistance against loads. The structure needs to be designed for 8.5g. This means that the structure of the aircraft needs to be inspected frequently and parts have to be replaced on a regular basis. Furthermore the mounting and dismounting system require more inspection because this is highly sensitive for damage during operations.

The propulsion system is the most complex component of the aircraft. This system is moving at high angular velocities to make the aircraft maintain airspeed. Engine wear is very common and needs to be checked frequently.

The landing gear is designed safe life and has to be inspected frequently as well. Tires and breaks will wear and need to be replaced in within the time as specified by the manufacturer of these specific components.

Safety
The safety of the system is determined by it's impact on the environment. Parameters like fuel type, flying velocity and flying altitude are important here.

Loss of control is one of the main hazards for unmanned aerial flight. An uncontrollable aircraft may crash, which leads to either a high energy impact on a small area on the ground or, a low energy impact on a wider spread area. Depending on whether the aircraft stays intact or disintegrates in the air before chrashing into the ground.

The UAV is flying on aviation gasoline (avgas) which is a variation of gasoline used in cars. This fuel is flammable in case it is spark-ignited. The flammable fuel oils can fatally damage the wings in such a way that the aircraft burns down and crashes. Because avgas is the most used fuel in general aviation, the protection of fuel tanks and safety systems are well designed and the probability of occurrence is very unlikely.

The high velocity and low altitude flights over densely populated areas creates a direct hazard to local residents. Safe modes in the FMC are designed to land the aircraft safely in case of loss of communication or engine failure. The safe modes must be designed in such a way that the crash rate of the UAV is less than 1 out of 10 million flight hours.

To sum up, comparing with other UAVs, the system is reliable because of the conventional and most important proven concept. The availability is very dependent on the allocation of the UAV. The maintainability is compared with other aircraft UAVs a disadvantage since retractable landing gear is used and the loads are high. At last the safety is beneficial and forming an important role in design. As an overall conclusion, it can be said that the calibration UAV based system is designed in a way that high quality is guaranteed.

Table 15.4: Reliability of system components. [7]

Component	**Chance of loss [%]**	**MTBF [hrs]**	**MTBO [hrs]**	**Notes**
Power & propulsion	32	5,500	1,500	
Avionics & Flight controls	28			
Autopilot		*2,500*		
Flight critical avionics		*12,500*		
Instruments		*15,000*		
Non critical avionics (Payload)		*300*		
Servos		*3,000*		
Communications	11	2,500		Redundant system, so the final redundancy level will be larger.
Control	22			
Ground control		*5,500*		
Human operator		*650,000*	*10*	
Airframe	7	125,000	3,000	

15.5. CRASH RATE

The crash rate of the aircraft is very important for the confidence by customers in a design. The crash rate is defined by the number of crashes divided by the total flight hours. The UAV requirement is a crash rate of 1 in 10 million flight hours a crash occurs. This requirement gives a very low crash probability with respect to other unmanned systems. This in mainly because unmanned systems are designed to be cheaper and have less to spend on development costs. Levels of redundancy are lower and less testing is done as acceptable for manned aircraft. [7] Confidence in a system is needed when flying over populated areas. The crash rate of the system

is dependent on the failure rate of critical subsystems. Those can be connected by OR-trees or AND-trees. The AND-trees are redundant system, where multiple subsystems need to fail in order to get a system failure. The top-level of the fault-tree is shown in Figure 15.5. As can be seen, the communication system is a redundant system, where all subsystems need to fail in order to cause a crash.

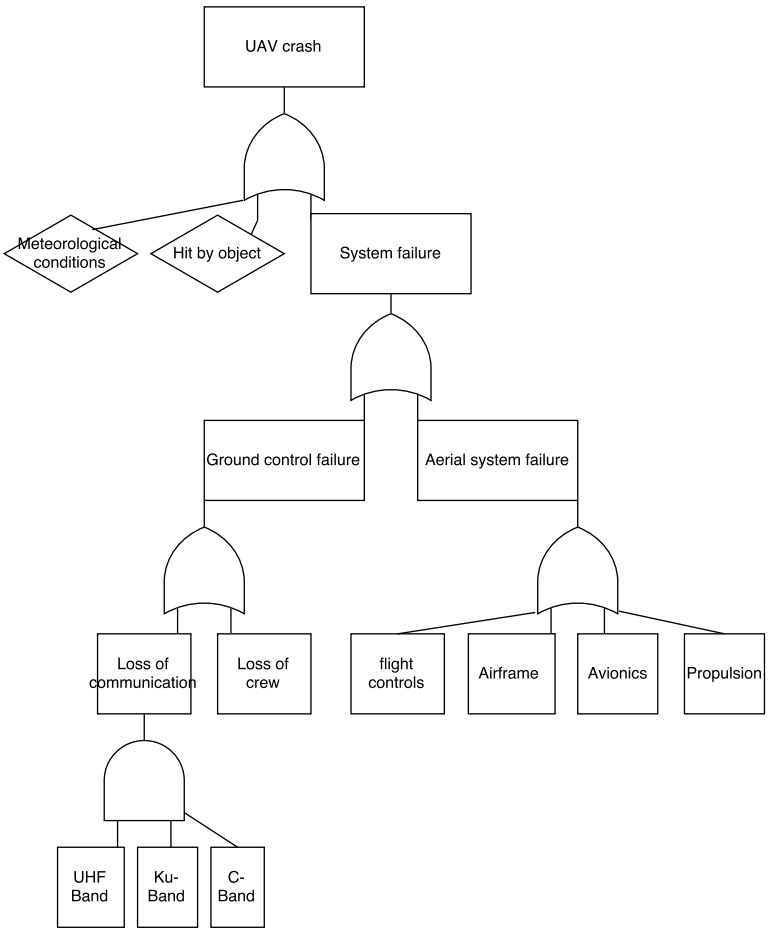

Figure 15.5: Fault tree for the UAV system.

15.6. COST AND PROFIT BREAKDOWN

Before the UAV is developed, an analysis needs to be done to know if this project is profitable. This will be done by analysing the return on investment. To be able to do this analysis, research on development cost, production cost, customer price architecture and operating cost is needed. All those parameters are discussed in these section.

15.6.1. DEVELOPMENT COST ESTIMATION

The development cost is basically all the money that is to spend to develop a fully certified aircraft/UAV. The development costs of aircraft include not only the design phase but also a lot of resources are needed for the experimenting and testing of during the design.

To estimate the development cost of the UAV, reference data was used from [7] and is listed below:

Table 15.5: Reference estimated development cost

UAV	Estimated development cost [$M]	Empty Operational mass [kg]
Outrider	268.5	185 [9]
Predater	209.9	512 [10]
Global Hawk	370.3	5150 [11]
DarkStar	326.9	2000 [12]

With this information, the development cost of the UAV is estimated to be 250 million dollars. This estimation is made by using linear regression to determine the relationship between the development cost and the OEW.

15.6.2. PRODUCTION COST

The production costs of the airborne system is a major consideration with respect to the feature feasibility of this project. In this section three different methods will be used to estimate the production cost of the airborne system. These methods include all the costs that incur for the manufacturer to produce a UAV from blueprint. In this estimation the costs include the production of the airframe, avionics, aircraft systems, communications etc. All three methods are based on UAV statistics and draw relationships between the production costs of UAVs and specific aircraft parameters. Important to mention is the fact that these estimation do not include the production of the payload system. This is because the payload systems can differ substantially depending on the specific mission of the UAV. Payload system costs can differ substantially from each other depending on the specific mission the UAV has to fulfil.

The first cost estimation method as shown in Equation 15.4 is proposed by Gundlach [7] and is a function of the OEW only. In 2004 the average production costs of UAVs was estimated to be 1500 $\$/lbs$.

$$C_P = \$1500 \cdot OEW \cdot ICF \cdot D2E = 1500 \cdot 752.4 \cdot 1.27 \cdot 0.89 = €1.27 million \tag{15.4}$$

In this case the OEW is in pounds and because this estimation was made in the year 2004 the 1500 $ has to be corrected for inflation since that year up till now. The inflation correction factor ICF is computed using the Consumer Price Index CPI of 2004 and the one of may 2016. Because the relationship from 15.4 that uses the dollar as a reference, the CPI of the United States is used provided by the Bureau of Labor Statistics. It was stated that the CPI for the fiscal year of 2004 had an average value of 188.900 and the CPI of May 2016 had a value of 240.236. The ICF can now be computed using 15.5. To convert to the euro currency a conversion rate $D2E$ of 0.89 from dollar to euro is used which was the current rate on June 18, 2016. As can be seen from the result of 15.4, the production costs of 1 UAV unit is estimated to be around 1.27 million euros.

$$ICF = \frac{CPI_{2016_{may}}}{CPI_{2004}} = \frac{240.236}{188.900} = 1.27 \tag{15.5}$$

The second estimation method as shown in Equation 15.6 is developed by Technomics [42] which includes both the max endurance E_{max} of the aircraft(19 hours) as well as the payload weight in pounds W_{PL} to compute the production costs. Other input variables for this method are the year of first flight FF_{Year}, which is set for 2016 and the f_prod, which is a correction constant set on 0.3981.

$$C_P = \$118750 \cdot (E_{max} \cdot W_{PL})^{0.587} \cdot e^{-0.01 \cdot (FF_{Year} - 1900)} \cdot f_{prod} \cdot ICF \cdot D2E = €1.58 million \tag{15.6}$$

The third estimation method has also been developed by Technomics [42] and includes only the $MTOW$ as a aircraft parameter to compute the productions costs. Equation 15.7 shows how the costs are a function of the $MTOW$ but also again is dependent on a correction factor which for this method is 1.379.

$$C_P = \$12550 \cdot MTOW^{0.749} \cdot f_{prod} \cdot ICF \cdot D2E = €3.23 million \tag{15.7}$$

The first method shows the lowest production costs but is still 5 times higher than the requirement that was set by the customer. This result will largely influence the future feasibility of the project and new revenue strategies.

15.6.3. CONSUMER PRICE

To estimate the consumer retail price, some research has been done on other UAVs. The unit customer price has been defined by [7] and their results are listed below: [ht]

[9] http://www.designation-systems.net/dusrm/app2/q-6.html [cited 16 June 2016]
[10] http://www.bga-aeroweb.com/Defense/MQ-1-Predator-MQ-9-Reaper.html [cited 16 June 2016]
[11] http://www.bga-aeroweb.com/Defense/RQ-4-Global-Hawk.html [cited 16 June 2016]
[12] http://www.militaryfactory.com/aircraft/detail.asp?aircraft_id=1152 [cited 16 June 2016]
[13] http://www.militaryfactory.com/aircraft/detail.asp?aircraft_id=326 [cited 16 June 2016]
[14] http://www.designation-systems.net/dusrm/app2/q-2.html [cited 16 June 2016]
[15] https://grabcad.com/library/drone-us-navy-mq-8b-firescout-uav-helicopter-1/files [cited 16 June 2016]

Table 15.6: Reference customer price

UAV	Unit Customer Price [$M]	Empty Operational mass [kg]
RQ-7A	0.45	75[13]
RQ-2B	0.75	178 [14]
RQ-8B	4.73	940.3 [15]
MQ-1B	3.12	512 [10]
MQ-9A	6	2223 [10]

After this research a unit customer price for a UAV with a OEM of 342kg was estimated (with use of linear regression) to be equal to 1.8676 $M.

15.6.4. ACHIEVABLE MARKET SHARE

It is very difficult to make a proper estimation of the achievable commercial market share, since at the current stage, UAV's are illegal for civil use.

As man hours are very expensive, [16], industry strives to automate as much processes as possible.

One of the direct stakeholders of the project is the NLR (Nederlands Lucht- en Ruimtevaartcentrum) who is currently providing the NavAid calibration for all dutch airfields and belgian military airfields. It can be assumed that they will order such a UAV when it is certified.

As mentioned before companies want to decrease their labour cost. For that reason it is expected that over time more and more companies will step over to the UAV[17] calibration method which will lead to a increase of market share. Once the product is introduced to the market, other companies will become familiar with the product, increasing the market share.

15.6.5. OPERATIONAL COST

To convince the customer that operating a UAV is cheaper than a manned aircraft, research was done to support this presumption. The DOD reported that the operation cost of the Predator and the Reaper UAV are respectively $859 and $1,456 per flight hour[18], while the operational cost of the Blackhawk helicopter and the C-12 aircraft are around $5,897 and $1,370. Those operational costs are based on maintenance costs, asset utilisation costs, and military personnel costs.

Over a long period it becomes more profitable to employ an UAV instead of a manned aircraft.

15.6.6. RETURN ON INVESTMENT

To investigate the amount of profits produced due to a certain investment, an analysis on return of investment (ROI) is done. To calculate the ROI the equation below is used[43].

$$\text{ROI}(\%) = \frac{\text{Gain from Investment} - \text{Cost of Investment}}{\text{Cost of Investment}} \cdot 100 \tag{15.8}$$

The "gain from investment" can be formulated as Equation 15.9, and the "Cost of Investment" can be formulated as Equation 15.10. Note that the value of customer price, development cost and unit production cost are discussed previously in this in this section.

$$\text{Gain from Investment} = \text{customer price} \cdot \text{number of produced units} \tag{15.9}$$

$$\text{Cost of Investment} = \text{development cost} + (\text{unit production cost} \cdot \text{number of produced units}) \tag{15.10}$$

If the number of produced units will be equal to 100 (which is the initial requirement) the ROI will be as follows:

$$\text{ROI}(\%) = \frac{1.8676 \cdot 100 - (250.6614 + 1.4333 \cdot 100)}{250.6614 + 1.4333 \cdot 10} \cdot 100 = -52.6 \tag{15.11}$$

From Table 15.7 it can clearly been seen that that the initial requirements of 100 units result in a negative ROI with means that the company will make no profit. What also can be seen is that the ROI increases if the

[16] http://www.bls.gov/oes/current/oes_nat.htm#00-0000 [cited 17 June 2016]
[17] http://www.globalsecurity.org/intell/library/reports/2001/uavr0401.htm[cited 17 June 2016]
[18] https://www.quora.com/U-S-Air-Force-Is-the-future-of-military-aircraft-in-expensive-manned-craft-or-cheaper-disposable-U
18 June 2016]

Table 15.7: Return on investment for different numbers of produced units

Numbers of produced units	**ROI[%]**
100	-52.6
300	-17.7
500	-3.5
700	4.3

number of produced units goes up. With the estimated parameters the break even point (ROI is equal to 0) will be reached at 578 units.

If the UAV is used only for calibration purposes the the whole project will fail economically, since large number of UAV flight inspection systems will be large to sell. To be able to make profit it is recommended that the UAV be re-purposed to be used in other markets such as surveillance or geographical measurements.

16 Design Review

Now that the design is finalised, there is only one task remaining, and that is to verify and validate the entire product. This is done to prevent disasters that could have been prevented by checking whether the designed product is the product that was intended to be designed and whether the product is as the customer requested. This chapter shall provide a compliance matrix in Section 16.1 in which the product verification is presented, along a description of the verification method and an elaboration on the requirement. Then in Section 16.2, the product validation will be performed, in which an explanation will be provided on the techniques that can be used to validate the product, once it is built.

16.1. Product Verification

In order to verify the product, it needs to be checked whether the system that is developed meets the requirements that were set at the beginning of the design process by the customer, better known as the top-level requirements. For this, a compliance matrix Table 16.1 is constructed, which serves as a proof of compliance with the design solution specification and also includes a description of the compliance along with the verification method that is used. The verification methods that are available are explained below [44].

- **Inspection**: Inspection of the design documentation of the product to show compliance with the requirement.
- **Analysis**: Establish by mathematical or other analysis techniques that the product complies with the requirement.
- **Demonstration**: Establish by operation, adjustment or reconsideration of a test article its compliance with the requirement.
- **Test**: Test (a representative model of) the product's compliance with the requirement under representative conditions.

16.2. Product Validation

Validation is needed to check whether the designed product actually is what the customer requested. In this case, product validation is checking whether the UAV is able to calibrate aerial navigational equipment. All functions that are required to perform the mission are specified in the FBS back in Section 2.2. If the UAV is able to perform all these functions, it can be said that the product is validated. The functions are listed below, along with a description of how these functions are carried out.

Perform Flight This includes the ability to provide lift, thrust, stability and control. All these aspects are taken care of, meaning the UAV is able to fly.

Provide Navigation The UAV is equipped with multiple navigational antennas, as well as communication antennas to receive commands. Therefore it can be concluded that the UAV is able to navigate.

Provide Communication The UAV has a complete set of antennas, including back-up, with which a communication link can be established with the GS. This can be done using a direct link (line of sight) or a satellite link (SATCOM). Both links are available to the system. With the on-board computers and data buses, it is also able to store data and process data.

Provide Power The engine that is equipped on the UAV provides enough power to complete all possible missions.

Perform Inspection Inspection can be performed with the removable payload that is designed. This payload includes all receivers and a DAU to accurately measure the navigational signals that need to be calibrated.

Provide Structure For all critical parts, the structure is designed in detail, from which it became clear that the structure as it is now, will not fail due to the loads that can be experienced in the ultimate case.

[1] `http://www.navipedia.net/index.php/GBAS_Fundamentals` [cited 17 June 2016]

Provide Safety Safety has been taken into account during the entire design process. For example, the critical components of the avionics are all duplicated or even triplicated for redundancy. The on-board computers have a safe mode function which ensures that the system and its direct environment are safe.

From the above text, it can be concluded that, in theory, the product is validated as the customer requested. However, product validation can be done more accurately after the system has been produced, which is not the case. Should the system be produced, then a more elaborate product validation can be carried out. To do this, the following techniques can be used [44]:

- **End-to-End Information System Testing**: Show compatibility of project information systems (e.g. data, timing).
- **Mission Scenario Tests**: Demonstrate that flight hardware and software can execute the mission under flight-like conditions (nominal & contingency) without real timeline.
- **Operations Readiness Tests**: Demonstrate that all elements of the ground segment (e.g. software, hardware, people, facilities) accomplish the mission plan using real timeline.
- **Stress-Testing and Simulation**: Assess system robustness to variations in performance and fault conditions.

Table 16.1: Compliance matrix for the top-level requirements of the system.

ID	Requirement	Comp.	Method	Comment
1	The UAV shall have a range of at least 800 NM.	✓	Analysis/Test	It is shown in Chapter 11 that the maximum range of the UAV is 1736 NM.
2	The UAV's endurance shall be more than 4 $hours$.	✓	Analysis/Test	It is shown in Chapter 11 that the maximum endurance of the UAV is 19 hours
3	The UAV's maximum cruise speed shall be at least 200 kts.	✓	Analysis/Test	It is shown in Chapter 11 that the maximum cruise speed of the UAV is 204 kts at FL100
4	The UAV's service ceiling shall be higher than FL100.	✓	Analysis/Test	It is shown in Chapter 11 that the service ceiling of the UAV is FL190
5	The pre-programmed UAV shall be updatable in flight.	✓	Analysis	There is a telecommunication link available between the GS and the UAV, both within line of sight (direct link) and beyond line of sight (satellite link). These links are also used to provide commands to the UAV from the GS. An explanation can be found in Section 5.4.
6	The UAV shall be able to fly autonomously.	✓	Inspection	The UAV has several computers on-board that enable autonomous flight. These are presented in Section 5.5.
7	The UAV shall have a direct remote control system.	✓	Inspection	The GS consists of an operator control unit which includes a direct remote control system.
8	The crash rate of the system shall be less than 10^{-7} per flight hour.	???	Analysis	The crash rate could not be determined, because this needs to be based on test statistics. However, the interaction and dependencies of subsystems was described.
9	The UAV shall be compliant with relevant EASA standards.	✓	Inspection	The design is based EASA standards.
10	The UAV shall produce 20 dBA lower sound exposure level than a Cessna 550 on a 3° glideslope landing.	✓	Analysis	The sound exposure level is currently only 15 dBA lower than the Cessna 550, which is not enough yet, but still this is a huge improvement with respect to current practises. After discussing this with the customer, it turned out to be a satisfying result and therefore it can be said that the system complies with the noise requirement.
11	More than 80% of the empty weight shall be recyclable.	✓	Analysis	It is shown in calculations in Section 15.3 that the overall recyclability is 80.9 %.
12	The MTOW of the UAV shall be less than 500 kg.	✓	Inspection	The weight estimation in Chapter 6 shows that the MTOW of the UAV is 484 kg, thereby showing preliminary compliance with this requirement.
13	The system shall fit in a single LD6 aircraft container.	✓	Inspection	The outer dimensions of the UAV exceed that of the LD6, but as explained in Section 14.2, the UAV can be dismantled such that it can fit inside the LD6.
14	The production volume shall be 100 units.	X	Analysis	The profit related to 100 products is too low to compensate for the development cost. To match the development costs, at least 578 units shall be produced. To be able to sell all those units, a wider market is needed.
15	The unit production cost of the UAV shall not be more than €250,000.	X	Analysis	The production cost is estimated to be €1.27M which is five times higher than the requirement. But with respect to the customer price and development cost, a production cost of €1.27M seems perfectly reasonable
16	The UAV shall be able to carry flexible payload for possible future missions.	✓	Inspection	There is a special payload bay that can be dismantled.
17	The ground-based positioning system shall have an accuracy of less than 1 m.	✓	Inspection	The system makes use of GBAS near airports, which has an accuracy of less than 1 m [1]

17 FUTURE PLANNING

The future planning determines what activities have to be performed in order to get from this point of the project to a working system. For this, the project design and development logic is created together with a Gantt chart. After this, a cost-breakdown structure is created and a production plan is determined.

17.1. PROJECT DESIGN AND DEVELOPMENT LOGIC

The project design and development logic is the logical order of activities to be conducted after the DSE [45]. Figure 17.1 shows the first phase after the DSE which is the detailed design phase. Here a more thorough mission will be defined after which a detailed market, risk, RAMS and cost analysis will be performed. At the same funding must be acquired to continue the project as well as promoting the the calibration and testing UAV to potential costumers. On the technical side more detailed aerodynamics will be design from which a wind tunnel test will be conducted. Other aircraft systems, structures, propulsion and payload (calibration equipment) will be design further. The wind tunnel test will most likely mean changes must be made both aerodynamically and structurally. The weight and performance will be asses which is important for the detailed design review. If the review is passed the team can continue with the build and operation phase shown in Figure 17.2. If the review is failed, improvements must be made before a new review can be held.

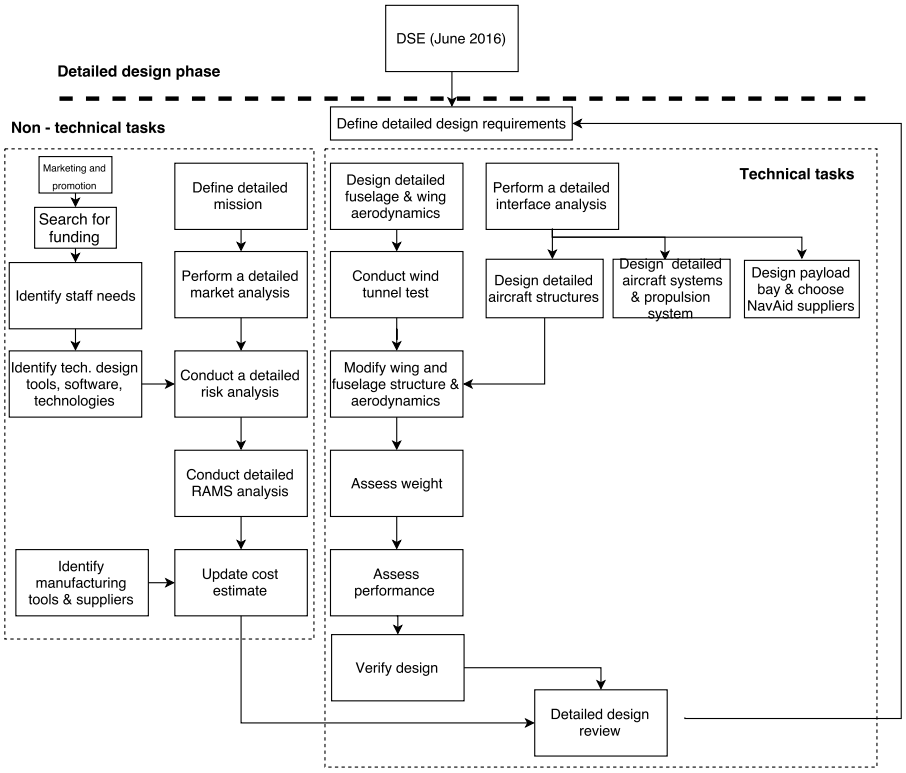

Figure 17.1: Project design and development logic for post-DSE

The build and operations phase begins with logistics planning for the production as well as schedule the production itself. At the same time documentation is prepared for the final product. Operational and maintenance procedures are defined based on work done during the detailed design. Manufacturing as well as assembly is carried out to build a prototype. This prototype is used for testing and validation. The operational phase consist of distribution of the product. After the UAV has gone to market maintenance and modifications must be carried out. Lastly, when the system is at its end-of-life, it must be disposed and recycled.

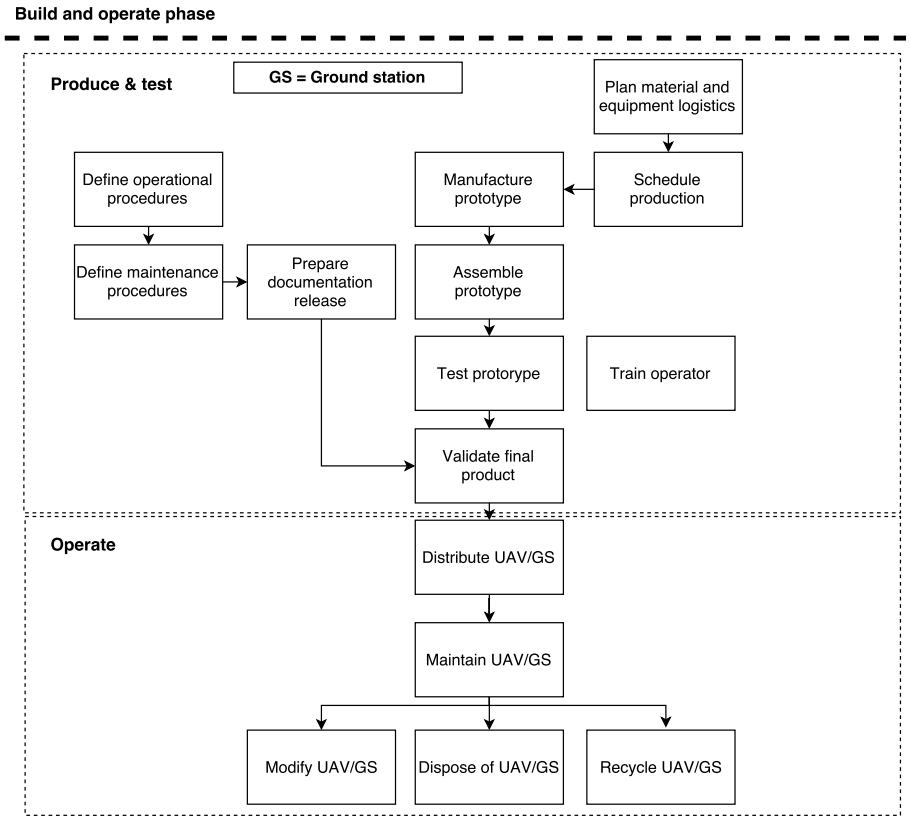

Figure 17.2: Project design and development logic for post-DSE

17.2. PROJECT GANTT CHART

The project Gantt chart (Figure 17.3 and Figure 17.4) shows the The project design and development logic in a timeline where the duration of each task is estimated. It is aimed to deliver the UAV and ground station system to customers in the last month of 2017 with development starting directly after the conclusion of the DSE. The maintenance, recycling and disposing of the system has been added, but since they are tasks done during operation, they do not have a duration specified.

ID	Task Name	Duration	Start	Finish
1	DSE Project			Thu 30-6-16
2	**Detailed Design Phase**	**231 days**	**Fri 1-7-16**	**Fri 19-5-17**
3	**Non-tectnical tasks**	**231 days**	**Fri 1-7-16**	**Fri 19-5-17**
4	Market and promote	200 days	Mon 15-8-16	Fri 19-5-17
5	Search for funding	100 days	Fri 1-7-16	Thu 17-11-16
6	Define detailed mission	20 days	Fri 1-7-16	Thu 28-7-16
7	Identify staff needs	10 days	Fri 15-7-16	Thu 28-7-16
8	Perform a detailed market analysis	30 days	Sat 30-7-16	Thu 8-9-16
9	Identify technical design tools, software & techonologies	20 days	Sat 30-7-16	Thu 25-8-16
10	Conduct a detailed risk analysis	20 days	Sat 10-9-16	Thu 6-10-16
11	Conduct a detailed RAMS analysis	20 days	Sat 10-9-16	Thu 6-10-16
12	Identify manufacturing tools and suppliers	30 days	Sat 1-10-16	Thu 10-11-16
13	Update cost estimate	30 days	Thu 1-12-16	Wed 11-1-17
14	**Technical tasks**	**205 days**	**Fri 1-7-16**	**Thu 13-4-17**
15	Design detailed fuselage and wing aerodynamics	90 days	Fri 1-7-16	Thu 3-11-16
16	Perform a detailed interface analysis	20 days	Fri 1-7-16	Thu 28-7-16
17	Conduct wind tunnel test	5 days	Thu 10-11-16	Wed 16-11-16
18	Design detailed aircraft structures	100 days	Fri 15-7-16	Thu 1-12-16
19	Design detailed aircraft and propulsion system	100 days	Fri 15-7-16	Thu 1-12-16

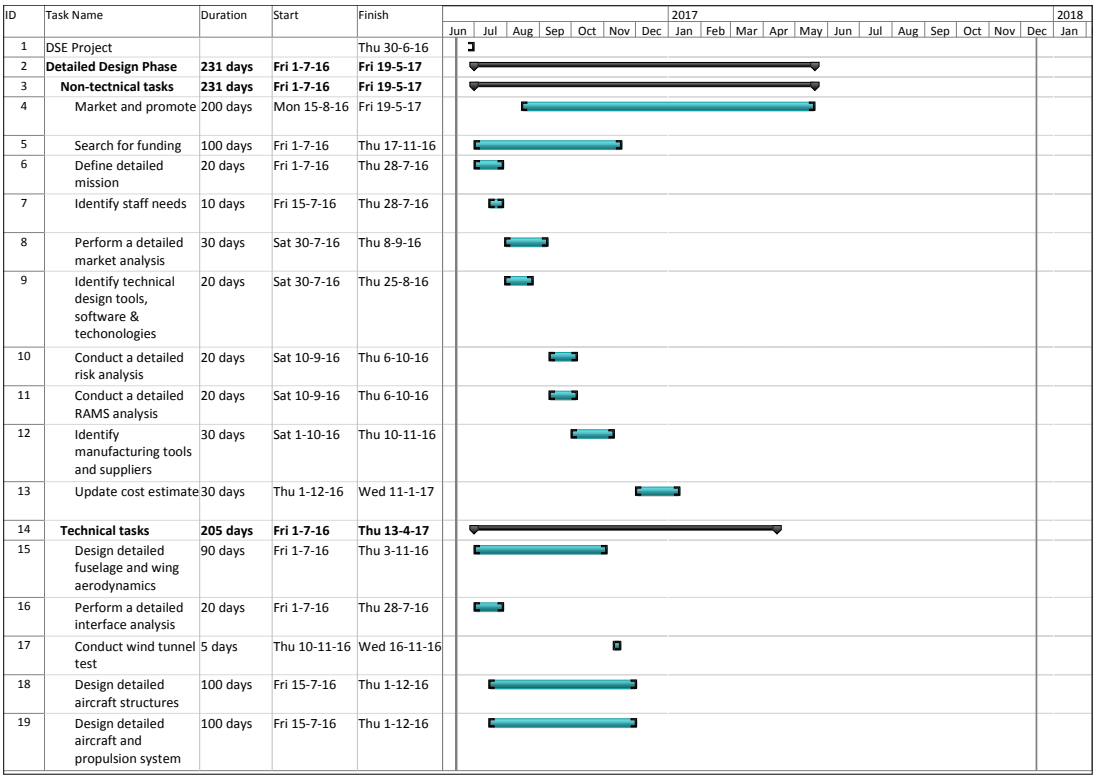

Figure 17.3: Project Gantt chart for post-DSE

ID	Task Name	Duration	Start	Finish
20	Design payload bay and choose NavAid suppliers	45 days	Fri 1-7-16	Thu 1-9-16
21	Modify wing and fuselage structure and aerodynamics	45 days	Sun 1-1-17	Thu 2-3-17
22	Assess weight	30 days	Wed 15-2-17	Tue 28-3-17
23	Assess performance	30 days	Wed 1-3-17	Tue 11-4-17
24	Verify design	20 days	Wed 15-3-17	Tue 11-4-17
25	Detailed design review	10 days	Sat 1-4-17	Thu 13-4-17
26	**Build and operate phase**	**154 days**	**Mon 15-5-17**	**Fri 15-12-17**
27	Define operational procedures	15 days	Mon 15-5-17	Fri 2-6-17
28	Plan material and equipment logistics	30 days	Mon 15-5-17	Fri 23-6-17
29	Define maintenance procedures	30 days	Thu 1-6-17	Wed 12-7-17
30	Prepare documentation release	30 days	Thu 15-6-17	Wed 26-7-17
31	Train operator	30 days	Thu 15-6-17	Wed 26-7-17
32	Schedule Production	15 days	Tue 30-5-17	Mon 19-6-17
33	Manufacture prototype	67 days	Thu 15-6-17	Fri 15-9-17
34	Assemble Prototype	45 days	Thu 20-7-17	Wed 20-9-17
35	Test prototype	55 days	Tue 1-8-17	Sun 15-10-17
36	Validate final product	16 days	Sun 1-10-17	Fri 20-10-17
37	Distribute UAV/GS	0 days	Fri 15-12-17	Fri 15-12-17
38	Maintain UAV/GS	0 days	Fri 15-12-17	Fri 15-12-17
39	Modify UAV/GS	0 days	Fri 15-12-17	Fri 15-12-17
40	Recycle UAV/GS	0 days	Fri 15-12-17	Fri 15-12-17
41	Dispose UAV/GS	0 days	Fri 15-12-17	Fri 15-12-17

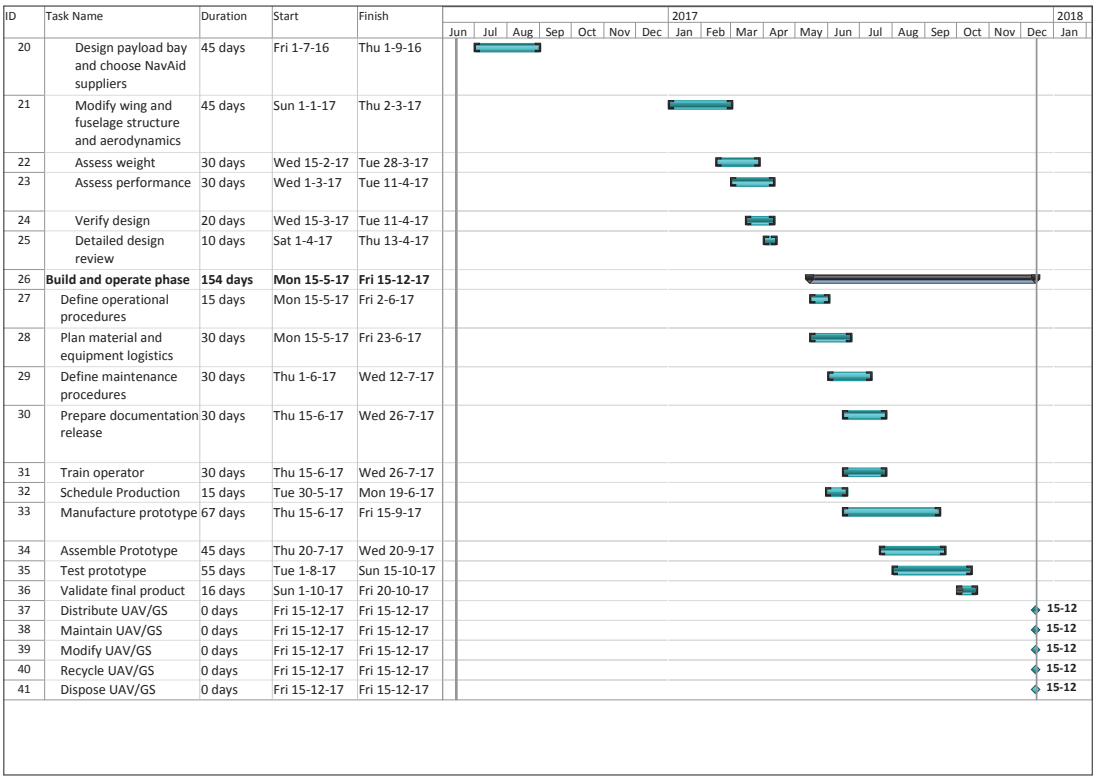

Figure 17.4: Project Gantt chart for post-DSE

17.3. COST-BREAKDOWN STRUCTURE

The cost-breakdown structure is aimed at identifying the total cost of the UAV and ground system. It is based on the project design and development logic from Figure 17.1 and Figure 17.2. A cost estimation will be based

the cost-breakdown structure

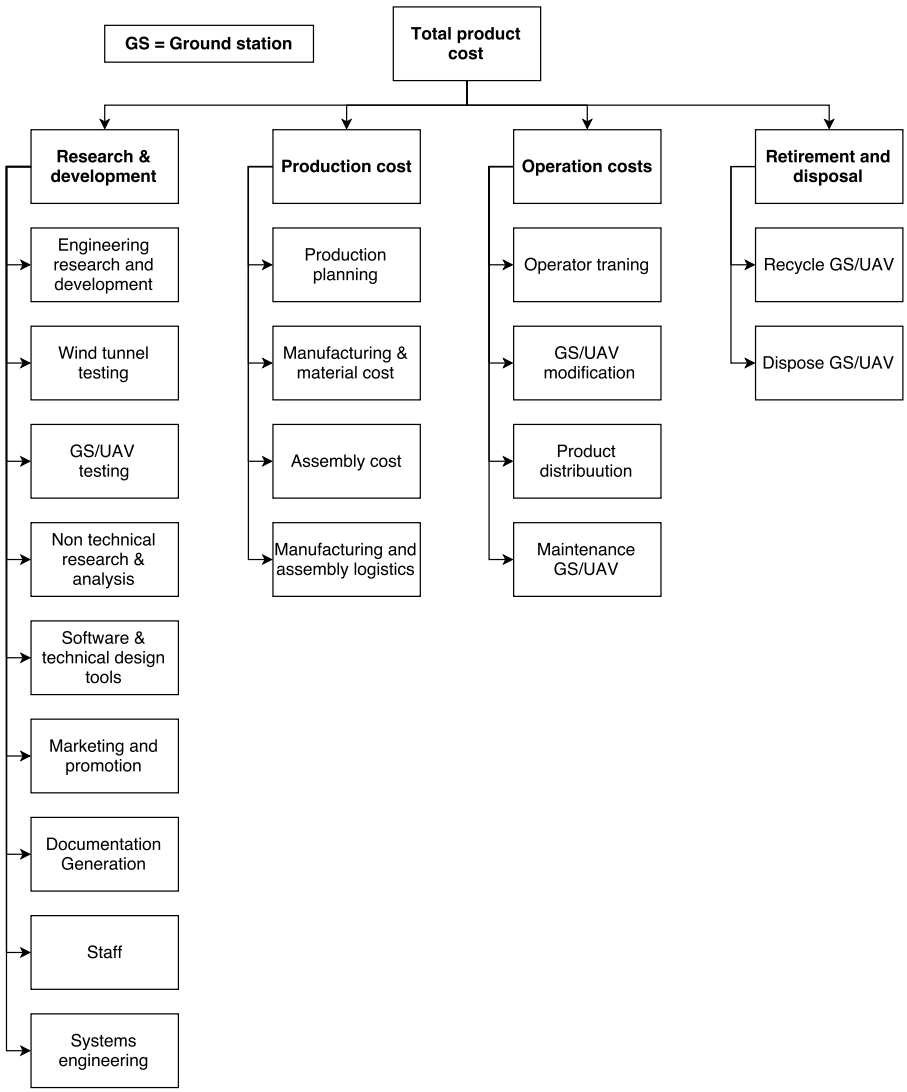

Figure 17.5: Project design and development logic for post-DSE.

17.4. PRODUCTION PLAN

As the UAV has to be transportable, and parts must have the possibility to be replaced independent of other components of parts. To make that possible the UAV will be made out of different parts. To make sure that production will smooth, a production plan will be made.

First you have to know which departments are involved in the production. Those are listed below:

- Main wing
- Tail
- Boom
- Landing gear
- Fuselage
- Engine
- Propeller
- Payload system

- Avionics

For some of those listed department you need to work with subcontractors, for example payload system, avionics and the engine. The other departments can be manufactures without subcontractors, which will reduce the production cost. Since the UAV is not a large aircraft, all components can be made in one factory. By doing this there will be almost no transportation cost.

First all the components has to be made which are not dependant on subcontractors. The engine, payload systems, avionics and propeller are expensive products that first has to be bought by the assemblage factory and later be charged to the buyer. Since this is a large cost you want to do it as late as possible. By knowing all this the production plan, as presented in Figure 17.6, can be made.

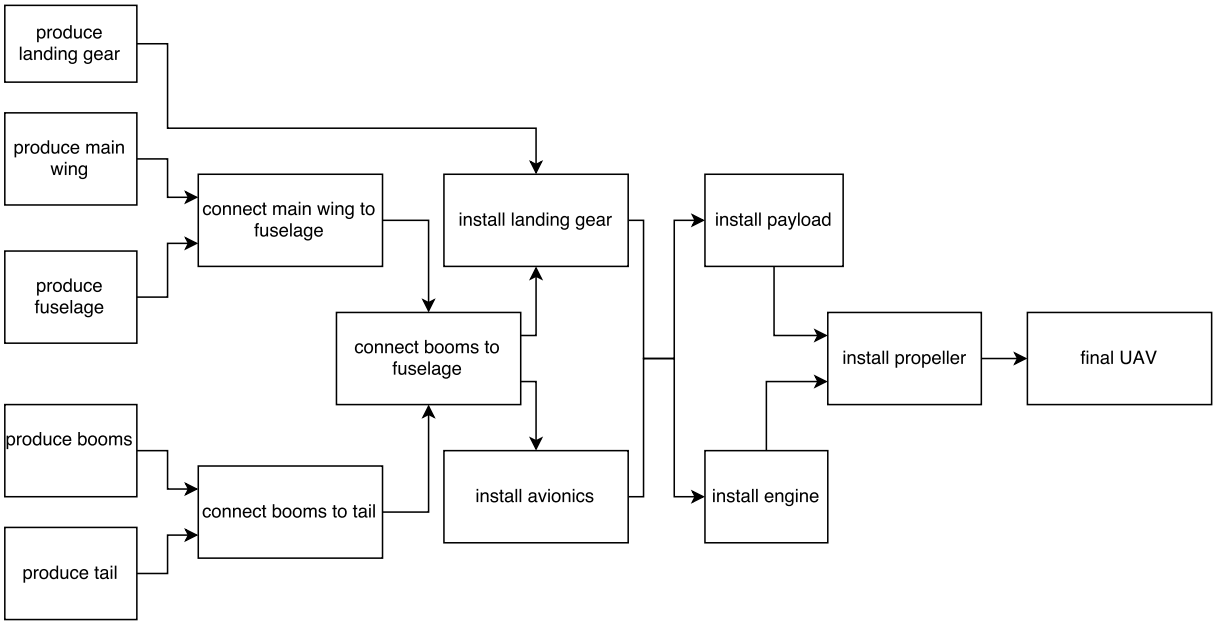

Figure 17.6: production plan

18 Conclusion and Recommendations

The aim of this report was to present a final concept design of a UAV based system able to replace the aircraft that are currently used for the calibration of aerial navigation equipment. During a ten week design process, a concept has been designed as presented in this final report. The UAV is equipped with multiple navigation receivers, as well as communication antennas to receive commands. Because of this, the system is able to calibrate aerial navigation equipment without a pilot and only requires a flight inspector on the ground. This significantly reduces the operational cost of the system compared to current flight inspection systems. Because the system is specifically designed for the altitude and speed at which flight inspection is performed and is smaller, it is able to perform the flight inspection more efficient, more sustainable, create less interference with aerodrome operations and produce less noise while still meeting the same performance requirements.

The main requirements of the system were described by the customer. Most of these requirements have been met, however, some are not and some have been altered in consult with the customer. At this point, the crash rate of less than 10^{-7} could not be analysed quantitatively, therefore no precise crash rate has been presented and the compliance with this requirement could not be proven. Furthermore, the sound exposure level was required to be 20 dBA lower than a Cessna 550 on a 3° glideslope. Reaching this value was deemed impossible after analysing the characteristics and a final value of 15 dBA was presented. The production cost of at most €250.000 could also not be met. First estimations calculated the production cost at €1.27M, however, this seemed perfectly reasonable after further debate with the customer. The real production cost can however only be analysed once the detailed design is finalised and a detailed production plan is created. Finally, the production volume of 100 units is according to first estimations not sufficient to compensate for the high development cost of the system, therefore, a wider market is required in order to be profitable. In order to achieve this, the UAV could be repurposed for other missions, which is already enabled by making the payload removable.

Some recommendations on the final design have to be made. First of all, more dynamic load cases should be analysed and specifically at points of load introduction as these cause local stress concentrations. In addition, an aeroelasticity analysis should be performed on the tail to determine the impact of its low stiffness on its aerodynamic performance, as large deflections impact the local angle of attack. Furthermore, a detailed design of the fuselage should be made, especially with considerations regarding composites. To reduce the structural loads due to gusts, which are currently driving in the V-n diagram, an iteration of the airfoil should be performed where a lower lift gradient should be opted for to reduce its sensitivity. This will be beneficial for possible high stability requirements for imaging payloads. Alternatively, gust alleviation systems may be analysed to reduce the accelerations caused by gusts and to improve fatigue life by reducing the load amplitude. Finally, because the requirements ask for a relatively small aircraft with a high cruise speed, the size and weight of the engine drive the overall design to a large extent (the engine weight is 25% of the OEW of the UAV). Researching new engine technologies for more compact and lighter engines could therefore significantly improve the overall design and performance of the system and should be looked at before further development of the system.

BIBLIOGRAPHY

[1] H. van Donge, S. Heyer, A.A.J. Hooijen, A. Khoshnewiszadeh, R.R.J. Krook, J. Meyer, J.R. van der Ploeg, T.S.C. Pollack, T.C. Schouten and S.C.E. Smets, *Design of a UAV based NavAid Calibration and Testing system - Project Plan,* (2016), DSE.

[2] H. van Donge, S. Heyer, A.A.J. Hooijen, A. Khoshnewiszadeh, R.R.J. Krook, J. Meyer, J.R. van der Ploeg, T.S.C. Pollack, T.C. Schouten and S.C.E. Smets, *Design of a UAV based NavAid Calibration and Testing system - Midterm Report,* (2016), DSE.

[3] H. van Donge, S. Heyer, A.A.J. Hooijen, A. Khoshnewiszadeh, R.R.J. Krook, J. Meyer, J.R. van der Ploeg, T.S.C. Pollack, T.C. Schouten and S.C.E. Smets, *Design of a UAV based NavAid Calibration and Testing system - Baseline Report,* (2016), DSE.

[4] T. Wede, *The future of the flight inspection world a crystal ball look into changes ahead, based on current trends and developments,* 14th International Flight Inspection Symposium (2006).

[5] Airbus, *Global market forecast flying by numbers 2015-2034,* (2015).

[6] S. Peasgood, *Drones: a Rising Market,* Sophic Capital (2015).

[7] J. Gundlach, *Designing Unmanned Aircraft Systems: A Comprehensive Approach* (American Institute of Aeronautics and Astronautics, Inc., 2011).

[8] S. N. Zealand, *Handbook: Risk management guidelines-companion to AS/NZS ISO 31000:2009* (NSW SAI Global Limited, New Zealand, 2013).

[9] K. Munson, *Jane's Unmanned Aerial Vehicles and Targets* (Peer Tree Image Processing, United Kingdom, 1996).

[10] I. Wilmes, *Flight Inspection Manual NLR*, NLR (2016).

[11] T. Macnamara, *Introduction to Antenna Placement & Installation* (John Wiley & Sons Ltd, London, 2010).

[12] T. Heinke and T. Feuerle, eds., *Flight Inspecting Ground Based Augmentation Systems (GBAS)*, 15th International Flight Inspection Symposium (International Committee for Airspace Standards and Calibration, Oklahoma City, 2008).

[13] *Manual on Testing of Radio Navigation Aids*, International Civil Aviation Organization, Quebec, 4th ed. (2000).

[14] A. Cervone, *AE2111-II Aerospace Design and Systems Engineering Elements II lecture slides,* (2014).

[15] A. J. Chaput, *Design of UAV Systems,* `www.southampton.ac.uk` (2003).

[16] F. A. Administration, *Airplane Flying Handbook* (U.S. Department of Transportation Federal Aviation Administration, 2004).

[17] *Aviation Maintenance Technician Handbook-Airframe*, FAA (2012).

[18] T. Saaty, ed., *Decision making with the analytic hierarchy process*, Vol. 1, No. 1, University of Pittsburgh (Int. J. Services Sciences, 2008).

[19] M. H. Sadraey, *Aircraft Design - A Systems Engineering Approach* (John Wiley & Sons Ltd, Wiltshire, United Kingdom, 2013).

[20] R. Eppler, *Airfoil Design and Data*, 1st ed. (Springer-Verlag Berlin Heidelberg GmbH, New York, 1990).

[21] I. Abbott and A. von Doenhoff, *Theory of Wing Sections* (Dover Publications, Inc., New York, 1958).

[22] J. Mariens, A. Elham, and M. van Tooren, *Quasi-three-dimensional aerodynamic solver for multidisciplinary design optimization of lifting surfaces,* Journal of Aircraft **51** (2014).

[23] G. La Rocca, *Systems Engineering and Aerospace Design,* Delft University of Technology (2016).

[24] X.-S. Yang, *Engineering optimisation : An introduction with meta-heuristic applications* (Wiley, 2010).

[25] J. John D. Anderson, *Fundamentals of Aerodynamics*, 2nd ed. (McGraw-Hill, 1991).

[26] D. P. Raymer, *Aircraft Design: A Conceptual Approach* (AIAA, 1992).

[27] A. van der Wees, J. van Muijden, and J. van der Vooren, *A fast and robust viscous-inviscid interaction solver for transonic flow about wing/body configurations on the basis of full potential theory,* AIAA Paper (1993).

[28] D. Steenhuizen, *Aerospace design and systems engineering elements ii, wing design part 3,* Delft University of Technology (2013).

[29] J. A. Mulder, W. H. J. J. van Staveren, J. C. van der Vaart, E. de Weerdt, C. C. de Visser, A. C. in 't Veld, and E. Mooij, *Flight dynamics lecture notes,* Aerospace Engineering Faculty – Delft University of Technology (2013).

[30] S. Gudmundsson, *Chapter 7 - selecting the power plant,* in *General Aviation Aircraft Design*, edited by S. Gudmundsson (Butterworth-Heinemann, Boston, 2014) pp. 181 – 234.

[31] E. Torenbeek, *Synthesis of Subsonic Airplane Design* (Kluwer Academic Publishers, 1996).

[32] G. J. J. Ruijgrok, *Elements of airplane performance*, 2nd ed. (VSSD, 2009).

[33] S. Gentile and M. Glicksman, *Spitfire Mk I & II Pilot's Handbook*, A2A (1946).

[34] G. E. Wright and F. M. d. Piolenc, *Ducted fan design. Vol. 1.* (Mass Flow, West Covina, 2001).

[35] J.Roskam, *Airplane design. Pt. 4. Layout design of landing gear and systems* (Ottawa, Kansas: Roskam Aviation and Engineering., 1985).

[36] E. A. S. Agency, *Certification Specifications and Acceptable Means of Compliance for Normal, Utility, Aerobatic, and Commuter Category Aeroplanes CS 23*, amendment 4 ed. (2015).

[37] E. Torenbeek, *Development and Application of a Comprehensive, Design-Sensitive Weight Prediction Method for Wing Structures of Transport Category Aircraft*, Tech. Rep. (Delft University of Technology, 1992).

[38] F. A. Administration, *Aviation Maintenance Technician Handbook—Airframe Volume 1* (U.S. Department of Transportation federal aviation administration, 2012).

[39] International Aluminium Institute, European Aluminium Association, and Organisation of European Aluminium Refiners and Remelters, *Global Aluminium Recycling: A Cornerstone of Sustainable Development,* (2009), URL: `http://www.world-aluminium.org/media/filer_public/2013/01/15/fl0000181.pdf` [cited april 20, 2016].

[40] K. Binnemann, P. T. Jones, B. Blanpain, T. V. Gerven, Y. Yang, A. Walton, and M. Buchert, *Recycling of rare earths: a critical review,* Journal of Cleaner Production **51**, 1 (2013).

[41] R. Austin, *Unmanned Aircraft Systems UAV's Design, Development and Deployment* (John Wiley & Sons Ltd, Wiltshire, United Kingdom, 2010).

[42] J. Cherwonik, *Unmanned aerial vehicle system acquisition cost estimating methodology,,* Technomics, 37th DOD Cost ANalysis Symposium (2004).

[43] Sarah Major, *Return on Investment (ROI),* (2016), URL: `http://jwilson.coe.uga.edu/EMAT6450/Class%20Projects/Major/Teacher's%20Guide%20ROI.pdf` [cited June 20, 2016].

[44] E. Gill, *Systems Engineering and Aerospace Design,* Delft University of Technology (2016).

[45] P. Roling, *Project Guide Design Synthesis Exercise*, Tech. Rep. (Delft University of Technology, 2016).

A PAYLOAD COMPONENTS

Table A.1: Overview of example payload components with their size, mass and power.

Type	Product name	Manufacturer	Size [l/w/h] [mm]	Mass [kg]	Power [W]
Avionics Sensor Unit					
VOR/ILS	AN/ARN-147	Rockwell Collins	105/127/305	3.6	28.5
Receiver	ANV-141	SELEX	336/124/87	5.5	42
DME Interrogator	ANV-211	SELEX	322/90.5/194	6.25	50
Marker Receiver	MB-10	PS-Engineering	22/66/123	0.18	8.25
ADF Receiver	ARG-80	SELEX	336/124/87	3.5	16.2
TACAN Interrogator	TCN-550	Rockwell Collins	177.8/172.2/304.8	6.48	500
GPS/SBAS (WAAS)	CMA-5024	Esterline	66 x 216 x 24	2.5	20
	CMA-4124	IntegriFlight	168 /102 /15	0.23	12
VHF DATA BROADCAST (VDB)	RE9009	TELERAD	483/430/44.5	4	41.4
Data Acquisition Unit					
DAU	AT-930 SPU	Airfield Tech.	550/300/190	9*	500
	AT-940 SPU	Airfield Tech.	550/350/200	11*	600
Telemetry System					
Omnidirectional blade antenna	6125	Haigh-Farr	76/14.2/30.2	0.02	0
	GMS Part # 501-078	Cobham	76/14/30.2	0.02	0
	Telemetry Antenna S04E102-E4	Spectrum Antennas	62/16.5/44	0.044	0
	ANT-625202	Aero Telemetry	76/-/112	0.369	0
Telemetry transmitter	TT40	SEMCO	76/51/25	0.17	2
	VTX 5540 NT	VITEM	100/80/23	0.39	10
	VTX 5533 NT	VITEM	80/75/23	0.3	2
Airborne amplifier	VTA 5543	VITEM	100/100/21	0.45	20
Linear airborne amplifier	VTA 5540 L	VITEM	210/175/75	3.9	60
Airborne amplifier	VTA 5540	VITEM	100/80/21	0.39	10